Polyurethane nanocomposites as potential drug delivery systems

Author:
Chung, Johnson Hsiang-Yu

Publication Date:
2011

DOI:
https://doi.org/10.26190/unsworks/15273

Polyurethane Nanocomposites
as
Potential Drug Delivery Systems

by

Johnson Hsiang-Yu Chung

A thesis submitted for the degree of Doctor of Philosophy

Graduate School of Biomedical Engineering

The University of New South Wales

Sydney, Australia

August, 2011

Originality Statement

I hereby declare that this submission is my own work and to the best of my knowledge it contains no materials previously published or written by another person, or substantial proportions of material which have been accepted for the award of any other degree or diploma at UNSW or any other educational institution, except where due acknowledgement is made in the thesis. Any contribution made to the research by others, with whom I have worked at UNSW or elsewhere, is explicitly acknowledged in the thesis. I also declare that the intellectual content of this thesis is the product of my own work, except to the extent that assistance from others in the project's design and conception or in style, presentation and linguistic expression is acknowledged.

Signed: …….....

Date:…….....

Abstract

Polymer nanocomposites (NCs) are materials with remarkable potential in the field of controlled drug delivery. There are a range of factors proposed to perturb the release mechanisms in polymer NCs, but little focus has been directed towards the understanding of interactions between the drug and NC which can also affect the drug release behaviour. The objective of this research was to examine the potential of polyurethane nanocomposites (PUNCs) as controlled drug delivery systems. Specifically, the aims were to investigate the impact of adding a drug on the silicate dispersion and release behaviour of PUNCs, as well as to assess the impact of fabrication method on the biological interactions of PUNCs and the activity of released drugs. Organically modified silicates (OMS) were prepared using OMs with varying alkyl chain length. The resulting OMS were incorporated at various loadings into PU matrices and solvent cast to form PUNCs. Findings revealed that the optimum dispersion was achieved from samples with lower clay loadings and longer alkyl chains. A better dispersed sample also conferred an increase in strain while maintaining the Young's modulus and tensile strength of the material. The drug release behaviour of PUNCs was significantly impacted by the properties of the added drug. Results showed that drug release was restricted by the size of the drug. For cases using lower molecular weight drugs that can be released, release of hydrophobic drugs was more sustained than for hydrophilic drugs. However, where strong attractive interactions existed with the host polymer, hydrophilic drugs also showed sustained release. The subsequent introduction of silicates modulated drug release based on the charge and polarity of the drug. Positively charged drugs had a

tendency to interact with clay to a greater degree and release was significantly reduced by the introduction of clay, while anionic and neutral drugs were modulated to a lesser extent. If the charge of the added drug had a repulsive nature with clay, then increasing clay loading promoted the release. PUNCs fabricated both as films and as coatings demonstrated good cell viability and low cell growth inhibition. Biological assays to assess drug activity showed that drugs remained active after release. PUNCs show promise as drug delivery systems, where the drug release profile and mechanical properties can be modulated through changes in modifiers, clay loading and understanding of component interactions.

Acknowledgements

After countless hours of work, I owe my deepest thanks to many people, whom without their help I would not be writing this acknowledgments page.

Firstly, my supervisor Prof. Laura Poole-Warren and co-supervisor Prof. Anne Simmons for their guidance, encouragement and unfailing support right from the beginning of my project. Thank you for providing me with lots of great advice and guiding me to look at things from a different perspective. I have experienced and gained so much. Thank you!

The experience would not have been so enjoyable in The Netherlands without these people: Prof. Leo H. Koole for your help and guidance with the heparin work in your lab, Dr. Menno Knetsch for your endless knowledge in basically everything in the lab. Thanks to Leika, Robert, Jorrit for making work so interesting and most importantly your generosity for donating blood! Without you, I would probably be blood deficient by now. Thanks to Dr. Qinghua Zeng for the modelling work, Dr. Ross Odell with stats and drug release (I now always plot against square root of time!) and staff from the analytical centre. Thank you Dr. Yu Wang and Jenny Norman with help in analysing data and equipment issues.

To the PUNC team, Brooke Farrugia and Nicole Fong, thanks for sharing all the advice and tips in the project. People at GSBME: Bill, Sung, Cara, Jenny, Khoon, Eman for their friendship and support. Naatasha for knowledge on everything U937. Thanks Moon, for making my PhD life happy and interesting. Without you I would not have made it so far, Thank you.

Most importantly, thank you Mom, Dad and Neena for putting up with my ups and downs and especially when I am extremely stressed. Thanks for the support, encouragement and love at times when I needed it most. Finally I made it!

Table of Contents

Abstract ..... **iii**
Acknowledgements ..... **vi**
Table of Contents ..... **vii**
List of Figures ..... **xiii**
List of Tables ..... **xvii**
List of Abbreviations ..... **xix**
Chapter 1: Introduction **1**
1.1. Thesis aim and hypotheses 4
Chapter 2: Background and literature review **7**
2.1 Components in polymer NCs 9
2.1.1 Polymer matrix 10
2.1.1.1 Polyurethane 11
2.1.2 Nanofillers 14
2.1.2.1 Metals and metal oxides 15
2.1.2.2 Carbon nanotubes and fibres 16
2.1.2.3 Layered double hydroxides (LDH) 17
2.1.2.4 Smectite clays 18
2.1.3 Surfactant 20
2.1.4 Polymer Nanocomposite preparation 22
2.2 Morphology of NCs 23
2.3 Exploitation of barrier properties for drug delivery 26
2.3.1 Drug delivery approaches in polymer NCs 27
2.3.1.1 Type 1 28
2.3.1.2 Type 2 29
2.3.1.3 Type 3 32
2.3.1.4 Type 4 33
2.3.1.5 Mathematical models 34
2.4 Properties of polyurethane clay nanocomposites 38

2.4.1 Mechanical properties 38
2.4.2 Barrier properties 40
2.4.3 Polyurethane nanocomposites in drug delivery applications 46
2.4.4 Considerations in drug delivery 47
2.5 Summary and thesis structure 48
Chapter 3: Impact of alkyl chain length on dispersion of nanoparticles within polyurethane nanocomposites 50
3.1 Introduction 50
3.1.1 Silicate modification and arrangements 50
3.1.2 Modification and resulting morphology of NCs 51
3.2 Materials and methods 53
3.2.1 Polymer nanocomposite components: 53
3.2.1.1 Polyurethane 53
3.2.1.2 Layered silicates 54
3.2.1.3 Organic modifiers 54
3.2.2 Polyurethane Nanocomposite fabrication: 55
3.2.2.1 Polyurethane suspension 55
3.2.2.2 Modification of Silicates 55
3.2.2.3 Nanocomposite preparation 56
3.2.3 Materials Characterisation 57
3.2.3.1 Thermogravimetric Analysis 57
3.2.3.2 X-ray Diffraction 58
3.2.3.3 Transmission Electron Microscopy 59
3.2.3.4 Tensile testing 60
3.3 Results 61
3.4 Discussion 73
3.5 Conclusion 76
Chapter 4: Assessment of Polyurethane Nanocomposites as anti-thrombotic coatings using heparin 78
4.1 Introduction 78
4.1.1 Application focus 78

4.2 Materials and methods 83
4.2.1 Sample preparation and coating 83
4.2.1.1 Scanning electron microscopy 85
4.2.2 Drug delivery 85
4.2.2.1 *In vitro* heparin release 85
4.2.2.2 Surface heparin 86
4.2.3 Biological activity of coating 87
4.2.3.1 Static thrombin generation assay 87
4.2.3.2 Dynamic thrombin generation assay 90
4.3 Results 91
4.3.1 Coating 91
4.3.2 Drug release 93
4.3.2.1 *In vitro* heparin release 93
4.3.2.2 Surface heparin 95
4.3.3 Biological activity 96
4.3.3.1 Static thrombin generation assay 96
4.3.3.2 Dynamic thrombin generation assay 100
4.4 Discussion 102
4.4.1 Feasibility study in blood related application 103
4.4.2 Identification of issues for future research 104
4.5 Conclusion 107
Chapter 5: Impact of structure and release of model drugs with different properties 109
5.1 Introduction 109
5.2 Materials and methods 112
5.2.1 Nanocomposite preparation 112
5.2.2 Attenuated Fourier Transform Infrared Spectroscopy 114
5.2.3 In vitro drug release 116
5.3 Results 119
5.3.1 Silicate dispersion and interactions 119
5.3.1.1 X-ray diffraction 119

5.3.1.2 Attenuated Fourier Transform Infrared Spectroscopy 123
5.3.2 *In vitro* drug release 131
5.4 Discussion 136
5.4.1 Impact of interactions on PUNC dispersion 136
5.4.2 Impact of interactions on drug release behaviour 141
5.5 Conclusion 143
Chapter 6: Impact of structure and release of active drugs with similar chemistry 145
6.1 Introduction 145
6.2 Materials and methods 149
6.2.1 Nanocomposite preparation 149
6.2.2 Material characterisation 151
6.2.2.1 X-ray Diffraction 151
6.2.2.2 Transmission Electron Microscopy 151
6.2.2.3 *In vitro* drug release 151
6.2.2.4 Attenuated Fourier Transform Infrared Spectroscopy 152
6.2.2.5 MD simulation 154
6.3 Results 155
6.3.1 Physical experimentation 155
6.3.2 MD simulation 166
6.4 Discussion 168
6.4.1 Impact of interactions on PUNC structure 169
6.4.2 Impact of interactions on drug release behaviour 171
6.5 Conclusion 173
Chapter 7: Polyurethane Nanocomposites as carriers of therapeutic drugs 176
7.1 Introduction 176
7.1.1 Drug activity and release 177
7.1.1.1 Paclitaxel 177
7.1.1.2 Dexamethasone 178
7.1.2 Biological response of PUNCs and PUNC coatings 179
7.2 Methods 182

7.2.1 Nanocomposite preparation 182
7.2.2 *In vitro* Ptx release 182
7.2.3 Biological response assays 183
7.2.3.1 Cell culture 183
7.2.3.2 DexA films-cell growth inhibition assay 184
7.2.3.3 DexA films-CGI inhibition level 185
7.2.3.4 Ptx coils-cell growth inhibition assay 185
7.2.3.5 Ptx coils-CGI inhibition level 186
7.2.4 Drug activity assays 186
7.2.4.1 DexA films-cell growth assay 186
7.2.4.2 DexA films-TNF-α determination by enzyme-linked immunosorbent assay (ELISA) 187
7.2.4.3 DexA films-TNF-α suppression level 189
7.3 Results 190
7.3.1 *In vitro* Ptx release 190
7.3.2 Biological response 192
7.3.2.1 PUNC films loaded with DexA 192
7.3.2.2 PUNC coils loaded with Ptx 194
7.3.3 Drug activity 197
7.4 Discussion 200
7.4.1 Paclitaxel release 200
7.4.2 Biological response of PUNCs 203
7.4.3 Drug activity 204
7.4.3.1 Dexamethasone 204
7.4.3.2 Paclitaxel 206
7.5 Conclusion 208
Chapter 8: Conclusions and Recommendations for Future Work 210
8.1 Introduction 210
8.2 Overall conclusions 210
8.2.1 Silicate dispersion and biological interactions with PUNCs 210
8.2.2 Impact of drug addition on the structure and drug release of PUNCs 213

8.2.3 Drug activity....216
8.3 Recommendations for Future Work....219
8.3.1 PUNC structure....219
8.3.2 Drug-NC interaction....220
8.3.3 Drug release....221
Bibliography....225
Appendix A- Statistical analysis....247
A.1 Mechanical testing data....247
A1.1 Chapter 3-Table 3.3....247
A.2 Blood compatibility assays....251
A2.1 Chapter 4-Table 4.2....251
A2.2 Chapter 4-Figure 4.6....252
A2.3 Chapter 4-Figure 4.8....254
A2.4 Chapter 4-Figure 4.9 & Figure 4.10....254
A2.5 Chapter 4-Table 4.3....256
A.3 Cell studies....258
A3.1 Chapter 7-Figure 7.9....258
A3.2 Chapter 7-Figure 7.10....259
Appendix B....260
B.1 Static thrombin generation assay....260
B.2 Dynamic thrombin generation assay....261
Appendix C....263
C.1 ATR-FTIR spectra of 16CH_3MMT and 12CH_3MMT....263
C.2 Release kinetics of crystal violet and bromophenol blue....264
Appendix D....271
D.1 Cell growth inhibition assay of DexA and DexP....271

List of Figures

Figure 1.1 Polymer NC consisting of A) three components; B) four components. 3

Figure 2.1 Polymer NC consisting of three components 10
Figure 2.2 Urethane linkage 11
Figure 2.3 Morphology of polyurethane. 12
Figure 2.4 Structure of polyurethane showing (A) microphase separation; and (B) packing of hard segments 13
Figure 2.5 Structure of MMT. 20
Figure 2.6 Arrangement of alkyl chains in clay minerals 21
Figure 2.7 Illustration of (A) conventional; (B) intercalated; (C) exfoliated polymer clay NCs. 24
Figure 2.8 Morphology of polymer silicate NCs 25
Figure 2.9 Types of approaches for drug delivery in non-degradable polymer NCs. 28
Figure 2.10 The concept of the tortuous pathway. 35

Figure 3.1 Molecular structure of Poly (ether) urethane. 54
Figure 3.2 Atomic structures of organic modifiers. 55
Figure 3.3 TGA thermograms of OMS used in this study. 63
Figure 3.4 XRD diffractograms for: A) MMT, B) 12CH3MMT, and C) 16CH3MMT. .64
Figure 3.5 XRD diffractograms for a) neat PU, and PUNCs modified with 12CH3MMT at loadings b) 1wt%, c) 3wt%, and d) 5wt%. 65
Figure 3.6 XRD diffractograms for a) neat PU, and PUNCs modified with 16CH3MMT at loadings b) 1wt%, c) 3wt%, and d) 5wt%. 65
Figure 3.7 Representative TEM images of PUMMT-1 and P12C-1.....67
Figure 3.8 Representative TEM images of P12C-1 and P16C-1 68
Figure 3.9 Representative TEM images of P12C-5 and P16C-5 69
Figure 3.10 Young's modulus for PU and PUNCs.. 71
Figure 3.11 Ultimate tensile stresses for PU and PUNCs.. 71
Figure 3.12 Ultimate strains for PU and PUNCs.. 72

Figure 4.1 The intrinsic, extrinsic and common pathway of blood coagulation 82
Figure 4.2 Coils in PRP for static thrombin generation assay. 89
Figure 4.3 Setup of the dynamic thrombin generation assay 90
Figure 4.4 Representative SEM images of coated coils.....92
Figure 4.5 Cumulative release of samples incorporated with heparin.. 94
Figure 4.6 Total amount of surface heparin on the surface of the coil. 95
Figure 4.7 Summary of heparin released, surface bound and those remaining in the bulk polymer. 96
Figure 4.8 Static TGT of PU+H and P16C-5+H under washing times of 1 day, 2 days, and 1 week......97
Figure 4.9 Static TGT for coils with and without heparin. 98
Figure 4.10 Peak thrombin of coils with and without heparin. 99
Figure 4.11 Dynamic TGT of samples with and without heparin.....100

Figure 5.1 Illustration of the types of interfacial interactions occurring in polymer-organoclay nanocomposites. 110
Figure 5.2 Plates consisted of 9 glass cylinders. 117
Figure 5.3 XRD diffractograms for : A) PU+1%CV, B) P12C-1+1%CV, C) P12C-3+1%CV, D) P12C-5+1%CV, E) P16C-1+1%CV, F) P16C-3+1%CV, and G) P16C-5+1%CV.....120
Figure 5.4 XRD diffractograms for : A) PU+1%BB, B) P12C-1+1%BB, C) P12C-3+1%BB, D) P12C-5+1%BB, E) P16C-1+1%BB, F) P16C-3+1%BB, and G) P16C-5+1%BB. 121
Figure 5.5 XRD diffractograms for : A) PU+1%CB, B) P12C-1+1%CB, C) P12C-3+1%CB, D) P12C-5+1%CB, E) P16C-1+1%CB, F) P16C-3+1%CB, and G) P16C-5+1%CB. 122
Figure 5.6 ATR-FTIR spectra of OMS added with CV. 124
Figure 5.7 ATR-FTIR spectra of OMS added with BB. 124
Figure 5.8 ATR-FTIR spectra of OMS added with CB. 125
Figure 5.9 ATR-FTIR spectra of OMS added with model drugs at wavenumbers between 3000-2800cm^{-1}.. 126

Figure 5.10 ATR-FTIR spectra of OMS added with 30mg of model drugs at wavenumbers between 1550-1450cm^{-1} 127
Figure 5.11 ATR-FTIR spectra for PUNC-3wt% with varying concentration of CV. .. 127
Figure 5.12 ATR-FTIR spectra for PUNC-3wt% with varying concentration of BB ... 128
Figure 5.13 ATR-FTIR spectra for PUNC-3wt% with varying concentration of CB. .. 128
Figure 5.14 Cumulative release profile of samples incorporated with CV. 133
Figure 5.15 Cumulative release profile of samples incorporated with BB 134
Figure 5.16 Cumulative release profile of samples incorporated with CB 134
Figure 5.17 Interactions that could occur between the model drugs and OMS. 139

Figure 6.1 XRD diffractograms for : A) PU+1%DA, B) P12C-1+1%DA, C) P12C-3+1%DA, D) P12C-5+1%DA, E) P16C-1+1%DA, F) P16C-3+1%DA, and G) P16C-5+1%DA. 156
Figure 6.2 XRD diffractograms for : A) PU+1%DP, B) P12C-1+1%DP, C) P12C-3+1%DP, D) P12C-5+1%DP, E) P16C-1+1%DP, F) P16C-3+1%DP, and G) P16C-5+1%DP. 156
Figure 6.3 Representative TEM images of P12C-1 with DexA or DexP. 158
Figure 6.4 Representative TEM images of P12C-5 with DexA or DexP 159
Figure 6.5 Cumulative release profile of samples incorporated with a) DexA, and b) DexP over 5 weeks (n=3). 161
Figure 6.6 ATR-FTIR spectra for MMT, OMS and OMS incorporated with DexA and DexP. 163
Figure 6.7 ATR-FTIR spectra for PUNC-3wt% with varying concentrations of DexA.. 164
Figure 6.8 ATR-FTIR spectra for PUNC-3wt% with varying concentrations of DexP.. 165
Figure 6.9 ATR-FTIR spectra of PUNC-3wt% loaded with a) DexA and b) DexP. 165
Figure 6.10 Models of MD results of exfoliated NCs. 166

Figure 7.1 U937 cells; a) not activated and b) activated by PMA (U937*). 188
Figure 7.2 Cumulative release profile of coils incorporated with Ptx. 191
Figure 7.3 Cumulative release profiles of coils with respect to square root of time.. 191

Figure 7.4 Cell growth inhibition assay of samples loaded with DexA.....193
Figure 7.5 CGI standard curve for DexA.....193
Figure 7.6 Cell growth inhibition assay of samples loaded with Ptx.....195
Figure 7.7 CGI standard curve for Ptx.....195
Figure 7.8 Comparison of cell growth inhibition of PU and P16C-1 196
Figure 7.9 Cell growth assay of samples loaded with DexA over 10 days.....197
Figure 7.10 TNF-α release from samples.....199
Figure 7.11 Standard curve for TNF-α suppression by DexA 199

Figure 8.1 General guide for predicting the drug release profile from PUNCs. 217

Figure B.1 Representative thrombin generation curves for: A) PU and B) P16C-1.....260
Figure B.2 Dynamic thrombin generation curve of A) PUNC controls and B) incorporated with heparin. 261

Figure C.1 ATR FTIR spectra for NaMMT, 12CH_3MMT and 16CH_3MMT 263
Figure C.2 Zero order release kinetics. The ratio of cumulative release of CV.....265
Figure C.3 First order release kinetics. The logarithm of cumulative release of CV.....266
Figure C.4 Higuchi's square root model. The ratio of cumulative release of CV. 267
Figure C.5 Zero order release kinetics. The ratio of cumulative release of BB.....268
Figure C.6 First order release kinetics. The logarithm of cumulative release of BB.....269
Figure C.7 Higuchi's square root model. The ratio of cumulative release of BB.....270

Figure D.1 CGI standard curve for: a) DexP (n=2) and b) DexA (n=3).....271

List of Tables

Table 1.1 Medical applications of polymers 1
Table 2.1 Notation and chemistry of common smectites 18
Table 2.2 Theoretical models in predicting barrier properties of polymer NCs 37
Table 2.3 Mechanical properties of PUNCs.....41
Table 2.4 Barrier properties of PUNCs 44
Table 3.1 Materials investigated within Chapter 3 57
Table 3.2 XRD results for PU and PUNCs 66
Table 3.3 Summary of mechanical properties of PUNCs. 72
Table 3.4 The effects on silicate dispersion and mechanical properties from increasing loading and modifier chain length.....76
Table 4.1 Materials investigated within Chapter 4 84
Table 4.2 Summary of total heparin released.....94
Table 4.3 Summary of dynamic TGT for all samples 101
Table 4.4 Summary of coils with added heparin.....102
Table 5.1 Materials investigated within Chapter 5 113
Table 5.2 PUNCs incorporated with model drugs with same clay loading 115
Table 5.3 OMS incorporated with model drugs 116
Table 5.4 Structure and chemical properties of model drugs 118
Table 5.5 XRD results for PU and PUNCs incorporated with CV 120
Table 5.6 XRD results for PU and PUNCs incorporated with BB 121
Table 5.7 XRD results for PU and PUNCs incorporated with CB 122
Table 5.8 FTIR band assignments of MMT, OMS and model dyes 129
Table 5.9 FTIR band assignments of PUNCs and model dyes 130
Table 5.10 Coefficient of determination and k 135
Table 5.11 Theoretical assumptions of the interactions between model drugs and OMS. 137
Table 6.1 Materials investigated within Chapter 6 150

Table 6.2 Structure and chemical properties of drugs.....152
Table 6.3 PUNCs incorporated with drugs with same clay loading 153
Table 6.4 OMS incorporated with drugs.....153
Table 6.5 X-ray diffraction results for PUNCs incorporated with DexA or DexP 157
Table 6.6 Coefficient of determination and k 162
Table 6.7 Interaction energies (kcal/mol) between any two components in an exfoliated PUNC at equilibrium.....167
Table 6.8 Interaction energies (kcal/mol) between any two components in PU-drug systems at equilibrium.....168
Table 7.1 Materials investigated within Chapter 7 183
Table 8.1 Summary of silicate spacing, morphology and mechanical properties of PUNCs.....211
Table 8.2 Summary of drugs used in this study.....214

List of Abbreviations

$8CH_3$	Octylamine
$12CH_3$	Dodecylamine
12COOH	Aminododecanoic acid
$16CH_3$	Hexadecylamine
$18CH_3$	Octadecylamine
AFM	Atomic force microscopy
ANOVA	Analysis of Variance
AUA	Aminoundecanoic acid
ATIII	Anti-thrombin III
ATR-FTIR	Attenuated total reflection-Fourier transform infra-red spectroscopy
BB	Bromophenol blue
BDO	1,4 Butanediol
CB	Coomassie Blue
CEC	Cation exchange capacity
CGI	Cell growth inhibition
CNF	Carbon nanofibre
CNT	Carbon nanotube
CTAB	Cetyltrimethyl ammonium bromide
CV	Crystal violet
DBTDL	Dibutyltin dilaurate
DES	Drug eluting stents

DEB	Drug eluting balloon
DEX	Dexamethasone
DEXA	Dexamethasone acetate
DEXP	Dexamethasone phosphate
DMAc	Dimethylacetamide
DPBS	Dulbecco's phosphate buffered saline
DSC	Differential scanning calorimetry
EDA	Ethylene diamine
ELISA	Enzyme-linked immunosorbent assay
EMEM	Eagle's minimal essential medium
EQ	Ethoquad ® O/12PG
FBS	Foetal bovine serum
FTIR	Fourier transform infra-red spectroscopy
LDH	Layered double hydroxide
LMWH	Low molecular-weight-heparin
LPS	Lipopolysaccharide
MD	Molecular dynamic
MDI	4,4' diphenylmethane diisocynate
MMT	Montmorillonite
NC	Nanocomposites
NIR	Near infrared
NMP	1-methyl-2-pyrrolidone
NMR	Nuclear magnetic resonance

OM	Organic modifier
OMS	Organically modified silicate
PES	Polyether sulphone
PBS	Phosphate buffered saline
PMA	Phorbol 12-myristate 13-acetate
PPG	Polypropylene glycol
PRP	Platelet rich plasma
P/S	Penicillin/Streptomycin
PTMEG	Polytetramethylene glycol
PTMO	Poly (tetramethylene oxide)
PTX	Paclitaxel
ROI	Reactive oxygen species
RPMI	Roswell Park Memorial Institute
PU	Polyurethane
PUNC	Polyurethane nanocomposite
SEM	Scanning electron microscopy
TEM	Transmission electron microscopy
TGA	Thermogravimetric analysis
TGT	Thrombin generation lag time
TNF	Tumour necrosis factor
UTS	Ultimate tensile strength
XRD	X-ray diffraction

Chapter 1: Introduction

Polymers have become increasingly popular in medical applications due to design flexibility, lower manufacturing cost compared to other classes of materials, and the continuous increase in the use of disposable medical products [1, 2]. Their greatest advantage is the ability to undergo chemical modifications, giving them unlimited diversity in chemistry, structure and function [3].The United States represents the largest market for medical polymers valued at $6.55 billion, accounting for 45-47% of the global market. This is followed by the European Union which accounts for 30% of the global market [1, 4]. Of the medical polymers produced, 56% of those are used for packaging and 44% used in medical supplies and equipments [1]. Table 1.1 lists some applications of polymers in the medical industry.

Table 1.1 Medical applications of polymers [5, 6]

Implants	Supplies & Equipment	Disposables	Others
Breast prostheses	Tubing	Contact lens	Drug delivery systems
Vascular grafts	Blood Bags	Syringes	Suture material
Hip/Knee prostheses	Bandage	Medical Packaging	Catheters
Heart valves			

When applied as coatings onto medical devices, polymers can deliver drugs locally, as well as minimise the host response through releasing anti-inflammatory or anti-

thrombotic agents. Examples of such devices include catheters, drug eluting stents (DES), drug eluting balloons (DEB) and guidewires. The use of elastomers is often preferable in these applications as they can flex and extend in response to stress and retain their structural integrity after stress is removed. Among the different elastomers available, polyurethane (PU) has become increasingly popular as a potential coating for drug delivery applications due to its high tensile strength, chemical stability and good compatibility with tissues and blood [7, 8]. PU has been examined as carrier for anti-tumour drugs to treat cancer [9], as a coating to reduce inflammation after stent placement [10], and in vascular applications for releasing anti-thrombotic agents [11, 12].

However, one major issue related to the use of PU or other polymers as drug delivery systems in long-term applications is the sudden release of drugs initially, referred to as the burst effect [13]. Once in contact with the release medium, polymers can lose a large proportion of drug within a short period of time and the therapeutic effects cannot be maintained. Some strategies to sustain and modulate drug release include modifying the composition or morphology of the polymer [13], chemically attaching the drug to polymer backbone [3, 14], or coating with an additional layer of polymer [15, 16]. However, these strategies involve extra processing steps that increase cost and time, as well as introducing additional materials with new chemistries that can lead to regulatory concerns. Thus, further research and development is required to identify suitable materials for use in the controlled drug delivery field.

A means to modulate release mechanisms of polymers without negatively impacting the physical properties of a polymer is by the incorporation of layered silicates to obtain a

polymer nanocomposite (NC). As illustrated in the schematic in Figure 1.1a, NCs are materials reinforced with nanoscale fillers that can provide improvements in mechanical, thermal and barrier properties when they are well separated, or dispersed throughout the matrix [17, 18]. When uniformly dispersed, these filler nanoparticles not only strengthen the matrix [19, 20], but can also significantly reduce the permeability of moisture and gases. These interesting properties have been explored for packaging materials in a variety of food and beverage products, but have yet to be widely exploited for medical applications [21, 22].

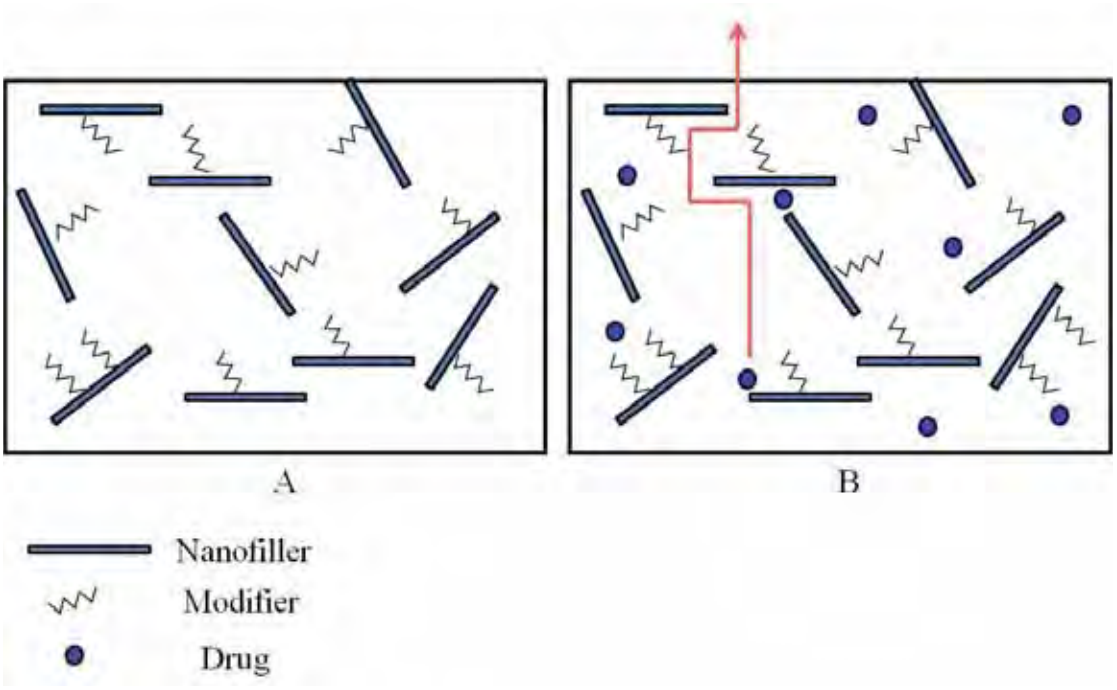

Figure 1.1 Polymer NC consisting of A) three components: nanofillers, organic modifier, both of which are incorporated in a polymer matrix; B) four components: nanofillers, organic modifier, drugs, all of which are incorporated in a polymer matrix. Arrow represents the diffusion path for drugs which can depend on filler content, dispersion and interactions between the drug and the components within NC.

The observation that barrier properties can be modulated in polymer NCs may have significant implications in the field of drug delivery. Drug permeability in polymer NCs can be significantly perturbed by the variation of component properties such as filler content and quality of dispersion as depicted in Figure 1.1b. However, drug interactions with the NC system may also impact on silicate dispersion, drug diffusion and the release mechanism. Thus, a continuing challenge for the field is to understand the key interactions between the drug and the polymer, nanofiller and modifier. This knowledge will contribute to the development of more accurate models that will ultimately allow for the prediction of drug release behaviour in a polymer NC system.

1.1. Thesis aim and hypotheses

This thesis aims to explore the use of polymer NCs as potential drug delivery coatings for medical devices. The ability to modulate barrier properties through manipulation of filler parameters will be potentially beneficial for drug delivery purposes due to likely influences on dissolution rate, release mechanisms and drug uptake. In this research, the NC system investigated was a polyurethane (PU) based NC with organically modified silicates as the nanofiller. Of interest, is the application of these materials to accommodate and deliver a wide variety of drugs for anti-thrombotic, anti-proliferative or anti-inflammatory purposes. The overall objective of this research was to examine the potential of PUNCs as controlled drug delivery systems and devise a guide for predicting the drug release profile based on the different physical and chemical properties of the added drug.

The main hypotheses driving this research were:

1. Modification of silicates using longer alkyl chain length modifiers promotes exfoliation of silicates within the PU matrix, which in turn sustains drug release via the tortuous path effect (Figure 1.1b). These improvements occur without detrimentally affecting the biological performance of PU.

2. Silicate dispersion and thus release behaviour is affected by interactions arising from the addition of a fourth component (the drug) into the PUNC system. The interactions occurring between the four components comprising of polymer, clay, modifier and drug, depends on the physical and chemical properties of the added drug.

3. The drugs that are released from the NC system remain biologically active and are not affected by fabrication methods. That is, drugs incorporated and then released from PUNCs fabricated either as films or as coatings maintain their function and capacity for producing the desired therapeutic effect.

The focus of the current research was directed towards the fundamental understanding of drug-PUNC interactions to allow accurate predictions of the drug delivery behaviour. The specific aims of this project were to:

1. Identify the most suitable modifier and clay loading to achieve a NC structure with maximal silicate dispersion.

2. Examine and understand the interactions that occur when incorporating a drug in a PUNC system, and the implications on silicate dispersion and drug release behaviour.

3. Assess the *in vitro* mammalian cell response of PUNCs and use this as a measure of the material's biocompatibility.

4. Assess the activity of drugs released from PUNCs through various *in vitro* biological assays.

5. Examine the feasibility of using PUNCs as coatings for medical devices by coating it onto metallic substrates.

Chapter 2: Background and literature review[1]

Composite materials are defined as materials comprised of two or more distinct components including a matrix and a filler that are combined on a macroscopic scale. These components are incorporated such that the resulting new material exhibits the desirable properties of its constituents, such as increased mechanical strength, stiffness, fatigue resistance and wear resistance. With mechanical properties being the major driver, composite materials have been widely used in automotive and aerospace applications where high strength-to weight and stiffness-to-weight ratios are required [23].

Much like traditional composites, NCs are comprised of two or more components, however, at least one dimension, either the length, width, or the thickness of one of the components is in the size range of 1 to 100nm [18]. Significant improvements in properties can be achieved when fillers are well dispersed in the matrix, otherwise they may act as conventional filler particles. When the filler particles are well dispersed, NCs typically require 1 to 5wt% filler content in comparison to the 10 to 70wt% in conventional composites to achieve property enhancement [24]. These filler nanoparticles reinforce and strengthen the matrix which can be constructed of metallic,

[1]Parts of this chapter were adapted to from a review article: J.H.Y Chung, A. Simmons, L.A Poole-Warren, 2011, Non-degradable polymer nanocomposites for drug delivery, *Expert Opinion on Drug Delivery*, **8(**6) 765-778, and are reproduced here with copyright permission from the publisher. The contribution by the author of this thesis to this paper included: outline of the content and concepts, and major part of the structure and writing.

ceramic or polymeric base materials [19, 20]. In this review the focus will be on polymer matrices.

The origin of polymer NCs can be traced back to the early 1950s when Hauser discovered that by replacing inorganic cations in nanoclays with an organic base, the ability of the clay to swell in water was diminished and the surfaces became organophilic [25]. This finding laid the foundation for incorporation of such modified nanoclays into organic polymers, the modifier having a "compatibilising" effect on the normally hydrophilic clay. In the absence of surface modifiers, the ability to disperse typically polar nanofillers within a largely non-polar organic matrix is limited.

Much research investigating swelling behaviour of layered clays and intercalation chemistry of polymers has been conducted [26-28], but the findings were not translated into NC applications until the 1990s. In 1993, researchers from the Toyota group successfully polymerized ε-caprolactam in a cation exchanged montmorillonite (MMT) to produce a nylon-6 clay based NC [29, 30]. The resulting NC was well dispersed and showed dramatic improvements in mechanical and physical properties and heat distortion temperature at very low layered silicate concentrations [29, 30]. This enabled research into other potential fillers such as carbon nanotube (CNT), carbon fibre (CNF), glass and metals [22, 31, 32].

The improvements in material properties observed in polymer NC systems make them particularly attractive for biomedical applications. Having the ability to improve mechanical properties without altering the chemistry of the polymer matrix is a useful

tool to overcome regulatory concerns with new chemistries in the biomedical environment. Similarly, barrier properties are known to be impacted by addition of nanofillers and this property may have significant implications in the field of drug delivery. Drug delivery systems typically aim to provide therapeutic levels of active agents at the target site in a controlled manner. Such systems theoretically provide appropriate concentrations of drug at a local site which usually would not be possible through systemic administration. Control of drug release locally is also able to overcome issues of adverse side effects and systemic toxicity that can be associated with systemic drug delivery.

This chapter aims to provide background knowledge on polymer NCs with specific reference to the PU organosilicate NCs studied in this thesis. An overview will be presented on the components making up polymer NC systems, the properties relevant to drug delivery systems and the delivery approaches and applications relating to the use of polymer NCs in drug delivery. Finally, areas that require further understanding will be discussed.

2.1 Components in polymer NCs

Polymer NCs are comprised of the polymer matrix material and the nanofiller, but in many cases a third component, the organic modifier (OM) is required to enhance compatibility of inorganic nanofiller with the organic polymer matrix as illustrated in Figure 2.1. Existing polymers for controlled delivery include non-degradable and degradable polymers, hydrogels and biopolymers [33].

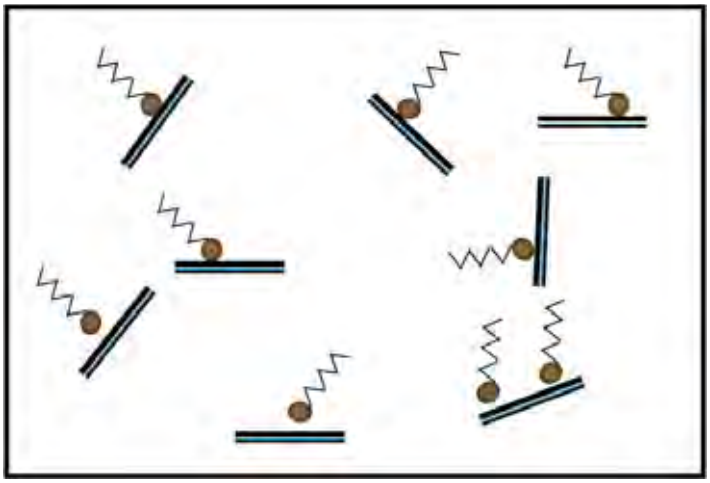

Figure 2.1 Polymer NC consisting of three components. The inorganic nanofillers (rectangular stacks) modified through electrostatic interaction with organic surfactants (sphere shaped head group and tail), both of which are incorporated in a polymer matrix (Reproduced from Chung et al. 2011 [34]).

2.1.1 Polymer matrix

Choice of polymer matrix often depends on the application, with much research concentrated on NCs based on epoxies [35], polyimide [36], polystyrene [37], polypropylene [38], polyethylene [39] and polyurethane [40]. Polymers have a variety of desirable attributes in selected medical applications, such as flexibility, toughness, weight/volume ratio, design flexibility and low electrical conductivity [2, 41].

Due to the processing ease, polymers find use as tubing, sutures, blood contacting devices, medical packaging, lenses, dialyzers and syringes [6]. The increased use of disposable devices has also expanded the use of polymers. For application such as catheters, stent coatings, drug eluting balloons and guidewire, the use of elastomers are

often preferable. Elastomers are loosely cross-linked polymers that have characteristics similar to rubber and can retain their structural integrity after stress is removed. Common elastomers used as matrices for polymer NCs include polyurethane, silicone, ethylene-vinyl acetate and rubber [42, 43]. The major focus of this research will be on polyurethane organosilicate nanocomposites.

2.1.1.1 Polyurethane

PUs are defined as polymers having urethane linkages shown in Figure 2.2 [8]. They are versatile polymeric materials with desirable properties such as high abrasion resistance, tear strength, excellent shock absorption and flexibility [44]. PUs are elastomers that are used in a variety of applications including automotive, screens, roller systems, coatings , adhesives, and medical applications [40].

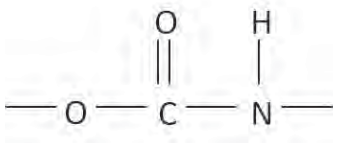

Figure 2.2 Urethane linkage (adapted from Gunatillake [8]).

In general, PUs are segmented copolymers (Figure 2.3) consisting of soft segments made of high molecular weight polyester or polyether macrodiol, and hard segments which are composed of diisocynate and a low molecular weight diol or diamine. PU can be synthesised by one or two-step process [45]. In the one step process, all components are mixed and reacted with the presence of a catalyst, while the two-step process does not involve the use of a catalyst. The macrodiol is initially reacted with diisocynate to

form a prepolymer and the prepolymer then reacts with a chain extender to form the polymer. The selection of reactants, ratios and process of synthesis (one or two step process) can influence the microstructure and final properties of the resulting PU [46].

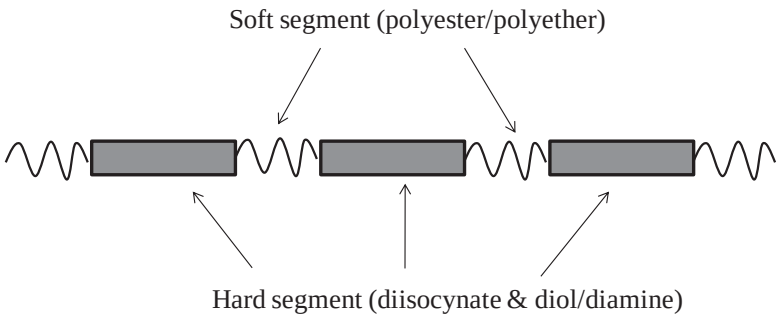

Figure 2.3 Morphology of polyurethane (adapted from Hyvarinen [45]).

Microphase separation within the PU due to thermodynamically incompatible soft segments (amorphous) and hard segments (semicrystalline) give PU attractive mechanical and physical properties. The soft phase imparts flexibility and softness, while the hard phase contributes to the strength and stiffness of the polymer. The degree of microphase separation can be influenced by a lot of factors, including the hard-soft segment ratio, composition of each, solubility, length and crystallisability [8]. An early model proposed by Estes *et al*. [47] illustrated in Figure 2.4A, showed a two-dimensional cross section of the domain structure in undeformed PU. The hard domains exist as interconnecting network. Both phases are continuous and interpenetrating with some urethane blocks dispersed in the matrix due to incomplete phase separation [47]. The average hard block is around 55Å [48] with an interdomain repeat distance of approximately 50-90nm depending of the hard/soft segment content [49] . Hard domain

sizes of around 12-32nm [49] can form due to the aggregation of the hard phase. The aggregation is assisted by hydrogen bonding of the urethane groups (Figure 2.4B) and by π-electrons (aromatic diisocynate) [50].

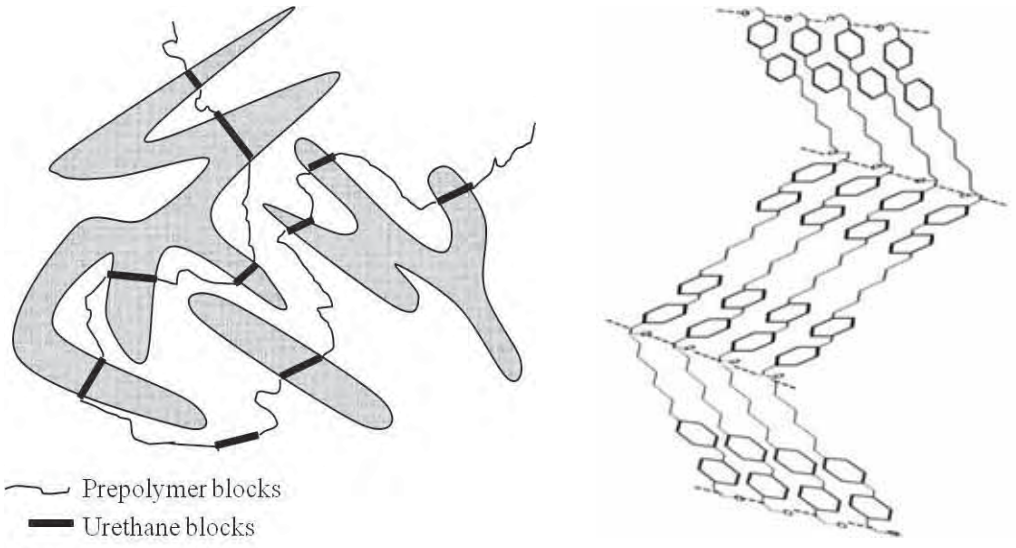

Figure 2.4 Structure of polyurethane showing (A) microphase separation (adapted from Estes [47]); and (B) packing of hard segments (adapted from Blackwell [50]).

Synthetic elastomers are frequently used for the construction of implantable medical devices, where silicon rubbers and PUs are often the choice due to their good chemical stability in a biological environment [8]. The use of silicon rubbers is limited to applications that are suited to their weak mechanical properties, tear, abrasion and fatigue life. On the other hand PUs have good resistance to mechanical degradation and their tensile strength is significantly greater than that of silicon rubber [45].

Boretos and Pierce in 1967 were the first to recognize the potential of using PU in medical implants [51]. Since then, PUs have been used in a variety of biomedical applications including blood sacs in ventricular assist devices, catheters, vascular grafts, and suture materials [52]. The potential of PU as drug delivery systems has also been studied by several research groups. Iskakov *et al*. examined PU as a carrier for anti-tumour drugs in treating cancer [9]. Depending on the solubility of drug and amount incorporated, the release of cyclophosphane, thiophosphamide and vincristine all showed diffusion controlled mechanisms and the total amount was released in 6 to 7 days for cyclophosphane, 5 to 6 days for thiophosphamide and 2 to 3 days for vincristine.

Other researchers evaluated dexamethasone loaded PU systems for the prevention of postoperative adhesions after strabismus surgery [53]. Adhesion during postoperative healing inhibits delayed adjustment of the eye since the alignment of the eye may drift over time [53, 54]. Using this system, delay of the adjustment was possible for up to 6 weeks postoperatively in a rabbit model without frequently applying steroids [53]. The incorporation of anti-inflammatory agents, anti-thrombotic and anti-proliferative agents for vascular applications has also been reported [11, 12]. Up to this point, the PU matrix alone was applied for drug delivery. To formulate a NC, fillers need to be added and choice of the filler is a key decision that can impact on the function of the NC.

2.1.2 Nanofillers

Various types of nanoparticle fillers have been used as reinforcement for rubber and plastics. This section will briefly discuss some of the common nanofillers reported in

biomedical applications and in particular drug delivery systems, such as metals [55, 56], metal oxides [57], carbon nanotubes (CNT) and nanofibres (CNF) [58, 59], layered double hydroxides (LDH) [60-62], and smectite clays [63, 64]. The latter is the nanoparticle of choice in this research and therefore the primary emphasis is on the smectite clays.

2.1.2.1 Metals and metal oxides

Metal oxides such as TiO_2 are spherical nanofillers that have been studied as fillers in various polymer types. Ng *et al.* [65] showed a dramatic increase in both modulus and scratch resistance using TiO_2 particles with an average diameter of 32nm and 10wt% loading in epoxy, while micron sized TiO_2 only demonstrated increased modulus. In the field of bioengineering, TiO_2 can be used as a drug carrier for active drug molecules due to its oxidising properties and chemical inertness. NCs based on poly(lactic acid) and nano-TiO_2 as a carrier of anticancer drugs showed more efficient delivery and potentially higher loading capacity due to the large surface area. This was attributed to electrostatic interactions and non-covalent binding between the drug and TiO_2 creating a self-assembled surface that could readily adhere to the surface of the targeted cancer cells and enhance drug permeation [66]. In addition, there have been reports on the use of nano-Ti in urinary tract applications because of their encrustation-resistant properties and decreased adhesion of *S. epidermidis* [57].

Both gold (Au) and silver (Ag) have been explored in NCs as fillers possessing desirable biological properties. An improvement in thermal and mechanical behaviour was found by Hsu and co-workers when Ag/Au nanoparticles were incorporated in a poly (ether)

urethane. Following implantation in porcine models, these materials also demonstrated improved *in vivo* biostability compared to neat PU which was attributed to free radical scavenging by the Ag/Au nanoparticles [55, 56]. Silver is well known for its antimicrobial ability and has been used in catheters to prevent infection [67]. Incorporation of silver nanoparticles in poly (ether) urethane showed enhanced cellular proliferation, reduced monocyte activation and lower bacterial adhesion [68]. Gold on the other hand is a noble metal that has low cytotoxicity and does not elicit pro-inflammatory cytokines. Gold incorporated poly (ether) urethane NCs also demonstrated lower bacteria adhesion and platelet activation [69].

2.1.2.2 Carbon nanotubes and fibres

Carbon nanotube (CNT) and carbon fibres (CNF) are unique structures with high aspect ratios and excellent mechanical (flexibility and strength), electrical and thermal properties, making them the subject of intensive research as reinforcements for polymer, metal and ceramic composites [58]. CNT were first discovered by Iijima in 1991 at the NEC fundamental research laboratory in Japan [70]. CNT can be visualized as rolled sheets of graphitic carbon either as a single-walled structure with diameter as small as 0.4nm or multi-walled with outer diameter from 5 to 100nm [61]. CNF can encompass a range of morphologies from disordered bamboo-like structures to layers of 'cup stacked' structures with diameter in the order of 50-200nm. Polymer NCs based on CNT and CNF show improved mechanical strength at low volume fractions. Chang *et al.* [59] showed a threefold modulus increase with 1wt% CNT in polypropylene matrix, while a 13% improvement in fracture toughness and 33% improvement in bending strength were

observed in CNF reinforced alumina NC loaded with 2.5 and 5.0 (v/v) respectively [58]. Most of the research on such NCs however, was in microcatheters or blood compatible materials rather than for drug delivery applications [71, 72]. A major obstacle in the widespread application of CNT is the debate on the safety of CNT in long term implants [61].

2.1.2.3 Layered double hydroxides (LDH)

LDH are anionic clays that can also accommodate organic compounds through ion-exchange reactions from its interlayer anions. The chemical formula for LDH can be generalized as $[M^{II}_{1-x}M^{III}_{x}(OH)_2]^{x+}(A^{n-})_{x/n}\cdot yH_2O$, where M^{II} and M^{III} are divalent and trivalent cations respectively, and A^{n-} is the anion. They can be of synthetic and natural origin. The most commonly known natural occurring LDH is hydrotalcite, having the formula $Mg_6Al_2(OH)_{16}CO_3\cdot 4H_2O$. Therefore LDHs are also known as hydrotalcite-like compounds [73, 74]. LDHs can easily be synthesised in the laboratory to have high chemical purity, structural homogeneity and tunable chemical properties [75]. Therefore most of the LDHs reported in literature were synthesised.

The use of LDH in drug delivery systems has been extensively studied for antibiotic [76], anti-cancer [77], anti-inflammatory [78, 79], DNA and lipid regulating drug delivery systems [80, 81]. The use of LDH as nanofillers in NCs have also been reported [76, 82]. Tammaro *et al*. [76] investigated the release of the antibiotic, chloramphenicol succinate, from LDH-polycaprolactone NC. In addition to the improvement in the elastic modulus, yield strength, and fracture strength, NCs loaded with the same drug loading as neat polycaprolactone retarded 70% of the initial burst release [76].

2.1.2.4 Smectite clays

There are generally three types of layered silicates (phyllosilicate) used in the synthesis of polymer clay NCs. They are the 2:1 type, 1:1 type and layered silicic acids. The smectite group, or 2:1 type, are the most widely used for the production of polymer NCs, because of their high aspect ratio and remarkable ability to exchange ions [63, 64]. Smectites commonly used in NCs, either natural or synthetic are shown in Table 2.1.

Table 2.1 Notation and chemistry of common smectites (Reproduced from Chung et al. 2011 [34])

2:1 type	Substitution	Cell Formula
Natural		
Montmorillonite	Octahedral	$(Na,Ca)_{0.33}(Al,Mg)_2Si_4O_{10}(OH)_2 \cdot nH_2O$
Hectorite	Octahedral	$Na_{0.3}(Mg,Li)_3Si_4O_{10}(OH)_2$
Saponite	Tetrahedral	$(Ca_{0.5},Na)_{0.3}(Mg,Fe^{2+})_3(Si,Al)_4O_{10}(OH)_2 \cdot 4(H_2O)$
Synthetic		
Fluorohectorite	Octahedral	$Li_{1.12}[Mg_{4.88}Li_{1.12}][Si_8O_{20}]F_4$
Laponite	Octahedral	$Na_{0.7}[Mg_{5.4}Li_{0.4}]Si_8O_{20}(OH)_4$

To date, montmorillonite (MMT) is the most widely used layered silicate because of its abundance in nature, low cost and ease of chemical modification. Most importantly, MMTs have silicate layers 0.96nm thick and approximately 100 to several hundred nanometers in length, resulting in a high surface area of around 750 m^2/g [83-86]. This

high surface area provides more polymer-clay reinforcement than conventional micron-sized composites [87].

The structure of MMT consists of a repeating triple layer composed of two silica tetrahedral sheets sandwiching an octahedral sheet of alumina, as shown in Figure 2.5. Isomorphic substitution of Si^{4+} for Al^{3+} in the tetrahedral layer and Al^{3+} for Mg^{2+} in the octahedral sheet will generate negative charges within the layers. This behaviour is then counterbalanced by cations such as Na^{+}, Ca^{2+}, Li^{+} occupying the 'interlayer' or 'gallery' [84, 88]. The layers with high aspect ratio are stacked via weak dipole forces and the cations occupying the gallery are generally responsible for the swelling of clay in water [17]. Due to the strong electrostatic attraction between silicate layers, clay minerals are not naturally of nanometer size since they exist as stacked tactoids. These tactoids can be exfoliated or delaminated into single "platelets" with thickness about 1 nm, allowing clay to be a candidate filler in polymer NCs [87].

The ability of clays to exchange the interlayer cations with other cations is referred to as the cationic exchange capacity (CEC). CEC is highly dependent by the isomorphic substitutions within the interlayer and therefore varies among different clay minerals. The CEC also determines the amount of modifiers present between the silicate layers which could influence the structure of the resulting NC [35, 64]. As noted earlier, a practical problem in the synthesis of polymer NCs is to disperse the inorganic nanofiller in an organic polymer matrix. This process typically requires modification of the surface of the nanoparticle using molecules that compatibilise the particle with the polymer matrix.

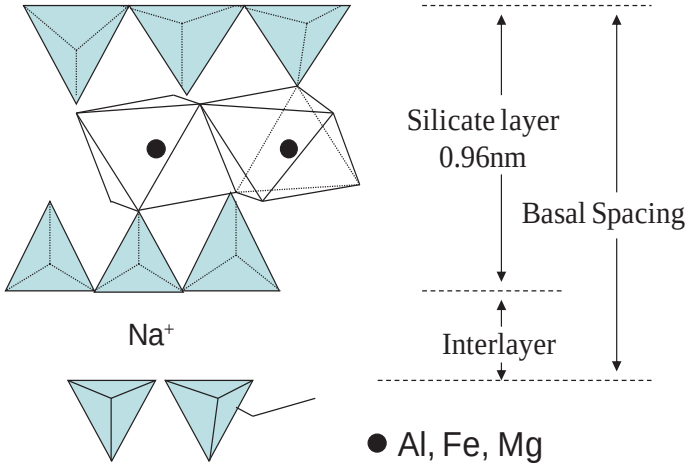

Figure 2.5 Structure of MMT (modified from Kato [89]).

2.1.3 Surfactant

The principle underlying organic modification of nanofillers is that an amphiphilic molecule can interact both with charged surfaces of the filler and with the non-polar matrix. For example, cationic-organic surfactants, such as alkylammonium cations, are commonly used in rendering clays organophilic [18, 37, 90]. They lower the surface energy by reducing the van der Waals interaction of the clay layers which allow organic species to diffuse into the layers and achieve separation of the silicate layers [17]. The degree of separation is dependent on alkyl chain length [29, 35], degree of quarterisation [91, 92] and the amount of alkylammonium ions. On the other hand, anionic surfactants such as dodecyl sulfate, dodecyl benzenesulfonate and laurate, are commonly used to modify the positively charged surfaces on LDH nanofillers [73]. Carbon nanotubes (CNT) undergo similar aggregation and can be separated with surfactants such as triton X100 and anionic sodium dodecyl chloride, with separation dependent on the nature and surface charge of the surfactant [93, 94].

Depending on the length of alkyl chain and the amount of alkylammonium ions, surfactants in clay minerals can adopt either a monolayer, bilayer, pseudotrimolecular or paraffin-like structure as shown in Figure 2.6 [92]. The monolayer type arrangement contributes to the smallest increase in clay spacing while the largest spacing is from the paraffin type, where chains radiate away from the surface and the extent of separation is largely dependent on the alkyl chain length [92].

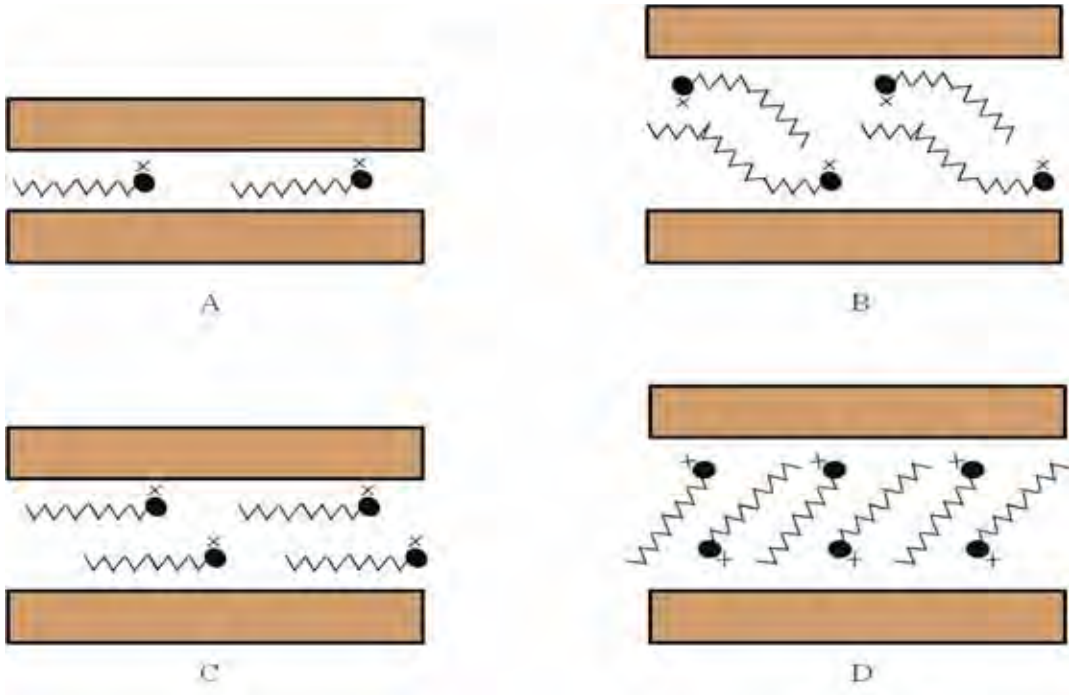

Figure 2.6 Arrangement of alkyl chains in clay minerals could be in the form of: a) monolayer, b) bilayer, c) pseudotrimolecular layer and d) paraffin structure (adapted from Lagaly [92]).

Using the same concept, surfactants with biological features could also be used to modify nanofillers. Examples of such include the use of single stranded DNA to modify CNT, where π-stacking interactions between nucleic bases and the side-wall of CNTs allow DNA to wrap around the surface [95, 96]. The use of antibacterial chlorhexidine

to modify MMT, and the antibiotic drug, chloramphenicol succinate (CFS) with LDH have also been reported [76, 97]. Thus any polymeric molecule having the ability to interact with the charged nanofiller surface and also having regions that can interact with the polymer matrix can conceivably be used to compatibilise a nanofiller with an organic polymer.

2.1.4 Polymer Nanocomposite preparation

There are three main methods used in the literature to fabricate polymer NCs: *in situ* polymerisation, melt intercalation and solution casting.

In situ polymerisation involves swelling the organically modified silicate (OMS) in a liquid monomer or monomer solution. The monomer then migrates into the galleries of silicates so that upon polymerisation, the silicate sheets will be pushed apart. The reaction can be initiated by heat, radiation or from suitable initiators [98]. This method was used by researchers from the Toyota group in their pioneering research on Nylon 6-MMT NCs [29, 30].

Polymer melt intercalation involves heating the polymer and clay above their melting temperature, and blending them through a screw head so that the two components combine and form a NC [21]. Vaia *et al*. [99] successfully used this method to produce the first polystyrene-MMT NC which greatly attracted interest from the industry. Since the process requires no solvent, it is more environmentally friendly and has less concern on the compatibility between polymer, clay and solvent [21]. In addition, NCs can be

fabricated through ordinary extruders or mixers which minimises the cost to purchase new equipment.

Solvent casting uses an organic solvent to aid the penetration of polymers between clay layers. Forces between layers of silicates can be reduced when immersed in a suitable solvent, thereby allowing polymer chains to penetrate into the galleries. Upon removal of the solvent under vacuum or precipitation, the sheets of silicates reassemble to sandwich the polymer and form an NC [98]. The process of polymer chain penetration can be assisted by vigorous mechanical mixing or sonication. This method has several advantages over the other two methods especially when NCs are aimed for medical use.

First, the low processing temperature as compared to *in situ* polymerisation or melt intercalation, where temperatures can reach ~200°C, allows biological agents to be added to NCs [30, 40, 100]. This is very important for NCs to be used in drug delivery where the biological agent needs to remain active and not degraded during the fabrication stage. Secondly, the absence of residual monomers can prevent undesirable effects within a biological environment [101, 102]. Since solvent casting has been widely used in the manufacture of PU medical devices [52] and in the studies related to PUNCs [103-105], this method was chosen as the processing method in this thesis.

2.2 Morphology of NCs

Varying degrees of nanoparticle dispersion are usually achieved in polymer NCs. In the case of clay particles in polymer NC, three broad types of morphologies can exist: 1) conventional composite, 2) intercalated NC, or 3) exfoliated NC, as illustrated in Figure

2.7. In conventional composites, clay particles existing in agglomerated stacks or tactoids are intact and there is no intercalation of polymer between clay layers [17, 20]. In intercalated NCs, polymer chains are inserted into the gallery of the clay minerals resulting in a well ordered multilayer morphology with a repeating distance of a few nanometers. Exfoliated NCs occur when the clay platelets are completely separated and dispersed in a continuous polymer matrix. The expansion of the layered silicate is so large that the interaction between the layers is not strong enough to keep the ordered morphology [106].

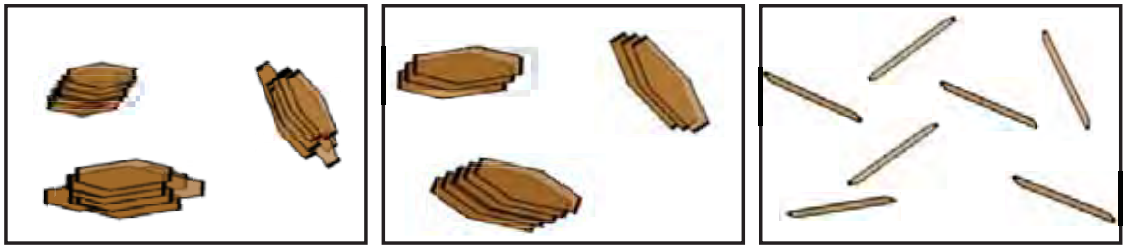

Figure 2.7 Illustration of (A) conventional; (B) intercalated; (C) exfoliated polymer clay NCs (Reproduced from Chung et al. 2011 [34]).

The ideal exfoliated morphology is where the individual silicate layers are completely separated and uniformly dispersed in the polymer matrix. Practically, morphologies of fabricated NCs usually fall between these idealised morphologies and a partially exfoliated structure is the result [107]. Figure 2.8 shows TEM (transmission electron microscopy) images of polymer NCs at various magnifications to illustrate typical morphologies observed.

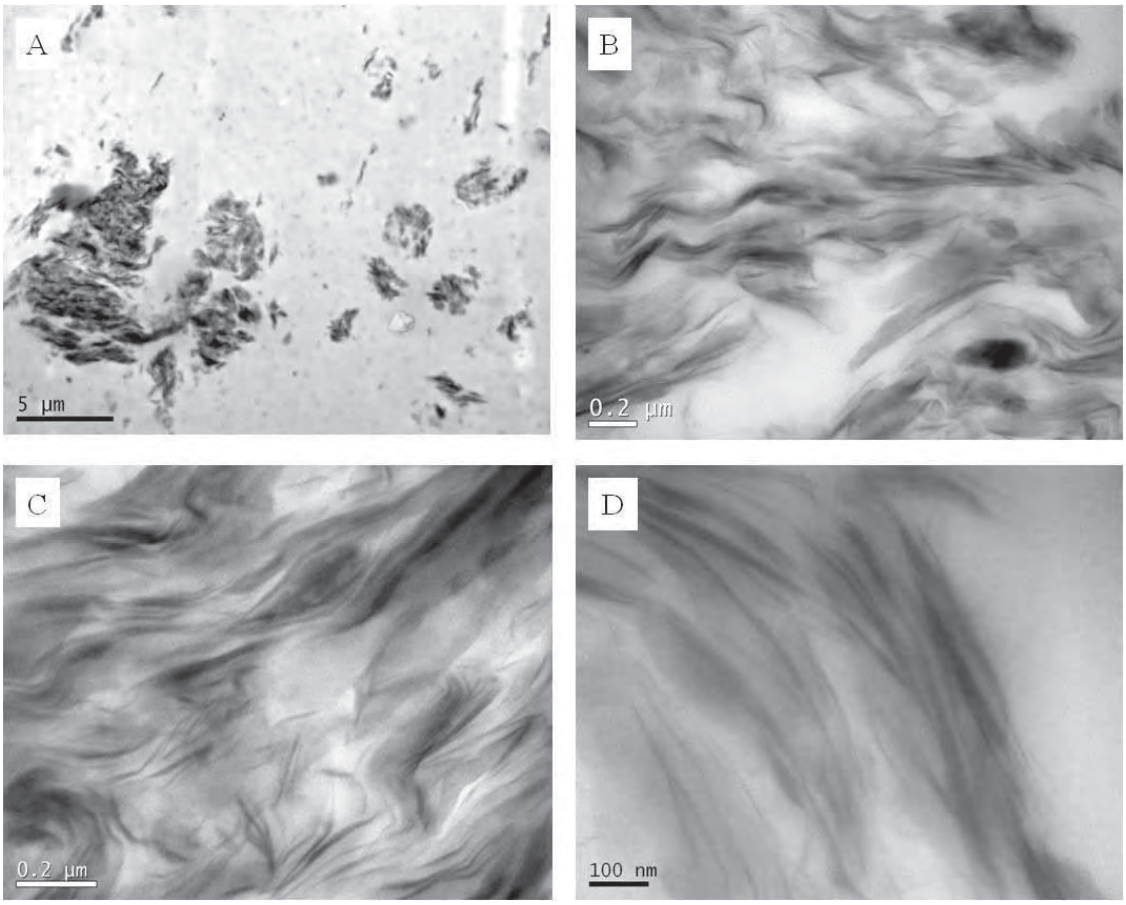

Figure 2.8 Morphology of polymer silicate NCs showing (A) tactoids and agglomerated stacks; (B,C) intercalated morphology; and (D) partially exfoliated structure showing individual silicate sheets at 5000x, 60000x, 100000x and 150000x magnification respectively (Reproduced from Chung et al. 2011 [[34]).

To optimise the benefits that NCs have to offer with regards to material properties, filler particles should be exfoliated throughout the matrix material to increase the number of available reinforcing elements that can carry applied load and deflect cracks. Complete exfoliation is difficult to achieve and most NCs have been found to contain some intercalation in their structure. Uniform separation of nanofillers is not only reflected by their enhanced mechanical performance but also by their significant decreases in gas or

water permeability. This is a useful property in terms of drug delivery applications and will be discussed in the next section.

2.3 Exploitation of barrier properties for drug delivery

Barrier properties refer to those characteristics of a material that prevent permeation of gases, water vapour or liquids. Materials with good barrier properties are resistant to or can retard diffusion of the permeating molecule. This is especially important in packaging of food and beverages where the loss of carbon dioxide in carbonated soft drinks and moisture penetration into sealed foods can lead to product spoilage. Materials with good barrier properties can be particularly useful in drug delivery systems when prolonged dosage and controlled release to prevent fluctuations in drug concentration are required. Polymers are often used as drug carriers but may not provide sustained therapeutic doses within the desired time frame and release mechanisms are mainly via diffusion. Diffusion can be perturbed by a number of approaches such as adjusting the composition of the polymer, coating with an additional layer of polymer, or covalently attaching the drug to the polymer backbone [14, 33].

Nanofillers have the capacity to alter the barrier properties of the base polymer by either acting as obstacles and retarding permeation of molecules, or by enhancing penetration by acting as carriers of penetrants. The alteration in barrier properties is potentially beneficial for drug delivery purposes as this can have a direct influence in dissolution rate, release mechanisms and drug uptake. Many polymers such as PET (polyethylene terephthalate), polyurethane, nylon, HDPE (high density polyethylene) and epoxy,

demonstrate a reduction in permeability up to an order of magnitude with a low percentage of fillers added [21, 108]. An example given by Runt and co-workers, showed that water vapour permeability of polyurethanes could undergo a 5 fold reduction at 20wt% silicate loading even under conditions where the NCs were not fully exfoliated [7, 105].

The altered barrier properties of polymer NCs, such as significantly reduced permeability of moisture and gases, has been explored for packaging materials, containers and in a variety of food and beverage products. However, these properties have not been widely exploited for medical applications [21, 22, 109]. The following section outlines the types of drug delivery approaches and applications for polymer NCs.

2.3.1 Drug delivery approaches in polymer NCs

Drug delivery approaches using polymer NCs can be broadly categorised into four types as illustrated in Figure 2.9. All delivery types described are based on non-degradable polymer NC systems where release is via diffusion or from activation through external stimulus. Depending on the various filler and surfactant combination, the drug release could either be fast, pulsatile, or sustained. The PUNC system investigated in this thesis is a Type 3 drug delivery approach where organosilicates were incorporated within a PU matrix.

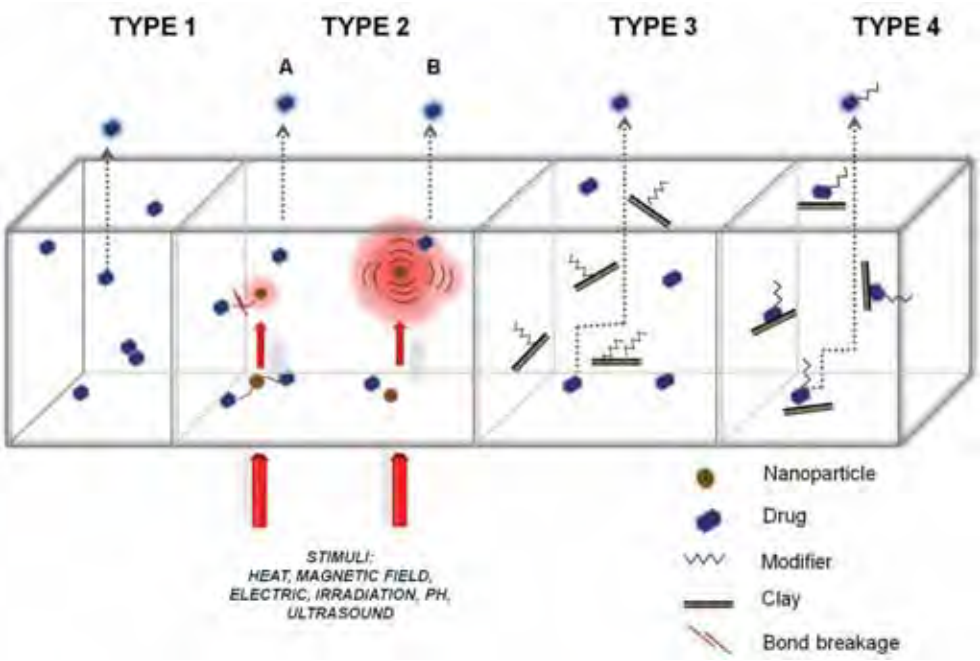

Figure 2.9 Types of approaches for drug delivery in non-degradable polymer NCs. Dotted lines represent the pathway of release. Nanoparticles activated by external stimuli are highlighted in red. Type 1 approach is when the nanoparticle is the drug. Type 2 requires an external stimulus for drug delivery. Activated nanoparticles can cleave the bonded drug (type 2A) or cause a physical change to the polymer (type 2B), thereby inducing release. Type 3 is where drugs are added as a fourth component. Finally, in the type 4 approach, the drug is used as the modifier or a component of the modifying system (Reproduced from Chung et al. 2011 [[34]).

2.3.1.1 Type 1

Type 1 approaches represent cases where the nanoparticle is the drug. Drugs are released by diffusion from the polymer matrix and release can be modulated by modifying the polymer composition or concentration of the drug. This type of drug delivery approach is prevalent in anti-bacterial applications, such as urinary catheters, joint arthroplasty, and medical packaging [110, 111]. Damm *et al.* [111] compared the antimicrobial efficiency of silver nanoparticle and silver microparticle incorporated in polyamide 6.

The NC was able to completely eliminate *E. coli* within 24 hours of release at a loading of 0.06wt % while polyamide silver microcomposites only killed 80% of bacteria in the same time with loadings much higher than NCs. The silver released from NCs was therapeutically active and released at a higher concentration than from microcomposites due to the larger surface area of nanoparticles. Hsu and co-workers [68] on the other hand incorporated either silver or gold particles in poly (ether) urethanes. These silver and gold NCs showed much lower bacterial adhesion and reduced monocyte activation compared with neat polyurethane [68]. In addition, following implantation in porcine models, these materials also demonstrated improved *in vivo* biostability compared to neat polyurethane due to their capacity for free radical scavenging [55, 69].

2.3.1.2 Type 2

Type 2 drug delivery represents polymer NCs that require an activator or external stimulus to assist release. This type can be further separated into two subtypes where the nanoparticles are bound to the drug and can be activated to release the drug (Type 2A), or stimuli-responsive nanoparticles could cause a reversible physical or chemical change to the polymer matrix, thereby enhancing release (Type 2B).

Nanoparticles that respond to external stimulation have attracted significant interest in the past few years owing to their potential applications in drug delivery [112, 113]. By responding to specific external stimuli and releasing drugs in a pulsatile manner, the release is independent of the biological environment and can provide trigger-precise drug doses [114, 115]. Drug release under non-stimulated states is dependent on diffusion as well as interactions between the drug and nanoparticle. While under

stimulation, a burst release of drug occurs. To date, systems have been developed to respond to irradiation [114-117], heat [118], magnetic fields [119-123], magnetic induced heat [124], pH [125], ultrasound [126], electrical stimuli [127] and even combinations of some of the above [128]. Although the nanoparticles in Type 2 are often used alone or incorporated within a stimuli-responsive polymer hydrogel, this approach can also be applied to non-hydrogel polymers to minimise the loss of drug after repetitive stimulation and potential leaching of cytotoxic nanoparticles.

Electromagnetic radiation in the range of 380-2500nm has been applied externally to NCs to switch drug release on and off [114]. Wavelengths in the visible light range typically cannot penetrate more than 1 cm in the body due to scattering. Therefore near infrared (NIR) light (650-900nm) is often used to allow deeper penetration into the tissue [129]. Tanaka *et al.* [117] reported coumarin-modified mesoporous silica nanoparticles loaded with the steroid cholestane which respond to UV light. Mesoporous silica nanoparticles are cylindrical structured materials containing a hexagonal array of pores (0.5-1.5 cm^3g^{-1}) that allow easy loading of drugs. The release of cholestane was achieved through the cleavage of the cyclobutane ring of the coumarin dimer [117] by applying UV light at a wavelength of 250nm. Similarly Wu *et al.* [115] reported a light responsive silica nanoparticle prepared by covalent conjugation of photoactive *o*-nitrobenzyl bromide molecules with amino groups on the particle surface. Drugs with either carboxylic, phosphate, or hydroxyl groups were covalently attached and irradiated at 310nm. Upon irradiation, the photoactive groups transformed to cause an irreversible cleavage of drug-particle bond, inducing drug release [115].

Gold filled NCs are also materials that display remarkable potential in activated drug delivery systems [112]. The incorporation of NIR-sensitive gold nanorods into a temperature sensitive hydrogel was reported by Wei *et al.* [118]. NIR radiated gold nanorods delivered localised heat to the polymer matrix and induced a phase transition of the polymeric chains from coiled to globular. The drug release was observed to be faster in periods of NIR exposure due to the breakage of hydrogen bonds between drug and polymer from heat induced conformational change [118].

The concept of using external magnetic fields to achieve pulsatile release from polymer composites was first investigated by Kost *et al.* [119]. Insulin release was demonstrated from a magnetic bovine zinc insulin ethylene-vinyl acetate copolymer (EVA) composite using a low frequency oscillating magnetic field [119]. This is a very attractive technique since the use of magnetic nanoparticles linked to insulin can provide a sudden influx to the patient when required, such as after a meal. The remaining insulin can then be released more slowly at other times [119].

Alternatively, heat responsive magnetic nanoparticles are also gaining interest in hyperthermia cancer treatment and areas of chemotherapy where imprecise targeting can be overcome and drugs can be localised and triggered precisely [130]. Magnetically modulated release can be accomplished by either: (1) the aggregation of magnetic particles embedded in a polymer matrix, leading to shape deformation to promote release [120, 121]; or (2) magnetic heating of nanoparticles embedded in a thermally responsive polymer [124]. In (1), problems can arise from insufficient force to create an opening in polymer matrix, and chain loosening from repeated friction between the

nanoparticles and matrix [121]. Problems related to case (2) would be the loss of drug after each burst and the mesh size eventually becoming comparable or less than the drug so no release of drug will happen. Therefore for implantable drug delivery which requires drug delivery from weeks to months, further improvement of this type of approach is required [124].

2.3.1.3 Type 3

Type 3 represents cases where the drug is added in polymer NCs that contain inorganic nanofillers, most commonly silicates. Drugs are released through diffusion but are forced to follow a longer path due to the presence of impermeable nanoparticles. Mathematical models developed to predict barrier properties of this type are the most common in literature and will be discussed in later sections. Drugs in this type of NC delivery system are added as a fourth component in the system [131]. Specific examples of application of this type of drug delivery system can be found in anti-inflammatory agent delivery systems [43, 132]. Studies on the incorporation of dexamethasone into PUNCs showed that the drug did not lead to a disturbance in morphology and demonstrated an adequate reduction in inflammatory response over 14 days [132]. Similarly, a study by Cypes *et al.* [43] also showed that the controlled release of dexamethasone in this system was achieved by addition of silicate and there was a dependence on silicate loading [43].

Oral chemotherapy is another area of drug delivery that may benefit from NC delivery approaches. Methylmethacrylate chloromethylstyrene copolymer NC (PMMA-MMT) incorporated with active 1,2,4-triazine derivatives were investigated by Salahuddin *et al.*

for this purpose [133]. The incorporation of cationic 1,2,4-triazine and their derivatives, resulted in a range of release profiles that varied according to pH and the condition of the buffer (acidic or neutral) [133]. Another interesting area using NC as drug delivery systems is in transdermal pressure sensitive adhesives. This is to obtain better control over the drug release kinetics and to improve adhesive properties in pressure sensitive patches [134]. A model dye, solvent blue 35, with physiochemical characteristics similar to commercial drugs in transdermal systems was used to study the release kinetics. Up to 75% reduction in dye released was observed with 10wt% clay over a 10 day period with little burst effect. Shear strength also showed a 2.5 fold increase due to the reinforcement of polydimethylsiloxane (PDMS) matrix [134].

2.3.1.4 Type 4

Finally, in Type 4 approaches, the drug is used as the modifier or a component of the modifying system. Polymer molecules which have the ability to interact with the charged nanofiller surface and also regions that can interact with the polymer matrix can conceivably be used to compatibilise a nanofiller with an organic polymer. A novel approach different to other types is where the therapeutic activity was achieved through the selection of organic molecules that have dual function, being a modifier and drug at the same time [97, 135].

The use of chlorhexidine (CHX) as both a drug and modifier in PDMS and PUNCs have been reported [97, 136]. PUNCs modified with CHX resulted in a range of morphologies that depended on the amount of clay and saturation level of CHX. In both cases where MMT was 100% ion-exchanged with CHX and where free CHX was added, the

bacterial number of *S. epidermidis* dropped almost 2 orders of magnitude [97]. Styan *et al*. [135] previously reported that modifiers, such as Ethoquad ® O/12PG (EQ) and 1-aminoundecanoic acid (AUA), possess biological activity either used alone or co-modified. While AUA alone showed no inhibition of bacterial growth but maintained cell viability, an increase in EQ resulted in an increase in activity against *S. epidermidis* but decreased cell growth. These studies suggested the possibility of controlling antibacterial activity by adjusting levels of EQ [135].

2.3.1.5 Mathematical models

Mathematical models predicting the permeability of polymer NCs are often applied to assess diffusion through polymer matrices with added fillers (Type 3). Theoretical models developed for this type of system will be the focus of this section and are more complicated than Types 1 and 2, where diffusion is through a non-degradable, non-swelling or swelling type polymer membrane [21, 137]. Enhanced barrier properties can be explained by the concept of tortuous paths as shown in Figure 2.10, where nanoparticles act as impermeable barriers forcing the permeating molecules to travel around and follow the longer and more tortuous pathway in order to diffuse through the NC. The tortuosity factor is defined as the ratio of the actual distance the penetrant has to travel to the shortest distance it would travel in the absence of obstacles and is expressed as:

$$\tau = \frac{\text{Actual distance}}{\text{Shortest distance}} = 1 + \frac{\text{L}}{2\text{W}}$$

From this expression, it can be seen that the sheet-like morphology of silicates is likely to be more efficient than spherical particles in maximizing the path length due to their large length-to-width ratio [21, 31].

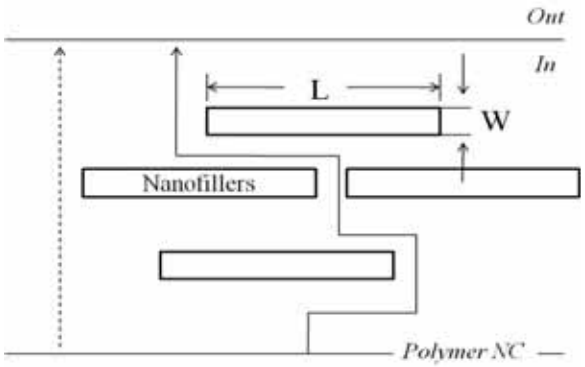

Figure 2.10 The concept of the tortuous pathway showing the actual distance (filled line) a molecule has to travel in the presence of nanofillers as compared to the shortest distance (dotted line) (Reproduced from Chung et al. 2011 [34]).

Accurate predictions from various mathematical and computer simulations of barrier properties and drug release behaviour are difficult due to the complexity of polymer NC systems. A model commonly referred to in the literature is the tortuous path theory developed by Nielsen [138]. Although highly simplified, it is often used as a preliminary estimation of the permeability behaviour in NCs as well as the starting point for development of further mathematical or computer based permeability models. It assumes that nanoparticles in the form of platelets with length L and thickness W are distributed evenly and aligned perpendicular to the diffusion direction as shown in Figure 2.10. The equation is as follows:

$$\frac{P_c}{P_p} = \frac{V_p}{1 + \frac{L}{2W} V_f}$$

where P_c is the permeability of the composite, P_p is the permeability of the polymer, V_p is the volume fraction of the polymer, and V_f is the volume fraction of the filler.

This relationship shows that the relative permeability of NCs decreases with increasing amount of filler and increasing aspect ratio. Limitations of Nielson's model are that it is only valid if the clay loading is less than 1wt% and the assumption of uniform dispersion, size and orientation is often not the case in reality. Several other models that have been proposed to predict the barrier properties of NCs are shown in Table 2.2. Many of these are similar to Nielson's model but have also considered factors such as particle orientation [139], particle shape [140-142], state of aggregation, resistance [143], and polymer clay interactions within the NC system [144].

The experimental deviation in Neilson's model was observed by Yano *et al*. [145] when the permeability of polyimide-clay hybrid incorporated with four different types of clay minerals was examined. Hectorite and saponite were shown to contain aggregates and were not fully exfoliated, therefore calculated values overestimated the permeability of these respective NCs [145]. Several studies have noted that although the predicted curve based on Nielson's model did not completely match the experimental result as it did not take into account the degree of dispersion, the agreement is satisfactory and can provide a general trend in the permeability behaviour in polymer NCs [146, 147]. In particular, a study conducted by Choudalakis *et al*. [137] compared several mathematical models as a function of platelet volume fraction and aspect ratio. It was concluded that Nielson's simple model is adequate in describing the reduction in the relative permeability in polymer NCs.

Table 2.2 Theoretical models in predicting barrier properties of polymer NCs (Reproduced from Chung et al. 2011 [34])

Model	Filler type	Formula
Nielson	Ribbon	$\frac{P_c}{P_p} = \frac{1-\Phi}{1+\frac{\alpha}{2}\Phi}$
Cussler (regular array)	Ribbon	$\frac{P_c}{P_p} = (1+\frac{\alpha^2\Phi^2}{1-\Phi})^{-1}$
Cussler (random array)	Ribbon	$\frac{P_c}{P_p} = (1+\frac{\mu'\alpha^2\Phi^2}{1-\Phi})^{-1}$
Fredrickson-Bicerano	Disk	$\frac{P_c}{P_p} = \frac{1}{1+\mu\alpha^2\phi^2}$ where $\mu = \frac{\pi^2}{16\ln^2\alpha}$
Gusev and Lusti	Disk	$\frac{P_c}{P_p} = \exp\left[-\left(\frac{\alpha\phi}{3.47}\right)^{0.71}\right]$
Bharadwaj	Ribbon	$\frac{P_c}{P_p} = \frac{1-\Phi}{1+\frac{\alpha}{2}\Phi\left(\frac{2}{3}\right)\left(S+\frac{1}{2}\right)}$

For ribbon α=length/thickness

For disk α= radius/thickness

Φ= volume fraction of the filler

P_c= permeability of composite

P_p=permeability of polymer

α= aspect ratio (width to thickness)

μ´=geometric factor

S= orientation factor (from -1/2 to 1)

In summary, most of the models assume that the fillers are a regular and uniform shape in a regular array in space. The assumption is also that fillers are in complete exfoliation and that the physical characteristics of the polymer remain unchanged with the addition of the inorganic particles. The arrangements are usually perpendicular or have an average orientation at an angle to the main direction of diffusing gas molecule. Despite these shortcomings, these models can provide a preliminary guide to the relative permeability of polymer NCs and be used to design systems with desired outcome.

2.4 Properties of polyurethane clay nanocomposites

2.4.1 Mechanical properties

Wang and Pinnavaia [148] were the first to demonstrate the improvement of PU properties by addition of clay nanofillers. They found that MMT exchanged with long chain onium ions were easily solvated with several polyols and by adding 10wt% organoclay, the modulus, strain at break, tensile strength all increased by 100%. Since then, much research in PUNCs have focused on enhancing the barrier properties [7, 105], improving the thermal properties [149, 150] and to a lesser extent, improving viscoelastic properties [151-153]. The bulk of the research focuses on improving the dispersion or mechanical performance based on modifications in the constituents in PUNCs. This is achieved by varying hard/soft ratio of PU [83, 103, 154], varying clay [103, 155, 156], modifiers [40, 150] and using different types of polyols [40, 152]. The possibility of co-modifying the clay [104] and investigations of polymer blends-clay NCs [157] have also been investigated.

A simple explanation proposed to account for improvements in polymer mechanical properties was described by Pavlidou *et al*. [21], where the higher modulus of rigid fillers can bear significant portions of the applied load from the softer polymer matrix. The magnitude of load transfer is dependent on the area of contact between the filler and polymer. Therefore high surface area nanofillers such as layered silicates (~750 m^2/g) provide drastic improvements in modulus at much lower concentration compared to conventional composites. In general, if a force is applied to a specific volume of a conventional composite reinforced by 1000 micro-sized particles, the force applied in the same volume of material can be distributed over 1 million nano-sized particles in the case of NCs [158].

The addition of clay particles act as indestructible centres for the concentration of stress inside the composite and allow external forces acting on the material to be redistributed. However, if the dispersion and compatibility between particles and matrix is poor, these nanoparticles will act as lubricants instead of stress concentrators. Therefore the mechanical properties of NCs provide an indirect indication of both silicate dispersion and the affinity between the polymer and filler [21, 159]. The general trend observed in literature, as shown in Table 2.3 is that by inclusion of silicate particles, particularly at low loadings in polymer matrices, ultimate tensile strength is increased or at least maintained. The ultimate strain and Young's modulus are also increased with low clay loadings. However, as clay content increases, strain and ultimate tensile strength decreases. Furthermore, the rate of modulus increase levels off at higher clay contents. These results demonstrated that improvement in mechanical properties is highly dependent on the degree of dispersion [84, 160-162].

2.4.2 Barrier properties

A summary of the key findings in barrier properties of PUNCs published from literature is presented in Table 2.4. As mentioned in the previous section, the permeability of oxygen and water vapour decreases with increased filler content. Although NCs that are not fully exfoliated can still result in a significant reduction [7, 105], the largest reduction in permeability can often be correlated with samples showing the best dispersion[163, 164].

A case where the addition of silicates in PU does not result in a decrease in permeability is when there is filler aggregation or poor compatibility between the components of the system [165]. Osman *et al*. [166] observed that the addition of organoclay could result in a phase separation between the clay and PU matrix which leads to an increase in free volume at the interface, thereby allowing oxygen to pass through [166]. On the other hand, some studies have shown that phase separation was not disrupted by the addition of silicate particles in the PU system [103, 156]. Molecular dynamics simulation by Zeng *et al*. [159] showed that there was no obvious phase separation in the NC due to competitive interactions between the soft segment with alkyl chain and hard segment with clay [159]. The silicate layers can create large interfacial areas where the -OH groups can form hydrogen bonds with the hard or soft segment of PU [165]. These studies demonstrated that the enhancement in permeability from polymer NCs is dependent on dispersion, filler content, and more importantly the compatibility and interactions between each of the components in the system.

Table 2.3 Mechanical properties of PUNCs

Ref	PU constituents [a]	Modifiers [b]	Dispersion [c]	Loading [d]	UTS [e]	ε [e]	E [e]
[155]	MDI, PTMO, BDO	Cloisite 15A	I	3	1.18	1.17	1.24
				7	0.76	1.14	1.24
[103]	MDI, PTMO, BDO	Closite 30B	PE	3	0.69	0.98	1.84
				7	0.47	0.91	3.2
[167]	MDI,PTMEG,BDO	12COOH	PE	1	1.14	1.05	
			PE	3	1.14	1.64	
			PE	5	0.8	0.82	
		Benzidine	E	1	2.16	3.09	
			PE	3	1.95	2.68	
			I	5	1.93	2.73	
[154]	MDI,PTMEG,BDO	Benzidine	I	1	1.29	1.27	1.22
				3	1.16	1.25	1.01
				5	1.05	1.24	1.0
[7]	MDI, PTMO, EDA	Closite 15A	I	1	1.15	1.11	0.55
				3	1.15	1.19	1.28
				7	1.17	1.3	1.47
				13	1.27	1.44	2.61
				20	1.36	1.54	3.41
[90]	PU	Closite 25A	I	1	1.67	1.04	1.85
				4	1.69	1.11	1.87

Table 2.3 Mechanical properties of PUNCs (cont)

Ref	PU constituents [a]	Modifiers [b]	Dispersion [c]	Loading [d]	UTS [e]	ε [e]	E [e]
[168]	PU	Synthetic	I	2.5	1.63	2.31	0.81
		fluoromica	I	5	2.13	3.23	0.75
			I	7.5	2.75	5.08	0.42
			I	20	3.38	3.08	0.78
[169]	PPG,MDI,BDO	12COOH	I	1	1.92	1.30	1.47
			I	3	2.5	1.61	1.55
			I	5	3.02	1.94	1.55
			I	7	3.48	2.22	1.56
[104]	PPG,MDI,BDO	AUA	I	5	1.31	1.5	1.37
		CTAB	I	5	1.38	1.39	1.39
[40]	MDI,PTMEG,BDO	Closite 30B	PE	1	1.02		1.37
			PE	3	1.07		1.44
			PE	5	1.11		1.58
		Closite 25A	I	1	0.88		1.13
			I	3	0.94		1.13
			I	5	0.9		1.16
		Closite 15A	I	1	0.87		1.03
			I	3	0.88		1.08
			I	5	0.82		1.18
[44]	PPG, MDI,BDO	CTAB	I	2	1.31	1.06	
			I	5	1.39	1.14	

Table 2.3 Mechanical properties of PUNCs (cont)

Ref	PU constituents [a]	Modifiers [b]	Dispersion [c]	Loading [d]	UTS [e]	ε [e]	E [e]
			I	8	1.43	1.18	
			I	10	1.33	1.1	
[170]	MDI,PTMEG,BDO	Closite 30B	PE	1	0.7	0.42	1.09
			PE	3	0.46	0.41	1.92
			PE	5	0.4	0.45	2.21

[a] PU Constituents: MDI = 4, 4 diphenylmethane diisocyanate; PTMEG = polytetramethylene glycol; PPG= polypropylene glycol; PTMO = poly (tetramethylene oxide); BDO = 1, 4-Butanediol; EDA=ethylene diamine

[b] Modifiers: 12COOH= aminododecanoic acid; AUA=aminoundecanoic acid; CTAB=cetyltrimethyl ammonium bromide
Commercially available OMS: Closite 15A =dimethyl deydronated tallow, quaternary ammonium; Closite 25A = dimethyl, dehydrogenated tallow, 2-ethylhexyl; Closite 30B= methyl, tallow, bis-2-hydroxylehtyl, quaternary ammonium

[c] I: intercalated, PE: partially exfoliated, E: exfoliated

[d] Loadings are represented as wt% (g organically modified silicate/ 100g PU)

[e] Values are presented as ratio to the neat PU

Table 2.4 Barrier properties of PUNCs

Ref	PU constituents [a]	Modifiers [b]	Dispersion [c]	Loading [d]	Permeability [e]	
					O_2	H_2O
[7]	MDI, PTMO, EDA	Closite 15A	I	1		0.85
				3		0.73
				7		0.48
				13		0.32
				20		0.22
[171]	MDI,PEAD,BDO	Organosilicate	PE	1	0.76	
				3	0.64	
				5	0.59	
[167]	MDI,PTMEG,BDO	12COOH	PE	1	0.76	
			PE	3	0.88	
			PE	5	0.94	
		Benzidine	E	1	0.82	
			PE	3	0.94	
			I	5	1.00	
[166]	PU	Nanofil 804	PE	4	0.79	
			PE	6	0.76	0.63
			PE	8	0.73	
			PE	10	0.73	

Table 2.4 Barrier properties of PUNCs (cont)

Ref	PU constituents [a]	Modifiers [b]	Dispersion [c]	Loading [d]	Permeability [e]	
					O_2	H_2O
[90]	PU	Closite 25A	I	2	0.81	
			I	3	0.78	
			I	4	0.65	

[a] PU Constituents: MDI = 4, 4 diphenylmethane diisocyanate; PTMEG = polytetramethylene glycol; PTMO = poly (tetramethylene oxide); BDO = 1, 4-Butanediol; EDA=ethylene diamine; PEAD= poly (ethylene adipate) diol

[b] Modifiers: 12COOH= aminododecanoic acid

Commercially available OMS: Closite 15A =dimethyl deydronated tallow, quaternary ammonium; Closite 25A = dimethyl, dehydrogenated tallow, 2-ethylhexyl; Nanofil 804= bis(2-hydroxylethyl) hydrogenated tallow ammonium

[c] I: intercalated, PE: partially exfoliated, E: exfoliated

[d] Loadings are represented as wt% (g organically modified silicate/ 100g PU)

[e] Values are presented as ratio to the neat PU

2.4.3 Polyurethane nanocomposites in drug delivery applications

Information on PUNCs used in drug delivery applications is scant in literature. Studies conducted by Runt *et al*. [7] proposed using PUNCs based on a biomedical PU, Biospan, and Cloisite 15A as the clay [7, 105]. Their objective was to develop a novel NC for reducing gas permeability for biomedical PU membranes. However, compatibility of these materials in a biological environment was not reported. Using Type 1 delivery approach, Hsu and co-workers incorporated silver or gold nanoparticles into PU and showed superior antimicrobial properties with good dispersion and mechanical properties [68, 69]. The release of Ag or Au ions showed much lower bacteria adhesion and reduced monocyte activation compared to neat PU [68].

Silva *et al*. [132] examined the potential of PUNCs for anti-inflammatory purposes and found that the incorporation of dexamethasone into PUNCs did not lead to a disturbance in morphology. *In vivo* biocompatibility studies demonstrated an adequate reduction in inflammatory response over 14 days [132]. A novel approach mentioned in earlier sections, where the biological property of PUNCs was achieved through modifiers that possess dual functionality was reported by Fong [97] and Styan [135]. PUNCs, modified with chlorhexidine (CHX) decreased the number of *S.epidermidis* by almost 2 orders of magnitude [97]. Of the same principle, Ethoquad ® O/12PG (EQ) and 1-aminoundecanoic acid (AUA), either used alone or co-modified were also found to inhibit bacterial growth but maintain good cell viability [135].

2.4.4 Considerations in drug delivery

The reduction in permeability for sustained or controlled drug delivery in Type 3 NC systems depends largely on the amount of silicates and quality of exfoliation [43, 172, 173]. In other words, the amount of drug released can be modulated simply by silicate loadings if the system has an exfoliated structure and when there are no mutual interactions between the drug and components of an NC system. However, fillers are typically not "perfectly" exfoliated and the components within an NC system can interact with each other, thus affecting structure and permeability [159, 174]. With the drug being considered as a fourth component, interactions in Type 3 delivery system should be more complicated than the original three component NC system. The addition of clay can now actively promote or retard release due to drug-clay or drug-polymer interactions.

Interestingly, there is an absence from published literature investigating the effect of drug additives on the structure of NCs. Since drug release is dependent on the dispersion of silicates, the effect of drug additives on the overall NC formation is very important. It has also not been shown how the competitive charges and molecular interactions between drug additives and the NC system could affect drug release. The often adapted tortuous pathway model and most other mathematical models that describe the barrier properties of polymer NCs do not consider the interactions between the diffusing molecule and the polymer, filler, or modifier. With the addition of an extra component, drug permeability in polymer NCs can be significantly perturbed by the varied properties of the components that impact on drug diffusion and partitioning. Interactions

could be become dominant, causing the release profile to deviate from the commonly accepted tortuous pathway model. These processes are not currently well understood and are questions that this research aims to investigate.

2.5 Summary and thesis structure

Over the last 20 years, polymer NCs have been widely investigated due to dramatic increases that can be achieved in the mechanical and thermal properties of the base polymer. Furthermore, these improvements can be achieved at filler concentrations much lower than conventional composites, greatly reducing the mass of the material. The marked improvement observed in mechanical properties of NCs initially sparked interest in the automotive and aerospace industry. However the subsequent discovery of altered barrier properties has resulted in the study of NCs as alternatives to existing medical device materials.

This thesis explores the feasibility of polyurethane nanocomposites as drug delivery coatings on existing medical devices. The subsequent chapters aim to provide a better understanding of structure-property relationships through the variation in modifier chain length and clay loading. In particular, a variety of model and active drugs were selected to examine the impact of an additional 4^{th} component on the structure of NCs, drug release behaviour and drug interactions that could occur within the system. Finally, an assessment of drug activity and biological interactions was investigated. Outlines of each of the chapters to achieve these objectives are described below:

Chapter 3 details the methods used in PUNC preparation. The effect of modifier chain length and clay loading on the structure, dispersion and mechanical properties is explored.

Chapter 4 investigates the feasibility of coating PUNCs onto metallic substrates. The compatibility of PUNCs with blood is examined through the incorporation of an anti-thrombotic drug.

Chapter 5 assesses the impact of a fourth component on the structure and drug release behaviour of NCs through model dyes with different size, surface charge and polarity.

Chapter 6 further investigates the effect of component interactions by using active drugs with similar size and chemistry, but of different charge and solubility. That is, one being hydrophobic (neutral) and the other being hydrophilic (negative). The release mechanisms and interactions are studied through both physical experimentation and computer simulation.

Chapter 7 investigates the impact of fabrication method on the cellular response of PUNCs and most importantly, to assess the activity of the released drug. In addition, the effect of drug size and hydrophobicity on the drug release behaviour of PUNCs is further investigated.

Chapter 8 provides the overall conclusion arising from the current research, along with the recommendations for future work.

Chapter 3: Impact of alkyl chain length on dispersion of nanoparticles within polyurethane nanocomposites

3.1 Introduction

Modification of the inorganic clay by surfactants or organic modifiers is a crucial step in the successful fabrication of polymer NCs. One of the main roles played by organic surfactants is to reduce the van der Waals interaction between clay layers and assist the diffusion of organic species into the gallery. The resulting 'organoclays' are able to swell in an organic liquid but not water [25, 175]. The swelling behaviour of these layered silicates has been investigated extensively to further understand the mechanisms of exchange and the criteria for optimum swelling [176, 177].

3.1.1 Silicate modification and arrangements

Alkylammonium cations (or protonated alkylamines) are commonly used agents to modify clay minerals [18]. The packing density and conformation of alkylamines within the interlayer are found to be dependent on several factors including the length of the alkyl chain [29, 35], the degree of quaternisation [91, 92], amount of alkylammonium ions [84], size [178] and layer charge of the clay[179, 180]. As proposed by Lagely *et al*. [92], alkylammonium cations in the interlayer can adopt either a monolayer, bilayer, pseudotrimolecular or paraffin-like structure (see Figure 2.6). In the case of mono- and bilayer type conformations, the chains lie flat and parallel to the silicate surface. For pseudotrimolecular conformations, the chains "kink" and shift on top of each other. The

paraffin type arrangement consists of chains radiating away from the surface that can gradually move to a perpendicular position (all-trans conformation) depending on the length of modifier [92].

The effect of alkyl chain length on the expansion of clay layers was studied by Le Pluart and co-workers [181], who found that the increase in spacing of MMT was proportional to the increase of the carbon chains of alkylamines from 8 to 18 units. A paraffin structure was observed only at chain lengths greater than 12 [181]. Similarly, Usuki *et al.* [29] also showed that the swelling of MMT modified with amino acids was limited when carbon numbers were 8 or less, but increased when the carbon number was greater than 11. It was hypothesised that, as the chain length increased, the tilting angle (α) between the modifier and surface of the clay increased, moving the chains from a titled orientation to a perpendicular position [92]. The behaviour of NCs following incorporation of modified clays in an organic polymer matrix is likely to be further perturbed in a manner that depends on the properties of the modifier, polymer and the interactions between the components.

3.1.2 Modification and resulting morphology of NCs

The impact of alkyl chain length has been investigated in a variety of polymer NC systems including rubber [182], polypropylene [183], epoxy [20, 184] , polyethylene [185] and polyvinyl chloride [84]. It was generally found that NCs with better properties often had larger silicate spacings and that this is closely related to the length of the modifier. A study looking at the use of alkylamines with chain lengths of 8, 12 or 18 in

polyvinyl chloride (PVC) was conducted by Kalendova *et al*. [84]. It was found that the use of 18 carbon chain modifiers (octadecylamine) resulted in the best dispersion and resulted in a bilayer arrangement. The use of 8 carbon chain modifiers on the other hand, showed an inhomogeneous morphology, while 12 carbon chains demonstrated a mixed arrangement (monolayer and bilayer) [84].

A similar observation was found in polypropylene (PP) matrices where 12 carbon chain modifiers improved the modulus and yield strength of pristine PP by 55% and 24% respectively, whereas 8 carbon chain modifiers only improved the properties by 40% and 10% respectively [183]. The property enhancements were related to better dispersion and increased silicate spacing [183]. The use of longer modifiers not only promotes mechanical performance but may also improve processing conditions as suggested by reduced scorch time and improved curing time of nitrile rubber NCs via use of longer alkyl ammonium salts during the vulcanisation process [182].

Studies related to the impact of alkyl chain length on dispersion and properties of PUNCs are largely absent from the literature. Most of the studies related to PUNCs use only a primary alkylamine [90, 186-188], with $18CH_3$ being the most common length utilised [7, 189-191]. The reason for using primary amines appears to relate to improved dispersion and bonding strength compared with other classes of amines [17, 179, 180].

Ammonium ions can be classified in terms of the nitrogen head group into primary, tertiary and quaternary amines. A comparison between silicate spacings produced by different classes of amines of the same carbon chain length was conducted by Lan *et al*.

[180]. The resulting NC modified with primary amine showed no diffraction peaks whereas tertiary and quaternary amine modified NCs displayed strong peaks indicative of a intercalated morphology [180]. As a result of improved dispersion, mechanical properties were enhanced as demonstrated by Zilg *et al*. [17], where the incorporation of MMT with protonated primary amines in epoxy resin resulted in an improved toughness and stiffness balance. Consistent with these findings, Xu *et al*. [189] also demonstrated improved compressive and tensile strength of PUNCs when MMT was modified with primary octadecylamine rather than the tertiary form [189].

It is hypothesised that the choice of modifier chain length will impact on the structure of PUNCs and the use of longer chain length modifiers can provide better dispersion and mechanical properties. Specific aims were: 1) to assess the dispersion of silicates by varying OM chain length and clay loading , and 2) to identify the most suitable modifier for further study.

3.2 Materials and methods

3.2.1 Polymer nanocomposite components:

3.2.1.1 Polyurethane

Poly (ether) urethane, shown in Figure 3.1, was synthesised by Urethane compounds (Melbourne, Australia) and consisted of polytetramethylene oxide (PTMO) (1000g/mol), 4,4'-methylene diphenyl diisocynate (MDI) and 1,4 butanediol (BDO) as the chain extender. The poly (ether) urethane used in this thesis, herein referred to as PU, was

combined in the ratio of 100:7.5:46.3 respectively, with 0.003 dibutyltin dilaurate (DBTDL) added as catalyst. It has chemical components equivalent to the commercially used Pellethane 2363® series[2] without the processing wax, bisethylene stearamide.

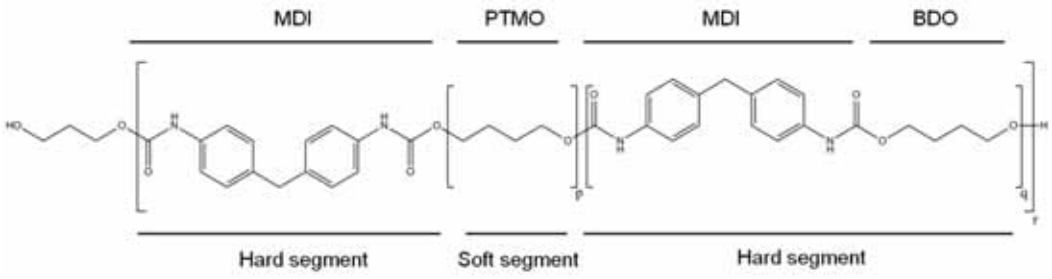

Figure 3.1 Molecular structure of Poly (ether) urethane.

3.2.1.2 Layered silicates

Unmodified clay natural montmorillonite (MMT) (Cloisite Na^+) with chemical formula $Na_{0.33}$ $[(Al_{1.67}Mg_{0.33})Si_4O_{10}(OH)_2]$ H_2O and CEC of 92.6meq/100g clay from Southern Clay Products (Texas, USA) was used. A schematic of the proposed structure is shown in Figure 2.5.

3.2.1.3 Organic modifiers

Organic modifiers (OM), dodecylamine ($12CH_3$, ≥ 98%) and hexadecylamine ($16CH_3$, ≥99%) were obtained from Sigma-Aldrich Pty Ltd. These are primary alkylamines and are shown in Figure 3.2.

[2] Pellethane 2363®-80A are a series of polyurethane produced by the Dow Chemical Company for biomedical applications including blood bags, catheters and pacemaker leads

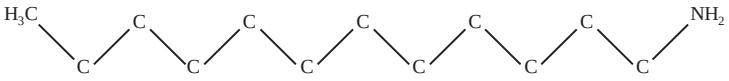

(A) Dodecylamine

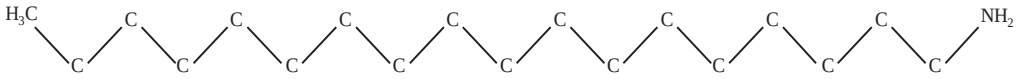

(B) Hexadecylamine

Figure 3.2 Atomic structures of organic modifiers. Both with methyl terminal groups but differ by carbon chain length: (A) 12 carbon and (B) 16 carbon.

3.2.2 Polyurethane Nanocomposite fabrication:

3.2.2.1 Polyurethane suspension

PU was washed in Milli-Q water and dried at 60ºC overnight. The required amounts of PU and dimethylacetamide (DMAc, Sigma-Aldrich) were weighed to achieve 5wt% PU in DMAc suspension. This was to increase the chain mobility of PU and to facilitate intercalation between PU and layered silicates. PU was added to DMAc and allowed to stir at a temperature of 50^{o}C for a period of 7 days to ensure complete dissolution. Nitrogen was then applied to the head of the container which was then sealed with parafilm. The container was stored away from light for a maximum of 1 month until the polymer suspension was required.

3.2.2.2 Modification of Silicates

Organically modified silicates (OMS) were produced by cationically exchanging MMT with organic modifiers. A 5wt% solution of NaMMT was prepared in Milli-Q water and

left stirring at 50°C for a period of 24 hours. Prior to modification, this solution was diluted to 1wt% MMT in Milli-Q water and appropriate amounts of OM were added.

Compounds for organic modification were added in excess at 110% of the theoretical CEC of MMT calculated using equation 3.1.The suspension was stirred and HCl was added drop wise to bring the solution below the isoelectric point of the compound to allow cationic exchange between the silicate layers and modifying compound. The pH of the solution was checked by pH indicator strips and solutions were then stirred vigorously for 24 hrs at a temperature of 50°C. To isolate the OMS, the suspension was centrifuged at 30100g for 12mins at 18°C (Beckman J-14 Centrifuge). After centrifuging, the supernatant was discarded and the clay was placed in a Petri-dish and dried in an oven at 60°C for 24 hrs. The clay was then crushed using a mortar and pestle and passed through a 325 mesh (45µm sieve) and labelled either $12CH_3$MMT (dodecylamine modified) or $16CH_3$MMT (hexadecylamine modified).

$$\frac{x\%CEC}{100} \times MW_{OM}\frac{g}{mol} \times valence_{OM} \times \frac{1Eq}{1000mEq} \times \frac{92.6mEq}{100g\ silicate} = \frac{g}{100g\ silicate} OM \qquad (3.1)$$

3.2.2.3 Nanocomposite preparation

PUNCs were prepared by solvent casting. Required amounts of OMS were mixed with the 5wt% PU in DMAc suspension. The amount of OMS added was based on the % loading, i.e. 1wt% loading represents 1g OMS/100g PU. The mixture was then left to stir at 60ºC for 17 hrs to allow polymers to penetrate the clay interlayer. The mixture was then poured into a glass mould (220mm × 70mm) and the solvent was removed at

60ºC and 400mbar in a vacuum oven (Binder V23) for 48 hrs. Cast films were stored away from light for 7 days prior to characterisation to allow residual DMAc to evaporate.

Two types of modifiers were used to prepare PUNCs in this study: dodecylamine and hexadecylamine with prefix labelled as P12 and P16 respectively. A suffix was added according to the %OMS, i.e. a PUNC that contained the OMS $12CH_3$MMT at 1% OMS loading would be identified as P12C-1. The materials that were prepared and characterised for this study are shown in Table 3.1.

Table 3.1 Materials investigated within Chapter 3

Material ID	Type of OM	% loading[a]
PU	-	-
P12C-1	$12CH_3$MMT	1
P12C-3	$12CH_3$MMT	3
P12C-5	$12CH_3$MMT	5
P16C-1	$16CH_3$MMT	1
P16C-3	$16CH_3$MMT	3
P16C-5	$16CH_3$MMT	5

[a] % loading = % OMS (g OMS/ 100g PU)

3.2.3 Materials Characterisation

3.2.3.1 Thermogravimetric Analysis

Thermogravimetric analysis (TGA) was used to determine whether cation exchange had occurred between the modifier and the interlayer Na^+ within MMT. The experimental

percentage of exchange (CEC_{exp}) can also be determined through analysis of the TGA thermogram. Measurements were taken on a Perkin Elmer Pyris 1 thermogravimetric analyser. Samples were dried overnight in an oven at 60°C prior to analysis to remove all residual moisture. Approximately 5-10mg was placed in an aluminium crucible and heated to an initial temperature of 50°C. Samples were then raised to 800°C at a rate of 30°C/min under N_2 and compressed air.

TGA thermograms were obtained both in the form of weight percentage (%) and derivative weight percentage (%) plotted against temperature (°C). An estimation of the experimental amount of % CEC can thus be calculated using equation 3.2.

$$\%\ CEC_{exp} = \frac{Weight\ of\ OM_{experiment}}{Weight\ of\ OM_{theoretical}} \times 100\% \qquad (3.2)$$

Weight of $OM_{experiment}$= Weight loss of OMS (800-200°C) - Weight loss of NaMMT (800-200°C)

3.2.3.2 X-ray Diffraction

XRD is a common technique used to evaluate the spacing between clay layers due to its ease and availability. Any change in shape, position and intensity of the basal peaks can provide useful information on the clay structure [192]. The distance between the silicate layers (d spacing) can be calculated using Bragg's law (equation 3.3), where λ is the wavelength of the incident beam, 2θ is the diffraction angle and *d* is the distance between silicate layers. As more polymer penetrates the interlayer, the d-spacing

increases and so the diffraction angle (θ) decreases. Exfoliation occurs when the spacing is sufficiently large that the reflection peaks disappears.

$$\lambda = 2d\sin\theta \tag{3.3}$$

Samples of ~15mm × 60mm were cut into strips selected randomly from the cast sheets. The distance between silicate layers in the NC was determined on a Philips PW-1830 x-ray diffractometer with CuKα radiation of 0.15406nm at 40kV and 40mA. Strips were scanned from 1.8 to 9^o at a rate of 0.00133^o/s and a step size of 0.01^o. A $1/12^0$ divergence slit and $1/12^0$ anti-scattering slit was used and the data were collected using X'pert Data Collector software. Post-test adjustment corrections were required to account for the sample thickness when placed on the sample holder. The same surface should be flat when exposed to the x-ray beam at zero $^o2\theta$. Equation 3.4 was used to correct the data obtained where *s* is the sample thickness (mm), *R* is the goniometer radius (173 mm for PW-1830), and θ is the incident x-ray beam angle (radians).

$$2\theta = \frac{2s\cos\theta}{R} \tag{3.4}$$

3.2.3.3 Transmission Electron Microscopy

TEM can provide a direct visualisation of the morphology and spatial distribution of the clay platelets. Variations in a material's electron density can provide image contrast as electrons are either transmitted through, or scattered from the sample. High resolution images can be produced in this way and give qualitative data regarding the orientation of

the clay platelets and whether the individual aggregates have been well dispersed. Therefore TEM is often used as a complement to XRD to confirm the d-spacing in polymer NCs. It can also clarify situations where the absence of basal reflections detected by XRD, usually implying exfoliation, could in fact be the result of a wide distribution of layer spacing and that the NC is still intercalated.

In this study, a small section of the cast NC films was cryosectioned using a Leica FC6 Cryo-Ultramicrotome at a temperature of -120ºC. Slices were cut at a rate of 0.15-3mm/s to approximately 90-110nm in thickness and collected onto a 200- mesh copper grid for analysis. Images of the samples were taken using a JEOL 1400 TEM, with an accelerating voltage of 100kV, at various magnifications (5000x-100000x). Each sample was imaged at multiple locations and one representative image of the material was chosen for presentation.

3.2.3.4 Tensile testing

Tensile testing can provide an indirect indication of silicate dispersion, as the quality of dispersion is proportional to the degree of mechanical enhancement [21, 109]. Samples were subjected to a constant deformation longitudinally until failure. The amount of force required for a change in length can be translated into a stress-strain curve and the ultimate tensile strength (UTS, σ), strain (ε) and Young's modulus (E) can be measured by equations 3.5, 3.6, and 3.7 respectively.

$$Stress(\sigma) = \frac{F}{A_0} \tag{3.5}$$

$$Strain(\varepsilon) = \frac{l - l_0}{l_0} \tag{3.6}$$

$$Modulus(E) = \left.\frac{\sigma}{\varepsilon}\right|_{\text{linear region}} \tag{3.7}$$

Tensile testing of PUNCs was conducted according to ASTM D 882-02. Strips of length ~60mm × 7mm were punched from the cast sheets and the thickness of each strip was measured using a digital micrometer measured at three positions and then averaged. Each sample was tested at a strain rate of 100mm/min using an Instron 4302 testing machine with a 1kN load cell. The strips were gripped by a grip with a smooth rubber surface at a pressure of 400kPa. Data collected from each sample were plotted and properties such as ultimate strain (ε), stress (σ) and young's modulus (E) were calculated using equations 3.5, 3.6, and 3.7 respectively.

Statistical analysis was conducted using two-way analysis of variance (ANOVA) with a fixed factor (material) and a nested random factor (batch). Comparison between NCs and PU were made using Dunnett's test. A second two-way analysis of variance to assess the effects of loading and modifier type was performed without PU control. A p-value <0.05 was used to indicate a significant difference. A detailed description of the statistical analysis can be found in Appendix A.1.

3.3 Results

Solvent cast PUNC films appeared transparent, colourless and smooth on both surfaces (contact with glass and contact with air). Films with higher loadings (5wt%) were more

opaque due to the presence of silicate particles. Successful modification of MMT with alkylamines was assessed via TGA and XRD. Silicate spacing and structure of NC was confirmed via XRD and TEM.

TGA confirmed that cationic exchange has occurred between the OM and silicate layers. Thermograms of MMT, $12CH_3MMT$ and $16CH_3MMT$ are shown in Figure 3.3. The decomposition of MMT is generally represented by two regions; the evolution of free and interlayer water between 100-400˚C, and the dehydroxylation of the aluminosilicate lattice between 500-1000˚C [193, 194]. On the other hand, the thermo decomposition of OMS as described by Xie *et al*. [194] can be separated into 4 distinct regions: I) mass loss due to water and gaseous species below 180˚C; II) evolution of organic substances between 200-500˚C; III) dehydroxylation of aluminosilicate between 500-700˚C; and IV) evolution of carbonaceous residue between 700-1000˚C. These observations were in agreement with the decomposition phase in Figure 3.3, indicating that cationic exchange had occurred.

An estimation of the experimental amount of % CEC calculated using equation 3.2 showed that the exchange for $16CH_3MMT$ and $12CH_3MMT$ was 85.75±3.9% and 81.34±5.3% respectively. Both OMS displayed lower % CEC compared with the theoretical amount added suggesting that, although an excess of 10% OM was added to fully exchange interlayer cations in MMT, a fraction of exchange sites would still be available due to the position or arrangement of exchanged modifiers blocking the remaining exchange sites.

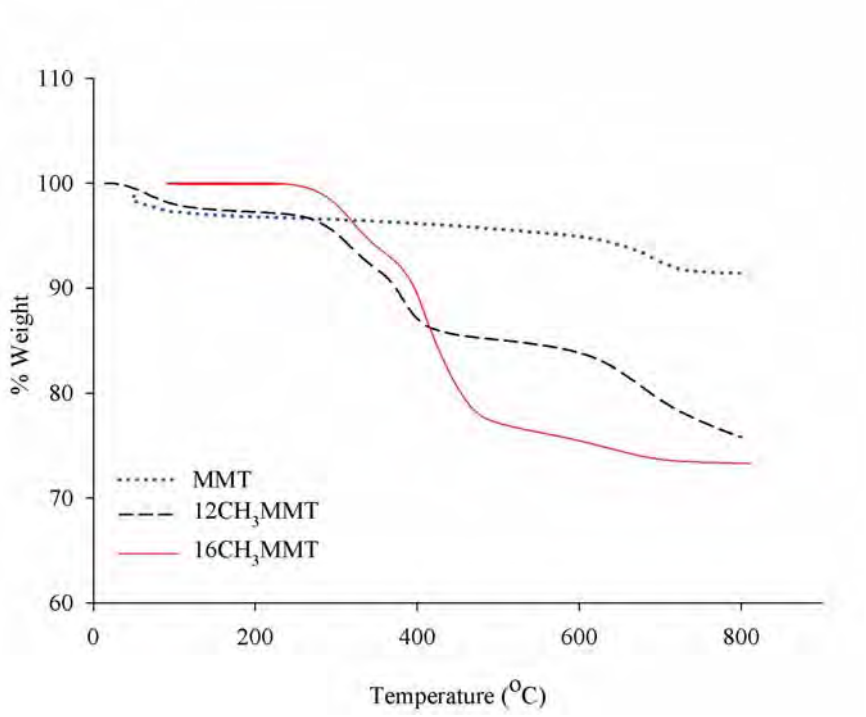

Figure 3.3 TGA thermograms of OMS used in this study.

Modification of MMT can also be determined by XRD analysis and is shown in Figure 3.4. An analysis of the peak of MMT using Bragg's law (equation 3.3) indicated a spacing of 1.39nm which is comparable with the results reported by the manufacturers of 1.17nm [195]. As OM was added to MMT, the spacings increased to 1.74nm and 1.89nm for $12CH_3MMT$ and $16CH_3MMT$ respectively. This suggested that OM successfully exchanged with the OM and aided the separation of silicate layers. An increase in spacing was also observed with the use of longer alkyl chain modifiers which is in agreement with findings in the literature [196].

The results for PUNCs at varying clay concentrations and different modifier lengths are shown in Figure 3.5 and 3.6. A summary of the silicate spacings are shown in Table 3.2. In general, it can be seen that, as clay content increases, the spacings decrease due to clay aggregation. The use of longer alkylamines, $16CH_3$MMT resulted in larger silicate spacings than PUNCs modified with $12CH_3$MMT. There was an absence of peaks for 1 wt% loading in both modifier types implying a partially exfoliated or fully exfoliated morphology.

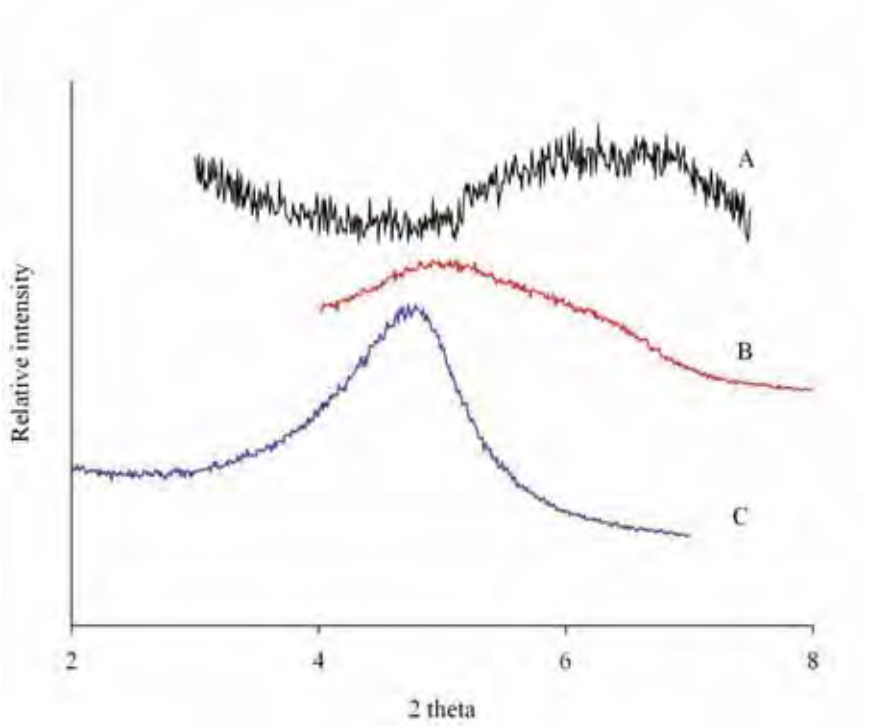

Figure 3.4 XRD diffractograms for: A) MMT, B) 12CH3MMT, and C) 16CH3MMT.

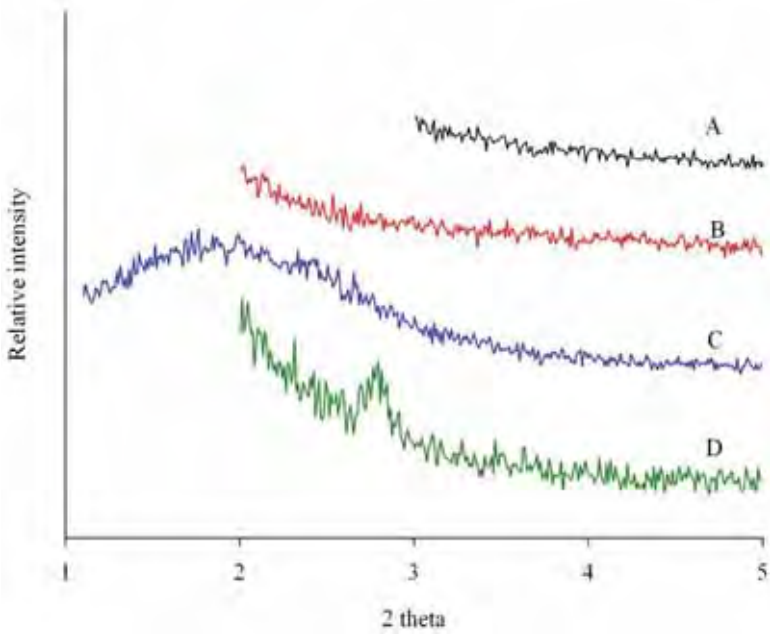

Figure 3.5 XRD diffractograms for a) neat PU, and PUNCs modified with 12CH3MMT at loadings b) 1wt%, c) 3wt%, and d) 5wt%.

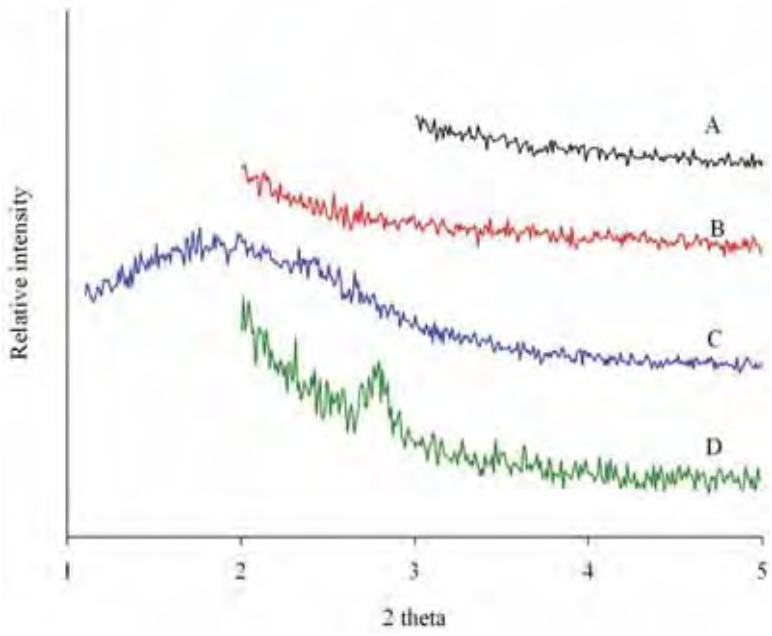

Figure 3.6 XRD diffractograms for a) neat PU, and PUNCs modified with 16CH3MMT at loadings b) 1wt%, c) 3wt%, and d) 5wt%.

Table 3.2 XRD results for PU and PUNCs

Material	2θ	Silicate spacing (nm)
PU	-	-
P12C-1	-	-
P12C-3	2.59	3.40
P12C-5	3.47	2.55
P16C-1	-	-
P16C-3	1.85	4.78
P16C-5	2.71	3.26

TEM confirmed the XRD findings relating to morphology of PUNCs as well as providing a direct visualisation of the structure and orientation of the silicate layers. Representative TEM images of PUMMT-1 and P12C-1 is shown in Figure 3.7. The importance of modifiers in the fabrication of NCs was clearly illustrated, since images from P12C-1 were able to show individual silicate layers while images from PUMMT-1 could not. The use of modifiers renders the clay organophilic to allow organic species (i.e. polymers) to diffuse into the layers and achieve separation of the silicate layers. Representative TEM images of both 1 and 5wt% loading for P12 and P16 taken at various magnifications are displayed in Figure 3.8 and 3.9. The increase in clay content resulted in an increased tendency to form clumps and the use of longer chain OM tended to result in smaller clumps, especially between P12C-1 and P16C-1. This was consistent with the XRD findings where increased clay loading decreases the silicate spacing and the use of longer chain length OM resulted in better dispersion.

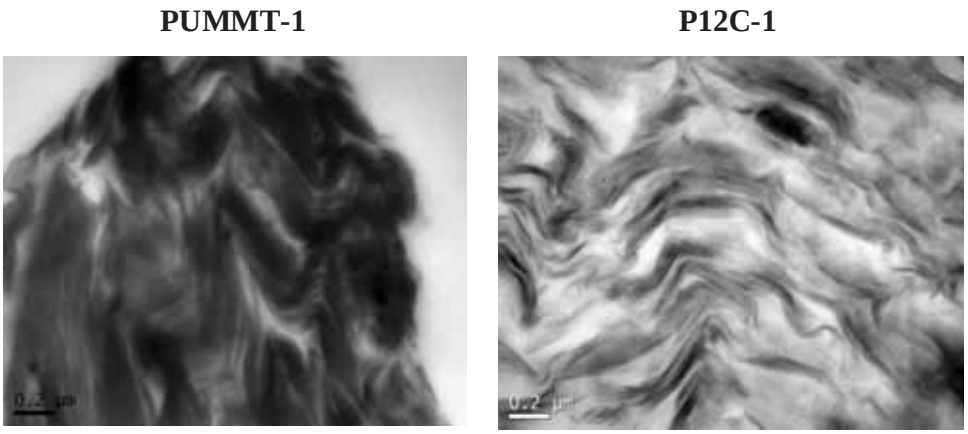

Figure 3.7 Representative TEM images of PUMMT-1 and P12C-1 taken at 60,000x (scale bar = 0.2μm).

At higher magnifications (Figures 3.8), both P12 and P16 at 1wt% loadings showed distinguishable individual silicate layers, but still contained regions where clay was not fully exfoliated. However, the XRD analysis for both of these NCs did not display a peak for an intercalated morphology. Therefore, by combining the results of both TEM and XRD, the structure for NCs modified with 1wt% loadings were classified as partially exfoliated and the absence of peaks from XRD was due to the distance between silicate layers exceeding the detection limit of this particular X-ray diffractometer.

Moving onto the 5wt% loadings, the increase in number of dark regions confirmed the higher tendency of those samples to form clay aggregates. In addition, at magnifications of ×60K and ×100K, a well ordered multilayer morphology was apparent. This was in agreement with the spacings determined from XRD that the morphology of 5wt% loaded PUNCs were intercalated. At higher magnifications, the differences in silicate spacing between P12 and P16 were less obvious than images taken at lower magnifications. However, P16 appeared to have less ordering and areas of dense aggregates than P12

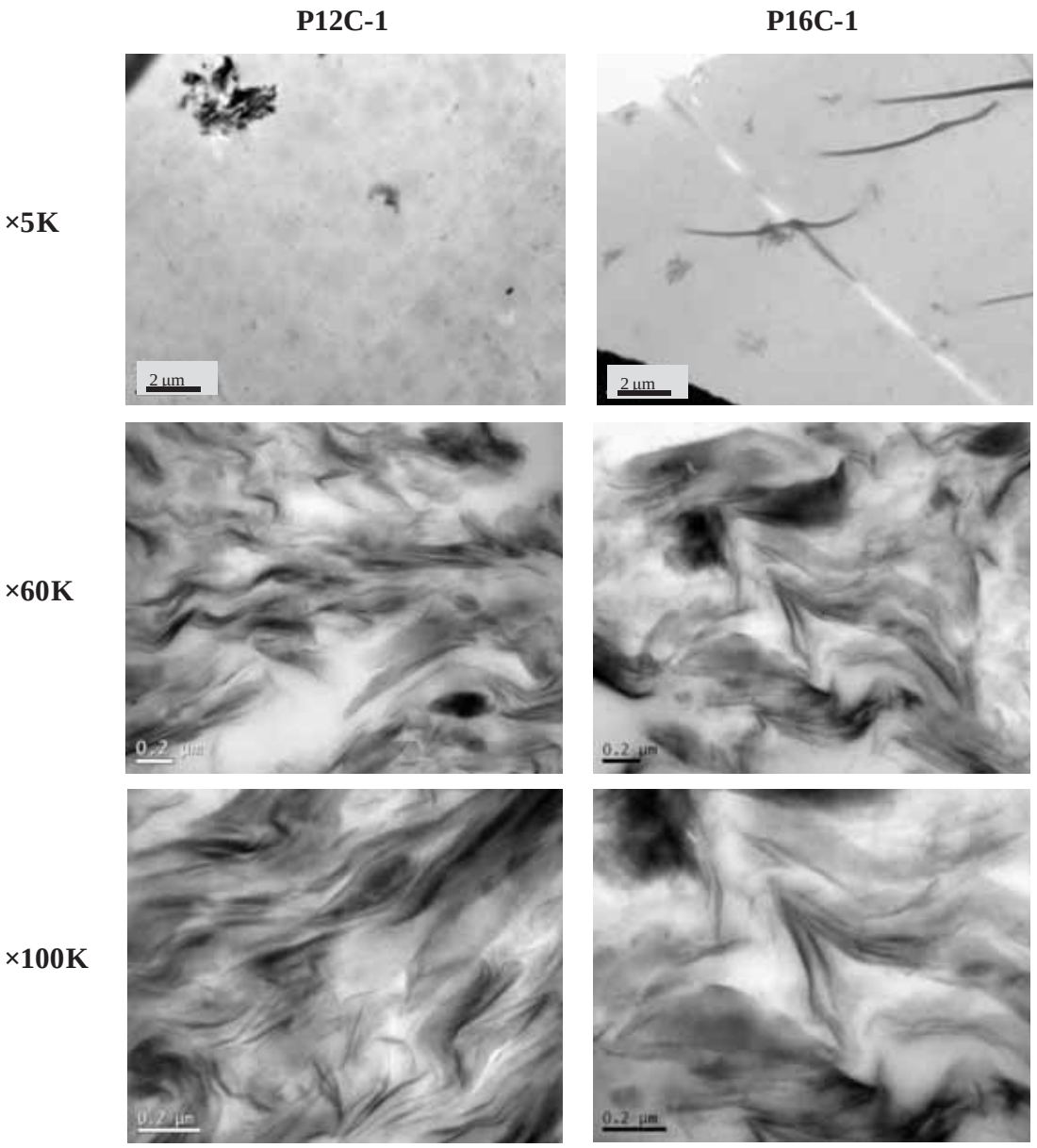

Figure 3.8 Representative TEM images of P12C-1 and P16C-1 taken at various magnifications of 5000x (scale bar= 2µm), 60,000x (scale bar=0.2µm) and 100,000x (scale bar= 0.2µm).

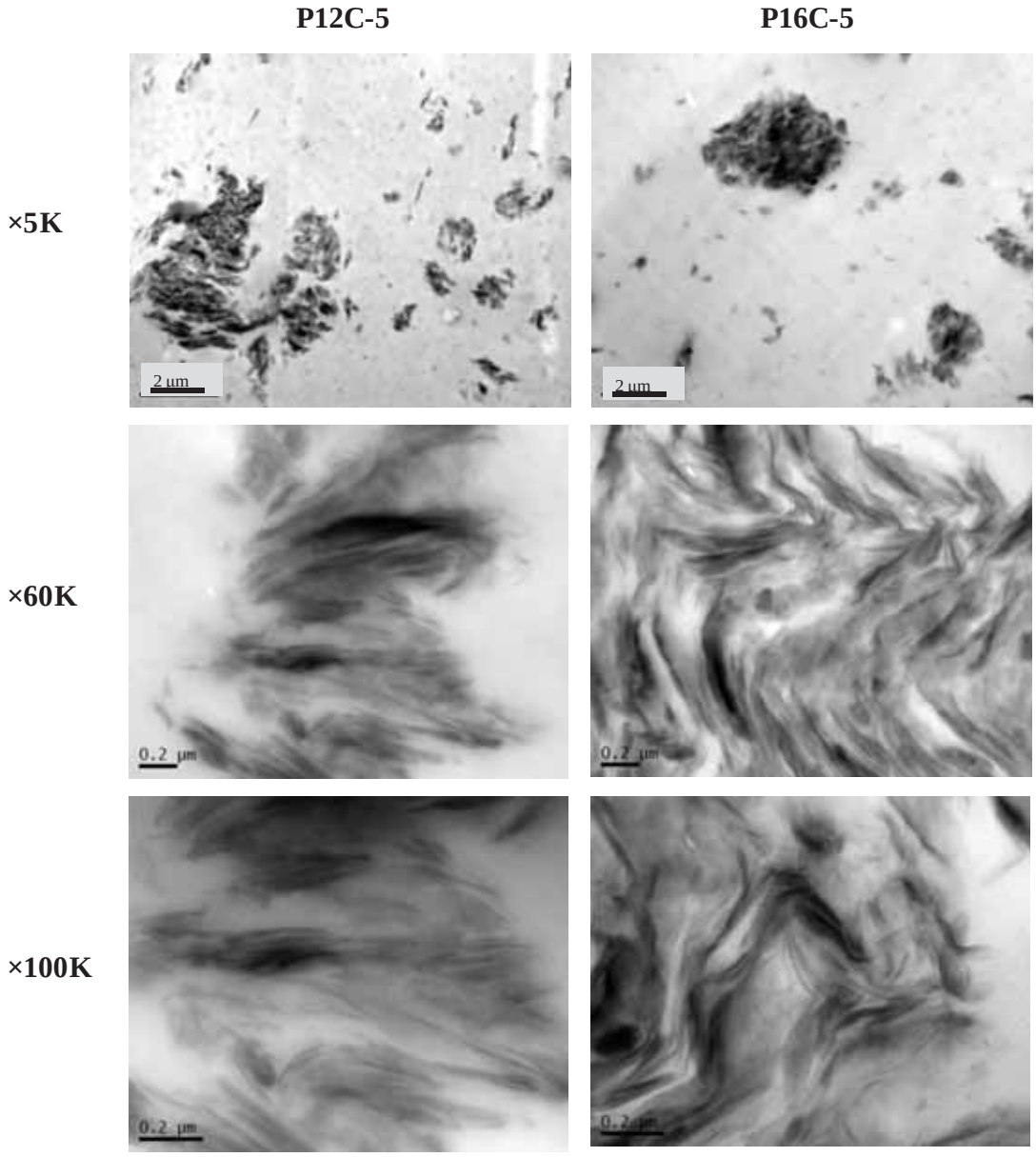

Figure 3.9 Representative TEM images of P12C-5 and P16C-5 taken at various magnifications of 5000x (scale bar= 2µm), 60,000x (scale bar=0.2µm) and 100,000x (scale bar= 0.2µm).

from images taken at ×100K. Therefore, although TEM is useful in providing a direct visualisation of the structure and orientation of the silicate layers, it is necessary to complement this technique with XRD to provide a more accurate understanding of silicate dispersion both visually and quantitatively.

The results for modulus, ultimate stress and ultimate strain of PUNCs are plotted in Figure 3.10-3.12 respectively and detailed in Table 3.3. PUNCs loaded at 1wt% for both types of OM maintained the Young's modulus of pristine PU and were not significantly different. However, the modulus increased with increasing clay loading with the greatest increase in modulus observed from sample P12C-5 ($p<0.05$). Statistical analysis of the effects of clay loading and modulus also suggested that the clay loading had a significant effect ($p=0.009$) on the modulus. Contrary to the results of Young's modulus, the ultimate stress decreased with the addition of clay and the lowest UTS was observed in samples with 5wt% loading. The ultimate stress of PUNCs were all significantly reduced when compared to PU ($p<0.05$) with the exception of P16C-1 (47.4MPa), which demonstrated similar strength to that of pristine PU (48.4MPa).

When compared to P12s, NCs modified with P16s appeared to have a lesser reduction in UTS across all clay loadings, suggesting that the length of modifier could have a significant effect ($p<0.05$). The effects of clay addition on strain showed that there was a significant increase in strain when using P16s across all clay loadings, but only seen at 1 wt% loading when using P12s ($p=0.0008$). Increasing the clay loading in P12 did not lead to an increase in strain. In fact, a loading at 5 wt% resulted in a significant reduction in strain ($p<0.05$) compared with pristine PU.

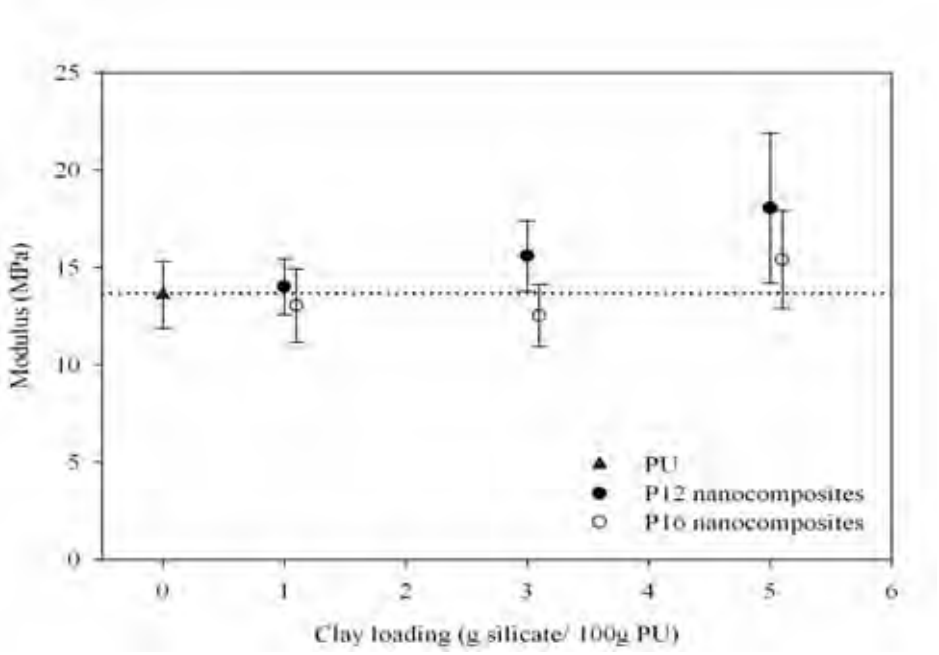

Figure 3.10 Young's modulus for PU and PUNCs. Mean ± standard deviation.

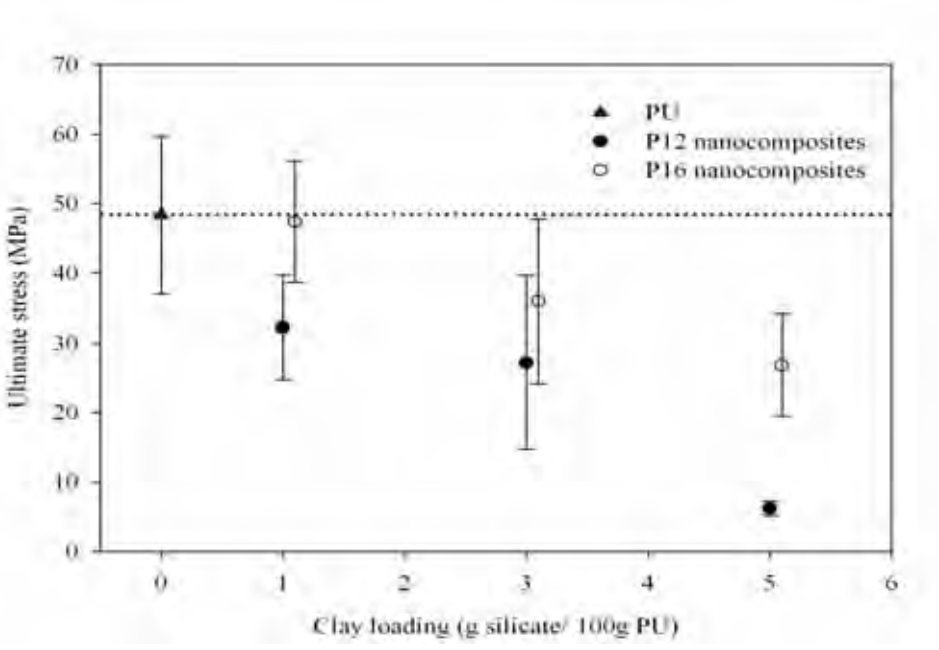

Figure 3.11 Ultimate tensile stresses for PU and PUNCs. Mean ± standard deviation.

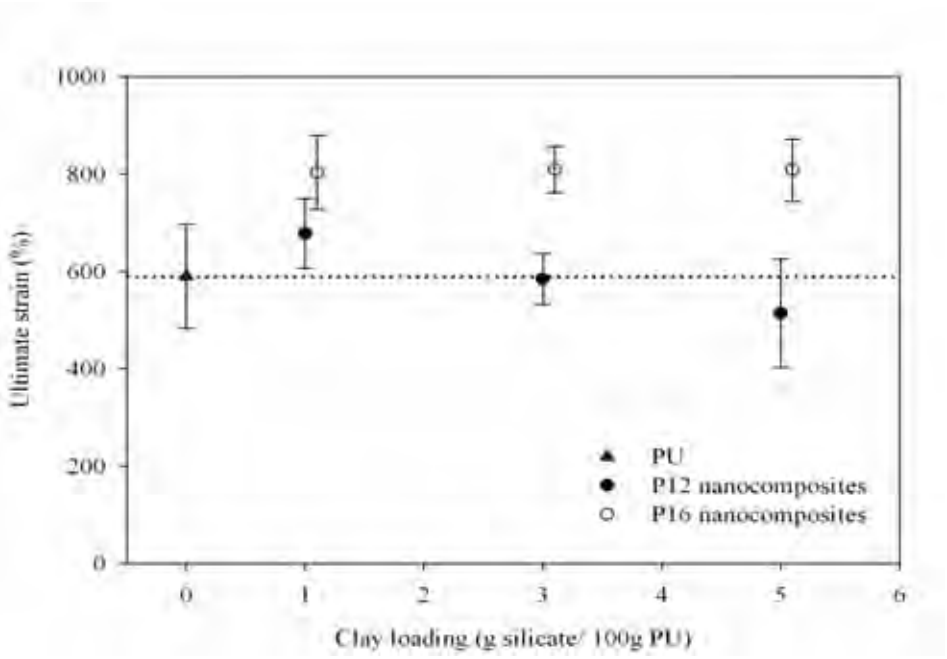

Figure 3.12 Ultimate strains for PU and PUNCs. Mean ± standard deviation.

Table 3.3 Summary of mechanical properties of PUNCs. Data presented as mean ± standard deviation

Material	Number of samples/batches	Ultimate stress (MPA ± s.d)	Ultimate strain (% ± s.d)	Modulus (MPa ± s.d)
PU	20/6	48 ± 11	590 ± 106	14± 2
P12C-1	25/6	32 ± 8 *	678 ± 72 *	14 ± 1
P12C-3	16/4	27 ± 12 *	584 ± 52	16 ± 2 *
P12C-5	22/5	6 ± 1 *	514 ± 112 *	18 ± 4 *
P16C-1	20/6	47 ± 9	803 ± 76 *	13 ± 2
P16C-3	20/4	36 ± 12 *	809 ± 47 *	13 ± 2
P16C-5	28/3	27 ± 7 *	808 ± 64 *	15 ± 3 *

* Indicates significant difference compared to PU control ($p<0.05$)

3.4 Discussion

Primary alkylamines with different chain length were used to modify silicates for the fabrication of PUNCs. The presented results demonstrated that a longer chain length modifier enhanced silicate spacing and that is maintained when the OMS was introduced in PU to produce PUNCs. Furthermore, although the optimal clay loading is of the order of 1wt% for both shorter and longer modifiers, there appears to be better dispersion at higher loadings in PUNCs based on longer chain modifiers.

The incorporation of OM into MMT as evidenced by XRD and TEM in Figure 3.4 and 3.7 showed an increase in silicate spacing in agreement with the published literature. Work conducted by Choi *et al*. [171] observed that the d-spacing of MMT increased from 1.18nm to 2.29nm after ion exchanging with OM. This increase was achieved with a CEC of only 74% [171]. A similar observation was reported by Lan *et al*. [180] where the addition of OM aided clay layer separation. This increase in separation of clay layers is due to the repulsive forces between the silicate surfaces after modification and the degree of separation is dependent on the length of alkyl carbon chain, density of modifier and arrangement of modifiers on the clay surface [92].

Silicate spacing measured by XRD is equivalent to the distance between the individual silicate layers along with the thickness of an individual layer. As MMT is known to have a layer thickness of ~0.96nm [83], the subtraction of this value from the determined XRD spacing of $12CH_3$MMT and $16CH_3$MMT can give an estimate of the distance between silicate layers of OMS. In this study, the calculated values were 7.8Å and 9.3Å

for $12CH_3$MMT and $16CH_3$MMT respectively. These were shorter than the theoretical length of alkylammonium ions calculated from the relationship proposed by Pluart *et al*. [181], where the lengths of $12CH_3$MMT and $16CH_3$MMT were estimated to be 16.9Å and 21.9Å respectively under an all-trans configuration. By relating the dimensions of the OMs and the spacing determined by XRD, it is possible that the OMs were not in an all-trans conformation but adopting a pseudotrilayer or paraffin-like structure in a titled angle to that of the silicate surface [181].

Based on XRD results, the use of longer chain modifiers appeared to improve dispersion within a PUNC system. However, the difference between P12C-1 and P16C-1 shown in Figure 3.8 did not indicate a substantial difference in clay separation. Given that TEM focuses on a small section at very high magnification, the images obtained may not represent the general dispersion in the bulk of the sample. As indicated previously, although longer chains disperse better, the structure at high clay loadings are still intercalated from both XRD and TEM analysis. Since the XRD peaks were broad, this implies that there are a range of clay aggregates with different sizes and it is still difficult to disperse individual clay layers uniformly throughout the matrix.

The improvement in mechanical properties along with lower filler requirements was the main driving force for continuous research and implementation in the field of polymer NCs [29, 197]. A summary of the effects of increasing clay loading and modifier chain length in dispersion and mechanical properties found in this study is shown in Table 3.4. From tensile testing, the addition of OMS at loadings above 3wt% resulted in an increase in modulus compared with neat PU ($p<0.05$). Often, the improvement in

modulus is related to dispersion and interfacial adhesion between the particles and the matrix. With better dispersion, interfacial areas over which the particles can interact with the matrix increases, and the mobility of the polymer chains become more restricted under loading [198]. However, as the structure of P12C-1 and P16C-1 were not fully exfoliated and still contained aggregates as seen from TEM, the improvement in modulus was limited, but at least maintained. With increasing clay content, increases in modulus can be attributed to the stiffening of clay nanofillers since clay has a higher modulus than that of PU.

The UTS on the other hand decreased with increasing clay content, an exception being P16C-1 which was able to show similar strength to that of neat PU. The results from all other PUNCs suggested that the addition of clay appeared to have a detrimental effect on the UTS ($p<0.05$). The decrease in UTS was mainly thought to be caused by agglomeration of clay particles creating a poor interface, therefore decreasing the number of available reinforcements. Chang *et al.* [90] investigated the mechanical properties of PU with various organoclays ranging from 0-8wt%. It was found that the UTS of PUNCs increased remarkably up to 3wt% loading but decreased with further addition [90]. This was also seen in others where the increase in strength starts to decrease above a certain clay loading [83, 103, 199]. From these results, it has been shown that there is an optimum amount of clay loading to achieve the required type of property enhancement. The most balanced enhancement in strain, UTS and modulus result from clays with better dispersion and lower loadings.

Table 3.4 The effects on silicate dispersion and mechanical properties from increasing loading and modifier chain length

Increasing	Dispersion	Modulus	Ultimate stress	Ultimate strain
OM Chain length	Increase	Minor increase	Minor decrease	Increase
Silicate loadings	Decrease	Increase	Decrease	Maintain

3.5 Conclusion

The impact of modifier chain length on the silicate dispersion within PUNCs was examined by the use of two alkylamines; $12CH_3$ or $16CH_3$. Although MMT was not fully exchanged with the OM, the amount that was successfully exchanged was still able to arrange in a pseudotrilayer or paraffin-like structure that aided further separation upon intercalation with PU.

The dispersion of silicates was dependent on both the type of modifier and the silicate loading. Results suggested that the optimum dispersion was achieved with P16C-1 that showed a partially exfoliated structure, whereas samples with higher clay loadings and shorter alkyl chains showed an intercalated morphology and larger aggregates. The better dispersed sample P16s also conferred an increase in ultimate strain while maintaining the Young's modulus and tensile strength of the material. Higher loadings of clay leads to increases in modulus, but could also result in lower UTS due to the higher tendency to form aggregates.

In summary, the use of longer chain length modifiers and lower clay loadings are desirable with respect to both dispersion and mechanical properties. Although the optimal clay loading is at 1wt% for both lengths of modifier, dispersion appeared to be better at higher loadings in PUNCs based on longer chain modifiers. The effects of chain length and modifier will be investigated further in subsequent chapters for their impact on drug delivery behaviour.

Chapter 4: Assessment of Polyurethane Nanocomposites as anti-thrombotic coatings using heparin

4.1 Introduction

The results of the previous chapter showed that longer chain length modifiers and lower clay loadings led to improvements in clay dispersion and mechanical properties of PUNCs. This chapter aims to extend the investigation of PUNCs based on 12 and 16 carbon chain alkylamine modified silicates into the field of drug delivery systems. Furthermore, the research aimed to conduct proof-of-principle studies on the feasibility of coating PUNCs onto metallic substrates and their use in blood related applications[3]. The rationale for conducting such studies was to assess key factors that may impact on the application of PUNCs for drug delivery and to identify challenges and issues for further research. The identification of these issues and uncertainties early in this work assisted in addressing unanswered research questions, as well as setting the scene for subsequent chapters of this thesis.

4.1.1 Application focus

Oral or intravenous administration of aggressive anticoagulants and anti-thrombotics is a typical approach to prevent device failure in blood related applications and to improve

[3] This work was largely conducted by the candidate during a lab visit to the Centre of Biomaterials Research at Maastricht University (The Netherlands) under the supervision of Prof. L.H. Koole and Dr. M. Knetsch

surgical outcomes. In the case of coronary stents warfarin, aspirin and clopidogrel are commonly used peri-operatively and for at least 1 year post-operatively [200]. Using anti-thrombotics for long periods of time may introduce bleeding and surgical complications as well as longer hospital stays and higher costs [201]. Some of the strategies used to improve blood compatibility of polymers and reduce requirements for systemic administration of drug therapy are the surface modification of polymers through covalent or non-covalent immobilisation with either anti-thrombotic agents, hydrophilic polymer chains, or incorporation and release of anti-thrombotic agents directly from the bulk material [202, 203].

Heparin, a potent anticoagulant drug, interacts strongly with antithrombin III (ATIII) in preventing the formation of a fibrin clot and is commonly chosen as a preferred agent in the aforementioned device modifications. Heparin acts as a catalyst that enhances the affinity of ATIII for thrombin or factor Xa, thereby forming a complex of thrombin and ATIII that loses the ability to participate in further blood coagulation processes [204, 205]. The complex then dissociates from heparin, which allows heparin to inactivate further thrombin molecules.

Extensive research has been conducted on development and evaluation of immobilised heparin on PU surfaces. This has been achieved through a variety of techniques including covalent linking via a spacer [206-209], layer-by-layer deposition [210-212], photochemical coupling [213], physical adsorption [214], or in the form of block copolymers [215, 216]. Conversely, it has been reported that heparin can be released from polymers through both ion-exchange mechanisms and via diffusion [217].

Although it has been reported that heparin via release from materials has higher bioactivity than when surface immobilised [218], the amount of heparin released is often not sustained and the majority released within the first few hours [217].

Control of drug release from polymers can be achieved by a number of approaches, such as modifying the composition or morphology of the polymer to decrease the mobility of the drug or the pore size of the polymer [13], adding an additional layer or coating to increase the diffusion pathway [15, 219], or modulating drug distribution to overcome the diminishing release rate [220]. These approaches however, involve extra processing steps and introduction of additional materials that may increase both the cost and time.

In theory, by adjusting the filler content and the dispersion of nanofillers, NCs could control drug release without the need for chemical modification, additional coatings or extra processing steps. Interestingly, reports in literature on polymer NCs for blood applications have focused more on the development of a blood compatible surface rather than achieving compatibility through controlled release of anti-thrombotic molecules [71, 221]. In a study conducted by Zhou *et al*.[222], phosphatidyl choline (PC) was incorporated as an antithrombotic molecule for release and as a surfactant in a polydimethylsiloxane (PDMS) based NC. The NC films demonstrated better blood compatibility than neat PDMS films but the drug release profile or approaches in modulating the release were not studied [222].

In addition, among the NCs reported for blood applications, carbon nanotubes were often selected as the nanofiller rather than MMT [71, 72, 222], and there have been no

reports in using PUNCs for blood contacting devices. In the majority of studies cited, materials were fabricated as films rather than as coatings, and are typically not focussed on anti-thrombotic applications [223, 224]. Therefore, the possibility of coating polymer NCs on metallic surfaces could be extremely useful for devices that have good physical properties but poor blood compatibility. In particular, using PU as the matrix could provide the coating with elasticity, strength, and good baseline blood compatibility [52].

When blood comes in contact with a foreign material, plasma proteins are rapidly adsorbed onto the surface [225]. Together with platelet aggregation, the coagulation cascade is activated and thrombus forms [226, 227]. Thrombus formation is triggered by two different pathways; the intrinsic and extrinsic coagulation pathway which ultimately converge into a common pathway as shown in Figure 4.1. The common pathway involves the activation of thrombin by factor Xa and factor Va (prothrombinase complex) in the presence of Ca^{2+} and phospholipids (PL). Thrombin induces the formation of fibrin fibres that cross-links to form a stable clot [202]. The intrinsic pathway, also referred to as 'contact activation' pathway, involves a cascade of sequential activation starting with factor XIIa that catalyses the formation of factor Xa in the common pathway [202]. On the other hand, extrinsic pathway is triggered by the generation of tissue factor (TF) present in the smooth muscle cells which is released when tissue damage occurs, such as in implants or surgical procedures. TF forms a complex with factor VII (TF:FVIIa complex) that also leads into the common pathway [202, 228] .

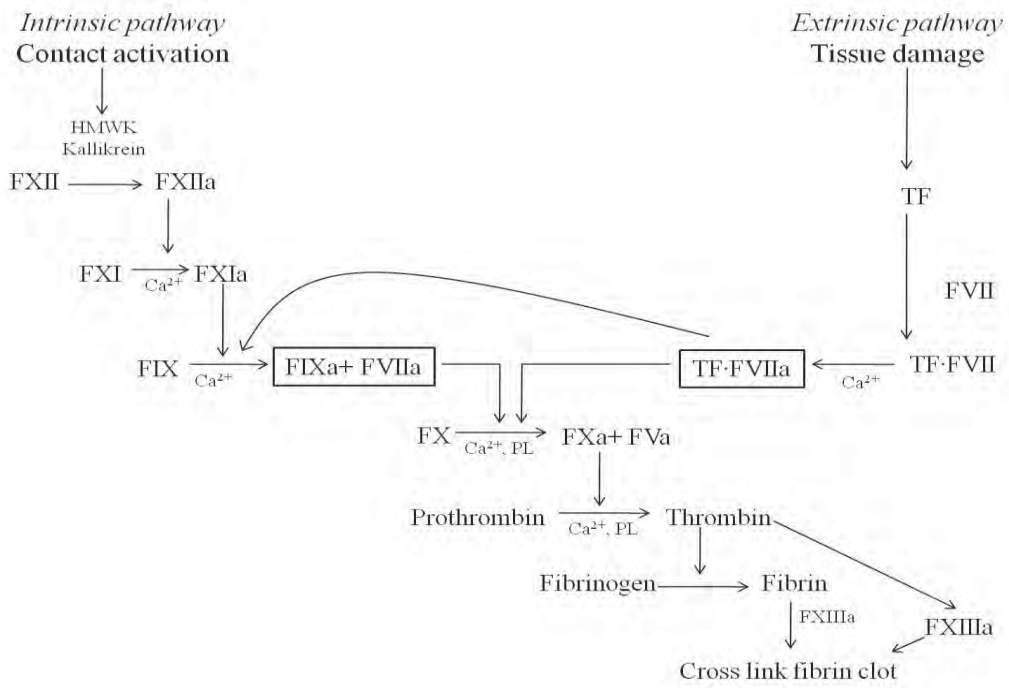

Figure 4.1 The intrinsic, extrinsic and common pathway of blood coagulation; PL= phospholipid; TF= tissue factor; HMWK= high molecular weight kininogen [202, 228-230].

The overall objective of this study was to identify key challenges and issues associated with the use of NC based drug delivery systems. The underlying hypothesis is that heparin released from PU can be modulated by introducing layered silicates and the associated variables (clay loading, quality of dispersion). In addition, silicates will not affect the blood compatibility of PU and the biological activity of heparin. The specific aims for this study were to:

1. Examine the coating of PUNCs onto stainless steel wires as a model for coating on stents.

2. Examine the impact of silicate loading and OM chain length in modulating heparin release.

3. Assess the comparative blood compatibility of PU and PUNCs.

4.2 Materials and methods

4.2.1 Sample preparation and coating

Due to processing requirements with the coating company (MCTec BV), the solvent NMP (1-methyl-2-pyrrolidone, Acros USA), which belongs to the same class of aprotic solvents as DMAc, was used to dissolve PU. The materials prepared for coating were mixed in the same manner as those described in Chapter 3, and were thus expected to have similar mechanical properties and silicate dispersions. Unfractionated heparin (Celsus Laboratories Inc, USA) was used as received. Heparin was present as the sodium salt and the activity was 197 units/mg.

Required amounts of PU and NMP were weighed to achieve 8%w/v PU in NMP suspension and stirred for a period of 5 days to ensure that the PU was completely dissolved. PUNC solutions for coating were prepared by mixing polymer suspension and modified clay overnight. For PUNCs incorporated with heparin, 10wt% heparin (g heparin/100g PU) dissolved in formamide (Sigma, Aldrich) was added to the NC solution. PUNCs were labelled according to abbreviations described previously in Chapter 3, and is shown in Table 4.1. Samples incorporating heparin have an additional "H" in the suffix. For example, a PUNC that contained the OMS $12CH_3$MMT at 1% OMS loading + heparin would be identified as P12C-1+H. PUNC samples modified with $12CH_3$ or $16CH_3$ are still labelled with prefix P12 or P16 respectively.

Table 4.1 Materials investigated within Chapter 4

Material ID	OMS	Loadings (g/100g PU)	
		Clay	Heparin
PUNC coils			
PU	-	-	-
P12C-1	12CH_3MMT	1	-
P12C-5	12CH_3MMT	5	-
P16C-1	16CH_3MMT	1	-
P16C-5	16CH_3MMT	5	-
PU+H	-	-	10
P12C-1+H	12CH_3MMT	1	10
P12C-5+H	12CH_3MMT	5	10
P16C-1+H	16CH_3MMT	1	10
P16C-5+H	16CH_3MMT	5	10

PU and PUNC solutions added with or without heparin were coated on stainless steel wires through an automated coating system at MCTec BV (Venlo, The Netherlands). Stainless steel wires (>1000m, diameter 171µm) were first cleaned with phosphoric acid and passed through a water bath to remove acid remnants. The wires were then pulled through the polymer solution at 1.1m/s and guided through a cylindrical oven (maximum temperature 300^{o}C, height approximately 6m) to evaporate the solvent (NMP). Thickness of the coating was monitored with an in-line continuous measurement. Wires used in this study were first coated with 1µm layer of polyether sulphone (PES) as a

binder. Following that, a second layer consisting of PUNCs (3µm) with or without heparin was coated by the same process.

The resulting diameter of the coated stainless steel wires was 176µm. Coated wires were then coiled by a speed controllable mandrel and a stainless steel core wire with a diameter of 690µm was used. Coils of approximately 50cm in length were made. These coils were used to conduct experiments as they allow more surface area with lesser materials.

4.2.1.1 Scanning electron microscopy

The integrity of the coated coils was evaluated using a Hitachi S3400-X SEM. Coils were cut into 2cm sections and fixed onto a specimen holder by carbon tape. An accelerating voltage of 10kV and current of 30mA were used. Each coil was imaged at multiple locations and one representative image of the material was chosen for presentation.

4.2.2 Drug delivery

4.2.2.1 *In vitro* heparin release

Heparin released from the coils was measured using the method described by Jaques *et al*. [231]. The method was based on the measurement of the metachromatic activity of heparin with Azure A. Coils (10cm) were cut into 4 smaller sections and released in phosphate buffered saline (PBS, 10ml) at 37^{o}C. Aliquots (400µl) were taken at regular intervals and the sink replenished for a total of 24 hours. Azure A was first dissolved in

PBS at 0.1mg/ml and this solution (60µl) was added to the sample (150µl). The solution was then mixed and absorbance measured by a spectrofluorometer at 492nm (SpectraMax M2, Molecular Devices, CA, USA). Standards were prepared by a dilution series of heparin and PBS. PU coils without heparin was used as a control. The assay was repeated three times, where two of the assays were released for a further 24 hours (total of 48 hours) to determine the point at which the drug release profile plateaus.

Statistical analysis was performed using a two-way analysis of variance (ANOVA) to assess the effects of release time (24 versus 48 hours). Individual comparisons between PU and the NCs were made with Dunnett's test. Significant difference was indicated by $p<0.05$. Details of the analysis can be found in Appendix A.2.

4.2.2.2 Surface heparin

The amount of heparin left on the surface of the coils after drug release was measured by a modified method which was initially developed by Smith *et al*. [232]. Toluidine blue reacts with heparin under acidic conditions and this complex dissociates in a basic medium where the dye concentration can then be measured through spectroscopy. Coils after drug release studies were added with HCl/0.2wt% NaCl (0.01M, 300µl) and 500µl of 0.04wt% toluidine blue in aqueous HCl/0.2wt% NaCl (0.01M). After 4 hrs of shaking with toluidine blue, the coils were carefully washed with HCl/0.2wt% NaCl (0.01M) until no toluidine blue was seen in the washing media. The coils were then added with 4/1 (v/v) mixture (200µl) of ETOH/0.1M NaOH. After 10 mins, the solution (150µl) was added with HCl (10µl, 2M) and the dye concentration was measured at 620nm.

Calibration curves were made by mixing various concentrations of heparin with PBS. Using the same method as described previously, each concentration (200µl) was added with HCl/0.2wt% NaCl (0.01M, 300µl) and subsequently 500 µl of 0.04wt% toluidine blue in aqueous HCl/0.2wt% NaCl (0.01M). The mixture was then shaken for 4 hrs and centrifuged at 14000rpm for 5 minutes. The precipitate was then carefully washed with HCl/0.2wt% NaCl (0.01M) and dissolved in 4/1 (v/v) mixture (200µl) of ETOH/0.1M NaOH. From this solution, 150µl was added with HCl (10µl, 2M) and the dye concentration was measured. Statistical analysis was conducted using a two-way analysis of variance (ANOVA) with a fixed factor (material). Comparison between coils was made using Tukey's method. A p-value <0.05 was used to indicate a significant difference. Detailed description of the statistical analysis can be found in Appendix A.2.

4.2.3 Biological activity of coating

4.2.3.1 Static thrombin generation assay

Blood was collected through venipuncture from donors[4] that had not taken aspirin or any anticoagulants for at least 2 weeks prior to the experiment. Blood (9 part) was collected in a plastic tube containing 0.13M sodium citrate (1 part). Platelet rich plasma (PRP) was isolated by centrifuging whole blood at 200 *g* for 15 min.

Each static thrombin generation assay was performed with PRP from a single donor to ensure consistency. A pilot study was first conducted on samples that have been washed

[4] Approved by the Ethical Committee of Maastricht University (Maastricht University Medical Centre)

for different periods of time. Samples were washed prior to the start of the experiment for 1 , 24 , 48 hours and 7 days. The aim of this experiment was to examine if the surface heparin was still active after extensive washing and to determine the time required to remove to all residue heparin that could have affected the clotting time. Samples tested were PU+H and P16C-1+H.

After determining the time required to remove all residue heparin from the pilot study described previously, static thrombin generation assay was conducted on the coated coils. Two donors on different days were tested. Each assay consisted of 4 independent samples and the assay was repeated at least three times. The coils were first washed with PBS for at least 24 hours (as determined from the pilot study) to remove all loosely attached heparin. A fluorogenic substrate for thrombin, Z-Gly-Gly-Arg-AMC (Bachem Holding, Switzerland) was added to PRP to achieve a final concentration of 400μM. The PRP was then recalcified by adding $CaCl_2$ (0.5M stock solution) to a final concentration of $CaCl_2$ (20mM). Recalcified PRP (200μl) containing the fluorogenic substrate was then quickly transferred into 96 well plates that contains the coils. Absorbance was measured by a spectrofluorometer (Figure 4.2). A kinetic measurement was taken at λ_{ex} = 368nm and λ_{em} = 460nm for a total duration of 90min at 30s interval. The sensitivity was at 15 and the plates set to shake at 2s intervals and prior to test. Teflon and blank wells were used as a positive and negative control respectively.

The intensity of the readings was then converted into a thrombin concentration in nanomolars as described by Hemker *et al.* [233]. A thrombin generation curve was generated to determine the thrombin generation lag time (TGT) and peak thrombin (a

typical thrombin generation curve is shown in Appendix B.1). TGT is defined as the time at which thrombin rises steeply, marking the start of clotting. The threshold value in this experiment is taken at 2nM and the estimated time between when the blood first contact the material to when it rises above 2nM is the lag time (TGT). Therefore, materials that are more thrombogenic have shorter TGTs compared to materials that are less thrombogenic.

Statistical analysis was performed using a two-way analysis of variance (ANOVA) to assess the effects of washing time on TGT. Individual comparisons between PU and NCs were made with Dunnett's test. A second two-way analysis (ANOVA) was performed to assess the difference between coils with and without heparin. Significant difference was indicated by $p<0.05$. Details of the analysis can be found in Appendix A.2.

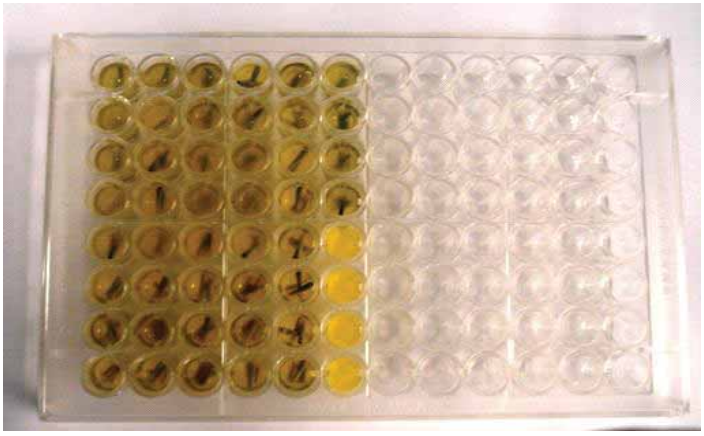

Figure 4.2 Coils in PRP for static thrombin generation assay.

4.2.3.2 Dynamic thrombin generation assay

Whole blood was collected in a similar procedure as the static thrombin generation assay but was used directly without the need of isolating PRP. The apparatus (37˚C) was set up according to the diagram illustrated in Figure 4.3. There were 2 inlet ports where the larger inlet port of the setup supplied citrated whole blood, while the smaller inlet port supplied $CaCl_2$ (0.2M). The coils were connected to the outlet port. Two syringe pumps (Harvard Apparatus, syringe infusion pump 22) were used to maintain constant flows of 76.5µl/min for citrated blood and 8.5µl/min for $CaCl_2$, generating a total flow rate of 85µl/min and a shear rate of approximately $44s^{-1}$ within the tubes. The total flow rate was chosen based on previous work conducted and to achieve a flow rate that could generate sufficient clotting within the time frame of the experimental setup [234].

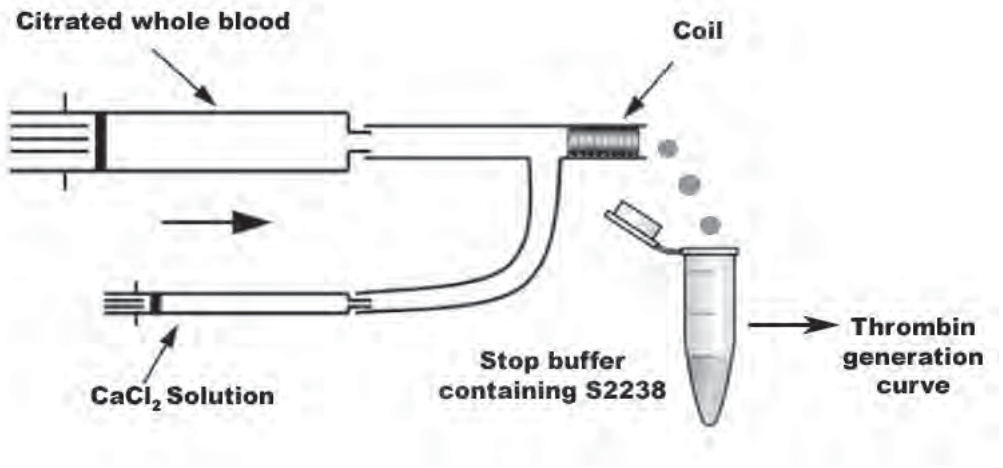

Figure 4.3 Setup of the dynamic thrombin generation assay (modified from [235]).

Prior to the start of the experiment, the coils were flushed with rinsing buffer (5ml) consisting of NaCl (140mM) and HEPES (20mM, pH 7.5) through a syringe to remove

unwanted contaminants. The effluent (25µl) was collected every 2 minutes directly into vials containing stop buffer (375ul) for a total duration of 1 hour. The vials were kept on ice to minimise enzymatic reactions. The stop buffer consisted of NaCl (140mM), HEPES (20mM), EDTA (20mM), bovine serum albumin (BSA,1mg/ml) and a thrombin-specific chromogenic substrate 2HCl·H-D-Phe-Pip-Arg-*p*Na (S2238, Celsus Biomat, 200uM dissolved in water). At the end of the experiment, the vials were centrifuged at 10,000 rpm for 5 seconds and the supernatant (200µl) was collected and transferred to a 96 well plate. Thrombin concentrations were measured using an Elx808 absorbance microplate reader (BioTek Instruments, Inc., USA) at 405nm (37^{o}C) and plotted against time to obtain the thrombin generation curve. Thrombin concentration in each vial was based on the rate of formation of *p*-nitroaniline (yellow) [236, 237]. Each assay was repeated twice from 2 donors performed on different days.

Statistical analysis was performed using Dunnett's test to compare coils without heparin to PU control. Subsequently, a two-way analysis of variance (ANOVA) was conducted to assess the effects of heparin on TGT. Significant difference was indicated by $p<0.05$. Details of the analysis can be found in Appendix A.2.

4.3 Results

4.3.1 Coating

Representative SEM images of PUNC coated coils are shown in Figure 4.4. Under SEM, the coated coils with and without heparin showed similar features and therefore only the coils without heparin were displayed. Notably, wires coated with PU showed a smoother

surface with minor debris, while NCs showed a rougher surface. The surface features between 1wt% and 5wt% loading were quite similar and the differences between P12s and P16s were not obvious.

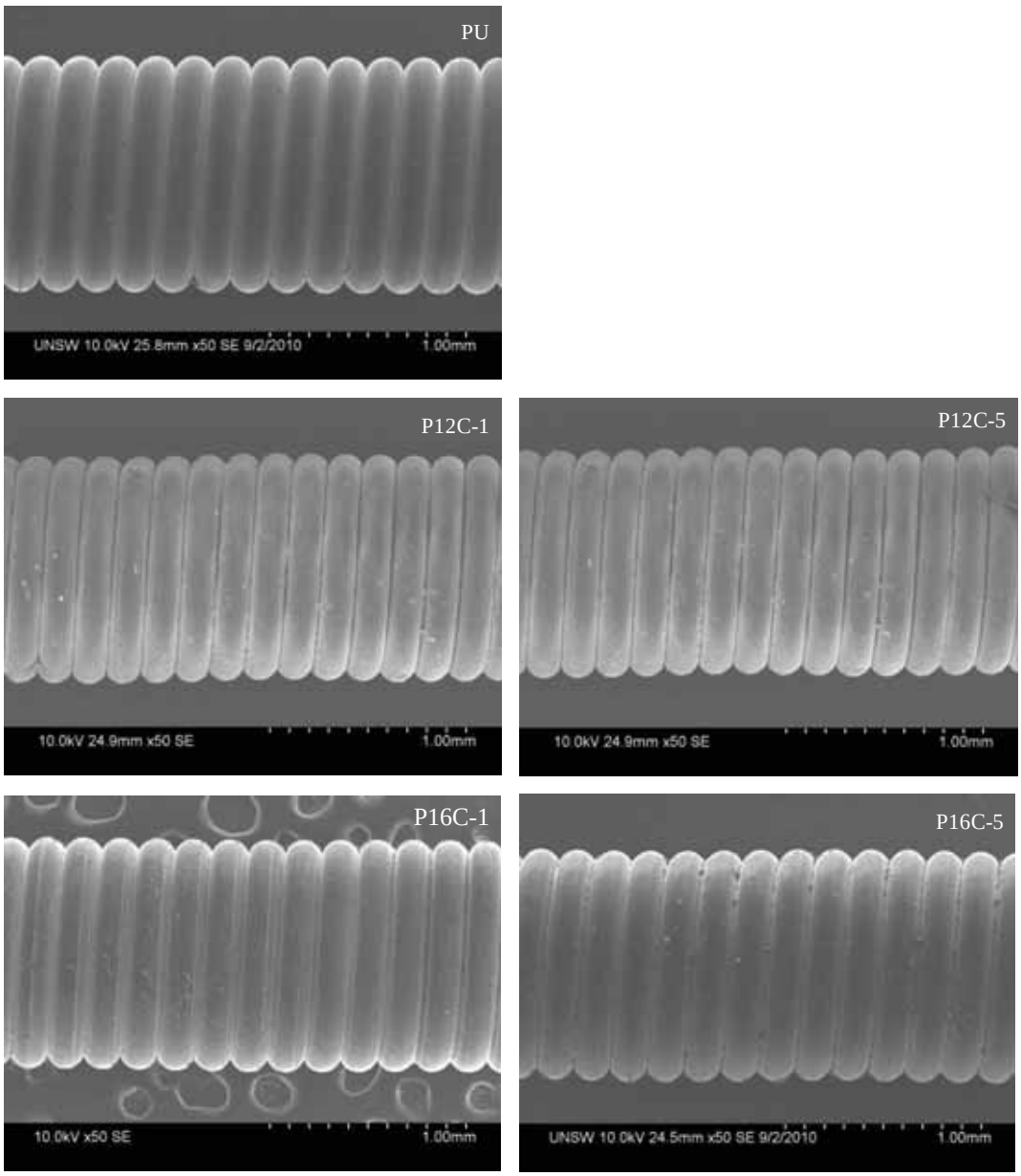

Figure 4.4 Representative SEM images of coated coils taken at 50x with incorporation of heparin (scale bar is 1mm).

4.3.2 Drug release

4.3.2.1 *In vitro* heparin release

Figure 4.5 shows the cumulative release profile of heparin from PUNC coils. All samples demonstrated a rapid initial burst followed by an early plateau. The total heparin released after 24 or 48 hours is summarised in Table 4.2, of which PU+H released the most (25% of total heparin) while P16C-1+H released the least (16% of total heparin) after 48 hours. There was minor difference in the amount of heparin released across all samples between 24 and 48 hours as indicated by the plateau in the release profile. A slight increase in heparin was observed from P16C-1+H in Figure 4.5 after 24 hours. However, when expressed in terms of percentage released, the increase was only 1-2% over 24 hours. This showed that the majority of heparin was released from the coils within the first 24 hours.

Heparin NCs modified by $12CH_3$ did not show a substantial decrease in heparin release when the clay concentration was increased from 1wt% to 5wt%. Using modifiers of longer alkyl chains ($16CH_3$), the amount of heparin released was lower than using shorter chains but the difference between the two were not significant. This implied that the majority of heparin released from the samples may be from loosely attached heparin residues on the surface after processing. The effect of silicate addition and dispersion therefore played a minor role on the release profile. However, a general trend was still observed, where PU demonstrated the fastest release and the release decreased by either increasing the clay concentration or using longer OMs.

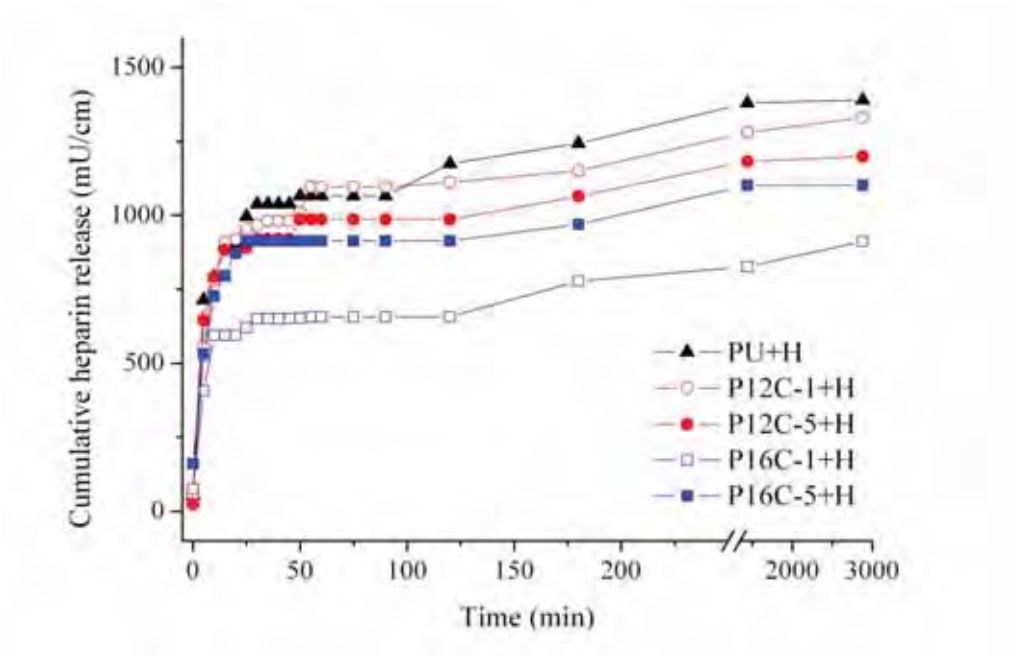

Figure 4.5 Cumulative release of samples incorporated with heparin for 48 hours (n=2). The error bars in this figure was neglected for ease of interpretation but included in Table 4.2. There was no significant difference in heparin released between 24 to 48 hours across all samples. Lines connecting each time point were included for a better representation of the trend of the samples.

Table 4.2 Summary of total heparin released. Mean % ± s.d

Material	Total heparin released (% released ± s.d)	
	24hr	48hr
PU+H	25 ± 2	25 ± 2
P12C-1+H	23 ± 1	24 ± 4
P12C-5+H	21 ± 2	21 ± 5
P16C-1+H	15 *	16 ± 2
P16C-5+H	20	20 ± 2

* Indicates significant difference compared to PU control (p=0.0586)

4.3.2.2 Surface heparin

The amount of surface heparin on the coils after release is shown in Figure 4.6. Results indicated that the amount of heparin present on the coils after 24 or 48 hours of release were not significantly different (p=0.272). This suggested that immersing coils in PBS for 24 hours would be sufficient to remove all residual heparin on the surface. This also correlated well with the heparin release study displayed in Figure 4.5, where the release profile eventually reached a plateau after 24 hours. Among the coils released for 24 hours, PU+H and P12C-1+H showed the highest amount of surface heparin with amounts of 799.8 and 776.55 mU/cm respectively.

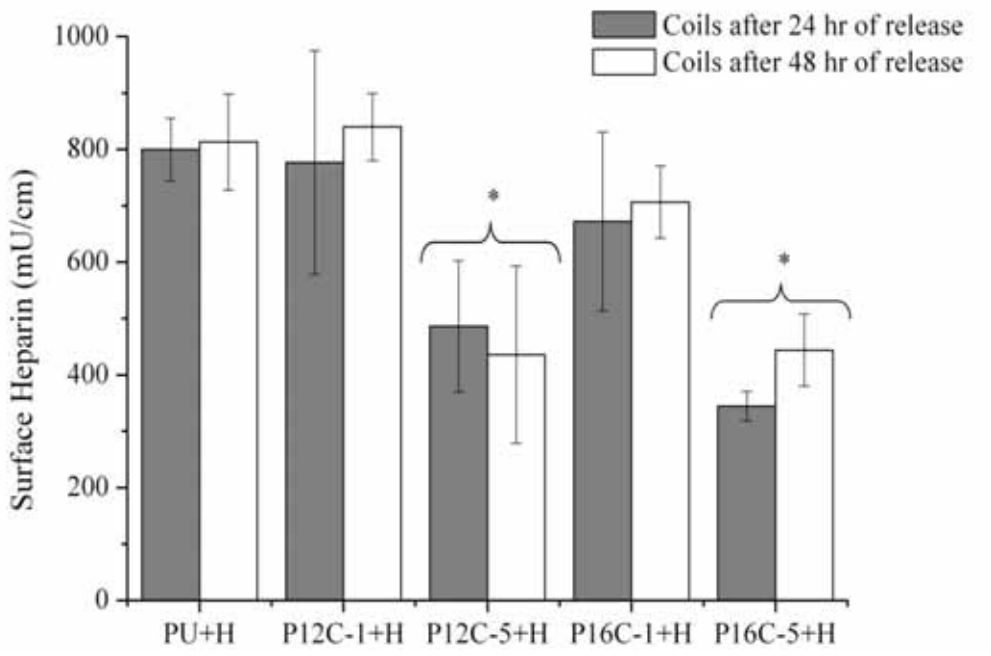

*Figure 4.6 Total amount of surface heparin on the surface of the coil. Data represents mean ± s.d. No significant differences were found between PU+H, P12C-1+H and P16C-1+H. *Denotes significant difference between 5wt% loaded NCs and 1wt% loaded NCs.*

A summary of the estimated distribution of heparin from coils released for 24 hours is presented in Figure 4.7. Interestingly, as the clay loading increases from 1wt% to 5wt%, the amount of surface heparin significantly decreases ($p<0.05$). Since this effect was observed in both modifiers, it suggested that interactions between the clay and heparin, most likely attractive interactions, could trap heparin within the bulk polymer leaving less heparin available on the surface.

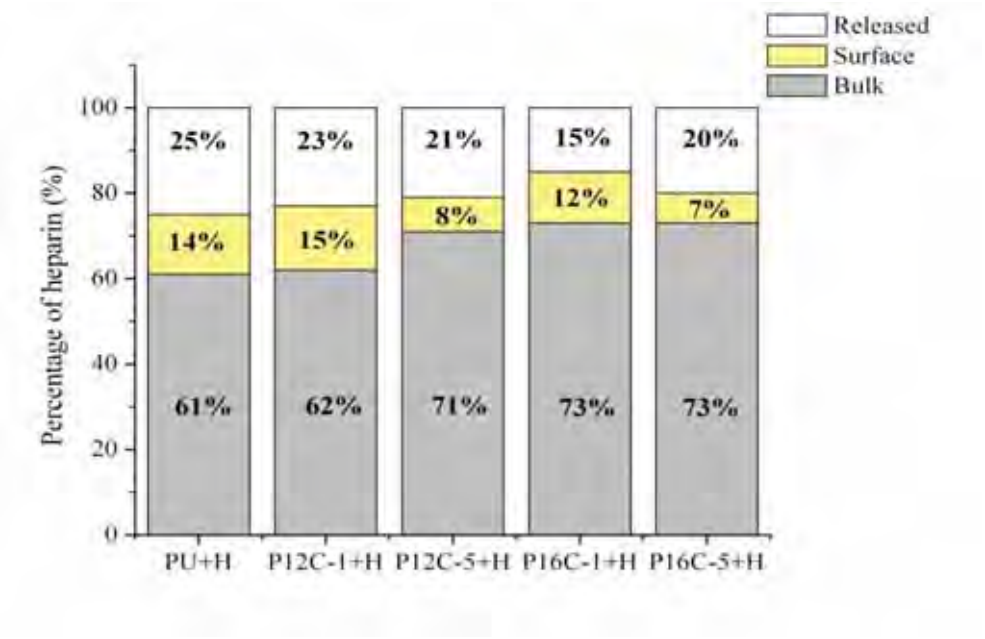

Figure 4.7 Summary of heparin released, surface bound and those remaining in the bulk polymer. Results based on coils released for a total for 24 hours.

4.3.3 Biological activity

4.3.3.1 Static thrombin generation assay

The activity of surface heparin was tested by static thrombin generation assays. Prior to testing, a pilot study to examine the effect of washing time on heparin activity was

conducted and is shown in Figure 4.8. Results suggested that all samples generated similar TGT despite the different washing times (p=0.131). This not only showed that the heparin bound on the surface was still active after washing, but a washing time of 24 hours prior to experimentation was sufficient to remove all loosely attached heparin residues. The continuous release of heparin can interfere with the results obtained from the static thrombin generation assay as the assay aims to test the activity of surface bound heparin.

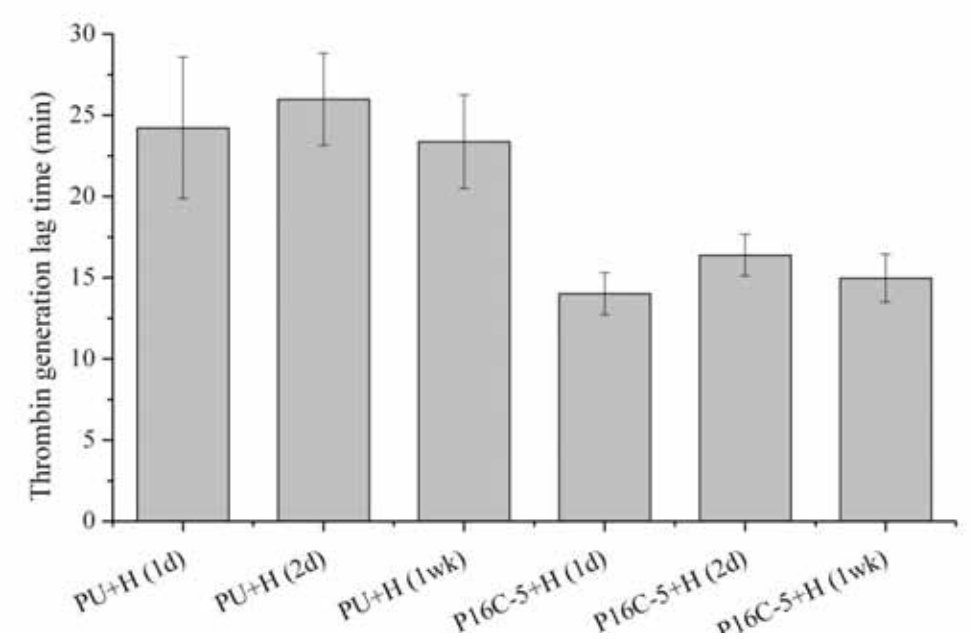

Figure 4.8 Static TGT of PU+H and P16C-5+H under washing times of 1 day, 2 days, and 1 week. Data represents mean ± s.d. Statistical analysis indicated no significant difference between the TGT of samples with respect to washing time.

Using coils that were washed for a minimum of 24 hours, the average TGT and peak thrombin for the coils is illustrated in Figure 4.9 and 4.10 respectively. Interestingly, PUNC coils without heparin displayed similar lag times to that of PU ($p=0.659$). This showed that the addition of silicate particles into PU did not increase the thrombogenicity of the material and the blood compatibility of PU was still maintained. The peak thrombin produced by the NCs without heparin was also similar to the amount produced by PU with no significant difference ($p=0.999$). On the other hand, coils loaded with heparin displayed significantly longer TGT ($p<0.05$) and lower peak thrombin ($p<0.05$) than their relative controls. This showed that the activity of heparin was preserved and was not lost during the coating process.

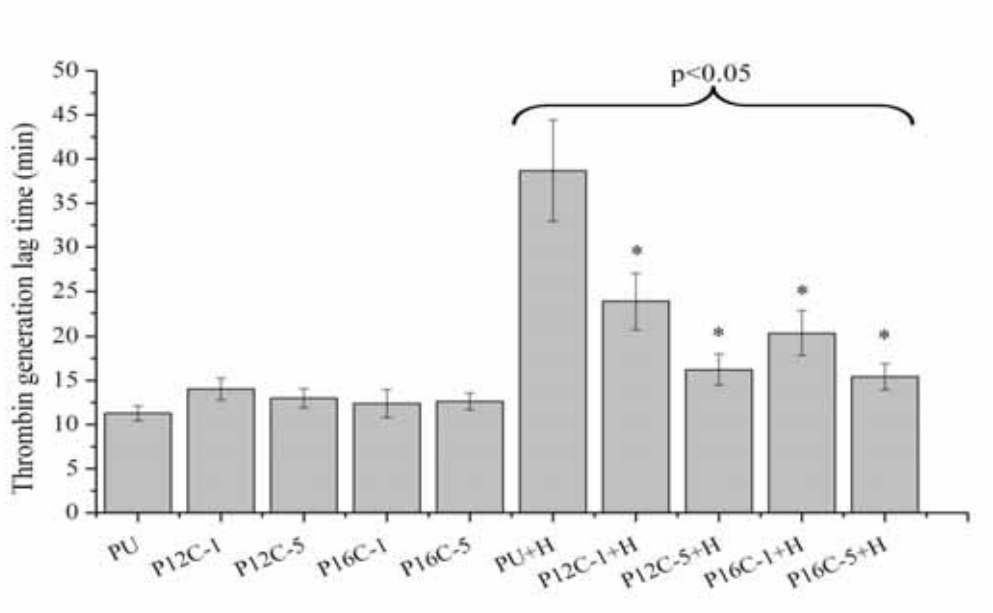

*Figure 4.9 Static TGT for coils with and without heparin conducted with PRP from 2 donors. Data represents mean ± s.d, n=3. The TGT of heparin incorporated coils were significantly different to coils without heparin ($p<0.05$). *denotes heparin incorporated coils significantly different to PU+H.*

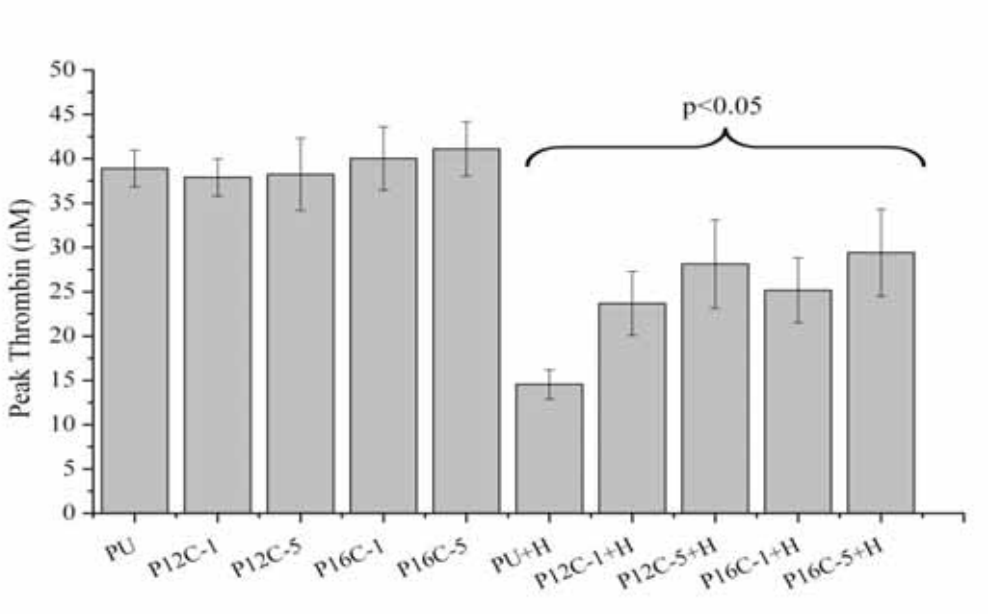

Figure 4.10 Peak thrombin of coils with and without heparin conducted with PRP from 2 donors. Data represents mean ± s.d, n=3. The peak thrombin of heparin incorporated coils were significantly different to coils without heparin (p<0.05).

The TGT for PU+H was the longest (38.67min) compared to all heparin loaded samples and was consistent with the amount of surface heparin presented previously in Figure 4.6. However, P12 NCs loaded with 1wt% clay (P12C-1+H) showed shorter TGT (23.89 min) as compared to neat PU (PU+H) despite acquiring similar amounts of surface heparin. The amount of thrombin generated was also more than PU, 23.68nM against 14.54nM. Therefore, it suggests that the interactions between clay and heparin may impact on the electrostatic interactions between the heparin, thrombin and ATIII, which decreases its activity to inhibit thrombus.

4.3.3.2 Dynamic thrombin generation assay

Dynamic thrombin generation assays allowed the interaction of the sample surface and blood to be studied continuously and closer to physiological conditions. Complete thrombin generation curves for PUNC coils with and without heparin are shown in Appendix B.2. As evident, the time taken for PU to reach the threshold (2nM) was much shorter than PU+H, reflecting the effect of heparin in preventing coagulation. The TGT under whole blood is illustrated in Figure 4.11. PU and PUNCs without heparin showed similar lag times ($p=0.190$), suggesting that adding silicate particles into PU did not decrease the thrombogenicity of PU. When compared to coils with added heparin, the TGT across all samples lengthened 2 to 3 times ($p<0.05$). The longest TGT was with PU+H, which delayed clotting to almost 4 times than that of PU.

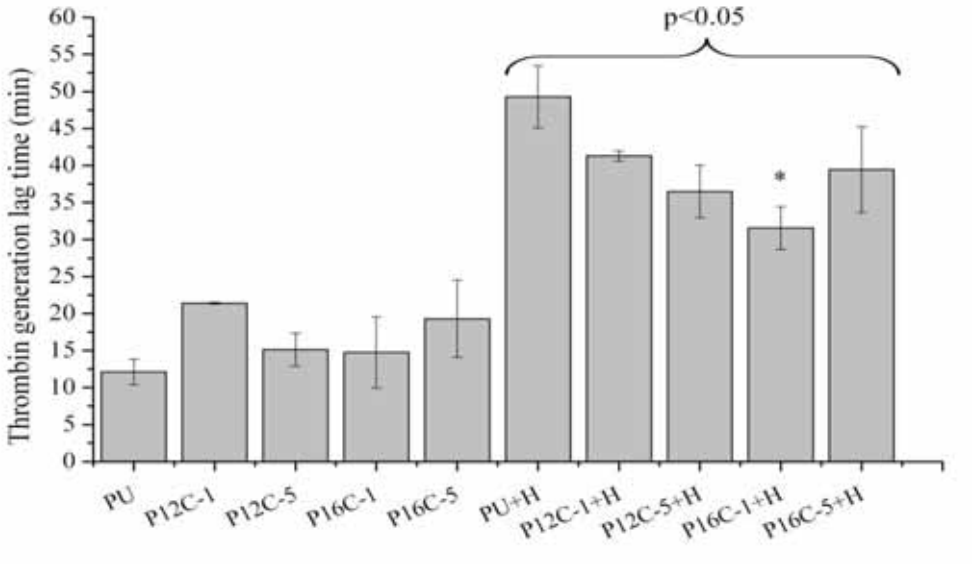

*Figure 4.11 Dynamic TGT of samples with and without heparin conducted with whole blood. The TGT of heparin loaded coils were significantly different to coils without heparin ($p<0.05$). *denotes heparin loaded coils significantly different to PU+H. Data represents mean ± s.d ($n=2$).*

A summary of the TGT of samples studied in contact with flowing whole blood is shown in Table 4.3. Similar to the findings in static thrombin generation assay, as the clay loading increased, the TGT of P12C-5+H decreased (36.5min) as compared to P12C-1+H (41.3min). This suggested that the addition of clay may have affected the activity of heparin to bind with thrombin. For ease of interpretation, Table 4.4 presents a summary of the results for coils with added heparin.

Table 4.3 Summary of dynamic TGT for all samples. Data represents min ± s.d

Material	Without heparin (min ± s.d)	With heparin (min ± s.d)
PU	12±2	49±4
P12C-1	21	41±1
P12C-5	15±2	37±4
P16C-1	13±5	32±3*
P16C-5	19±5	39±6

* Significant difference compared to neat PU control ($p<0.05$)

Table 4.4 Summary of coils with added heparin

	Amount heparin after 24 hours (mU/cm)		TGT (min)	
	Released	Surface	Static	Flow
PU+H	1380 ± 137	800 ± 56	39 ± 6	49 ± 4
P12C-1+H	1281 ± 74	777 ± 198	24 ± 3*	41 ± 1
P12C-5+H	1183 ± 120	486 ± 116*	16 ± 2*	37 ± 4
P16C-1+H	827 ± 3*	672 ± 159	20 ± 3*	32 ± 3*
P16C-5+H	1102 ± 361	344 ± 26*	15 ± 2*	39 ± 6

* Significant difference compared to PU+H control ($p<0.05$)

4.4 Discussion

The presented results showed that using static and dynamic thrombin generation assays, the addition of OMS did not alter the thrombogenicity of pristine PU. Both PU and PUNC coated coils demonstrated good bonding with no observable breakage. Due to the large molecular size of heparin, drug release results indicated a large burst release that was mainly from loosely attached heparin on the surface. Increasing the clay content however, led to a decrease in the total amount of heparin released which could be due to electrostatic interactions between the clay and heparin. Interestingly, heparin released from PUNCs was less effective in delaying thrombin generation than heparin that was released from pristine PU. It is possible that interactions between clay-heparin influenced the formation of the ternary complex between heparin, thrombin and ATIII.

4.4.1 Feasibility study in blood related application

PUNC coils without heparin were examined for their thrombogenicity as compared to neat PU. The addition of silicate particles increased the surface roughness and debris on the coating as evidenced by SEM, but had no effect on the blood compatibility as compared to neat PU. It was observed that the addition of clay to form a NC produced similar TGTs to that of neat PU. Although there were reports suggesting that the covalent binding of PU with linear alkyl chains (16 carbon chain or 18 carbon chain) could reduce the amount of thrombin deposition [238], the results obtained in this study showed no observable trends between clay loading and the use of longer OM chains. The alkylation of PU surfaces was known to increase the initial adsorption of albumin on the surface which reduces platelet and leukocyte adhesion, thereby inhibiting thrombus formation [225, 239]. Binding between albumin and alkyl chains arises from the hydrophobic interactions between the chains and the amino acids, and this binding strength was said to increase with increasing carbon chain length [240].

Comparing between PU and PUNCs, a trend of increasing TGT was not observed with the use of either 12 or 16 carbon chain modifiers. A slight increase in TGT between the PUNCs and PU in the dynamic setup was observed, but statistical analysis did not indicate a significant difference. It is possible that the binding of clay with OM prevented modifiers rising to the surface of the NC, therefore the chances for albumin to interact with free alkyl chains were largely limited. Nevertheless, TGT was maintained with the addition of clay, showing that PUNCs can be used in blood related applications.

The incorporation of heparin into both PU and PUNCs improved the TGT under static conditions, suggesting that heparin was not degraded during fabrication. To inhibit thrombin, heparin must directly bind to both thrombin and ATIII to form a ternary complex [241]. A minimum of 18 saccharide sequence of heparin is necessary to bind to thrombin and a high-affinity pentasaccharide sequence to bind ATIII. Unfractionated heparin used in this study consisted of varying lengths between 10-50 saccharides [241]. Chains lacking the 18 saccharide units, such as the majority of low molecular weight heparin (average 6-30 saccharides), still contain the pentasaccharide sequence necessary to bind to ATIII that can then directly bind to factor Xa [241]. This meant that although heparin expressed on the surface have chains still trapped within the polymer, the parts that were exposed were still sufficient to inhibit thrombus formation.

4.4.2 Identification of issues for future research

Heparin, being a direct inhibitor of thrombin and factor Xa, was chosen as the anti-thrombotic agent in this study. The accelerated binding of ATIII for thrombin was proposed by Byun *et al*. [205] to be from a heparin-induced conformational change in ATIII, which exposes the reactive sites for binding to thrombin. One of the specific aims for this chapter was to examine the impact of silicate loading and dispersion in modulating heparin release. However, the cumulative release of heparin from the coated coils suggested that heparin may not be the ideal drug to release from a NC system, but more of a drug for surface modification to improve blood compatibility.

Although a general trend in the release profile was seen to be related to the clay loading and OM chain length, the differences in total heparin released were small. Along with a large burst effect, results suggested that the heparin released was more from residues that were loosely attached on the surface of the coil. In addition, by correlating the drug release results with the amount of heparin on the surface (Figure 4.7), the retardation in heparin release with increasing clay content was more related to heparin being trapped within the bulk polymer by interactions with clay rather than through diffusion. Hence, PUNCs that uses longer alkyl chains (P16) allowed more interaction between clay-heparin since the dispersion was better, therefore leaving less heparin available on the surface as well as to be released.

Interactions between clay-heparin could actually retard the release if heparin was to follow the tortuous pathway model and diffuse out of the polymer. The fact that the release of heparin reached a plateau in the early stages, suggested that the trapping of heparin within the bulk polymer could also be related to the size of heparin. This was also observed in studies conducted by Lv *et al.* [242], where heparin was released quickly within the first hour reaching a maximum amount of only 6.15% and 7.19% for 3wt% and 5wt% loaded heparin respectively. The conventional heparin used in this study was unfractionated with a mean heparin molecular weight of 15000 Dalton [243]. Future studies involving heparin release could use low molecular-weight-heparin (LMWH) with an average molecular weight (MW) of 4500 Dalton or other anti-platelet drugs instead [243].

In relation to biological activity of the released heparin, despite having similar amount of surface heparin as PU (Table 4.4), P12C-1+H demonstrated a shorter TGT. A similar observation was also seen in P16C-1+H (20.3 min) when compared to PU+H (38.7 min). It was thought that the interactions between clay-heparin may have neutralised parts of the heparin which in result affected the formation of the ternary complex.

Supporting this from literature was that at physiological conditions, heparin and ATIII are both negatively charged and thrombin is positively charged. The accelerated action of heparin results from cooperative electrostatic interaction with thrombin and simultaneous non-ionic with ATIII, where tryptophanyl residues in ATIII were regarded as the non-ionic binding sites for heparin [244]. As OMS involves modifiers have positively charged head groups and regions of negative charges from non-exchanged clay surfaces, the interactions between clay-heparin most likely influenced the ability of heparin to bind to both ATIII and thrombin. Similarly, Heuck *et al*. [244] reported that the hydrolysis of a few N-sulfate residues (negatively charged) on heparin might be sufficient to terminate the action of heparin *in vivo*. The intra-molecular charge neutralisation after hydrolysis may prevent heparin from adapting a stretch out conformation, therefore the interaction sites available with further thrombin is impaired [244].

The decrease in TGT for all heparin added samples under the dynamic set up was less pronounced than static due to the combined effect of loosely attached heparin and surface bound heparin. The TGT of P12s at 1wt% loading with heparin was longer than at 5wt%, which was consistent with higher amounts of surface heparin and from the

lesser interaction between clay and heparin. Contrary to this, P16C-5+H showed longer TGT compared to P16C-1+H when the clay loading was higher and surface heparin was much less. Since the results from static thrombin assay indicated that P16C-5+H had shorter TGT than P16C-1+H, the longer TGT of P16C-5+H in the dynamic set up can be attributed to the effect of loosely attached heparin. Along with the observation that higher amounts of heparin was released from P16C-5+H than P16C-1+H, these results suggested that loosely attached heparin residues could have a more dominant effect on inhibiting thrombus compared to surface bound heparin. This was consistent to the study conducted by Park *et al*. [218] where the grafted heparin on PU surface had only 20% bioactivity as compared to raw heparin.

4.5 Conclusion

PUNCs were successfully coated onto stainless steel wires with no observable breakage or delamination when the wires were coiled. The addition of silicate particles increases the surface roughness and debris, but had no effect on the blood compatibility as compared to PU. Both PUNC and PU coated coils without heparin demonstrated similar TGTs, indicating that the NC system does not increase the material's thrombogenicity and would be suitable for blood contacting applications.

The large burst effect and low amounts of heparin released from coils suggested that the release was mainly from loosely attached heparin residues on the surface rather than via diffusion from the bulk polymer. A small change in release by using higher clay loadings and longer OM chain lengths was assumed to be from interactions between

clay-heparin trapping it within the polymer. The large molecular size of heparin also limited diffusion through the PU matrix. Investigations using LMWH, aspirin, or other such smaller size molecules might allow a better assessment on the impact of silicate loading and dispersion on drug release behaviour.

The addition of heparin into PUNCs prolonged the TGT, indicating that heparin was still active after the coating process. An improvement in TGT was most apparent in the dynamic thrombin generation assay, suggesting that loosely attached heparin was more effective in inhibiting thrombus than surface bound. An interestingly observation derived from the comparison between static thrombin generation assay and surface heparin was that the TGT of NCs were lower than PU when similar amounts of surface heparin was detected. This was thought to be from competitive interactions between clay-heparin that influenced the formation of the ternary complex between heparin, thrombin and ATIII.

In summary, the feasibility of using PUNC as drug delivery coatings was shown by the good uniformity in the coating and from the maintenance of thrombin generation time compared to neat PU. Through drug release and biological assays, the results indicated that the size of drug, interactions with the NC system, and biological activities are all important factors that needs to be considered for PUNC as a controlled drug delivery system. The understanding of these factors is essential in accurately predicting the release profile and will be investigated in subsequent chapters by examining drugs with different physical and chemical properties.

Chapter 5: Impact of structure and release of model drugs with different properties

5.1 Introduction

The controlled release of drug molecules from an NC system through modulating silicate loading is based on the concept that impermeable silicate particles can modulate permeability. As previously mentioned in Chapter 2, the often used tortuous pathway model and most other mathematical models for describing barrier properties of polymer NCs do not consider the interactions between the diffusing molecule and the polymer, filler or modifier. If heparin had no interactions with the constituents of the NC system, the release would be based on the tortuous pathway model and the variables modulating release would be silicate loading and dispersion. The fact that heparin release was likely affected by electrostatic interactions with clay and by the size of the molecule (see Chapter 4) highlights the need to understand the impact of drug interactions and drug properties in the release from an NC system.

It is well known that interactions arising from van der Waals (vdW), hydrogen bonding and cation exchange processes within a MMT-drug system could affect drug release behaviour [245, 246]. Basic molecules tend to form stronger bonds with MMT and retard the release, whereas anionic and non-ionic molecules exhibit much weaker interactions with MMT, resulting in a faster release [246, 247]. Polymers can also establish weak or strong interactions with the diffusing molecules and modulate release and adsorption profiles [9, 248].

First, it is essential to understand the interactions that occur between the three components making up the NC system. Possible interactions that can occur between components of a typical polymer NC system were illustrated by Pinnavaia *et al.* (Figure 5.1) [249]. Type A interactions represent interactions between the surface oxygen of clay layers and a polymer. It was proposed that these interactions were more important than interactions between the modifier and the polymer, referred to as type B [40, 249]. However, as the presence of modifiers is essential to allow polymers to be loaded in the galleries and to increase dispersion, type B interactions cannot be neglected. Hydrogen bonding between the hydroxyl side groups of clay and the polymer could also occur and are illustrated as type C interactions [7, 40]. The addition of a 4th component, such as a drug, further complicates the system and as such must be taken into consideration when designing a controlled drug delivery system.

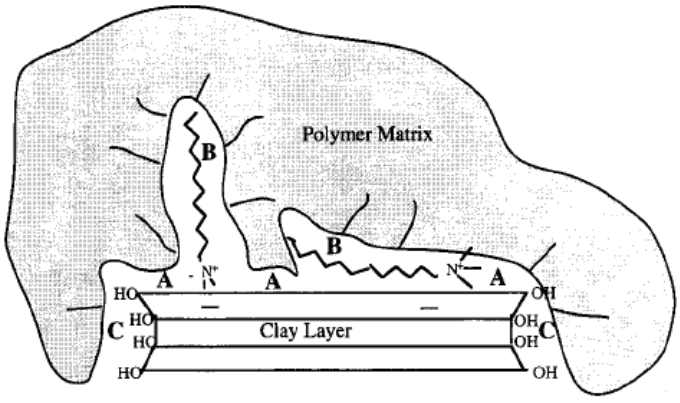

Figure 5.1 Illustration of the types of interfacial interactions occurring in polymer-organoclay nanocomposites showing direct binding of the polymer to the basal siloxane oxygen (type A interactions), modifier chains with the polymer matrix (type B interactions), and polymer binding to the hydroxyl groups at the edge (type C interactions) (Reprinted with permission from Shi et al.[249]. Copyright (1996) American Chemical Society).

Studies to date involving drug delivery from polymer NCs have shown drug release to be dependent on quantity of fillers, aspect ratio, the level of exfoliation and the ionic strength of the release medium [43, 172, 173, 250, 251]. Interestingly, very few studies have investigated the effect of drug interactions with NC components on release behaviour.

Lee *et al.* studied the release of model dyes from NCs based on negatively charged clays such as MMT (Closite® 30B) [173] and bentonite (modified with 3-acrylamidopropyl trimethyl ammonium chloride) [172], and positively charged clay hydrotalcite (modified with 2-acryloylamido-2-methyl propane sulfonic acid) [251, 252] in poly (acryl amide) or poly (acrylic acid) based hydrogels. As the gel was anionic, loading and release were found to depend on crosslink density and swelling ratio of the hydrogels when uncharged molecules were introduced [172, 251]. When the charge between the drug and the system was the same, a higher release ratio was observed. Conversely, when the charge between the drug and the system was opposite in charge, the release decreased due to attractive forces [173, 253]. It is important to note however, that these studies were performed in hydrogels that are based on hydrophilic polymer chains and have high water content. Organic thermoplastic elastomers are quite different in their morphology and behaviour as NC and as drug release systems.

Since NC barrier properties are related to structure and dispersion of the nanoparticle, developing knowledge on the impact of adding a fourth component, such as a drug on existing NC structures, is critical in understanding the release mechanisms. Therefore, the hypothesis in this study was that incorporating a fourth component into the PUNC system will affect the structure and resulting silicate dispersion. This

will impact on the drug release behaviour in a manner directly related to the physical and chemical properties of the added drug. The specific aims of this study were to:

1. Determine the impact of incorporating hydrophilic model drugs with different size, charge and polarity on the structure and silicate dispersion within a PUNC system.

2. Examine the specific inter-component interactions and their effects on the drug release behaviour of PUNCs.

5.2 Materials and methods

5.2.1 Nanocomposite preparation

Materials prepared in this study were similar to those described in Chapter 3, except that during mixing, the model drugs crystal violet (CV, Sigma Aldrich), bromophenol blue (BB, Sigma Aldrich), or Coomassie blue (CB, Sigma Aldrich) were added to the PU/DMAc solution simultaneously with the OMS.

The model drugs were added at 1wt% (g model drug/100 g PU) and as listed in Table 5.1. Samples listed in Table 5.1 were characterised by XRD using the same parameters described in Chapter 3 to examine the change in basal spacing after addition of the model drug. PUNCs were labelled according to abbreviations described previously in Chapter 3. PUNC samples modified with $12CH_3$ or $16CH_3$ are still labelled with prefix P12 or P16 respectively. Samples incorporated with model drugs however, have an additional suffix labelled either CV, BB, or CB.

Table 5.1 Materials investigated within Chapter 5

Material ID	OMS	Loadings (g/100g PU)	
		Clay	Model drug
Crystal violet			
PU+1%CV	-	-	1
P12C-1+1%CV	$12CH_3MMT$	1	1
P12C-3+1%CV	$12CH_3MMT$	3	1
P12C-5+1%CV	$12CH_3MMT$	5	1
P16C-1+1%CV	$16CH_3MMT$	1	1
P16C-3+1%CV	$16CH_3MMT$	3	1
P16C-5+1%CV	$16CH_3MMT$	5	1
Bromophenol blue			
PU+1%BB	-	-	1
P12C-1+1%BB	$12CH_3MMT$	1	1
P12C-3+1%BB	$12CH_3MMT$	3	1
P12C-5+1%BB	$12CH_3MMT$	5	1
P16C-1+1%BB	$16CH_3MMT$	1	1
P16C-3+1%BB	$16CH_3MMT$	3	1
P16C-5+1%BB	$16CH_3MMT$	5	1
Coomassie blue			
PU+1%CB	-	-	1
P12C-1+1%CB	$12CH_3MMT$	1	1
P12C-3+1%CB	$12CH_3MMT$	3	1
P12C-5+1%CB	$12CH_3MMT$	5	1
P16C-1+1%CB	$16CH_3MMT$	1	1
P16C-3+1%CB	$16CH_3MMT$	3	1
P16C-5+1%CB	$16CH_3MMT$	5	1

5.2.2 Attenuated Fourier Transform Infrared Spectroscopy

Attenuated total reflection FTIR (ATR-FTIR) was utilised to examine possible interactions between the model drug and constituents of the PUNC system by analysing the bond vibrations and the frequencies at which they occur. Samples were subjected to frequencies over the range of 4000-700cm^{-1}, at a resolution of 4cm^{-1} for a total of 32 scans, using a Bruker IFS66/S High End FT-NIR/IR Spectrometer with a diamond crystal ATR attachment. The ATR-FTIR spectrum was baselined at numerous locations across the spectral range using the supplied software (OPUS), and the data normalised to the C-C bond of the aromatic ring at 1414cm^{-1}. Each sample was scanned at 3 distinct regions and one of the spectra was chosen for representation.

FTIR was used to characterise PUNCs fabricated with 12CH_3MMT only since the spectra of 12CH_3MMT and 16CH_3MMT differed only by the intensity of CH_2 stretching (see Appendix C.1 for FTIR spectra). Therefore the analysis of one particular type of OMS would be sufficient to represent the interactions between the model drug and the PUNC system. Table 5.2 shows samples with various loadings of model drugs prepared for FTIR analysis.

In order to examine the interactions between just 2 components; OMS and the model drug, Hanley *et al*. [254] described a method used to prepare suspensions of OMS that can be mixed in with the model drug. A 5 w/w % (5 g/100 g total mixture) solution of 12CH_3MMT was prepared in Toluene. The solution was stirred for 30 minutes. Subsequently, methanol and water were added and stirred for another 30 minutes. Required amounts of model drug were added and stirred for a further 10

minutes before being dried overnight in a 60°C oven. The dried OMS was ground and stored away from light until analysis. Samples prepared by this method are listed in Table 5.3.

Table 5.2 PUNCs incorporated with model drugs with same clay loading

Material ID	Nanofiller	Loadings (g/100g PU)	
		Clay	Model drug
Crystal violet			
P12C-3+1%CV	$12CH_3MMT$	3	1
P12C-3+3%CV	$12CH_3MMT$	3	3
P12C-3+10%CV	$12CH_3MMT$	3	10
Bromophenol blue			
P12C-3+1%BB	$12CH_3MMT$	3	1
P12C-3+3%BB	$12CH_3MMT$	3	3
P12C-3+10%BB	$12CH_3MMT$	3	10
Coomassie blue			
P12C-3+1%CB	$12CH_3MMT$	3	1
P12C-3+3%CB	$12CH_3MMT$	3	3
P12C-3+10%CB	$12CH_3MMT$	3	10

Table 5.3 OMS incorporated with model drugs

Material ID	Nanofiller	Added clay(ml) (5wt% suspension)	Added model drugs (mg)
Crystal violet			
CV12MMT-1	12CH_3MMT	1	1
CV12MMT-30	12CH_3MMT	3	30
Bromophenol blue			
BB12MMT-1	12CH_3MMT	1	1
BB12MMT-30	12CH_3MMT	3	30
Coomassie blue			
CB12MMT-1	12CH_3MMT	1	1
CB12MMT-30	12CH_3MMT	3	30

5.2.3 In vitro drug release

In vitro drug release studies were conducted at an initial model drug loading of 1wt% (g drug/100g PU). This particular loading was chosen due to the similarity in drug concentration with commercially available drug eluting stents (140 ug/cm^2 for Cypher™ and 100-400 ug/cm^2 for Taxus™ [15]) . The concentration of model drugs in the films fabricated for this study was 168 μg/cm^2. Materials were cast directly into custom manufactured drug release pour plates as illustrated in Figure 5.2.

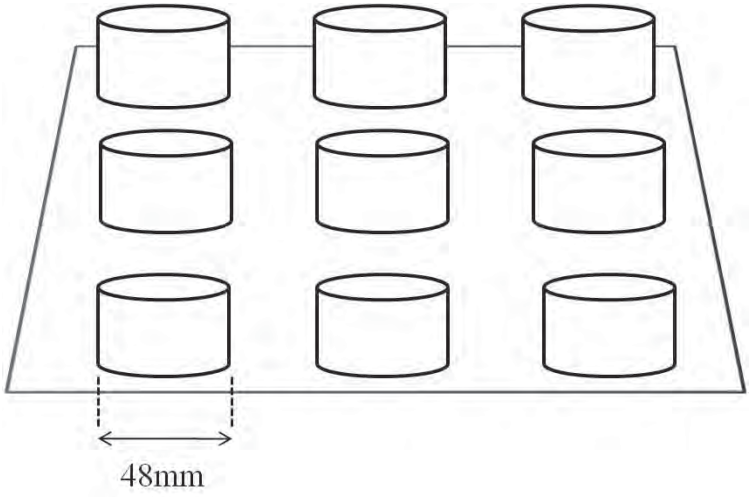

Figure 5.2 Plates consisted of 9 glass cylinders (48mm ID) attached by silicone glue to glass sheets. In this case, cast films will be consistent in thickness and will have equal area when exposed to the extracting medium.

A sink volume of 50mL (PBS, pH 7.4) was used and placed on an orbital shaker in a 37^{o}C incubator. Aliquots were taken at regular time intervals and replenished for a total of 4 weeks. The glass cylinders were sealed with paraffin to prevent evaporation. The assay was repeated in triplicate and each assay consisted of a triplicate of each material. Drug release was tracked using a UV- spectrophotometer (Varian Cary 300). The model drugs and their respective chemical structure, MW and absorbance peak are shown in Table 5.4.

Release kinetics were evaluated according to the following models: zero order kinetics (Equation 5.1), first order kinetics (Equation 5.2) and Higuchi's square root of time (Equation 5.3).

$$M = k_0 t \tag{5.1}$$

$$\ln M_t = \ln M_0 - k_1 t \tag{5.2}$$

$$M = k_H \sqrt{t} \tag{5.3}$$

Table 5.4 Structure and chemical properties of model drugs

	Crystal Violet	Bromophenol Blue	Coomassie Blue
Chemical structure	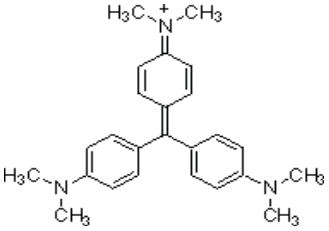	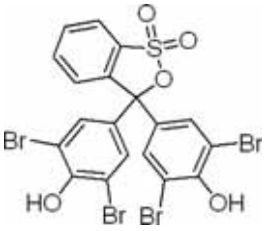	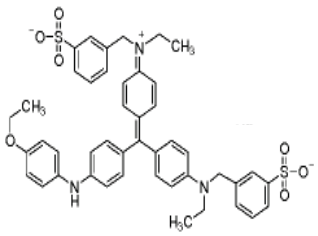
MW	407.98g/mol	669.96g/mol	825.97g/mol
Absorbance	570nm	590nm	595nm
Charge	Positive	Anionic	Positive, Negative
Solubility[a]	1mg/ml	4mg/ml	1mg/ml

[a]Aqueous solubility at 37°C [255-257]

where M is the cumulative amount of drug release, M_t is the amount of drug released in time t, M_0 is the initial amount of drug in the material, k_0, k_1 and k_H are respectively the zero order, the first order, and the Higuchi's release constant. The experimental diffusion coefficient (D) from a thin polymer film can be calculated using the equation for short time approximations, $M_t/M_\infty < 0.6$ [258-260] :

$$\frac{M_t}{M_\infty} = 4\sqrt{\frac{Dt}{\pi l^2}} \tag{5.4}$$

where M_t is the amount of drug released at time *t*, M_∞ is the total amount of drug released into the sink, *l* is the thickness of the film taken to be 140μm in this study. The diffusion coefficient can be calculated from the slope of M_t/M_∞ versus $t^{1/2}$.

5.3 Results

5.3.1 Silicate dispersion and interactions

5.3.1.1 X-ray diffraction

The effect of adding a fourth component on the dispersion of silicate particles was examined by XRD. Diffractograms of PUNCs loaded with CV, BB or CB are shown in Figures 5.3-5.5 respectively, and a summary of the silicate spacings is shown in Tables 5.5-5.7 respectively. Silicate spacings for BB loaded samples were smaller than samples without drugs added, with the exception of P12C-5+1%BB and P16C-5+1%BB that showed slightly larger silicate spacings than their relative controls. CV and CB loaded samples also showed smaller spacings compared with their relative controls, suggesting the presence of component interactions between the model drugs and the silicate particles.

Examining the spacings and diffractograms of PUNCs+CV in Table 5.5 and Figure 5.3 respectively, a peak was observed at 3.63˚ and 2.52˚ that corresponded to silicate spacings of 2.43 and 3.51 nm for P12C-1+1%CV and P16C-1+1%CV respectively. This indicated that the morphology of PUNC was intercalated even at 1wt% loading. As clay loading increases, silicate spacing decreases due to the higher tendency for clays to aggregate. On the other hand, no peaks were detected for P12C-1+1%BB and P16C-1+1%BB and the spacings were much larger than CV.

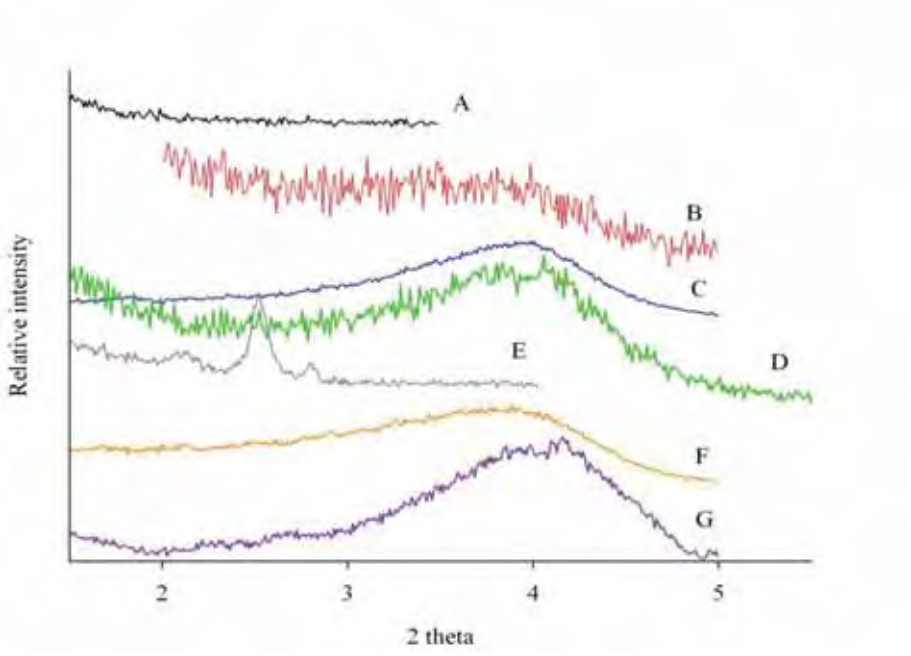

Figure 5.3 XRD diffractograms for : A) PU+1%CV, B) P12C-1+1%CV, C) P12C-3+1%CV, D) P12C-5+1%CV, E) P16C-1+1%CV, F) P16C-3+1%CV, and G) P16C-5+1%CV.

Table 5.5 XRD results for PU and PUNCs incorporated with CV

Material	2θ	Silicate spacing (nm)	
		With 1% CV	Control[a]
PU	-	-	-
P12C-1	3.63	2.43	-
P12C-3	3.82	2.31	3.40
P12C-5	3.89	2.27	2.55
P16C-1	2.52	3.51	-
P16C-3	3.72	2.38	4.78
P16C-5	3.93	2.25	3.26

[a] Silicate spacings reported in Chapter 3

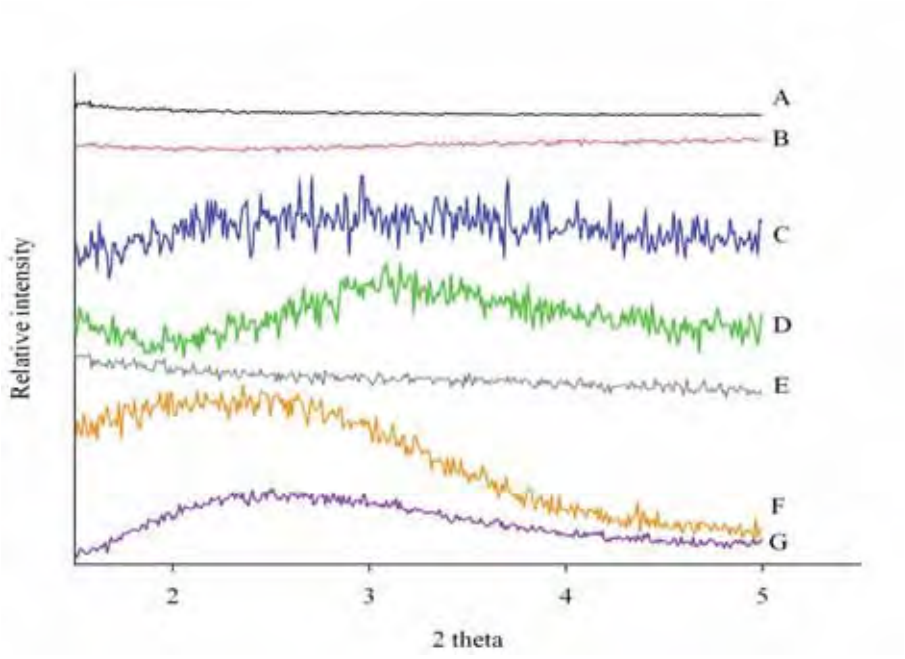

Figure 5.4 XRD diffractograms for : A) PU+1%BB, B) P12C-1+1%BB, C) P12C-3+1%BB, D) P12C-5+1%BB, E) P16C-1+1%BB, F) P16C-3+1%BB, and G) P16C-5+1%BB.

Table 5.6 XRD results for PU and PUNCs incorporated with BB

Material	2θ	Silicate spacing (nm)	
		With 1% BB	Control[a]
PU	-	-	-
P12C-1	-	-	-
P12C-3	3.04	2.91	3.40
P12C-5	3.2	2.76	2.55
P16C-1	-	-	-
P16C-3	2.25	3.93	4.78
P16C-5	2.62	3.37	3.26

[a] Silicate spacings reported in Chapter 3

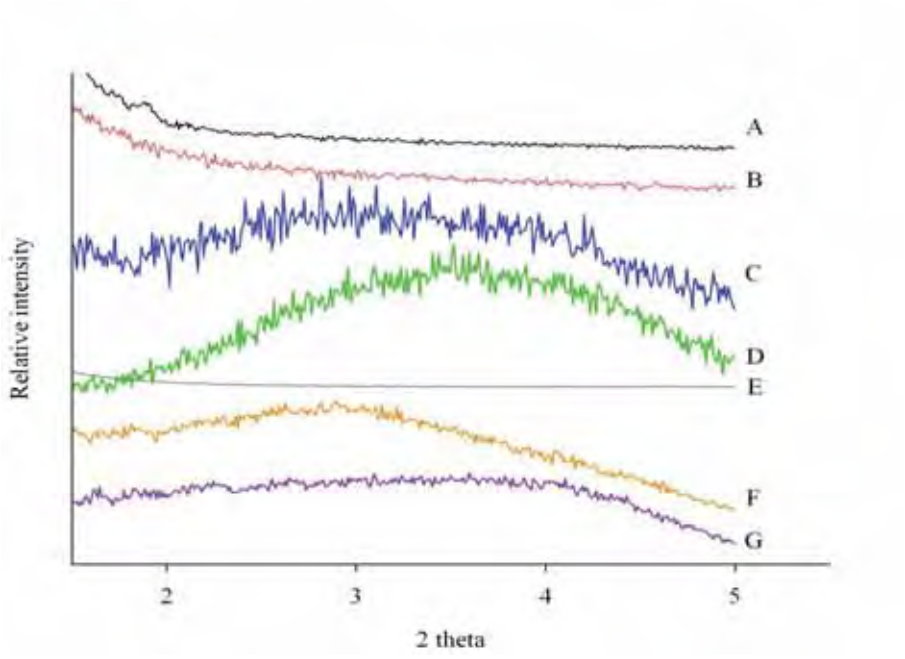

Figure 5.5 XRD diffractograms for : A) PU+1%CB, B) P12C-1+1%CB, C) P12C-3+1%CB, D) P12C-5+1%CB, E) P16C-1+1%CB, F) P16C-3+1%CB, and G) P16C-5+1%CB.

Table 5.7 XRD results for PU and PUNCs incorporated with CB

Material	2θ	Silicate spacing (nm)	
		With 1% CB	Control[a]
PU	-	-	-
P12C-1	-	-	-
P12C-3	3.03	2.91	3.40
P12C-5	3.46	2.55	2.55
P16C-1	-	-	-
P16C-3	2.8	3.16	4.78
P16C-5	3.11	2.84	3.26

[a] Silicate spacings reported in Chapter 3

Samples incorporated with CB also showed no peaks at 1wt% loading and had spacings larger than samples incorporated with CV. The use of longer chain modifiers improved the silicate spacings of PUNCs loaded with BB. This effect was not seen in samples loaded with CB. Similarly for CV, only P16 at 1wt% loading demonstrated an improvement in silicate spacing compared to P12 at 1wt% loading, while the 3 and 5wt% loading did not increase the spacing.

5.3.1.2 Attenuated Fourier Transform Infrared Spectroscopy

The ATR-FTIR spectra of OMS incorporated with various concentrations of model drugs are shown in Figures 5.6-5.8. The band assignment and wavenumbers for MMT, OMS and the three model dyes are displayed in Table 5.8. As the concentration of model drugs increases, the characteristic peaks of the model drugs become more apparent and are shown by the arrows in Figure 5.6 and 5.8. Characteristic peaks associated with BB were less apparent than CV and CB. Distinct peaks for MMT were in agreement with those reported in the literature [261, 262], and occurred at 3626 cm^{-1} (stretching of structural OH), 3425cm^{-1} (stretching of H-O-H water) and 986cm^{-1} (Si-O-Si stretch).

Successful modification of MMT was confirmed by the wavenumbers at 2926cm^{-1} and 2854cm^{-1} corresponding to the asymmetric and symmetric stretching of CH_2 respectively. The influence of incorporating model drugs in OMS structure between 3000-2800cm^{-1} is shown in Figure 5.9. OMS added with model drugs all showed similar decreases in the intensity of CH_2 stretching, but a larger shift was observed with adding CV (2927cm^{-1} to 2922 cm^{-1} and 2855 cm^{-1} to 2852 cm^{-1}). A shift was

also observed in CB but not in BB, showing that CV has stronger interactions for OMS followed by CB and lastly by BB.

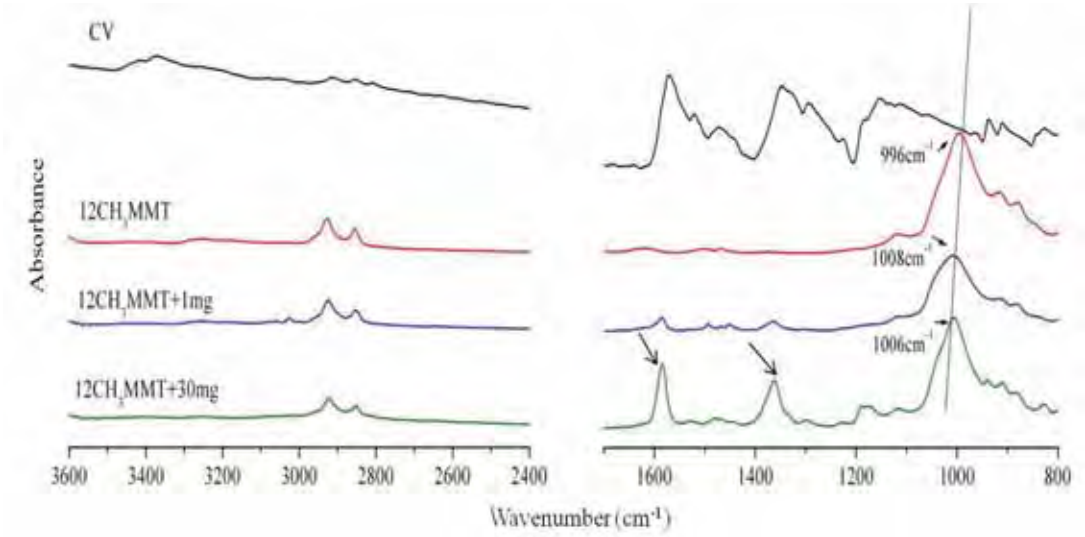

Figure 5.6 ATR-FTIR spectra of OMS added with CV. Arrow represents characteristic peaks for CV. Dotted lines represent shifts in Si-O stretch peak upon addition of modifier and drugs on MMT.

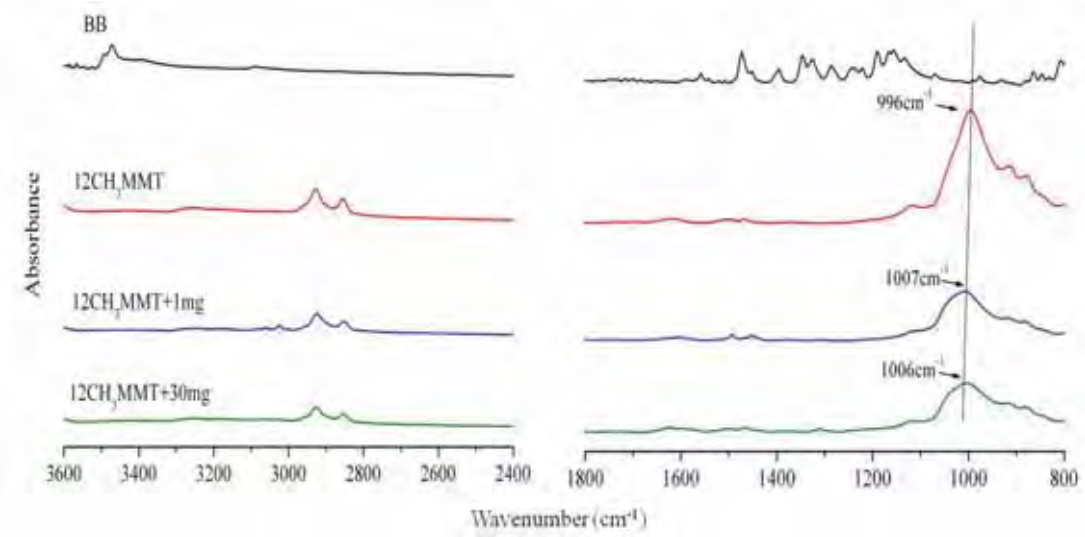

Figure 5.7 ATR-FTIR spectra of OMS added with BB. Dotted lines represent shifts in Si-O stretch peak upon addition of modifier and drugs on MMT.

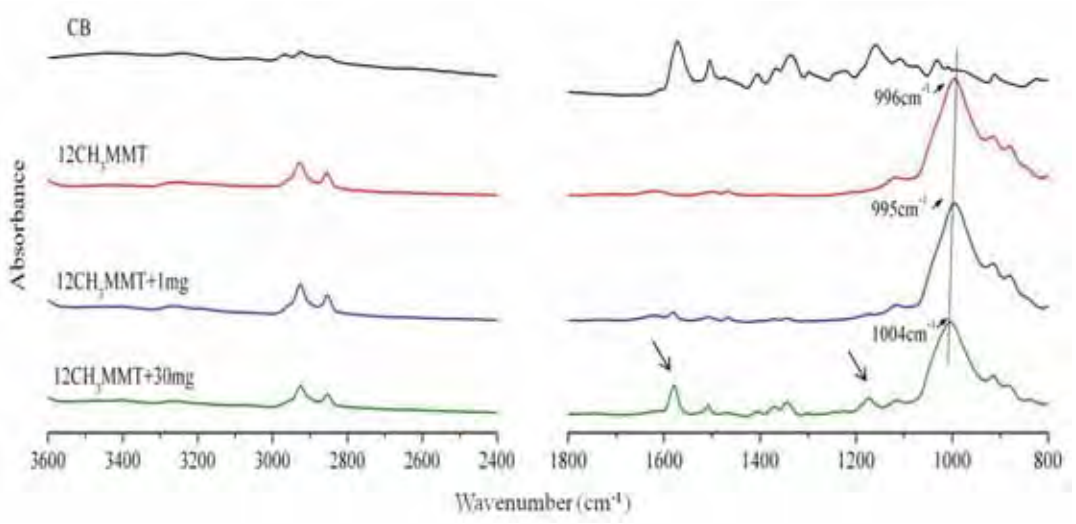

Figure 5.8 ATR-FTIR spectra of OMS added with CB. Arrow represents characteristic peaks for CB. Dotted lines represent shifts in Si-O stretch peak upon addition of modifier and drugs on MMT.

A comparison between OMS loaded with CV, BB or CB in regions 1550-1450cm^{-1} is illustrated in Figure 5.10. Peaks at 1501cm^{-1} corresponded to the bending of CH from the modifier head group [262]. The disappearance of this peak along with the formation of a doublet at 1480cm^{-1} for CV also indicated stronger interactions between OMS and CV. Contrary to this, there was neither a shift nor disappearance of peaks from the addition of BB and only a slight shift at 1508cm^{-1} was observed in OMS added with CB. FTIR spectra for PUNCs with model drugs in the regions 3600-2400cm^{-1} & 1800-800cm^{-1} are shown in Figure 5.11-5.13. All samples showed distinct peaks for PUNCs that corresponded to those reported in literature and are listed in Table 5.9 [263, 264]. Figures 5.11-5.13 compare samples with silicate loadings of 3wt% and varying in drug concentration. Any changes to the spectra from the P12C-3 control are mainly from interactions between PU and the drug. The addition of either drug did not introduce new peaks or cause major changes to PU peaks. The intensity increase at some locations was due to increases in drug concentration.

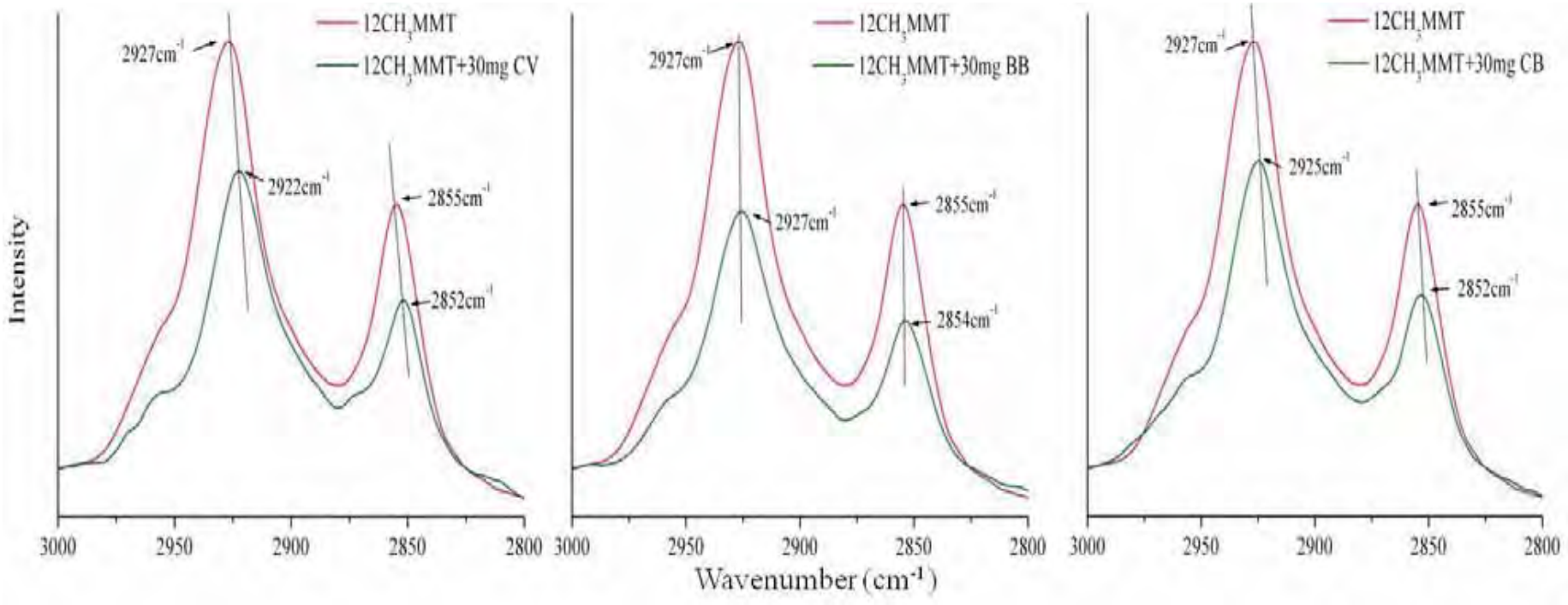

Figure 5.9 ATR-FTIR spectra of OMS added with model drugs at wavenumbers between 3000-2800cm^{-1}.Dotted lines indicate the shift in peaks and the arrows correspond to the asymmetric & symmetric stretching of CH_2 at 2927cm^{-1}and 2855cm^{-1} respectively [262].

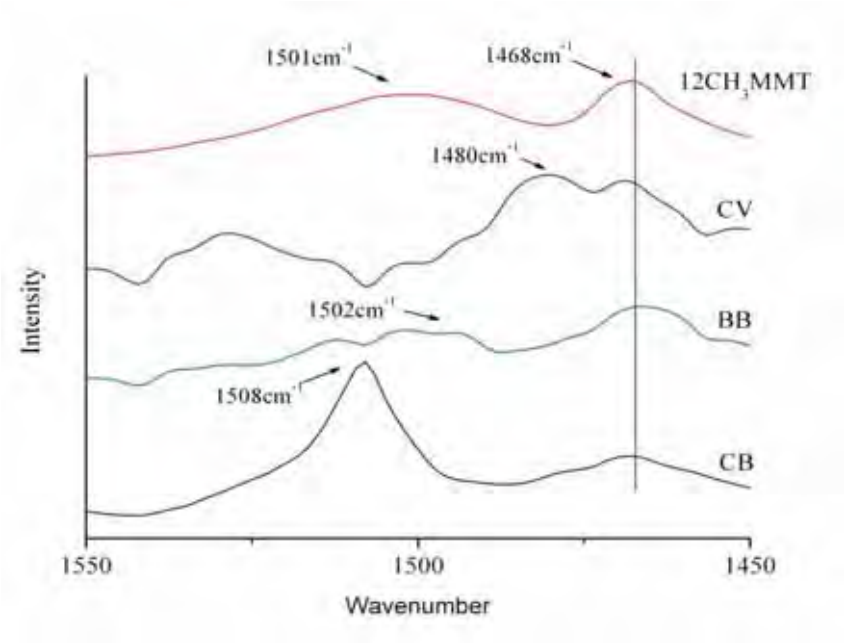

Figure 5.10 ATR-FTIR spectra of OMS added with 30mg of model drugs at wavenumbers between 1550-1450cm^{-1}.Dotted line indicates the peak corresponding to 1468cm^{-1} (Bending of CH_2).

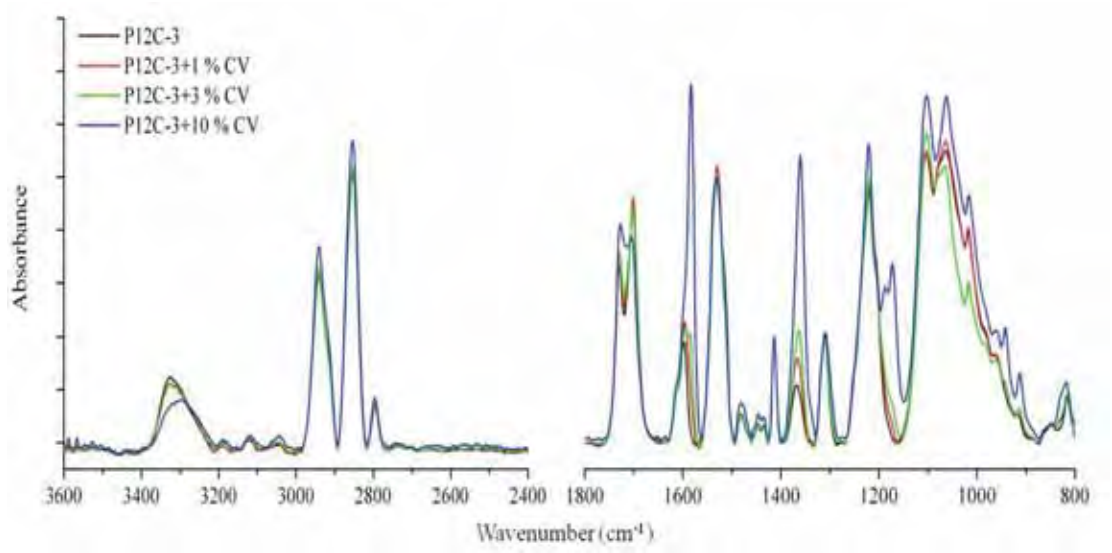

Figure 5.11 ATR-FTIR spectra for PUNC-3wt% with varying concentration of CV at wavenumbers 3600-2400cm^{-1} and 1800-800cm^{-1}.

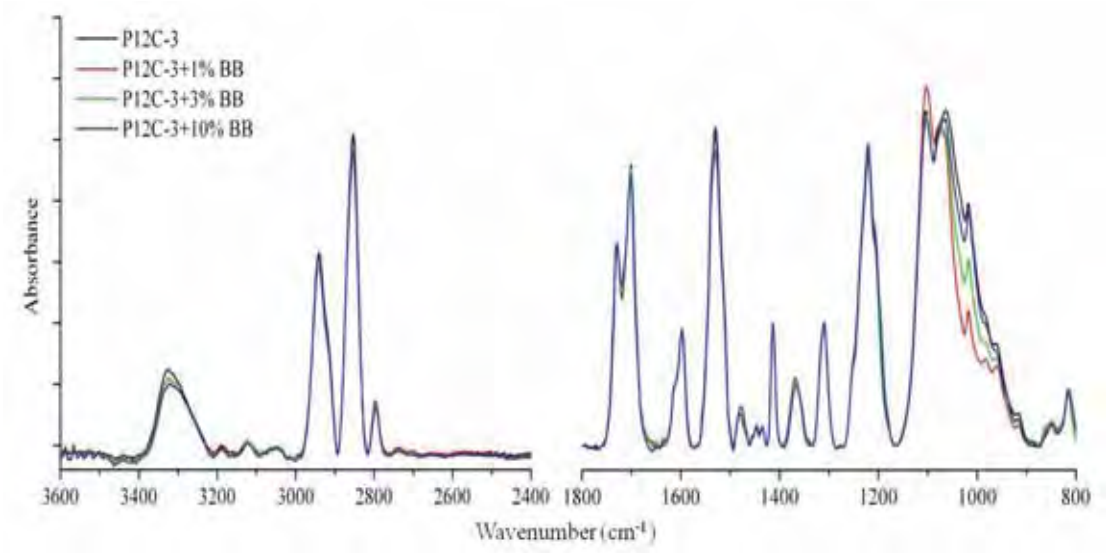

Figure 5.12 ATR-FTIR spectra for PUNC-3wt% with varying concentration of BB at wavenumbers 3600-2400cm^{-1} and 1800-800cm^{-1}.

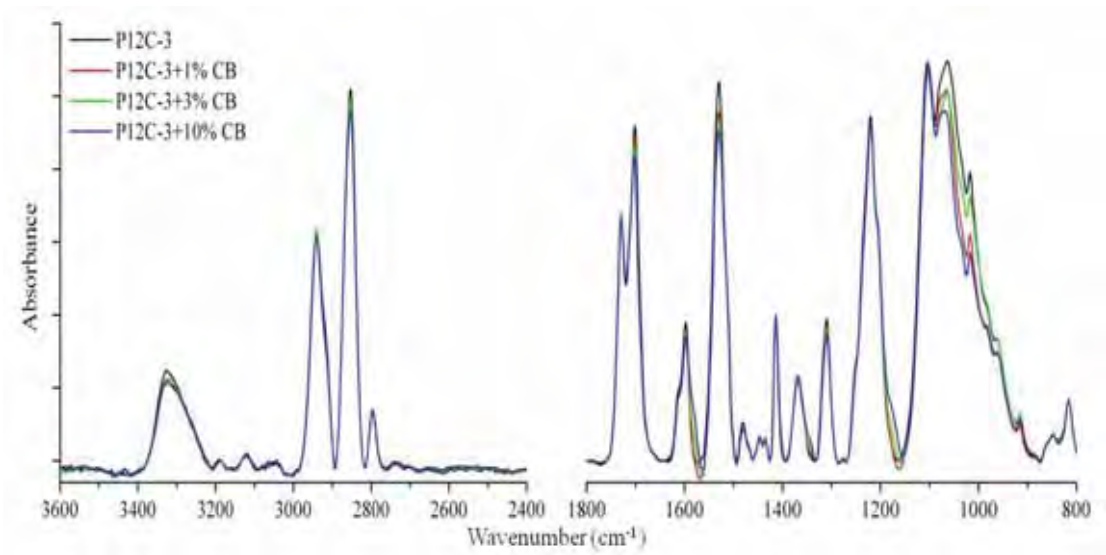

Figure 5.13 ATR-FTIR spectra for PUNC-3wt% with varying concentration of CB at wavenumbers 3600-2400cm^{-1} and 1800-800cm^{-1}.

Table 5.8 FTIR band assignments of MMT, OMS and model dyes [261, 265-269]

Wavenumber (cm^{-1})						Assignment
Literature	MMT	12CH_3MMT	CV	BB	CB	
3634-3618	3625					OH stretching vibration of structural hydroxyls
3440-3423	3425					Broad asymmetric and symmetric stretching of H-O-H water
3400-3300		3245				Asymmetric N-H stretch & symmetric N-H stretch
3330-3250						
2930		2927				Asymmetric stretching of CH_2
2856-2850		2855				Symmetric stretching of CH_2
1581			1571		1573	Symmetric stretching of aromatic ring C-C
1650-1580	1634	1618				Bending of H-O-H water & scissoring of N-H
1485		1501				Bending of C-H of CH_3
1467-1450		1468		1451,1473		Bending of CH_2 Asymmetrical bending of CH_3
1361			1348			Stretching of C-N of aromatic amine
1350-1300				1346*	1337	Stretching of C-N & asymmetric stretching of O=S=O
1172			1174			Stretching of C-N
1160-1120					1159	Symmetric stretching of O=S=O
1115-1091	1116					Stretching of Si-O-Si
1034-1027						
1005	987					
916-915	914					Bending Al_2OH
888	881					
735-715		729				Rocking of CH_2

*only asymmetric stretching of O=S=O

Table 5.9 FTIR band assignments of PUNCs and model dyes [154, 264, 270]

Wavenumber (cm^{-1})					Assignment
Literature	PU	CV	BB	CB	
3320-3305	3322				Stretching of N-H hydrogen bonded to carbonyl
2938	2941				Asymmetric stretching of CH_2
2852	2853				Asymmetric stretching of CH_2CH
2797	2797				Symmetric stretching of C-H in $–CH_2O-$
1733-1730	1730				Stretching of non-hydrogen bonded urethane carbonyl C=O
1703-1701	1702				Stretching of hydrogen bonded urethane carbonyl C=O
1597	1597				Stretching of C=C aromatic ring
1581		1571		1573	Symmetric stretching of aromatic ring C-C
1530-1529	1530				N-H bending and C-N stretching
1480-1430	1481		1451, 1473		Bending of CH_2
1367	1368				Wagging of C-H in CH_2
1361		1348			Stretching of C-N of aromatic amine
1350-1300			1346*	1337	Stretching of C-N & asymmetric stretching of O=S=O
1311-1309	1310				N-H bending and C-N stretching
1227,1219,1172	1220	1174			Stretching of C-N
1160-1120				1159	Symmetric stretching of O=S=O
1110	1103				Stretching of soft segment ether C-O-C
1081	1079				Stretching of hard segment ether C-O-C
1034-1005	1018				Stretching of Si-O-Si in MMT
960-770	961				Wagging of C-H aromatic ring

*only asymmetric stretching of O=S=O

5.3.2 *In vitro* drug release

In vitro drug release assays were conducted for samples with silicate loadings of 1 and 5wt%. Assays were conducted up to 4 weeks for CV and BB, while CB was conducted for up to 2 weeks since there was no CB detected up to that time point. Extracts from neat PU without added drugs did not interfere with the absorbance measurement for the model drugs as shown by the absence of peaks at 570nm or 590nm. All model drugs were tested for degradation in PBS or water for 2 months at 37˚C. There was no evidence of degradation with any of the drugs as there were no shifts or decreases in intensity at the absorbance peaks. The pH of model drugs in the sink medium before and after the assay were also tested. The pH of CV, BB and CB pre-assay were 4.28, 7.47 and 7.46, respectively, while the pH post-assay were 4.5, 7.35 and 7.36, respectively. The pH before and after the test were maintained, showing that all these model drugs were stable.

The cumulative release profiles of CV and BB are shown in Figures 5.14 and 5.15 respectively. In both cases, neat PU with model drugs demonstrated the largest initial release and highest total release. The initial slope for PU with BB was much steeper than PU with CV, indicating a faster initial release rate. When clays were introduced into PU, P12C-1+1%BB and P16C-1+1%BB samples still resulted in the same release profiles to that of PU+1%BB. Only when clay loading increased to 5wt%, a larger reduction in release was observed and the initial release rate became slower than both PU and the 1wt% loaded PUNCs. Contrary to this, the influence of clay addition on the release profile was larger in samples added with CV. That is, P16 NCs added with CV at clay

loadings of 1wt % and 5wt %, resulted in reductions from total release of around 25% and 80% respectively.

Interestingly, the reduction in CV release rate from increasing clay loading also resulted in a lower amount of CV released, as indicated by the plateau. Whereas for BB, the release profile for 5wt% showed lower release rates but no sign of plateau over the 4 weeks. This could imply that CV has larger interactions with silicates that prevented it from diffusing out of the system, while BB has weaker interactions with the silicates so the diffusion through the NC system is much easier. The benefit in using longer chain modifiers to further sustain the release by improving dispersion was not reflected in systems loaded with these model drugs. A lower release rate was observed in 5wt% PUNCs loaded with BB, but no difference was shown in the 1wt% loadings. On the other hand, a slightly higher release was reflected in CV loaded samples from the use of longer chain modifiers. These results suggested that the effect of clay loading had more impact to the release behaviour than modifier chain length. However, it also suggested that interactions between the OMS and model drug could play a more dominant role than clay loading in influencing the release behaviour from NC systems.

The materials containing CB did not release significant amounts of the model drug during the 2 week period as shown in Figure 5.16. The maximum release was at 2.4 %, while all other samples showed a total release between 0.1~2.1%. Therefore, CB was not studied further for its release kinetics. The limited amounts of CB released could be due to molecular size, interactions or sensitivity of the equipment. Solubility could also be another reason as it was observed that the release medium of samples with CB contained

tiny blue particles. It is unlikely that PU was degraded during the experiment, as degradation products would also be present in samples loaded with CV or BB if this was the case. Interestingly, the amount of particles were mostly found in CB loaded neat PU, followed by PUNCs at 1wt% loadings, and virtually none were found in CB loaded PUNCs at 5wt% clay loading. According to the MSDS provided by the manufacturer, CB is slightly insoluble in water, but can be made soluble by heating or constant stirring. Since sink conditions (sink volume of 50ml) were applied in the testing of CB (1mg/ml [255]), it is possible that the use of PBS as the sink environment may have an effect on the solubility of CB. An altered sink environment such as saline, distilled water or from changing pH, should allow a better assessment of the solubility of CB.

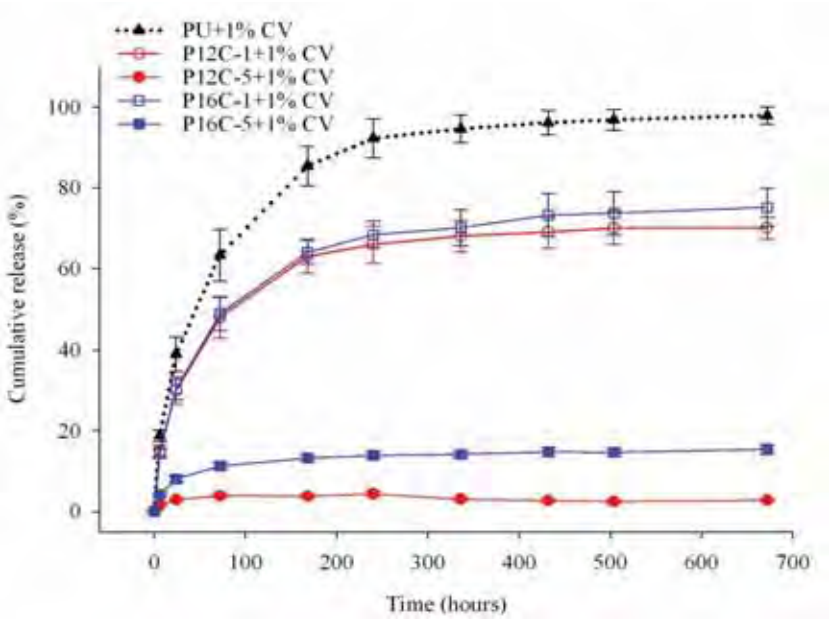

Figure 5.14 Cumulative release profile of samples incorporated with CV over 4 weeks (n=3). Data represents mean ± s.d.

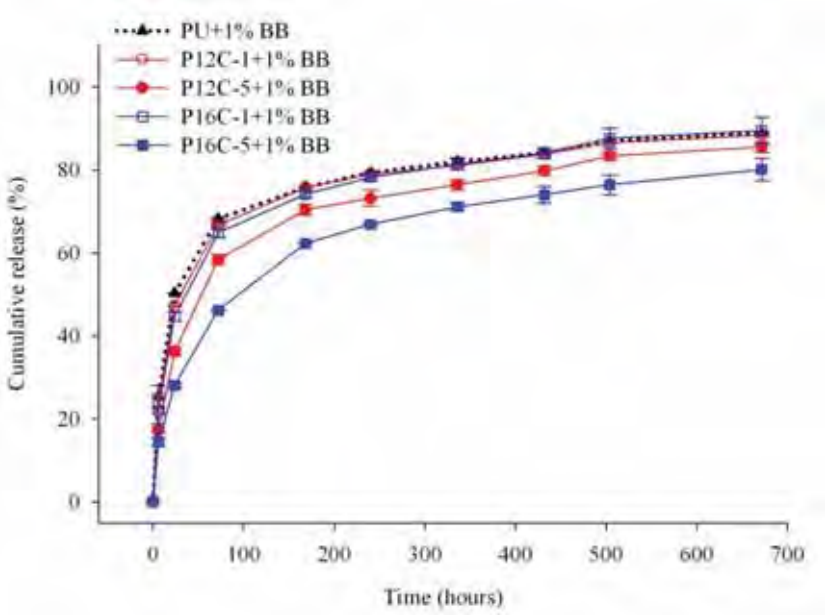

Figure 5.15 Cumulative release profile of samples incorporated with BB over 4 weeks (n=3). Data represents mean ± s.d.

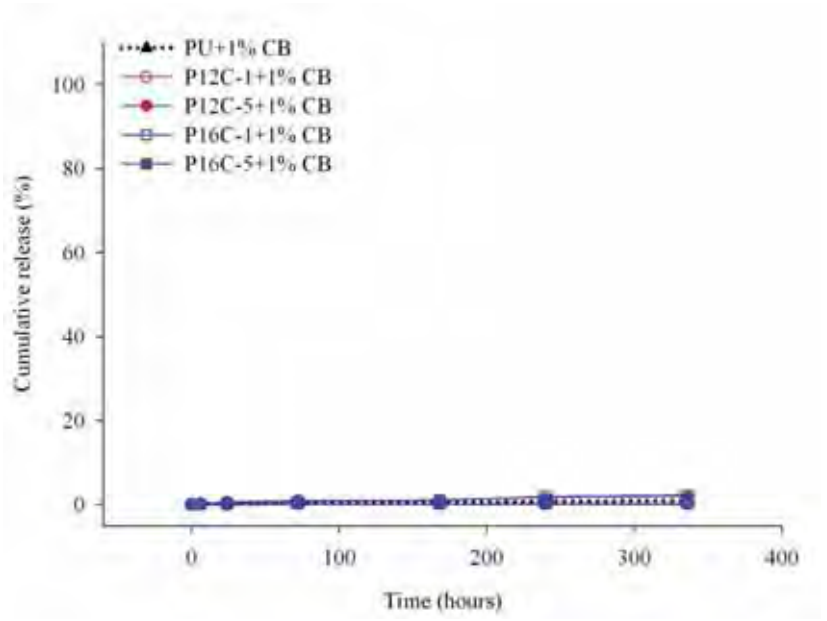

Figure 5.16 Cumulative release profile of samples incorporated with CB over 2 weeks (n=3). Data represents mean ± s.d.

The release kinetics of samples were evaluated using the zero order, first order and Higuchi's equation shown in Table 5.10. The regression plots for CV and BB from the above models were shown in Appendix C.2. The coefficient of determination (r^2) and release constant (k) for each sample are displayed in the table with the r^2 closest to unity underlined. The highest r^2 values for all samples were in the Higuchi's model, indicating

Table 5.10 Coefficient of determination and k

	Zero Order		First Order		Higuchi		Diffusion Coefficient[d]
	r^2	$k_0 \times 10^{3}$ [a]	r^2	$k_1 \times 10^{3}$ [b]	r^2	$k_H \times 10^{3}$ [c]	$D \times 10^7$ (cm^2/s)
CV							
PU+1%	0.86	4.52	0.77	7.95	<u>0.99</u>	66.34	0.24
P12C-1+1%	0.84	3.29	0.76	7.61	<u>0.98</u>	48.59	0.13
P12C-5+1%	0.73	0.44	0.79	10.58	<u>0.94</u>	4.50	6.5×10^{-5}
P16C-1+1%	0.84	3.38	0.75	7.79	<u>0.98</u>	49.98	0.14
P16C-5+1%	0.72	0.65	0.68	5.81	<u>0.93</u>	10.14	1.11×10^{-4}
BB							
PU+1%	0.79	8.09	0.61	13.43	<u>0.97</u>	80.35	1.44
P12C-1+1%	0.83	7.93	0.80	14.30	<u>0.98</u>	77.79	1.25
P12C-5+1%	0.89	7.15	0.86	16.98	<u>0.99</u>	67.94	0.19
P16C-1+1%	0.84	7.77	0.81	14.81	<u>0.98</u>	75.83	1.13
P16C-5+1%	0.89	5.68	0.88	16.52	<u>0.99</u>	54.02	0.040

[a] k_0 obtained from the slope of the plot M_t/M_0 against t. [b] k_1 obtained from the slope of the plot $ln(M_t/M_0)$ against t. [c] k_H obtained from the slope of the plot M_t/M_0 against $\sqrt{t}$. [d] Diffusion coefficient obtained from the slope of the plot M_t/M_∞ against $\sqrt{t}$.

that the release of CV or BB from the system was a diffusion dependent process. The release rate (*k*) was also found to be the highest in PU+1% for both model drugs and the values decrease as clay loading increases. Of note was that the release rate for BB was larger than CV, which is consistent with the observation from the drug release assay and from the weaker interactions with the PUNC system. The diffusion coefficients (D) were also consistent with the release profile for both model drugs and decreases with the addition of silicate particles. Values for BB were also greater than CV, indicating that BB can diffuse out of the system faster and easier than CV.

5.4 Discussion

The addition of a model drug disrupted the dispersion of silicates within a PUNC system, and the degree of disruption appeared to be dependent on the strength of electrostatic interactions and hydrogen bonding between the drug and OMS. Furthermore, the release of hydrophilic drugs was dissimilar. The release rate and level of retardation were governed largely by the charge, polarity and size of the incorporated drug. The release of positively charged drugs was significantly decreased by the introduction of clay, while the release of anionic drugs was modulated to a lesser extent. Although drug size was thought to impact release, it appears that the combined effects of interaction and solubility also influences drug release.

5.4.1 Impact of interactions on PUNC dispersion

The incorporation of CV in PUNCs as evidenced by XRD resulted in the smallest d-spacing compared to BB and CB. Since all of the silicate spacings of PUNCs with model

drugs were smaller than PUNCs without model drugs, this indicated that interactions between model drugs and OMS can disrupt the dispersion within PUNCs. However, it was clear that a decrease in silicate spacing did not directly correlate with the drug release profile and that other factors were of critical importance to impact the release behaviour. A theoretical consideration of the potential interactions occurring between the model drugs and OMS is summarised in Table 5.11. The interactions between each of the reactive side groups were ranked after considering the strength and type of interaction. The order of ascending interaction is: dipole-dipole (weak) and hydrogen bonding (weak); ion-dipole (weak to moderate); and ion-ion (strong) [271].

Table 5.11 Theoretical assumptions of the interactions between model drugs and OMS. (Interactions standing out are highlighted)

Drug		MMT		OM
		Surface	OH	N^+
CV	N^+	+++	++	---
BB	S=O	--	+	++
	OH	++	+	++
	Br	--	+	+
CB	S=O	--	+	++
	$S\text{-}O^-$	--	+	+++
	N^+	+++	++	---
	NH	+	+	++
	C-O-C	-	-	+

"+" represents attraction (strong +++; moderate ++; weak +)

"-"represents repulsion (strong ---; moderate --; weak -)

Focusing on the interactions between CV and OMS, a strong attractive interaction is seen between the positive nitrogen group (N^+) and negative charges across the MMT surface. At the same time, a strong repulsive interaction occurs between N^+ and the head group (N^+) from the OM. Contrary to this, the interactions between BB and OMS are at the hydroxyl (OH) side groups of MMT and are weaker compared to CV. This is consistent with the observations by Aguzzi *et al*. [246], where the adsorption studies of benzoic acid and CV on kaolin suggested that anionic species (benzoic acid) were adsorbed on the edge faces of the mineral and cationic (CV) species interact on the basal plane surface. The interaction between CB and OMS is more complicated due to the competitive interactions between the positive N^+ groups and negatively charged $S\text{-}O^-$ groups.

A hypothesis for the observed decrease in d-spacing based on both theory (Table 5.11) and experimental data, is that CV could potentially displace the amine groups (NH_3) on the surface of clay due to the simultaneous repulsive nature with the amine group and attractive nature with clay surface. The ion-dipole interactions with OH side groups of MMT could also contribute to the attraction of CV around the OMS leading to further displacement. BB however, only has weak interactions with the hydroxyl and amine group through its thionyl and hydroxyl groups, thus resulting in no displacement. The d-spacing of CB that lies in between CV and BB is represented by the conflicting interactions it has with the OMS. However, the spacings were still larger than CV due to the negatively charged thionyl group. An illustration of this hypothesis is illustrated in Figure 5.17. Since CV could potentially displace out the modifier, the spacings between silicates should be largely affected and this is evidenced by the intercalated structure at 1

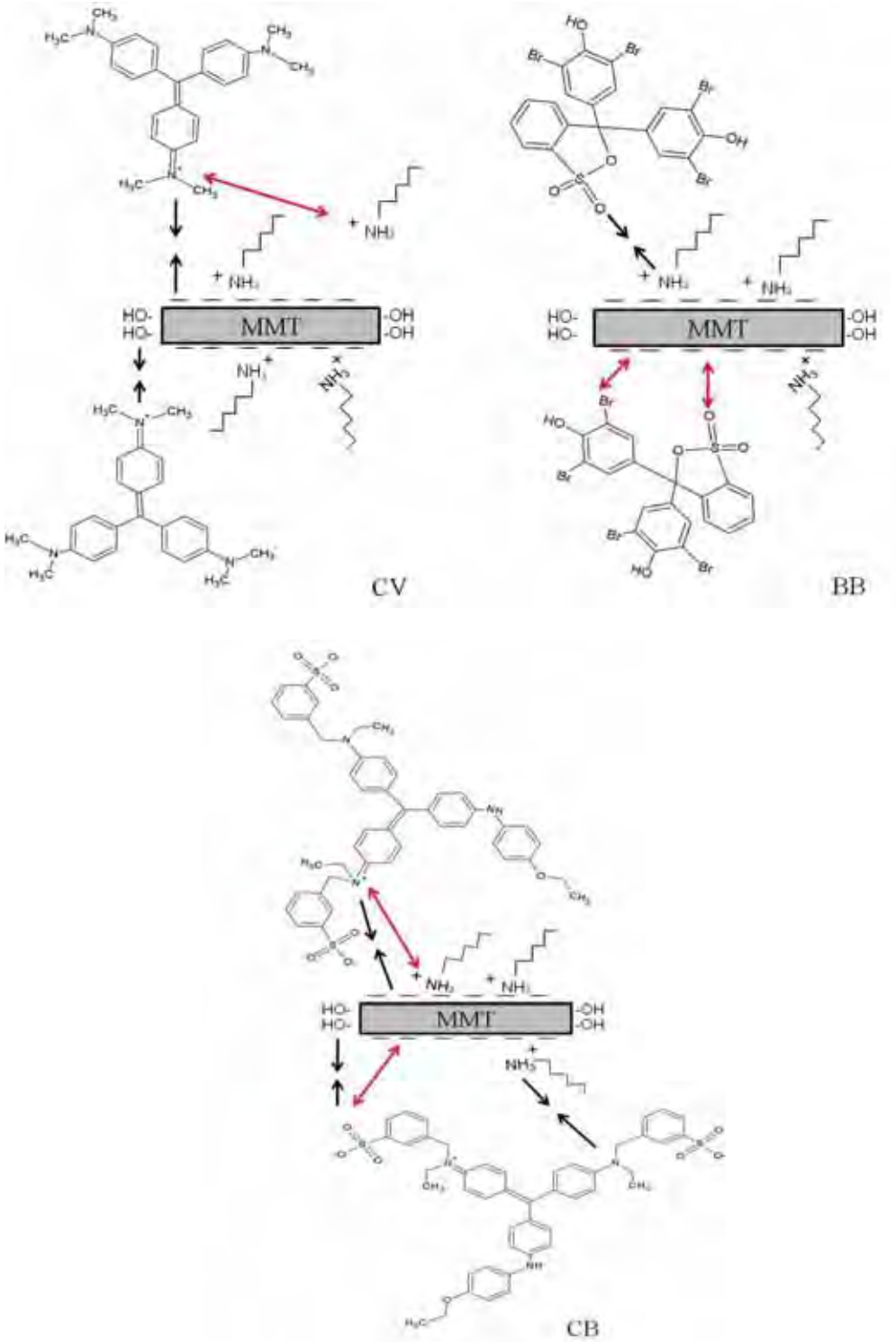

Figure 5.17 Interactions that could occur between the model drugs and OMS. The black arrows represent attractive interactions while the red represents repulsive interactions.

wt% of clay and the smaller d-spacing across all loadings as compared to BB and CB loaded samples.

In addition to XRD, interactions between OMS and the model drugs were also evidenced by FTIR analysis. For interactions to occur, changes would be expected at 2927cm^{-1} and 2855cm^{-1}, which corresponded to the asymmetric & symmetric stretching of CH_2 from the OMS. A shift of 5cm^{-1} at 2927cm^{-1} and 3cm^{-1} at 2922cm^{-1} was observed by the addition of CV, which indicated that CV showed stronger interactions at those regions. A slight shift was observed at both peaks for CB and virtually no shift was observed in OMS added with BB.

Another region of interest is between 1550-1450cm^{-1} (Figure 5.10). Immediately obvious was the disappearance of peak at 1501cm^{-1} along with the formation of a doublet at 1480cm^{-1} and 1468cm^{-1} when OMS was added with CV. The disappearance of peak at 1501cm^{-1} belonged to the bending of CH on the modifier head group [262], suggesting that CV may have displaced some of the modifier head groups from the MMT surface. On the other hand, the doublet formation was reported by Hongping *et al*. [266] to arise from inter-chain interactions between adjoining CH_2 groups, which also suggested that modifiers may have been pushed aside by CV. Comparing that change to changes resulted from adding BB and CB, spectra from both drugs still displayed a single unshifted peak at 1480cm^{-1} similar to the OMS control. Correlating this to XRD, these results demonstrated that silicate spacing was dependent on the strength of interaction between drug and OMS. Molecules bearing the same charge to the modifier could potentially displace the modifier, thereby reducing the quality of dispersion.

In relation to the interactions between model drugs and PU, there was no peak shift or major intensity changes from the FTIR spectra shown in Figures 5.11-5.13. This suggested that the interactions were not very strong between any of the drugs and PU. The main interactions between CV and PU were reported to be at the hard segments [272]. However, using the method described by Tien *et al*. [154] to calculate changes in the hard-soft segment linkages from the FTIR spectra, there were no changes across all drug concentrations when compared to that of neat PU. These findings showed that the interactions between CV and PU were not strong enough to be detected by FTIR.

Interactions between BB and PU were not reported in literature. However, it is hypothesised that the interactions are much weaker than between CV and PU since the burst effect and initial release rate shown in Figure 5.15 were much higher than CV. Similar to interactions with OMS, the interactions between CB with PU were also complicated by multiple attraction and repulsion. A stronger ion-dipole interaction between S-O and NH was observed, but there were no noticeable changes at 1530cm^{-1} or 1310cm^{-1}(δ N-H) from FTIR.

5.4.2 Impact of interactions on drug release behaviour

The cumulative release profiles conducted on all 3 model drugs indicated that the molecular size, charge and interactions can largely affect the drug release behaviour of an NC system. The release profiles of PU incorporated with CV or BB both indicated a rapid initial release followed by a plateau at latter times. The lack of strong interactions between CV-PU and BB-PU also supported less hindrance of release from those systems.

Some possibilities as to why only trace amounts of CB were released from the system are a) stronger interactions with the polymer, b) larger molecular size, and c) solubility. As discussed earlier, possible interactions between the $S\text{-}O^-$ from CB and the NH group from PU hard segment could limit the release. If this was true, the strong attractive interactions should be reflected by FTIR. The spectra however, did not indicate any changes in bond vibrations or intensities, suggesting that the interactions were actually not very strong. The two latter possibilities such as size or solubility are more likely to have prevented CB releasing from the system. Formation of insoluble particles as noted in earlier sections could affect the final concentration of CB measured through UV-spectrophometry. In terms of molecular size, while no studies were found concerning the release of CB from PU or PUNCs, the significantly smaller size of CB in relation to heparin (refer to chapter 4) might have still been too large to release out from the system.

For both CV and BB, a decrease in the total drug release was observed when silicate loadings were increased. The burst effect of CV was reduced considerably from the addition of clay, suggesting that attractive interactions exist between CV and OMS. This is consistent with the results obtained by XRD and FTIR discussed earlier. On the other hand, the maximum reduction of BB was only around 10% at the highest clay loading, indicating that the attractive interactions between BB and OMS were not very strong. Furthermore, while both model drugs are released via diffusion as shown in Table 5.10, the lower diffusion coefficient of CV than BB could also explain the weaker interactions between BB and OMS. These observations demonstrated that the effect of using longer chain modifiers to improve dispersion or by increasing clay loading to lengthen the diffusion pathway were less effective in modulating release than component interactions.

The large decrease in CV from PUNCs with 5wt% loadings was also partly due to the strong attractive interactions between CV and OMS, rather than entirely from the concept of impermeable particles from the tortuous pathway model.

In summary, the importance of component interactions in a PUNC system is reflected by the different release profiles observed between CV, BB and CB. Since interactions between the drug and the components within an NC system can play a dominant role in altering the release behaviour, drug properties such as the size, surface charge and polarity should also be considered when using NC as controlled drug delivery systems.

5.5 Conclusion

The addition of a fourth component to PUNCs was shown to disrupt silicate dispersion. Since the spacings from all three drugs decreased when clay content increased, a correlation could not be established between drug release behaviour and the increase or decrease observed in silicate spacings. A larger change in silicate spacing however, appeared in drugs that had greater interactions with the clay. The incorporation of positively charged drugs is able to displace modifiers from the MMT surface through electrostatic interactions and hydrogen bonding, thus resulting in a lower dispersion. As silicate dispersion can also affect the mechanical properties, it is desirable to minimise disruption through selecting drugs that can enhance or at least maintain the silicate dispersion.

The modulation of release from pristine PU was found to be dependent on the net charge and polarity of the drug. Positively charged drugs, such as CV, can be retarded to a

greater extent from the introduction of clay, while anionic BB was only modulated slightly. Findings in this study indicated that the reduction in release for both CV and BB was due to hydrogen bonding, dipole interactions and clays acting as impermeable barriers to decrease permeability. The trace amounts of CB measured were thought to be related to size and solubility. These results showed that the interaction between the drug and the NC system is equally important to factors such as filler content and dispersion in modulating barrier properties of PUNCs. The effect of charge and polarity on the structure and drug release of PUNCs will be further investigated in the subsequent chapter by using two drugs that are similar in size and chemistry but different in functional groups. In particular, focus will be on a hydrophobic drug that is electrostatically neutral and a hydrophilic drug that has a negatively charged phosphate group.

Chapter 6: Impact of structure and release of active drugs with similar chemistry

6.1 Introduction

The impact of incorporating a drug on the silicate dispersion and release behaviour of PUNCs was investigated in the previous chapter. Three hydrophilic model drugs with different molecular size, net charge and polarity were tested. It was found that none of the three model drugs showed strong interactions with PU and the release profile was mainly affected by interactions with the clay and the size of the model drug. Positively charged drugs have the potential to displace modifiers from the MMT surface through electrostatic interactions, while anionic drugs mainly interact with clay through hydrogen bonding and dipole interactions. As a result, the release of positively charged drugs is likely to be significantly decreased by introduction of clay, whereas the release of anionic drugs is impacted to a lesser extent.

Drug release behaviour was also affected by the size of the model drug. Coomassie blue, with a molecular weight of 826 g/mol, showed minimal release from either PU or PUNCs. This can be attributed to the size effect since there was no observable peak shift or major intensity changes from the FTIR spectra with pristine PU. Given the disparity in chemical structures, charge and size of the drugs tested in Chapter 5, further research studying interactions and release of two drugs of similar size and chemistry were proposed. Dexamethasone acetate (DexA) and dexamethasone phosphate (DexP) are

two drugs of similar size and chemistry but with different functional groups. The different chemistry of the functional groups of the chosen drugs resulted in one drug being hydrophobic (DexA) and the other being relatively hydrophilic (DexP). Therefore, a comparison between the release of hydrophilic and hydrophobic drugs can be conducted as well as focusing on the potential interactions that arise from drug charge and polarity. The drugs were also chosen on the basis of their potential for use in biomedical applications and the ability to assess drug function via assays, such as cell growth and *in vitro* inflammatory response.

Interactions that arise from the net charge and polarity of the incorporated drug could be in the form of electrostatic (positive or negative groups), polar (hydrogen bonding or van der Waals), or acid-base interactions [273]. Apart from these interactions, the type of drug and water solubility can also affect the release mechanisms [13]. Using drugs of different size and chemistry, the drug release behaviour of hydrophilic and hydrophobic drugs has been investigated in various polymeric systems [274, 275]. Chan *et al*. [274] compared the release behaviour of *p*-nitroaniline (hydrophobic) with brilliant blue G (hydrophilic) in poly (sebacic anhydride-*co*-ethylene glycol). It was found that the release of the *p*-nitrolaniline was slower than brilliant blue (in buffer, pH 7.4) over a period of 290 hours. The release of brilliant blue also showed a larger burst release than *p*-nitrolaniline, and a burst of 70% was seen from polymers with the highest drug loading (20wt%) [274]. There was also no further release after the initial burst, whereas *p*-nitrolaniline loaded at 20wt% showed no burst release and released only 50% over the same time frame [274].

Another study by Lao *et al*. [275] observed similar trends in the release profile. Poly(lactide-*co*-glycolide) (PLGA) films loaded with 5wt% metoclopramide monohydrochloride (hydrophilic) showed an initial burst of 50% that plateaued after 30 days, whereas paclitaxel, a hydrophobic drug, had no initial burst and released continuously for 90 days. A smaller burst was observed at lower drug loadings (1wt%) due to less agglomeration of undissolved drugs on the surface, however the time to reach complete dissolution was similar to the higher drug loaded films [275].

The release behaviour of drugs with similar molecular size but different water solubility was conducted by Huang *et al*. [276]. Hydrophilic propranolol hydrochloride (259.34g/mol) incorporated in polylactide (PLA) /polyethylene glycol (PEG) microparticulates released six times more drug than the hydrophobic lidocaine (234.34g/mol). Due to the lower solubility of propranolol hydrochloride in the polymer, most of the drug was crystallised and accumulated on the surface rather than dissolved in the polymer matrix. On the other hand, lidocaine with a higher partitioning coefficient, dissolved better in the polymer leading to slower release [276].

Studies examining the release of DexA and DexP from polymers are scant in literature. In addition, only one study has evaluated the release behaviour of DexA and DexP from PU matrices. Gurny and co-workers investigated the release of various chemical forms of dexamethasone from a poly (ortho ester) film [277]. Dexamethasone exists in three chemical forms; hydrophobic base (Dex), highly hydrophobic ester (DexA) and as a hydrophilic basic salt (DexP). The release of Dex was sustained up to 96 hours while DexA was not released from the polymeric matrix. Interestingly, DexP which is the most

hydrophilic of the dexamethasone series released only 20% of the amount loaded in 96 hours and did not reach maximum dissolution until day 10 [277]. It was believed that the basicity of DexP stabilised and buffered the system, thereby slowing down the release. This suggested that although the water solubility of drugs can affect the release profile, the acidic or basic properties of the drugs also play a dominant role as they can either promote or buffer the system which alters the release profile [277].

The release of DexA and DexP from polycarbonate based PU matrices (PCU) was examined by Kim *et al*. [278]. It was found that 60% of DexP was released in the first two hours from the polymer, whereas DexA released the same amount after 3 days [278]. In a review of NCs in the current literature, studies comparing hydrophilic and hydrophobic drugs from polymer NCs or PU based NC systems could not be found. However, the studies mentioned above demonstrated that drugs of hydrophilic nature generally have a faster and larger initial release rate compared to hydrophobic drugs as the drug particles are easily dissolved once immersed in aqueous release medium [279].

Therefore, the hypothesis of this study is that the release of hydrophilic drugs from PUNC systems will be less sustained than drugs of hydrophobic nature. The interactions between the drug and the PUNC system may however, impact on the structure and alter the release profile. These interactions are largely dependent on the charge and polarity of the incorporated drug and will be explored through a combination of computer modelling and experimental techniques. Specifically, the aims were to:

1. Examine the relative release behaviour of hydrophobic and hydrophilic drugs from neat PU and PUNC systems.

2. Understand the impact of drug charge and polarity on interactions between NC components.

6.2 Materials and methods

6.2.1 Nanocomposite preparation

Materials prepared in this study were similar to those described in Chapter 5, except that during mixing, active drugs: dexamethasone 21-acetate (DexA, Sigma Aldrich) and dexamethasone 21-phosphate (DexP, Sigma Aldrich), were added to the PU/DMAc solution simultaneously with the OMS. As per methods in Chapter 5, the model drugs were added at 1wt% (g model drug/100 g PU). PUNCs were labelled according to abbreviations described previously in Chapter 3, as listed in Table 6.1. Samples incorporated with DexA or DexP however, have an additional suffix labelled DA or DP respectively. PUNC samples modified with $12CH_3$ or $16CH_3$ are labelled with prefix P12 or P16 respectively.

Table 6.1 Materials investigated within Chapter 6

Material ID	OMS	Loadings (g/100g PU)		Test conducted[a]
		Clay	Active Drug	
DexA				
PU+1%DA	-	-	1	X
P12C-1+1%DA	12CH_3MMT	1	1	X,T
P12C-3+1%DA	12CH_3MMT	3	1	X
P12C-5+1%DA	12CH_3MMT	5	1	X,T
P16C-1+1%DA	16CH_3MMT	1	1	X
P16C-3+1%DA	16CH_3MMT	3	1	X
P16C-5+1%DA	16CH_3MMT	5	1	X
DexP				
PU+1%DP	-	-	1	X
P12C-1+1%DP	12CH_3MMT	1	1	X,T
P12C-3+1%DP	12CH_3MMT	3	1	X
P12C-5+1%DP	12CH_3MMT	5	1	X,T
P16C-1+1%DP	16CH_3MMT	1	1	X
P16C-3+1%DP	16CH_3MMT	3	1	X
P16C-5+1%DP	16CH_3MMT	5	1	X

[a] Characterisation methods to assess dispersion: X= x-ray diffraction (XRD); T= Transmission electron microscopy (TEM)

6.2.2 Material characterisation

6.2.2.1 X-ray Diffraction

XRD was performed as described in Chapter 3 to examine the distance between silicate layers in PUNCs. The analysis was determined on a Philips PW-1830 x-ray diffractometer with CuKα radiation of 0.15406nm at 40kV and 40mA. Strips of samples were scanned at three points from 1.8 to 9^{o} at a rate of 0.00133^{o}/s and a step size of 0.01^{o}.

6.2.2.2 Transmission Electron Microscopy

TEM analysis was conducted as described in Chapter 3. NC films were cryosectioned using a Leica FC6 Cryo-Ultramicrotome at a temperature of -120ºC and rate of 0.15-3mm/s. Images of the samples were taken using a JEOL 1400 TEM with an accelerating voltage of 100kV. Each sample was imaged at multiple locations and one representative image of the material was chosen for presentation.

6.2.2.3 *In vitro* drug release

Materials for i*n vitro* drug release assay were cast and the assay conducted as previously described in Section 5.2.3. A sink volume of 50mL (PBS, pH 7.4) was used and placed in an incubator (37^{o}C) on an orbital shaker. Aliquots were taken at regular time intervals and replenished for a total of 5 weeks. The assay was repeated in triplicate and each assay consisted of a triplicate of each material. Drug release was tracked using a UV-spectrophotometer (Varian Cary 300). The active drugs and their respective chemical structure, MW and absorbance peak are shown in Table 6.2.

Table 6.2 Structure and chemical properties of drugs

	Dexamethasone acetate	Dexamethasone phosphate
Chemical structure	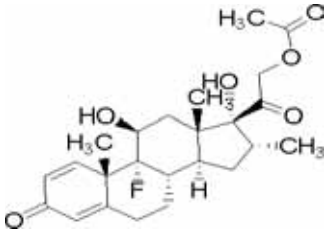	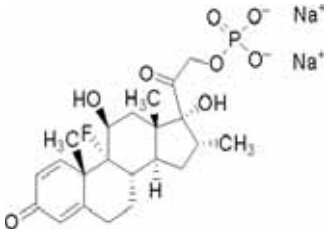
MW	434.49/mol	516.40/mol
Absorbance	242nm	242nm
Charge	Neutral	Negative
Type	Hydrophobic	Hydrophilic
LogP[a]	2.68	0.51

[a] Partition coefficient [280]

6.2.2.4 Attenuated Fourier Transform Infrared Spectroscopy

Attenuated total reflection FTIR (ATR-FTIR) was conducted using the same parameters as described in Section 5.2.2 to examine possible interactions between the drug and constituents of the PUNC system. Samples were scanned over the range of 4000-700 cm^{-1}, at a resolution of $4cm^{-1}$ using a Bruker IFS66/S High End FT-NIR/IR Spectrometer with a diamond crystal ATR attachment. The ATR-FTIR spectrum was baselined at numerous locations across the spectral range using the supplied software (OPUS), and the data normalised to the C-C bond of the aromatic ring at $1414cm^{-1}$. Each sample was scanned at 3 distinct regions and one of the spectra was chosen for representation. Table 6.3 shows samples with various loadings of DexA or DexP for

FTIR analysis. Similarly, FTIR analysis on OMS that was mixed with active drugs was conducted using the method as described in Section 5.2.2. Samples prepared by this method for FTIR analysis are listed in Table 6.4

Table 6.3 PUNCs incorporated with drugs with same clay loading

Material ID	Nanofiller	Loadings (g/100g PU)	
		Clay	Active drug
DexA			
P12C-3+1%DA	12CH_3MMT	3	1
P12C-3+3%DA	12CH_3MMT	3	3
P12C-3+10%DA	12CH_3MMT	3	10
DexP			
P12C-3+1%DP	12CH_3MMT	3	1
P12C-3+3%DP	12CH_3MMT	3	3
P12C-3+10%DP	12CH_3MMT	3	10

Table 6.4 OMS incorporated with drugs

Material ID	Drug	Added clay (ml) (5wt% suspension)	Added active drugs (mg)
DA12MMT-30	DexA	3	30
DP12MMT-30	DexP	3	30

6.2.2.5 MD simulation[5]

Molecular dynamic (MD) simulation was performed by using the Discover Module in Materials Studio – commercial software for materials modelling from Accelrys, Inc. The simulation model represented an exfoliated PUNC which consisted of one single clay platelet surrounded by a number of surfactant chains, PU chains, and drug molecules. The model of clay (e.g., MMT) was based on experimental structure and has a formula of $Na_{0.333}$ $[Si_4O_8]$ $[Al_{1.667}Mg_{0.333}O_2$ $(OH)_2]$ and cationic exchangeable capacity (CEC) of 90 mmol/100g. The MD cell had an overall dimension of a=25.959Å, b=27.0459Å, c=200Å, and $\alpha=\beta=\gamma=90^o$.

The force field employed was a modified CVFF (Consistent Valence Force Field) reported by Heinz *et al*. [281]. MD simulation was performed with a time step of 0.001ps and a total simulation time of 100ps. The van der Waals and Coulomb interactions were handled by the Ewald summation method. Initially, the model structure was relaxed for a certain period time, followed by NVT (canonical ensemble) MD simulation and data collection of the last 20ps for analysis. During the simulation, the clay platelet was treated as rigid body while the surfactants, PU chains and drug molecules were allowed to move flexibly.

Interaction energies between any two components in a system were calculated based on the equilibrated configurations and their extracted configurations. For a system containing *a* and *b* components, their total interaction energy (E_{ab}) as well as the

[5] Simulation conducted in collaboration with Dr. Qinghua Zeng in the School of Materials Science & Engineering at UNSW

individual contributions was calculated (i.e., electrostatic, van der Waals, and Born repulsion) by the following equation.

$$E_{a-b} = E_{ab} - E_a - E_b \tag{6.1}$$

where E_{ab}, E_a and E_b are the potential energies of the total two component system, component a, and component b, respectively.

6.3 Results

6.3.1 Physical experimentation

The effect of adding DexA or DexP on the dispersion of silicate particles was examined by XRD. Diffractograms of PUNCs loaded with DexA or DexP are shown in Figures 6.1-6.2 respectively, and a summary of the silicate spacings is shown in Table 6.5. PUNCs with DexA did not show a significant difference in spacing compared to PUNCs without DexA, suggesting that the drug did not disrupt the silicate dispersion within PUNCs. However, an increase in silicate spacing was observed in NCs when DexP was added. Since the spacings measured from P12C-3+1%DP and P16C-3+1%DP were much larger than their relative controls, adding DexP could have aided the separation of silicate layers by the repulsive charges on the phosphate group. This effect was dampened in PUNCs with higher silicate loadings.

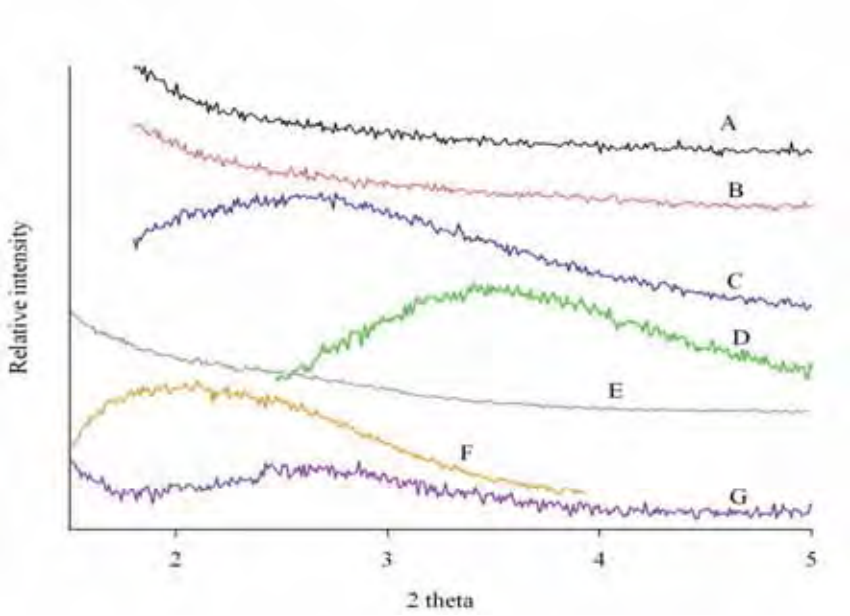

Figure 6.1 XRD diffractograms for : A) PU+1%DA, B) P12C-1+1%DA, C) P12C-3+1%DA, D) P12C-5+1%DA, E) P16C-1+1%DA, F) P16C-3+1%DA, and G) P16C-5+1%DA.

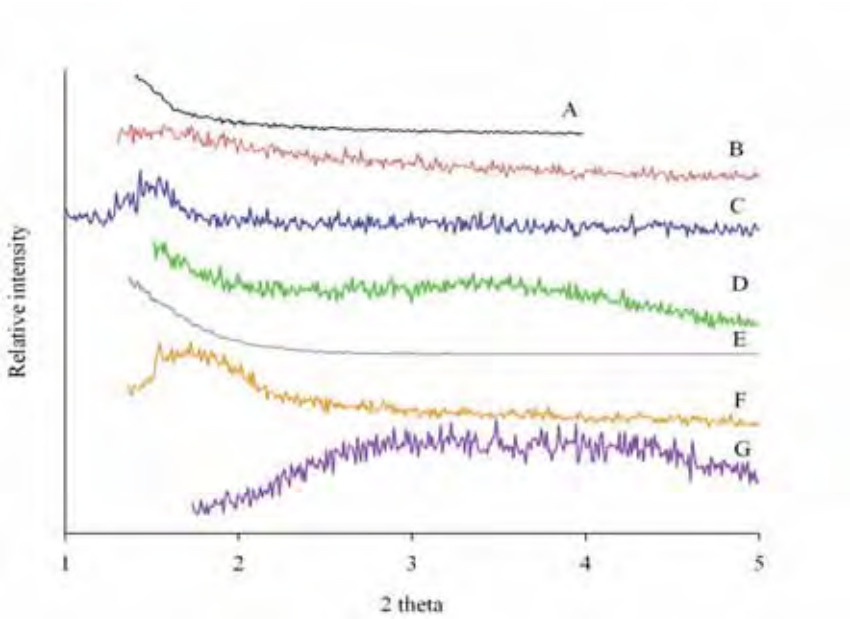

Figure 6.2 XRD diffractograms for : A) PU+1%DP, B) P12C-1+1%DP, C) P12C-3+1%DP, D) P12C-5+1%DP, E) P16C-1+1%DP, F) P16C-3+1%DP, and G) P16C-5+1%DP.

Table 6.5 X-ray diffraction results for PUNCs incorporated with DexA or DexP

Material	Spacing (nm)		
	Control[a]	With 1%DA	With 1%DP
P12C-1	No peak	No peak	No peak
P12C-3	3.40	3.40	5.88
P12C-5	2.55	2.58	2.62
P16C-1	No peak	No peak	No peak
P16C-3	4.78	4.55	5.46
P16C-5	3.26	3.46	2.56

[a] Silicate spacings as reported in Chapter 3

Representative TEM images of P12 NCs at 1 and 5wt% loadings with DexA or DexP are displayed in Figure 6.3-6.4. In general, it was found that increasing the clay loading of PUNCs from 1wt% to 5wt% increases the tendency to form bigger aggregates. At higher magnifications (Figures 6.3), both drugs at 1wt% loadings showed distinguishable individual silicate layers, but layers appeared to be better defined in DexP loaded samples. As both NCs at 1wt% still contained regions where the clay was not fully exfoliated, the structure for NCs at this loading was classified as partially exfoliated and the absence of peaks from XRD was due to the distance between silicate layers exceeding the detection limit of this particular X-ray diffractometer.

At 5wt% loadings (Figure 6.4), the increase in the number of dark regions confirmed the higher tendency of clays to aggregate. At high magnifications (×100K), DexA and DexP loaded samples showed similar morphology and were consistent with XRD results, where P12s at 5wt% loading incorporated with DexA and DexP showed similar silicate

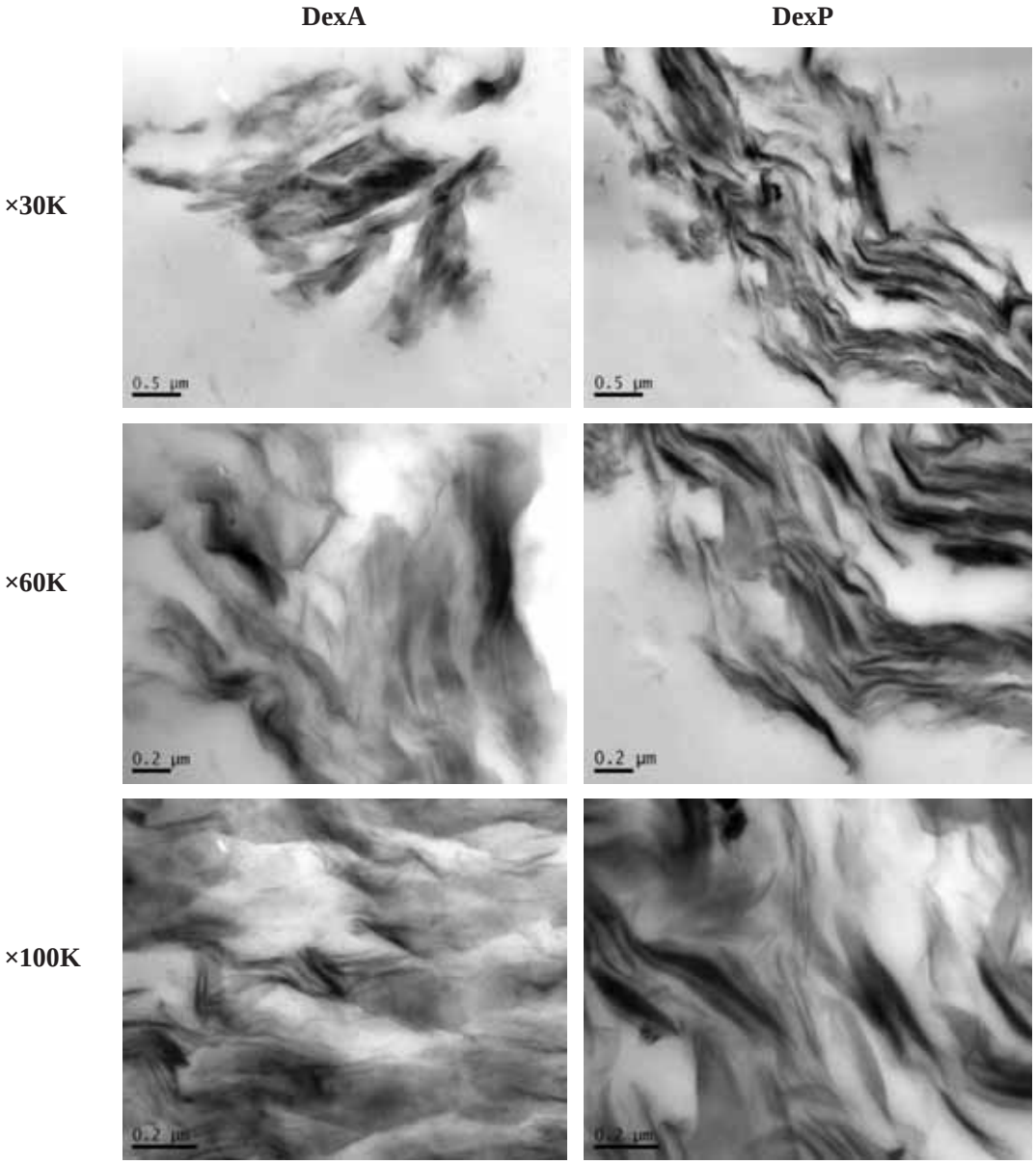

Figure 6.3 Representative TEM images of P12C-1 with DexA or DexP taken at various magnifications of 30,000x (scale bar= 0.5µm), 60,000x (scale bar=0.2µm) and 100,000x (scale bar= 0.2µm).

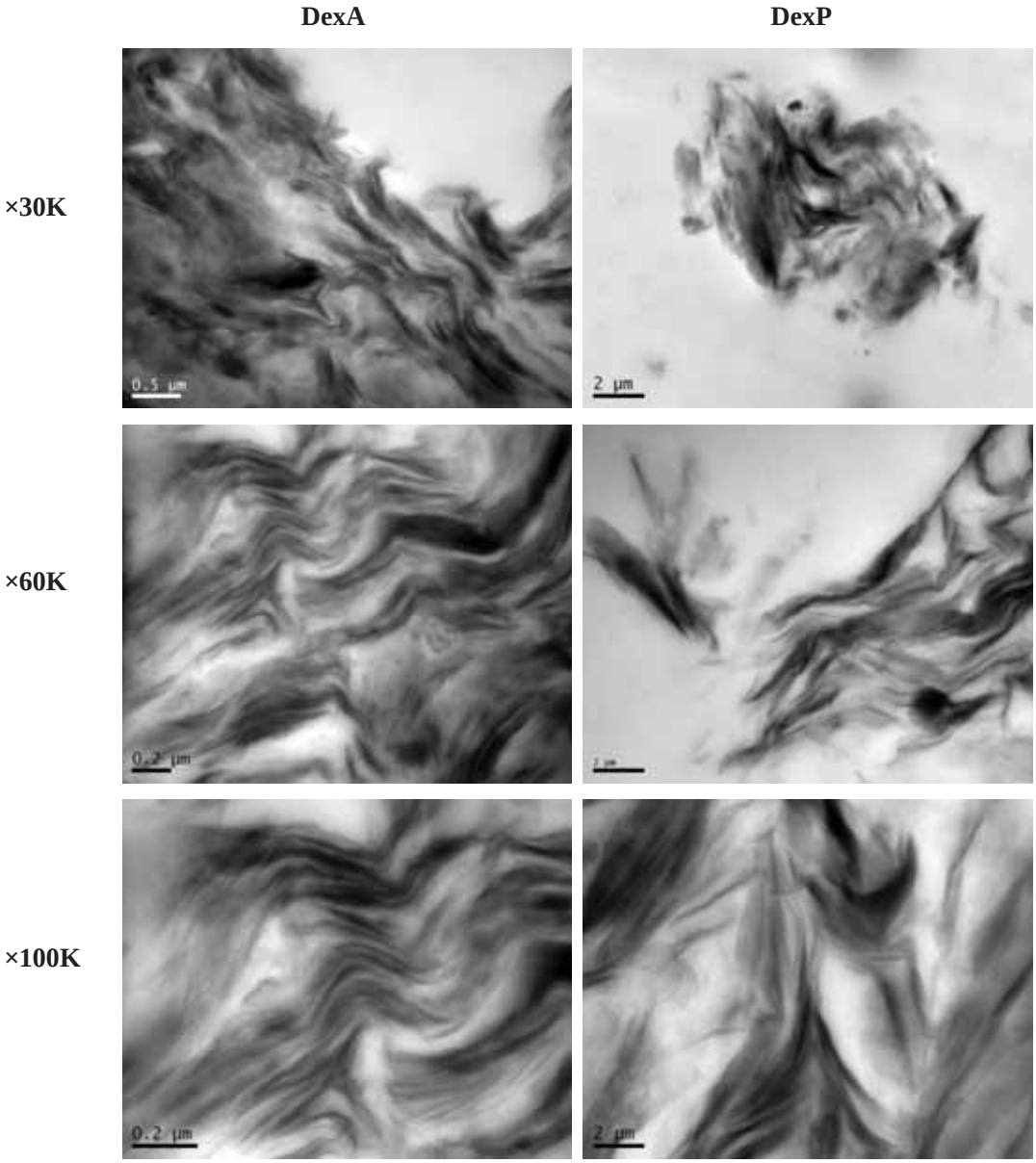

Figure 6.4 Representative TEM images of P12C-5 with DexA or DexP taken at various magnifications of 30,000x (scale bar= 0.5µm), 60,000x (scale bar=0.2µm) and 100,000x (scale bar= 0.2µm).

spacings of 2.58 and 2.62nm respectively. The well ordered multilayer morphologies observed from magnifications at ×60K and ×100K, were also in agreement with the spacings determined from XRD that the morphology of 5wt% loaded PUNCs was intercalated.

In vitro drug release assays for DexA and DexP were conducted over 5 weeks. Extracts from neat PU without added drugs did not interfere with the absorbance measurement for DexA and DexP as shown by the absence of peaks around 242nm. Both drugs were tested for degradation in PBS for 2 months at 37˚C and there were no signs of degradation of either drug. The pH of drugs in the sink medium were tested before and after the assay. The pH of DexA and DexP pre-assay were 7.34 and 7.48 respectively, while the pH post-assay were 7.4 and 7.41 respectively.

The cumulative release profiles of DexA and DexP are shown in Figure 6.5. There was minor perturbation of DexA release in PUNCs compared with neat PU as shown in Figure 6.5a. There was a slight impact on release that could be attributed to the chain length of the modifier and the silicate loading, with longer chain lengths and higher loadings being associated with lower total release over the 5 week period. The lowest total release (~52%) at 5 weeks was observed from P16s at 5wt% loading. Notably, when comparing the data presented in Figures 6.5a and 6.5b, the total release of DexA from neat PU was higher at 65% compared with DexP which only released 15% of the amount loaded. Looking at Figure 6.5b, this suggested that PU and DexP could have strong attractive interactions that prevented easy release of the hydrophilic drug. Interestingly, the rate of release in DexP was not affected by the surfactant chain length

but enhanced with the addition of clay. The larger rate of release also resulted in a higher amount of DexP released, with P12C-5+1% DP showing 65% of release at the end of 5 weeks.

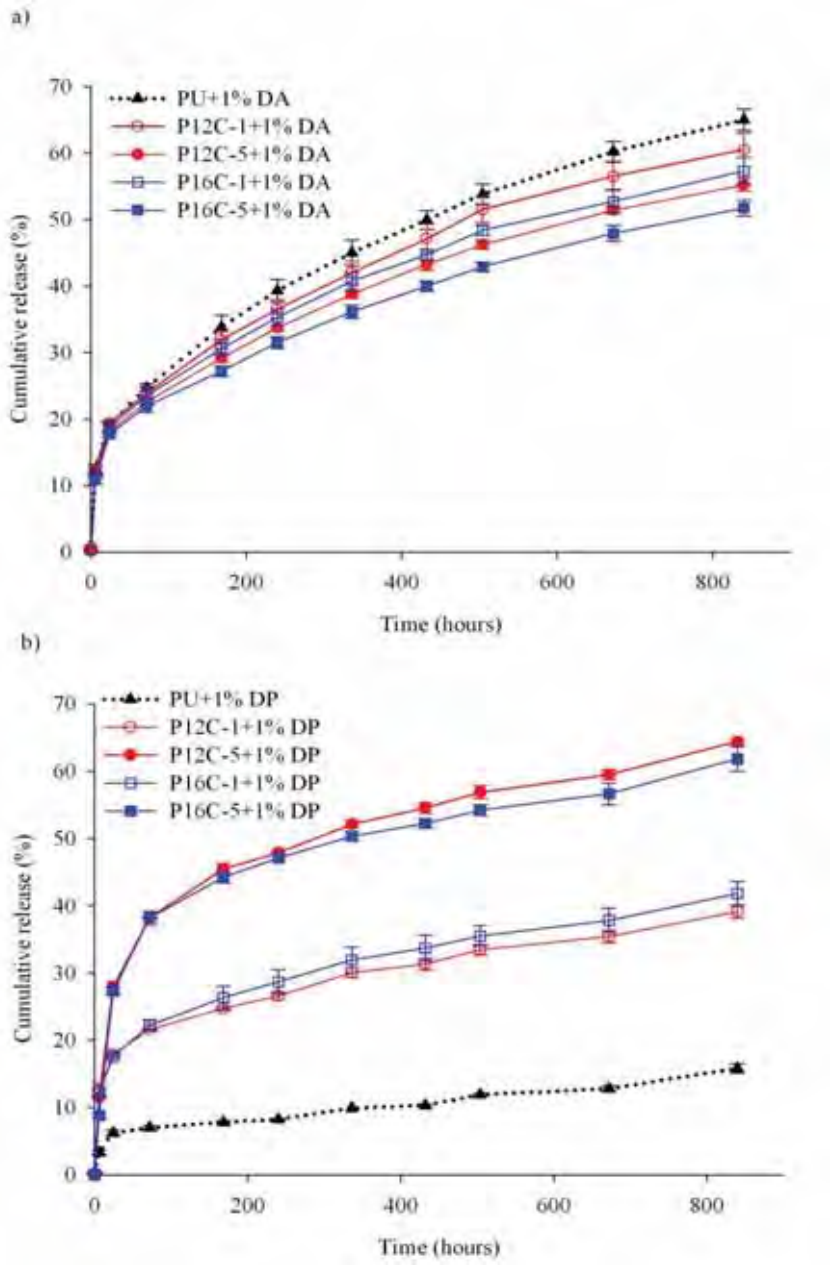

Figure 6.5 Cumulative release profile of samples incorporated with a) DexA, and b) DexP over 5 weeks (n=3).

Release data was also analysed using zero order, first order and Higuchi's models. The coefficients of determination (r^2) and release constants (k) are described in Table 6.6. The highest r^2 values and smallest deviation from 1 for DexA loaded samples were in the Higuchi's model, indicating that the release of DexA from the system was a diffusion dependent process. On the other hand, although displayed values of r^2 for DexP were also the highest in Higuchi's model, they are further away from 1 and the values deviate even further as the clay content increases. This indicated that additional mechanisms were involved in release process of DexP from PUNCs.

Table 6.6 Coefficient of determination and k

	Zero Order		First Order		Higuchi	
	r^2	$k_0 \times 10^{3\,a}$	r^2	$k_1 \times 10^{3\,b}$	r^2	$k_H \times 10^{3\,c}$
DexA						
PU+1%	0.94	0.68	0.79	1.69	0.99	19.88
P12C-1+1%	0.94	0.63	0.79	1.63	0.99	18.23
P12C-5+1%	0.93	0.57	0.79	1.59	0.99	16.40
P16C-1+1%	0.92	0.59	0.77	1.61	0.99	17.09
P16C-5+1%	0.94	0.52	0.79	1.55	0.99	15.02
DexP						
PU+1%	0.94	0.14	0.79	1.40	0.95	3.95
P12C-1+1%	0.90	0.34	0.78	1.09	0.99	9.21
P12C-5+1%	0.75	0.49	0.77	0.83	0.91	17.25
P16C-1+1%	0.89	0.31	0.76	1.18	0.98	10.37
P16C-5+1%	0.71	0.47	0.75	0.78	0.87	16.61

[a] k_0 obtained from the slope of the plot M_t/M_0 against t. [b] k_1 obtained from the slope of the plot $ln\ (M_0/M_t)$ against t. [c] k_H obtained from the slope of the plot M_t/M_0 against √t.

The ATR-FTIR spectra of OMS incorporated with DexA or DexP is shown in Figure 6.6. Distinct peaks for MMT are in agreement with those reported in literature [261, 262, 282]. They occur at 3626cm^{-1} (stretching of structural OH), 3425cm^{-1} (stretching of H-O-H water) and 986cm^{-1} (Si-O-Si stretch). Successful modification of MMT was confirmed by the wavenumbers at 2926cm^{-1} and 2854cm^{-1} representing asymmetric and symmetric stretching of CH_2 respectively. Distinct peaks of DexA and DexP occured at 1710cm^{-1}, 1668cm^{-1}, 1618cm^{-1}, 892cm^{-1} with three of the peaks illustrated by the arrows on the spectra [10]. Characteristic peaks associated with DexP were less apparent than DexA. The slight shifts in the Si-O peaks after modification of MMT reflect the electrostatic interaction between the positive alkyl ammonium head group and negative clay surface. A decrease in intensity and further shifting in the Si-O peaks after addition of drugs indicated that interactions with the clay were likely to occur at the clay surface.

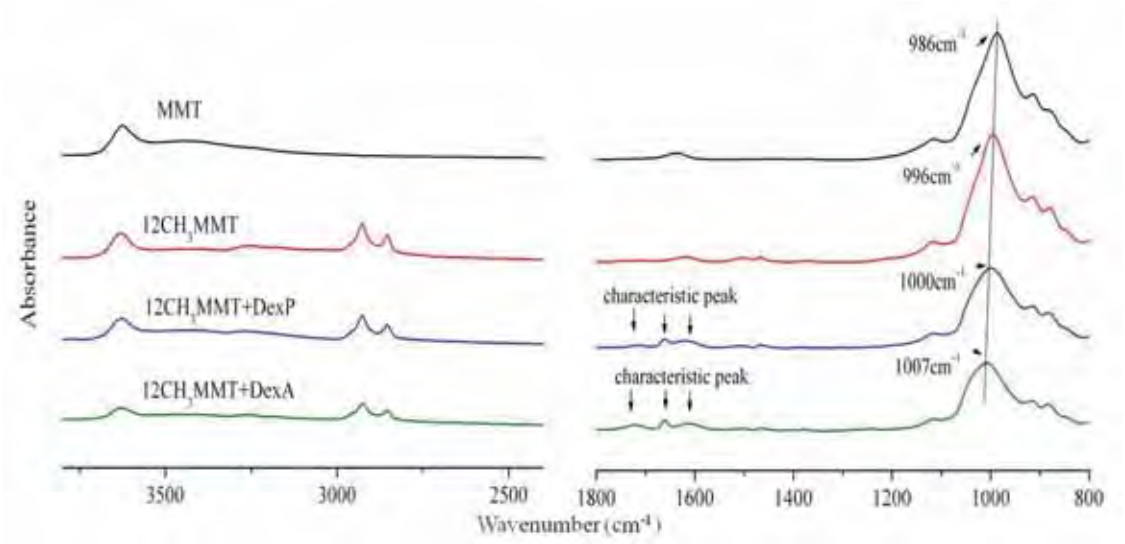

Figure 6.6 ATR-FTIR spectra for MMT, OMS and OMS incorporated with DexA and DexP. Characteristic peaks for DexA and DexP are illustrated with arrows. Dotted lines represent shifts in Si-O stretch peak upon addition of modifier and drugs on MMT.

FTIR spectra for PUNCs with DexA or DexP in the regions 3600-2400cm^{-1} & 1800-800cm^{-1} are shown in Figure 6.7 and 6.8 respectively. A magnified comparison between the two drugs in the region 1300-800cm^{-1} is illustrated in Figure 6.9. All samples showed the distinct peaks for PU that corresponded to those reported in the literature [263, 264]: 1728cm^{-1} (non-hydrogen bonded urethane carbonyl), 1702cm^{-1} (hydrogen bonded urethane carbonyl), 1102 cm^{-1} (soft segment C-O-C), 1078cm^{-1} (hard segment C-O-C) and 1018cm^{-1} (Si-O-Si). Samples compared were all loaded with 3wt% silicate so that changes in the resulting spectra could be attributed to the interaction with the drug. There were no apparent changes with small increases in DexA concentration but a large shift from 1064cm^{-1} to 1054cm^{-1} at the peak relating to the hard segment ether group (C-O-C) was observed when the concentration increased to 10wt%. In contrast, the addition of only 1wt% DexP resulted in large shifts from 1064cm^{-1} to 1043cm^{-1}, suggesting stronger interactions between DexP and PU.

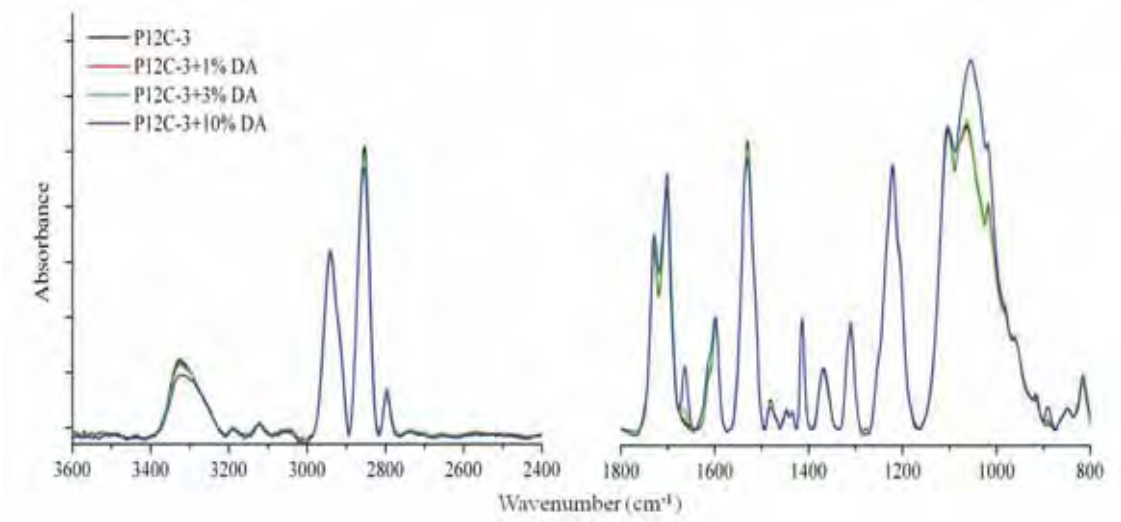

Figure 6.7 ATR-FTIR spectra for PUNC-3wt% with varying concentrations of DexA. Shifts from 1064cm^{-1}(aliphatic ether), to 1054cm^{-1} indicates preference for drugs to interact at those regions.

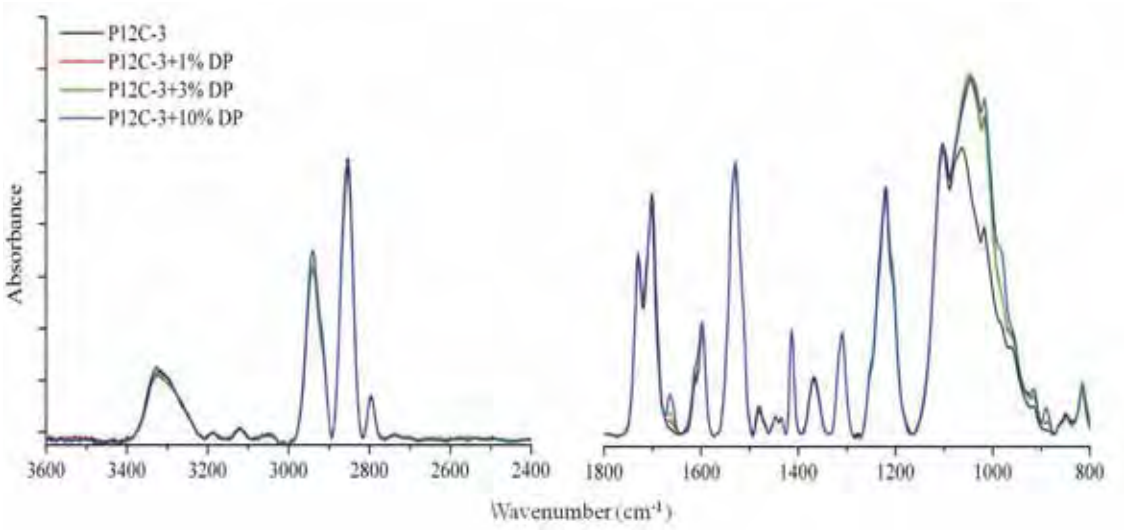

Figure 6.8 ATR-FTIR spectra for PUNC-3wt% with varying concentrations of DexP. Shifts from 1064cm^{-1}(aliphatic ether), to 1043cm^{-1} indicates preference for drugs to interact at those regions.

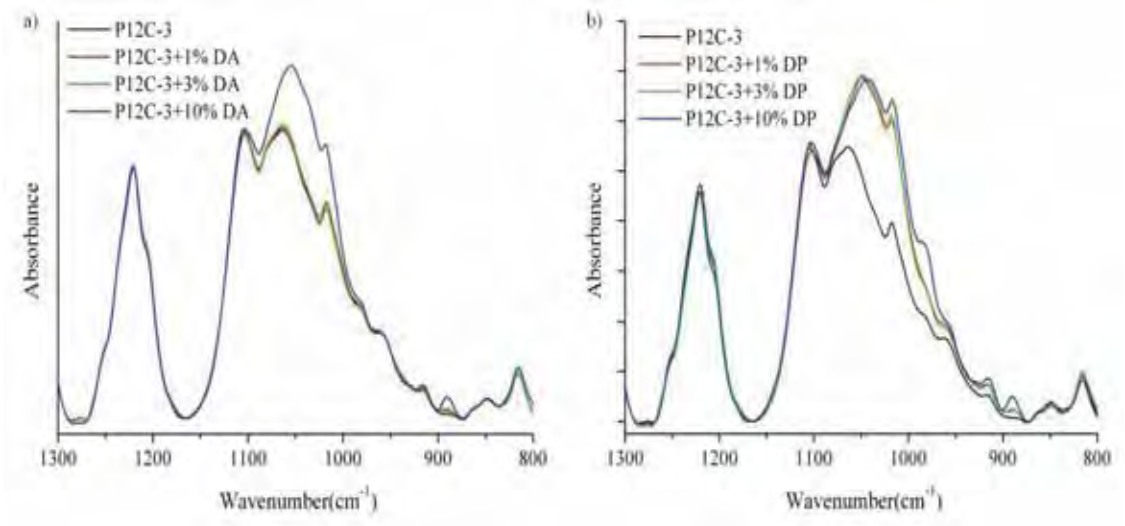

Figure 6.9 ATR-FTIR spectra of PUNC-3wt% loaded with a) DexA and b) DexP at wavenumbers from 1300-800cm^{-1}.

6.3.2 MD simulation

Models of three different NC systems with and without drugs are shown in Figure 6.10. At equilibration state, the modifiers in all three systems lie close to the clay surface. Some PU chains are also attached to the clay surface and the drug molecules are mixed with the PU matrix. Table 6.7 and 6.8 show the total interaction energies between any two components in the PUNC-drug and PU-drug system respectively. Each individual contribution is represented by electrostatic, van der Waals, and Born interactions.

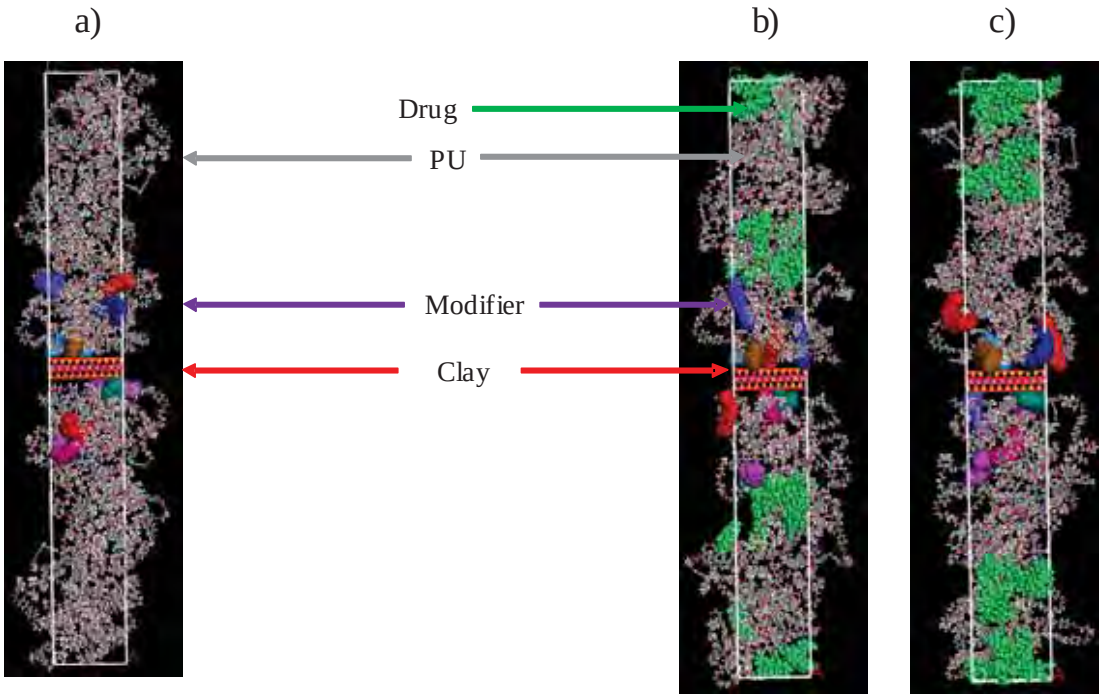

Figure 6.10 Models of MD results of exfoliated NCs: a) PUNC; b) PUNC-DexA; c) PUNC-DexP. Simulation cell: a=25.959, b=27.0459, c=200 Å, α=β=γ=90oC. Clay platelet (middle crystal sheet), modifiers (large colourful spheres), PU (ball and stick), and drug (small green spheres).

Table 6.7 Interaction energies (kcal/mol) between any two components in an exfoliated PUNC at equilibrium (average at last 20ps)

System (Molar ratio)	Pair interaction	Electrostatic	vdW	Born	Total
PUNC (clay:modifier:PU =1:0.333:0.467)	Clay-modifier	-7476.55	-68.81	56.74	-7488.62
	Clay-PU	-5501.72	-187.45	59.80	-5629.37
	Modifier-PU	196.11	-442.81	196.68	-50.00
PUNC+ DexA (clay: modifier: PU:DexA =1:0.333:0.4:1)	Clay-modifier	-8212.81	-92.95	85.65	-8220.11
	Clay-PU	-5022.71	-144.80	40.34	-5127.17
	Clay-DexA	-1933.89	-3.98	0.01	-1937.86
	Modifier -PU	283.13	-388.68	157.46	51.91
	Modifier -DexA	11.54	-18.89	9.63	2.28
	PU-DexA	-160.03	-2128.25	771.73	-1516.55
PUNC + DexP (clay: modifier: PU:DexP =1:0.333:0.4:1)	Clay- modifier	-7783.08	-88.39	81.67	-7789.80
	Clay-PU	-5144.83	-164.08	46.86	-5262.05
	Clay-DexP	-26770.75	-3.76	0.02	-26774.49
	Modifier -PU	274.44	-439.09	193.88	29.23
	Modifier -DexP	23560.08	-0.05	0.03	23560.06
	PU-DexP	515.60	-2020.17	2036.02	531.45

Table 6.8 Interaction energies (kcal/mol) between any two components in PU-drug systems at equilibrium

System	Pair interaction	Electrostatic	vdW	Born	Total
PU + DexA	PU-DexA	-80.38	-934.00	356.41	-657.97
PU + DexP	PU-DexP	-108.85	-1190.20	1089.62	-209.43

Clearly, there is a strong attractive interaction between clay-surfactant as well as between clay-PU, indicated by the negative interaction energies. For the clay-surfactant interaction, the main contribution was the electrostatic interaction between the positive head group and the negative clay surface, while for clay-PU interaction, it mainly came from both electrostatic and van der Waals interactions. Interestingly, the interaction between the drug and other components was quite different in both drug systems. In the PUNC-DexA system, there are strong attractive interactions between clay-DexA and between PU-DexA. However, in PUNC-DexP system, apart from the attractive interactions between clay-DexP, there is also a strong repulsive interaction between surfactant-DexP and a weaker repulsive interaction between PU-DexP.

6.4 Discussion

The results from these studies showed that the addition of negatively charged DexP increased the silicate spacing and that DexP was likely to interact with the hard segment ether groups of PU. This interaction between DexP and the PUNC system significantly affected the drug release profile and the release of DexP was enhanced by addition of clay. On the contrary, spacings remain unchanged with the addition of DexA and no

strong interactions with PU were shown by FTIR and MD simulation results. This low level of interactions translated into sustained DexA release that was directly impacted by the addition of clay and the use of longer chain modifiers.

6.4.1 Impact of interactions on PUNC structure

The incorporation of DexA in PUNCs as evidenced by XRD did not lead to significant changes in the silicate spacing. This was similar to the findings observed by Silva *et al*. [132], where the addition of DexA into biodegradable PUNCs did not change the silicate spacings [132].Contrary to this, the addition of DexP in PUNCs led to greater increases in spacings for PUNCs loaded with 3wt% clay. The spacings of P12C-1+1 DP were also expected to have better dispersion than P12C-1+1%DA based on the better defined silicate spacings displayed from TEM images. Given that the addition of positively charged CV from the preceding chapter showed attractive interactions that can potentially displace modifiers from the MMT surface, the increase in spacing from the addition of DexP in this study was thought to be from the repulsive action between the MMT surface and the negatively charged P-O^- groups on DexP.

On the other hand, there are no strong interactions between DexA and MMT that could attract or repel to induce significant changes to silicate spacings, thus the dispersion remains unaffected by the addition of DexA. The effect of DexP in assisting clay separation however was not seen in PUNCs with 5wt% loading, and the spacings measured by XRD were similar to PUNCs without added drugs. Along with the XRD findings obtained in the previous chapter with the three model drugs, this suggested that the addition of drugs can only impact silicate dispersion at lower clay loadings. NCs at

higher clay loadings will generally show a decrease in silicate spacing due to the higher tendency to form aggregates.

The FTIR spectra of PUNCs with drugs did not show any new characteristic absorption bands compared to PUNC systems without drugs, suggesting there was no obvious chemical reaction between the drug and the matrix which would impede its diffusion [132, 283]. However, there was evidence suggesting that stronger interactions occur between DexP and the PUNC system. For both drugs, the shift in absorption bands at the hard segment ether groups and dampened characteristic of the Si-O stretch, provided evidence for intermolecular interactions between the drug and the NC system and the preference for both drugs to interact at those regions. The instant shift in the peaks at the hard segment ether groups with only 1wt% of DexP as compared to the higher concentrations (10wt %) of DexA required to induce similar changes, suggested stronger interactions between PU and DexP. Theoretical considerations of the potential interactions that could occur between DexP-PU indicated attractive interactions between NH groups of PU and $P\text{-}O^-$ groups of DexP. Hydrogen bonding could also occur between NH and P=O groups. These attractive interactions at the hard segment could be responsible for the large shift in ether groups observed from FTIR.

Although FTIR could not provide information regarding the nature and magnitude of interactions from the addition of DexP, MD simulation indicated a large repulsive and attractive interaction with the modifier and clay respectively that was several magnitudes greater than that for DexA. This correlated well with the FTIR findings that DexP induced a stronger shift when incorporated in a NC system. The simulation between PU

and the drugs alone however, did not show a stronger attraction between PU and DexP as compared to PU and DexA but was accompanied with a larger Born energy (1089.62 kcal/mol). Born energy is the repulsive energy when two molecules come towards each other, suggesting that the incorporation of DexP into the NC system could have stronger attractions that required a larger repulsive energy to maintain it.

6.4.2 Impact of interactions on drug release behaviour

The cumulative release profiles of DexA and DexP in combination with the theoretical and experimental drug interaction studies indicated that interactions between the drug and the PUNC system can significantly impact the drug release behaviour. The release profile of DexA was dependent on the amount of clay and degree of dispersion. Improving the dispersion by using longer alkyl chains provided larger silicate spacings than shorter chains, thereby resulting in a more sustained release over time. This correlated well with the MD simulation where interaction energies between PU-DexA became stronger in a PUNC system (from -657 to -1516 kcal/mol). The presence of clay not only decreased the permeability of NCs due to the impermeable silicate particles, but the attractive interactions occurring between clay-DexA and PU-DexA also assisted in sustaining the release. In addition, as DexA is a neutral molecule which would not dissociate into ions, it is less likely to be affected by the charges present on the clay surface and therefore the addition of the clay with better dispersion (longer surfactants) could also retard the release.

As DexP is hydrophilic in nature, release into the medium should be quite fast [278, 284]. Interestingly, the release was only 15% from neat PU at the end of 5 weeks. This

suggests that the release of hydrophilic drugs from PU is not always characterised by a large burst release followed by an early plateau. The lower amounts of DexP released from neat PU could be due to strong molecular interactions with the host polymer. As discussed earlier, the large shifts in the hard segment ether groups from FTIR indicated strong interactions between DexP and PU that could have limited the release. This observation however, was not supported by the energies obtained from MD simulation. The simulation did not indicate very strong attractive interactions between PU-DexP (Table 6.8) that could explain the limited release seen in neat PU. However, as MD simulation was conducted on the basis of mutual interaction between components in an ideal environment, factors such as solvent, release medium and solubility between the drug and the polymer NC system, were not taken in consideration. These factors could have played an important role in retarding the release of DexP from PU through interactions that was not reflected by the calculated energies.

Studies have indicated that the acidobasicity of the incorporated drug can also play a major role in controlling drug release [277]. Einmahl *et al*. [277] observed that the release of DexP from poly (ortho ester) was only slightly higher than DexA and was not ideal when considering its hydrophilic nature and negatively charged functional groups [277]. It was suggested that the incorporation of the basic sodium phosphate salt DexP could have buffered the system and slowed down the release [277]. Furthermore, Kim *et al*. [278] reported that the use of DMAc is a good solvent for DexA but not for DexP which could also affect the surface topography of PU and hence, the release behaviour [278]. Although their studies reported a higher release of DexP than DexA, the initial

drug loading was higher (10wt%) and the matrix was a polycarbonate based PU system which would have different interactions with the incorporated drugs [278].

The release of DexP was enhanced by the introduction of clay. Unlike DexA, the release behaviour was also not sustained by further addition of clay or by the use of longer chain modifiers. According to the work conducted by Lee *et al*. [173], if the charge between the drug and the system is the same, then the release ratio is higher through repulsive interactions [173, 251, 253]. Since a repulsive interaction exists between the MMT surface and the negatively charged P-O^- groups on DexP, the addition of silicates could have promoted the release. This effect was more apparent when clay content increased from 1wt% to 5wt%, increasing the release amount of DexP from 39% to 64% in the case of P12s. The MD simulation for PU-DexP was also in agreement with the drug release assay, where the interaction energies between PU and DexP changed from attraction (-209.43 kcal/mol) to repulsion (531.45 kcal/mol) after clay was introduced.

6.5 Conclusion

The impact of interactions on the structure and release behaviour of PUNCs was further investigated in this study by using two drugs with similar size and chemistry. The incorporation of neutral drugs, such as DexA, to PUNCs did not led to significant changes in silicate spacings as evidenced by XRD. However, the addition of negatively charged DexP did increase the silicate spacings, possibly due to repulsive interactions with the MMT surface. Through techniques such as FTIR and MD simulation, both drugs indicated interactions with PU. However, the instant shift in the peaks at the hard

segment ether groups from FTIR with DexP as compared to DexA, suggested stronger interactions between PU and DexP. Although MD simulation did not indicate a stronger attractive interaction for PU-DexP, further simulations performed in the presence of solvents or release medium should allow a more accurate representation of the interactions present in PUNCs after fabrication and during release.

Interactions between the drug and PU were found to play a dominant role in the drug release behaviour. DexP showed limited release from neat PU due to attractive ion-dipole interactions between the negatively charged phosphate groups of DexP and the hard segments of PU, whereas the release of DexA from neat PU was unaffected by the weaker dipole interactions and was sustained mainly through its hydrophobic nature. The subsequent introduction of clays to modulate the release also largely depends on the interaction between the clay and drug. Drugs that are not affected by charges on the clay, such as DexA, can be sustained through hydrogen bonding, dipole interactions and the presence of impermeable silicate particles. On the other hand, drugs that possess the same charge as the clay are generally repelled from the system due to electrostatic interactions, thereby promoting the release.

In summary, the interactions arising from the addition of a drug into an NC system can impact on the silicate dispersion and drug release behaviour. Interactions between the drug and the host polymer can have a more dominant effect in perturbing the release behaviour than by the drug type: hydrophilic or hydrophobic. The addition of clay to PU to modulate drug release does not necessarily sustain the release but can actually promote the release if the drugs have a repulsive nature with clay. The complementary

use of physical experimentation and computational modelling has shown to be a powerful technique providing both qualitative and quantitative data on the structure and molecular interactions within the system. These results suggest that by understanding interactions and selecting appropriate drugs, polymer NC systems can be applied to various applications that require different release mechanisms. The following chapter will focus on the biological interactions of PUNCs along with a continuing investigation into the effect of molecular size on the drug release behaviour.

Chapter 7: Polyurethane Nanocomposites as carriers of therapeutic drugs

7.1 Introduction

In the preceding chapter, two molecules from the same class of steroid drugs with different charge and hydrophilicity were investigated for their impact on PUNC structure and release behaviour. Along with the initial findings in Chapter 5, it was demonstrated that release of hydrophobic drugs from PU and PUNCs was more sustained than that for hydrophilic drugs. However, when strong attractive interactions exist with the host polymer, it was found that hydrophilic drugs can become more sustained than hydrophobic drugs. These interactions were mainly due to the net charge and polarity of hydrophilic molecules, thereby allowing them to have greater interactions with PU or with clay. The subsequent introduction of silicates has an "additive" effect that perturbs the release profile based on the net charge of the drug. If the charge of the added drug has a repulsive action with clay, then increasing clay loading can promote the release. On the other hand, when the drug is neutral, the addition of clay can retard the release via the tortuous pathway model as it is less affected by interactions with clay.

This chapter extends the investigation of drug-PUNC interactions by selecting an alternative drug paclitaxel (Ptx), which is clinically relevant for stent applications in treating restenosis. Ptx is hydrophobic in nature and similar in size to Coomassie blue (CB). Some of the reasons for the limited release of CB in Chapter 5 were thought to be

due to molecular size and potential interactions with the PUNC system. Based on the observation in the preceding chapter that hydrophilic drugs (DexP) can demonstrate larger interactions with the PUNC system than hydrophobic drug (DexA), it is hypothesised that Ptx hydrophobicity will overcome any size restriction that was evident in CB. Furthermore, Ptx release from PU can be modulated by introducing layered silicates. The studies in this chapter also aim to investigate the impact of fabrication method on the cellular response to PUNCs and most importantly to assess the activity of the released drug.

7.1.1 Drug activity and release

7.1.1.1 Paclitaxel

Ptx is an anti-proliferative drug commonly used in cancer chemotherapy. It reversibly binds and stabilises microtubules, which are the structural components within the cytoskeleton of a cell [15]. Limiting flexibility of the cytoskeleton via this mechanism interferes with intracellular transport and cell division in the G0/G1 and G2/M phase. Ptx is also used in the prevention of restenosis due to its effect on stopping cell proliferation and migration [15, 285]. In a review of polymer NCs in the current literature, studies on PUNCs incorporating Ptx could not be found. However, studies related to Ptx delivery from PU matrices have been reported in areas of stent therapy. These include biliary [286], urethral [287], tracheal [288], gastrointestinal [289] and in coronary stents [11, 290]. Of all these studies mentioned above, only one study analysed the *in vitro* release behaviour from a non-degradable PU matrix [289]. The release of Ptx was found to be largely affected by the hydrophobicity of Ptx which can resist water

penetration and drug dissolution. It was shown in the study that PU matrices loaded with 0.45wt% of Ptx released 78% over 42 days, whereas Ptx loadings of 5.4wt% released only 8% in the same time frame [289].

7.1.1.2 Dexamethasone

Dexamethasone (Dex), employed in the previous chapter belongs to the glucocorticoids family and is one of the most potent anti-inflammatory drugs for treatment of chronic inflammatory disease and postsurgical inflammations [291]. Through direct interaction with the receptors in the cytoplasm as well as inhibition of transcription factors that regulate inflammatory gene expression, Dex is able to inhibit multiple inflammatory genes, such as cytokines, chemokins, adhesion molecules and enzymes [292]. In addition to suppressing inflammatory genes, glucocorticoids can also increase the synthesis of several anti-inflammatory cytokines (lipocortin-1, clara cell protein (CC10), and interleukin (IL)-1 and 10 receptor antagonist) to further enhance their effect [293]. Studies have also shown that the use of Dex decreases smooth muscle cell (SMC) or fibroblast (L929) growth by blocking cell cycle progression in the late G1 phase [294, 295].

Since there is a positive correlation between inflammation and growth of SMC, the incorporation of Dex into PU matrices can be found in the treatment of ocular diseases [296], post-strabismus surgeries [53], pacemaker leads [297] bronchial and also coronary stenting [10, 298, 299]. As reported from those studies, adding Dex suppresses inflammatory reactions which decreases cell infiltration and enzymatic activity [10, 299], decrease cell growth, and the formation of granulation tissues [298].

Studies in the literature regarding the use of PUNC systems to deliver Dex have been reported Silva and co-workers [132, 300]. A biodegradable PUNC based on MMT and poly (ethylene glycol) (PEG) or poly (caprolactum) (PCL) was investigated. An *in vitro* test conducted on PCL based PUNCs showed no release of toxic components after 7 days when placed in contact with human retinal pigment epithelial cells (ARPE-19) [300], while an *in vivo* mice model from PEG-PCL based PUNCs showed that the continuous release of Dex resulted in a reduction in inflammatory response over the 14 days tested [132]. The incorporation of Dex in both cases did not lead to a disturbance in morphology but was observed to create lesser defined phase separations between the hard and soft segments of PU [132, 300].

7.1.2 Biological response of PUNCs and PUNC coatings

Cell growth inhibition assays are common pre-clinical studies to test the biological response of samples as these assays can provide rapid screening of cytotoxic agents [301, 302]. Of the few in the literature that assessed the biological interactions of PUNCs, Styan *et al* [135, 303] showed that PUNCs modified with 1-aminoundecanoic acid (AUA) had no effect on mammalian cell growth. Both neat PU and PUNCs modified with AUA also did not affect cell growth and membrane integrity when analysed using flow cytometry [303]. Interestingly, an improvement in anti-bacterial activity against *S. epidermidis* was observed when PUNCs were co-modified with both AUA and Ethoquad ® O/12PG (EQ). However, increasing the concentration of EQ to above 50% CEC showed unacceptable levels of cell growth inhibition [135]. These studies suggested that through careful combination of suitable modifiers, PUNCs not only can

show good cell compatibility but can also possess additional functionality, such as anti-bacterial activity [135].

Of interest is the possibility of coating polymer NCs onto either metallic, polymeric surfaces or existing medical devices. Zaporojtchenko *et al*. [224] investigated the potential of co-sputtering noble metals (Ag and Au) with polytetrafluoroethylene (PTFE) to produce anti-bacterial coatings. A simultaneous sputtering of polymer and metals onto silicone or polycarbonate foils were tested for their ability to provide sustained anti-microbial properties. Although the interaction of these coatings with cells was not tested, the coatings demonstrated good bonding and dispersion from TEM and reduced bacterial growth (*S.aureus*) by five orders of magnitude as compared to neat PTFE [224].

In the majority of studies cited, PUNCs were fabricated as films rather than as coatings. In addition, studies of PUNC coatings onto metallic substrates are typically not intended for medical purposes [304-306]. However, there are reports using PUNCs based on polyhedral oligomeric silsesquioxane (POSS) with poly (carbonate-urea) urethane (PCU) for coatings on medical devices [307, 308]. These PUNCs were dip-coated onto mandrels for potential as microvascular grafts [308], or onto NiTi alloy by electro hydrodynamic spraying for stent coatings [307]. In both cases, coated POSS-PCU demonstrated good mechanical and bonding strength. Although there were no assays conducted to directly assess their toxicity within a biological environment, these coatings exhibited good integrity upon exposure to plasma or protein solutions up to 70 days [307], and also allowed endothelial cell proliferation [308]. Since the methods used in this study to fabricate PUNC films and coatings were quite similar, with the exception

of processing temperature and time, it is expected that PUNCs fabricated into coatings will show similar compatibility to those fabricated as films within a biological environment.

In summary, the research presented within this chapter sets out to examine the performance of fabricated PUNCs and PUNCs incorporated with drugs (Dex and Ptx) in a biological environment. The focus is on the biological performance of PUNCs fabricated using different methods and on assessing the retention of drug bioactivity in drugs post-release from PUNC systems. It is hypothesised that PUNCs fabricated either as films or coatings should not be cytotoxic, and will be capable of delivering bioactive therapeutic drugs. More specifically the aims of this chapter were to:

1. Investigate the drug release behaviour and activity of a larger hydrophobic drug, Ptx from PUNC coils.

2. Examine the impact of PUNC fabrication method on the cellular responses to the material.

3. Assess the activity of DexA released from PUNCs films and the efficacy of using PUNCs for prolonged release.

7.2 Methods

7.2.1 Nanocomposite preparation

DexA loaded films were prepared through the same methods described in Chapter 6 by solution casting. Paclitaxel (Ptx) coated coils were fabricated by methods as described in Chapter 4 and Ptx was added at 10wt% loading (g/100g PU). This loading, calculated to be 108 ug/cm^2, was chosen to be similar to the Ptx loading on Taxus ™ stent (Boston Scientific, USA) of 100 ug/cm^2 [15, 16, 309]. A summary of the materials investigated in this study is summarised in Table 7.1.

7.2.2 *In vitro* Ptx release

Drug release was conducted by immersing Ptx coils (15cm) into a sink volume (15ml) containing 10 vol% of methanol in PBS to ensure paclitaxel remains soluble. This also ensured that Ptx was not adsorbed into the glass moulds and plastic containers during the assay [310]. The samples were then placed on an orbital shaker in a 37^{o}C incubator. Aliquots (1.5 ml) were taken at regular time intervals, and replenished with fresh solution for a total of 3 weeks. The assay was repeated in triplicates and each assay consisted of a triplicate of each material. Drug release was tracked using a UV-spectrophotometer at 227nm.

Table 7.1 Materials investigated within Chapter 7

Material ID	OMS	Loadings (g/100g PU)		Biological tests[a]
		Clay	Therapeutic	
PUNC films			DexA	
PU	-	-	-	C, P, I
P16C-1	16CH_3MMT	1	-	C, P
P16C-5	16CH_3MMT	5	-	I
PU+1% DA	-	-	1	C, P, I
P16C-1+1% DA	16CH_3MMT	1	1	C, P
P16C-5+1% DA	16CH_3MMT	5	1	I
PUNC coils			Ptx	
PU	-	-	-	C
P16C-1	16CH_3MMT	1	-	C
P16C-5	16CH_3MMT	5	-	C
PU+P	-		10	C
P16C-1+P	16CH_3MMT	1	10	C
P16C-5+P	16CH_3MMT	5	10	C

[a] Biological test conducted on the samples: C= cell growth inhibition assay; P= cell growth assay; I= inflammatory response assay

7.2.3 Biological response assays

7.2.3.1 Cell culture

Model cell lines used to conduct biological assays in this study were L929 mouse fibroblast and U937 monocytic cell line, cultured in Eagle's minimal essential medium

(EMEM, Sigma Aldrich) and RPMI-1640 (R8755, Sigma Aldrich) respectively. Media were supplemented with 10% foetal bovine serum and 1% penicillin/streptomycin (P/S).

7.2.3.2 DexA films-cell growth inhibition assay

Cell growth inhibition (CGI) assay was conducted on PUNCs to determine the effects of material extracts on the growth of mammalian cells. Test materials were prepared in accordance to AS ISO 10993 standards [311]. Controls used in this assay included: latex (positive control), silicone (negative control, Dow Corning), 4% ethanol, 5% ethanol, 7.5% ethanol, vial only extraction media, and media only (null). Materials were punch-cut into 1.5'' diameter disc, placed into extraction vials made from borosilicate glass and sealed for sterilisation via ethylene oxide (EtO) gas (Prince of Wales Hospital, NSW). The materials were then left to degas in a laminar flow hood for 7 days.

L929 murine fibroblasts were used as a model cell line for this assay and seeded at a density of 5×10^4 cells/ml (2ml) into tissue culture dishes (35 mm) and incubated (37ºC, 5% CO_2) for 24 hrs. Vials containing the materials for extraction were also incubated for 24 hours alongside with the tissue culture dishes. The materials were extracted in EMEM (3.8ml). After 24 hours, the media were removed and replaced with the extraction fluid (1ml) followed by incubation for a further 48 hours. Samples that were not exposed to extraction media (null) were replenished with fresh media instead. Following the incubation period (48 hours), the extraction fluid containing cells that were not adhered onto the culture dish was first removed and put to the side. Subsequently, trypsin: osmol (1ml, 50:50 vol %) was used to detach the cells from the dish. Once the cells were detached from the surface, the extraction fluid was added back

to the cell suspension and the cell number and viability were determined using a Vi-Cell XR Cell viability analyser.

CGI was expressed as a ratio of the number of cells in test material to the number of cells in PU control. A ratio of 0.7 or higher was considered an 'acceptable level' of cell growth inhibition within this assay. Materials were performed in triplicates and the assay was repeated in triplicates.

7.2.3.3 DexA films-CGI inhibition level

A standard curve was produced to estimate the amount of DexA released from the materials in terms of the level of cell inhibition. The assay was conducted in the same manner as the CGI assay described earlier, but instead of exposing cells to material extracts, the cells were exposed to a range of DexA concentrations (0.01, 0.1, 1, 10, 100 and 500µM). DexA was prepared in EMEM media and the solution (1ml) was added to the cells after the first 24 hrs of incubation. At the end of the assay, the cell number and viability were determined using a Vi-cell XR cell viability analyser and the results were expressed as the ratio of cells in the test against cells in a tissue culture plate (TCP) with normal media (control).

7.2.3.4 Ptx coils-cell growth inhibition assay

Coils (4cm sections) were extracted in EMEM media (4ml) to give 0.1-0.2g/ml of extraction vehicle as suggested in AS ISO-10993 [311]. CGI of Ptx coated coils was sterilised and tested in a similar method described in Section 7.2.3.2. The controls used include: EMEM media (null), extraction media, 4% ethanol, 5% ethanol, 7.5% ethanol,

and a solution of Ptx. The concentration of added Ptx in solution (EMEM) was based on the amount released within the first 48 hours from the *in vitro* drug release profile of P16C-1+P. Results were analysed and displayed as a ratio of cells in the test material to cells in PU coils.

7.2.3.5 Ptx coils-CGI inhibition level

A standard curve for Ptx inhibition level was set up in a similar manner as described in Section 7.2.3.3. L929 fibroblasts were exposed to Ptx concentrations of 0.02, 0.2, 2, 100 and 200μM in EMEM media. Results were displayed as a ratio of cells in test to cells in a TCP with normal media (control).

7.2.4 Drug activity assays

7.2.4.1 DexA films-cell growth assay

In order to test whether the activity of the drug released was sustained over time, a growth assay using Vi-cell analyser was conducted. Samples were punch-cut into 7/16'' diameter disc, sealed and sterilised via ethylene oxide (EtO) gas. At day 0, L929 murine fibroblasts, were seeded with 3ml at the density of 2×10^4 cells/ml (37ºC, 5% CO_2) for 3 hours for cells to adhere. After the cells adhered onto the tissue well plate, test samples were added such that they were completely submerged in the media yet floating on top of the cells. Measurements were taken at days 1, 3, 5, 7 and 10. Fresh media was replenished at every second day. At every time point for measurement, samples were removed and the cell numbers were measured by Vi-cell XR cell viability analyser after detaching with trypsin: osmol (50:50 vol %) solution.

For null controls, wells were prepared with cells in culture media only. DexA in EMEM solution was also used as a control to examine the behaviour of cells exposed to only short periods of drug rather than continuous periods of exposure. Since the cells were replenished with fresh media on day 2, the added drug amount was equivalent to the first 48 hours of drug released from the release profile of PU+1% DA films. Statistical analysis was performed using a two-way analysis of variance (ANOVA) followed by a pairwise comparison between the samples using Tukey's method. Significant difference was indicated by $p<0.05$. Details of the analysis can be found in Appendix A.3.

7.2.4.2 DexA films-TNF-α determination by enzyme-linked immunosorbent assay (ELISA)

The ability of DexA to suppress pro-inflammatory mediators following release from PUNCs was assessed by an *in vitro* inflammatory response assay. U937 monocytic cell line was chosen as a model cell line for this assay and can be activated by phorbol 12-myristate 13-acetate (PMA, Sigma Aldrich) to possess characteristics of monocyte derived macrophages (MDMs). Activated cells are capable of releasing pro-inflammatory cytokines including tumour necrosis factor-alpha (TNF-α). TNF-α was monitored in this study as it is a potent inflammatory mediator produced when monocytes adhere onto material surfaces.

Samples were punch-cut into 1.5'' diameter disc, sealed and sterilised via ethylene oxide (EtO) gas. U937 cultured in RPMI-1640 was activated by PMA, herein referred as U937*. For every 10ml of 1×10^6 cells/ml, PMA (100uM stock solution) was added to achieve a final concentration of 1×10^{-7} M PMA and incubated (37ºC, 5%CO_2) for 72

hours. Following activation, as shown in Figure 7.1, the conditioned media were discarded and cells rinsed with sterile Dulbecco's phosphate buffered saline (DPBS) and trypsinised (3ml trypsin in a T75 tissue culture flask) for 2 min at 37 °C. The cells were then collected, centrifuged and counted by a Vi-cell XR cell viability analyser.

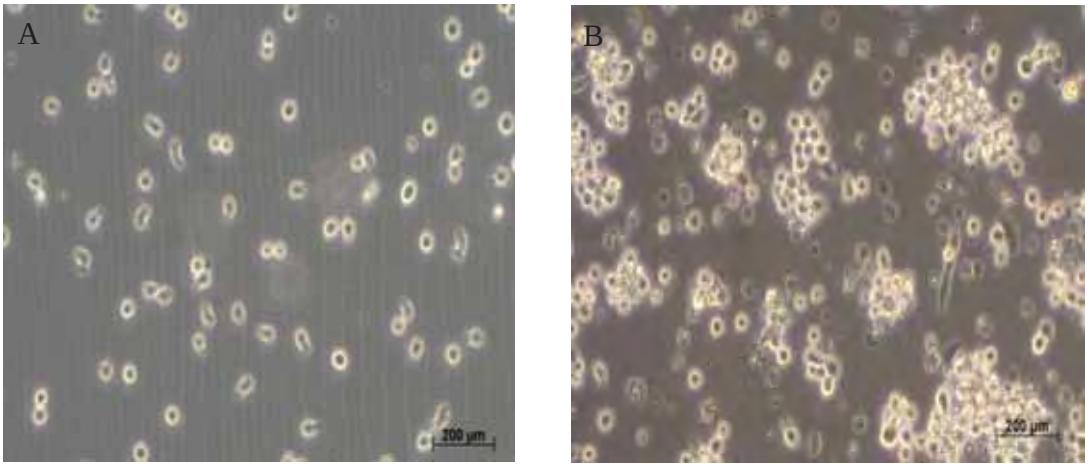

Figure 7.1 U937 cells; a) not activated and b) activated by PMA (U937).*

The experiment was conducted with the cell density of 1×10^6 cells/ml in each well. For test samples, activated cells were stimulated by lipopolysaccharide (LPS, Fluka Biochemika) to induce TNF-α secretion. Samples were then placed in contact with the stimulated cells and incubated for further 24 hours. After 24 hours, the supernatants were collected, centrifuged and then stored in Eppendorf tubes at -70ºC until analysed. The controls used in this assay include: U937* blank (negative control), U937*+LPS (positive control) and U937 not activated +LPS. DexA in RMPI-1640, equivalent to the amount released in the first 24 hours, was also used as controls, labelled: U937* +LPS +Dex and U937* +Dex. All samples were conducted in triplicates and the assay repeated at least three times.

A sandwich enzyme immunoassay technique was employed to quantify the amount of TNF-α release from either U937 or U937*. A 96 well ELISA plate pre-coated with monoclonal antibody specific for TNF-α was obtained from R & D systems (STA00C, Bioscientific). Buffered protein base (50µL) and 200uL of standard were added to each well. Subsequently, either the sample or control were added to the designated wells and incubated at room temperature (RT) for 2 hours. The standards were prepared as instructed by a dilution series of human recombinant TNF-α with serum. After washing with wash buffer, 200µL of TNF-α conjugated with horseradish peroxidise was added to each wells and incubated at RT for 1 hour. Wells were washed and 200µL of colorimetric substrate was applied and the plate was incubated in the dark for 20 mins. Stop solution (50µL) was then added and the absorbance of each well was measured at 450nm. The results were expressed as the percentage of TNF-α released compared to the positive control (U937*+LPS).

Statistical analysis was performed using a two-way analysis of variance (ANOVA) followed by a pairwise comparison between the samples using Tukey's method. Significant difference was indicated by $p<0.05$. Details of the analysis can be found in Appendix A.3.

7.2.4.3 DexA films-TNF-α suppression level

A standard curve was produced to estimate the amount of TNF-α suppressed by DexA. The assay was predominantly performed in the same manner as described in Section 7.2.4.2, however U937* was exposed to different DexA concentrations (5, 50, 100, 200, 250 and 500µM). U937* +LPS and U937* blank were used as a positive and negative

control respectively. The amount of TNF-α released was determined by ELISA and the results were plotted as the percentage of TNF-α reduced from positive control against DexA concentration. All concentrations were performed in triplicates within each assay and the assay was repeated three times.

7.3 Results

7.3.1 *In vitro* Ptx release

The cumulative release profile of Ptx coated coils into PBS is shown in Figure 7.2. All samples had an initial burst in the first hour with P16 at 1wt% loading showing the largest burst release of 12.30% and pristine PU displaying the smallest release of 7.18%. A plot of cumulative release with respect to square root of time is shown in Figure 7.3. The steeper gradient of P16C-1+P than P16C-5+P and PU+P indicated a faster initial release rate. However, the large burst effect of all samples suggested that the majority of Ptx released initially from the coils was from loosely adhered Ptx on the surface. A comparison between Ptx loaded PU and PUNCs indicated that all loosely bound Ptx was released from PU within 3 days, whereas Ptx loaded in PUNCs showed a small but continuous release up to the final time point at 3 weeks. The initial release rate and total release amount of P16 at 1wt% clay loading (41.23%) were higher than at 5wt% clay loading (36.71%), suggesting that the addition of higher loadings of silicate particle and interactions can still retard the release of Ptx, but only slightly.

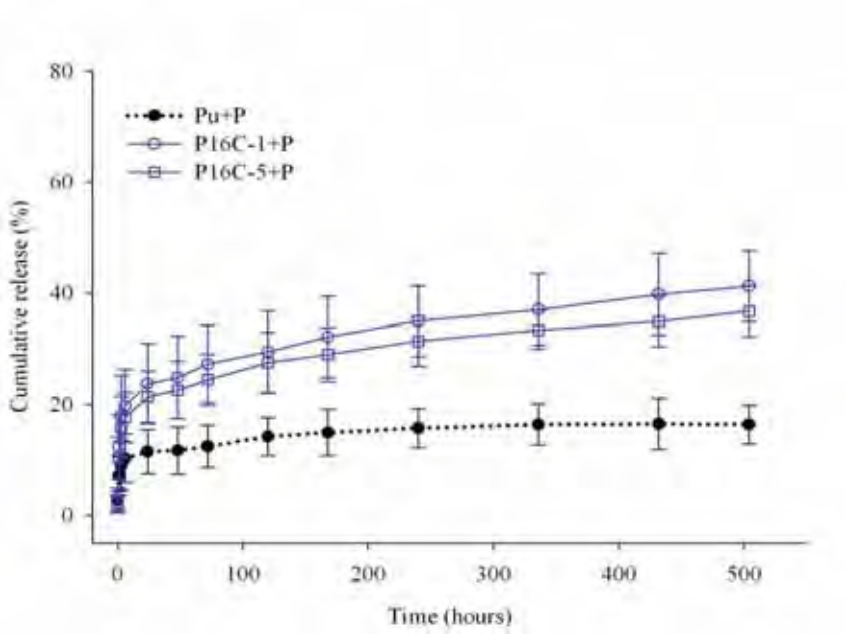

Figure 7.2 Cumulative release profile of coils incorporated with Ptx over 3 weeks (n=3). Data represents mean ± s.d.

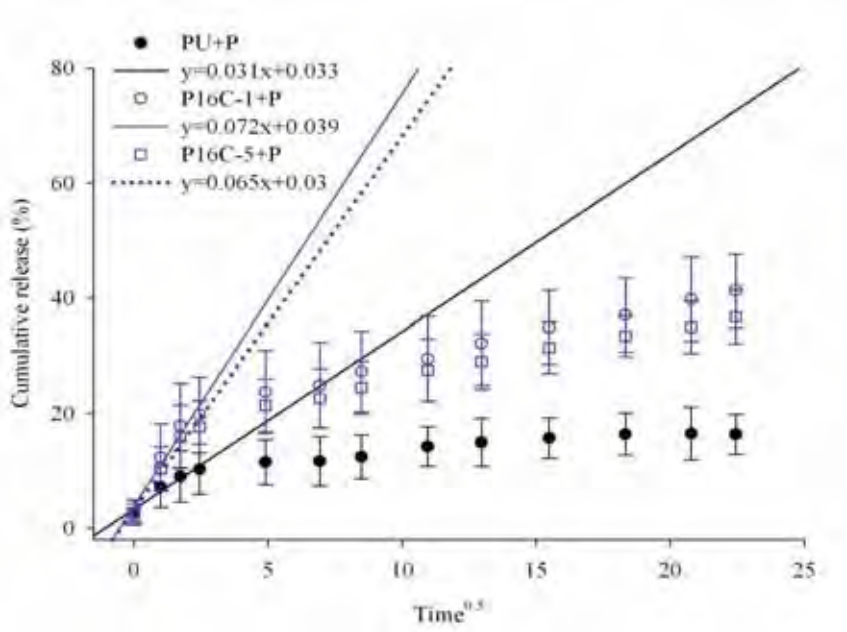

Figure 7.3 Cumulative release profiles of coils with respect to square root of time. Linear regression was performed on the initial burst of the release profile.

7.3.2 Biological response

7.3.2.1 PUNC films loaded with DexA

The CGI result is presented in Figure 7.4. Since the effect of DexA and DexP in cell growth inhibition were quite similar (shown in Appendix D), only DexA loaded materials were reported here. Although the addition of silicate particles in PU (P16C-1) showed slightly lower CGI ratio to that of pristine PU, no effect on cell viability was observed, indicating that PUNCs were not cytotoxic. The addition of DexA into PU and P16C-1 further reduced the CGI ratio but maintained high cell viability. There was no significant difference in CGI ratio between PU+1%DA and P16C-1+1%DA, suggesting that the amount of DexA released from the samples in the first 24 hours was quite similar.

In order to examine whether the decrease in CGI ratio from DexA loaded samples was due to the effects of DexA, a standard curve comparing CGI ratio to DexA concentration was established and shown in Figure 7.5. From the *in vitro* drug release profile conducted in the previous chapter, the amount of DexA released from PU+1%DA and P16C-1+1%DA was estimated to be 115μM and 109μM respectively. Using the standard curve, these concentrations should induce an inhibitory ratio of 0.41 ± 0.11. This was consistent with the CGI ratio observed for PU+1%DA and P16C-1+1%DA, where the ratios were 0.43 and 0.31 respectively. Therefore, the result indicated that the inhibition in cell growth from DexA loaded samples was due to addition of DexA.

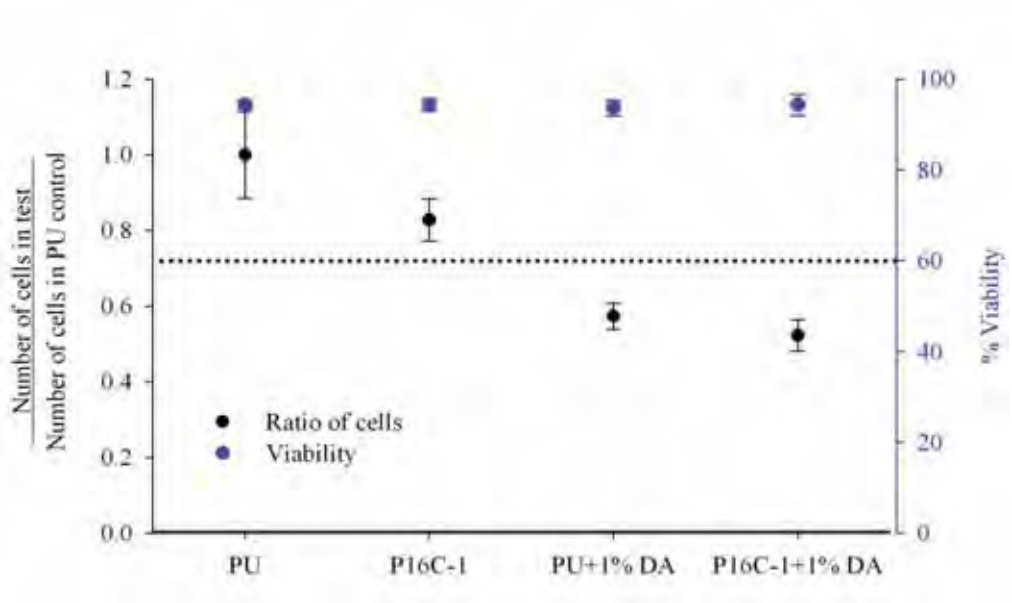

Figure 7.4 Cell growth inhibition assay of samples loaded with DexA versus the controls. Data presented represents a ratio of the no. of cells in test against no. of cells in PU control. Dotted line defines the threshold considered to be an acceptable CGI level. Mean ± s.d (n=3).

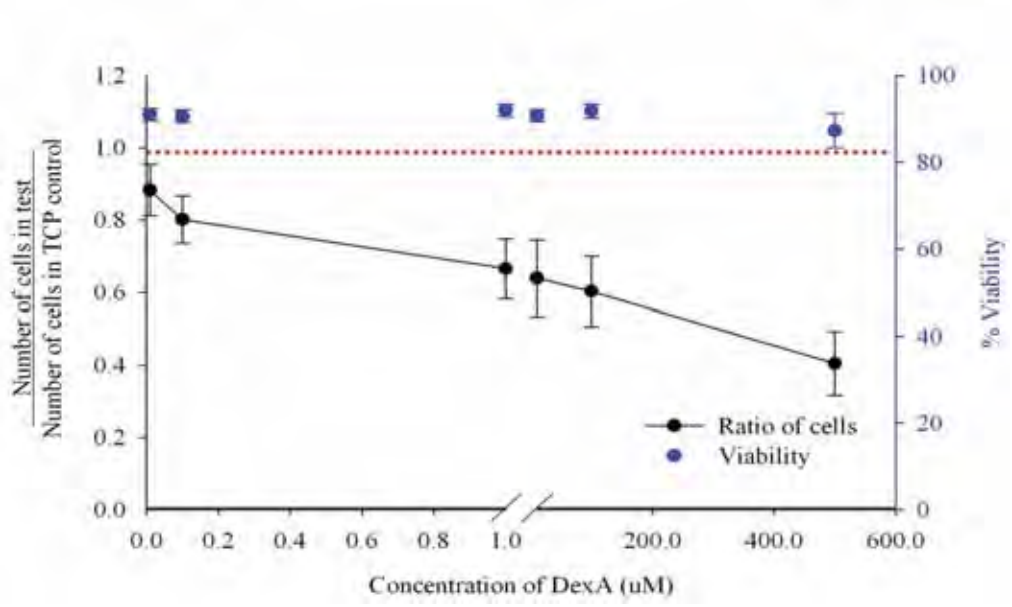

Figure 7.5 CGI standard curve for DexA. Data represents a ratio of cells in test against cells in positive control. Dotted line represents the positive tissue culture plate (TCP) control. Mean ± s.d (n=3).

7.3.2.2 PUNC coils loaded with Ptx

The CGI assay of coated coils is shown in Figure 7.6. PUNC coils without added Ptx demonstrated lower CGI ratio to that of neat PU. Both PUNCs modified with $16CH_3$ at 1wt% and 5wt% clay loading showed CGI bordering the 'acceptable limit' of 0.7, but still maintained a high viability of approximately 90%. On the other hand, the cell growth was largely inhibited in Ptx loaded coils regardless of the clay loading. To confirm if the decrease in CGI ratio was due to the effects of Ptx, a standard curve comparing mammalian cell growth to Ptx concentration was established and shown in Figure 7.7.

The CGI ratio decreased in a dose-dependent manner as Ptx concentration increased up to 2µM. However, the CGI ratio maintained at levels around 0.14-0.16 above 2µM. This indicated that there is a threshold concentration for Ptx to inhibit cell growth. The amount of Ptx that can be released from the coils within the first 24 hours was calculated from the release profile (Figure 7.2) and were 3.67, 8.01 and 7µM for PU+P, P16C-1+P and P16C-5+P respectively. This was consistent with the Ptx standard curve where concentrations above 2µM resulted in CGI ratios of 0.14-0.16. In addition, the viability across all concentrations of Ptx remained above 80%, indicating that the effect of Ptx inhibited cell growth but did not induce cell death.

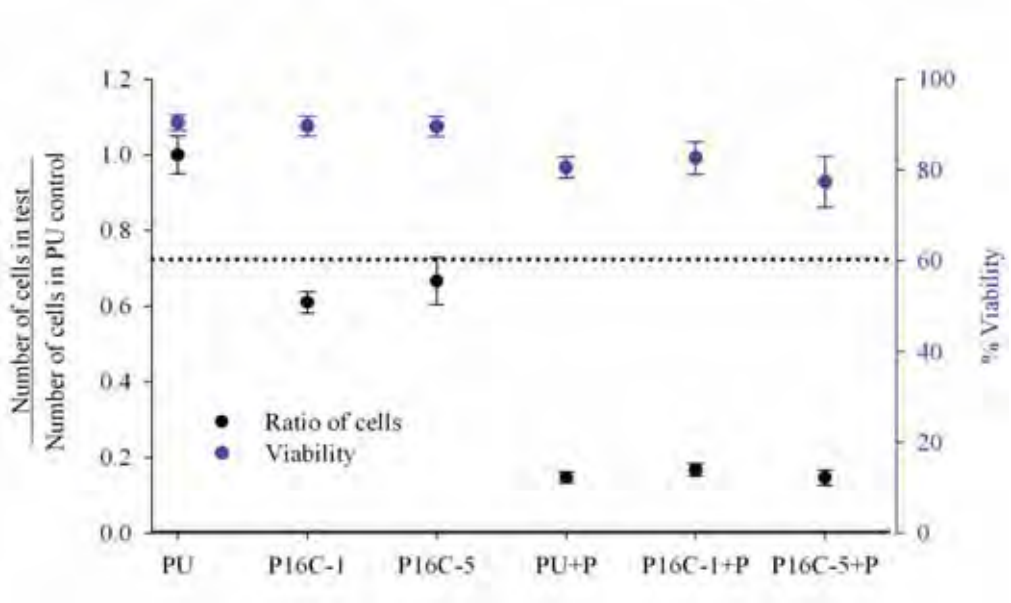

Figure 7.6 Cell growth inhibition assay of samples loaded with Ptx versus the controls. Data presented represents a ratio of the no. of cells in test against no. of cells in PU control. Dotted line defines the threshold considered to be an acceptable CGI level. Mean ± s.d (n=3).

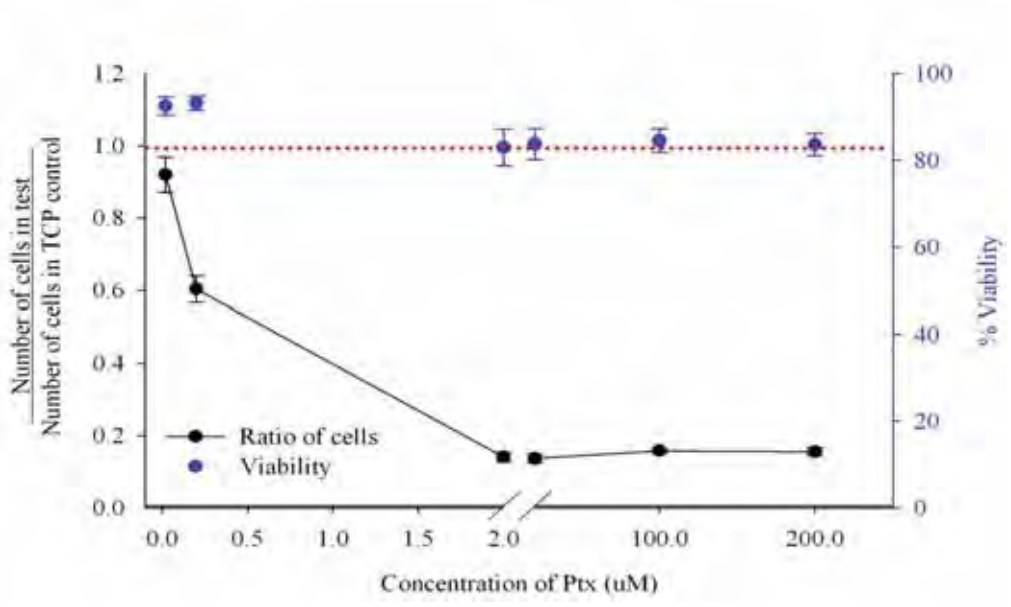

Figure 7.7 CGI standard curve for Ptx. Data represents a ratio of cells in test against cells in positive control. Dotted line represents the CGI ratio of the positive tissue culture plate (TCP) control. Mean ± s.d (n=3).

A comparison between the CGI ratio of PU and PUNCs without added drugs and fabricated differently is shown in Figure 7.8. PUNCs at 1wt% clay loading in both cases produced similar levels of inhibition and were not significantly different (p=0.535). On the other hand, the level of inhibition appeared to be lower for PU fabricated as coatings, but were not significantly different (p=0.130) to the films. The similarity in CGI ratio from both fabrication methods suggested that PU and PUNCs can be processed by the automated coating system at MCTec BV (Venlo, The Netherlands) without introducing by-products or contaminants that can affect the cell viability.

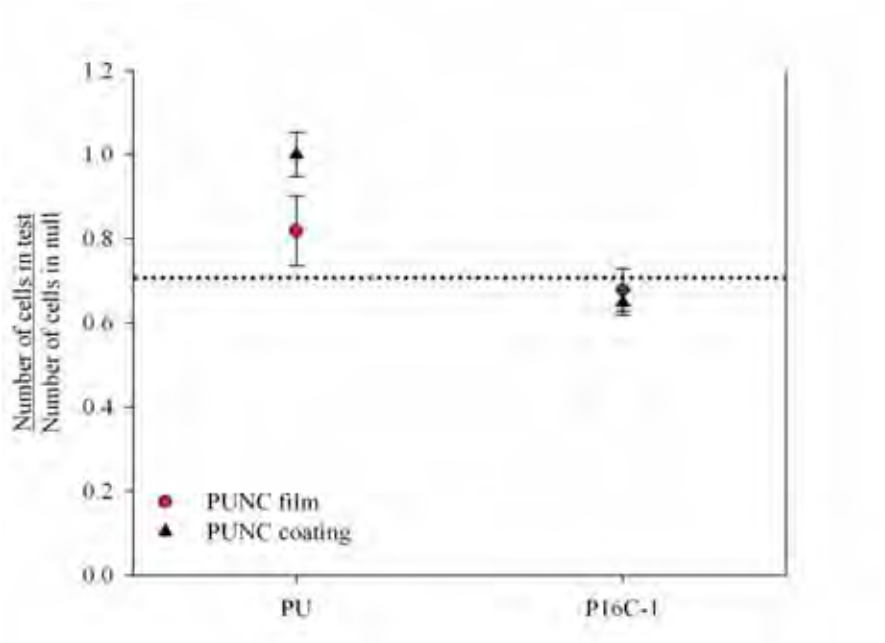

Figure 7.8 Comparison of cell growth inhibition of PU and P16C-1 fabricated in the laboratory (films) or industrially (coils). Data represents a ratio of the number of cells in the test samples against the number of cells in the null control (cells in media only). Dotted line defines the threshold considered to be an acceptable CGI level. Mean ± s.d (n=3).

7.3.3 Drug activity

Cell growth over 10 days in contact with DexA loaded PU and PUNCs is shown in Figure 7.9. Both PU and P16C-1 showed lower number of cells as compared to cells cultured in culture media alone over the 10 day period. The number of cells at day 10 between the two materials were not significantly different ($p=0.2478$). Materials loaded with DexA showed a further decrease in the number of cells compared to their corresponding controls ($p<0.05$).

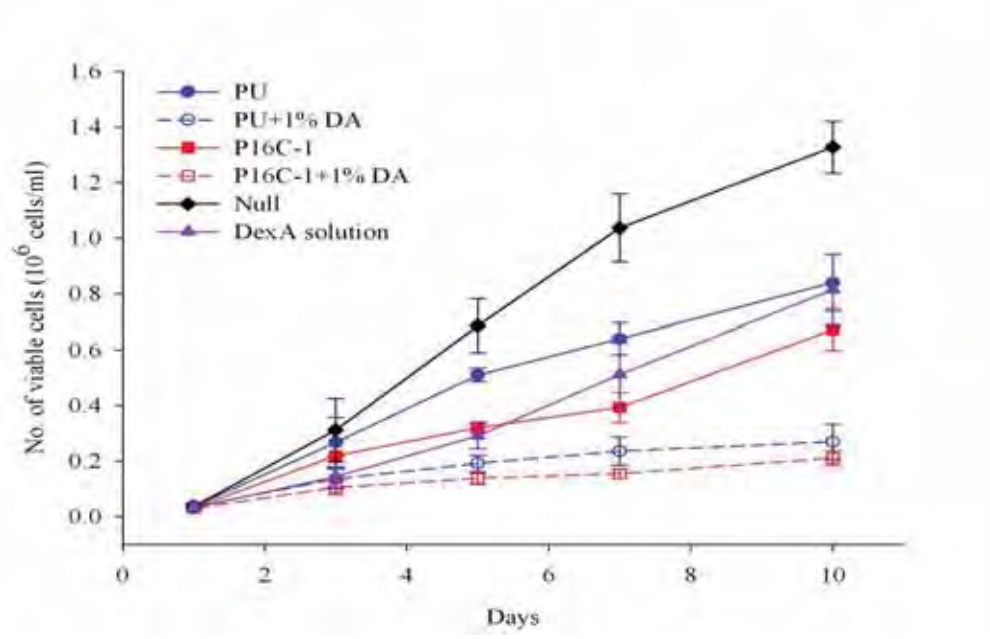

Figure 7.9 Cell growth assay of samples loaded with DexA over 10 days. Data represents mean ± s.d (n=3).As the difference in total drug release at day 10 for DexA loaded PU and P16C-1 was around 4% (Chapter 6), the cell numbers for DexA loaded PU and PUNCs maintained at a similar cell concentration over 10 days.

Noticeably, the cell numbers for DexA loaded PU and PUNCs maintained at a concentration of 0.15-0.2 $\times 10^6$ cells/ml, suggesting that DexA can inhibit cell growth

without reducing the cell viability. For cells that were exposed to DexA for short periods of time, a slow growth rate was observed up to day 3, after which cells proliferated and reached cell numbers similar to PU at day 10 ($p=0.9991$). This suggested that a continuous dosage of DexA may be required to inhibit cell growth and that the inhibition process is reversible after the drug has been removed from the cells.

The activity of DexA released from polymers was further tested in an *in vitro* inflammatory response assay. The amount of TNF-α produced by activated U937 (U937*) after 24 hours is shown in Figure 7.10. Results showed that the addition of DexA lowered the amount of TNF-α release by almost 50%. This was compared with the standard curve shown in Figure 7.11, which confirmed that the amount of DexA in media (Dex+L, approx. 220μM), can reduce the amount of TNF-α production by 50%. Given the small amounts of TNF-α produced from activated cells in the absence of LPS (U937* and Dex), the addition of LPS was necessary to stimulate the release of TNF-α so that the effect of DexA in suppressing the cytokine production can be exaggerated and examined readily.

Among the samples tested, both PU+1% ($p=0.0011$) and P16C-5+1% ($p=0.0162$) showed lower amounts of TNF-α compared to samples without added DexA. This demonstrated that DexA released from PUNCs was still effective against pro-inflammatory cytokines. Interestingly, the amount of TNF-α released in pristine PU was found to be much higher than cells incubated with PUNCs at 5wt% loading, possibly due to the higher affinity for cells and the higher susceptibility of neat PU to oxidation by adherent macrophages.

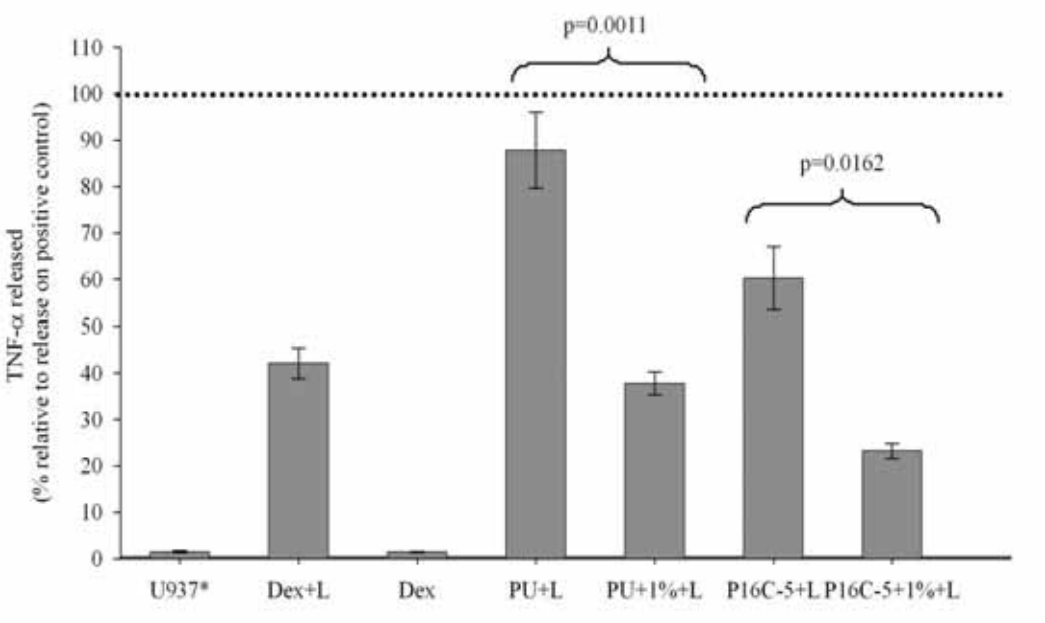

Figure 7.10 TNF-α release from samples. Expressed as a percentage of the amount of TNF-α released compared to positive control. Dotted line represents the positive control (U937+LPS). Mean ± s.d (n=3). * denotes significant difference relative to control without DexA.*

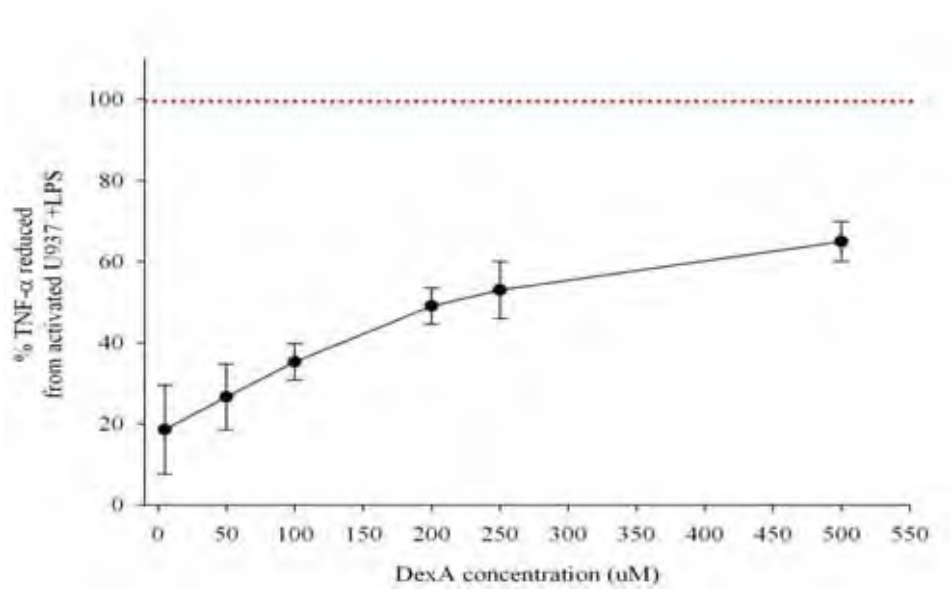

Figure 7.11 Standard curve for TNF-α suppression by DexA. The amount of TNF-α is expressed as a percentage of the amount of TNF-α reduced from U937+LPS. Dotted line represents the positive control (U937*+LPS). Mean ± s.d (n=3).*

7.4 Discussion

The results from these studies showed that both DexA and Ptx were active after release from polymers as DexA was found to reduce cytokine production and Ptx able to inhibit cell growth. PU and PUNCs fabricated either as films or coatings showed no significant differences in cell growth inhibition and were not cytotoxic in both cases. The majority of Ptx released from PUNC coatings was from loosely bound Ptx on the surface rather than through diffusion possibly due to the large molecular size of the drug. Interestingly, the introduction of silicates initially led to release by disrupting the NC structure and increasing the number of free volume for easier water penetration. Further addition of silicate particles retarded the release via the tortuous pathway model as well as weak interactions with Ptx.

7.4.1 Paclitaxel release

The cumulative drug release of Ptx coils conducted over 3 weeks demonstrated an initial burst similar to the release of heparin as shown previously in chapter 4. This indicated that the majority of Ptx released in the initial burst was due to Ptx residues on the surface rather than through diffusion. The difference in the release between PU and PUNCs in the second phase of the release profile was that Ptx from PU reached a plateau soon after the initial burst, while Ptx from PUNCs increased slowly until the end of the experiment.

Possibilities for the low amounts of Ptx released from pristine PU after the initial burst could be; i) strong molecular interactions, ii) solubility of Ptx, iii) the hydrophobic nature of Ptx, or iv) the molecular size. First, Ptx is a molecule similar to DexA which

has no net charge and consisted of mostly carbonyl and hydroxyl groups. Based on the similarity in both drugs, it is unlikely that the interactions between PU and Ptx were strong enough to completely prevent the release. As to the solubility, Ptx is known to have a poor solubility in water (0.3-1µg/ml) [312, 313] and PBS (5µg/ml in 0.1M, pH 7.4) [314]. The experiment however, was conducted in a mixed-solvent medium (90:10 (v/v) PBS: methanol) with frequent sampling time to ensure that Ptx remained soluble in the release medium and did not exceed more than 10% of the maximum solubility in PBS. The solubility of Ptx in PBS at the end of 3 weeks for PU+P, P16C-1+P and P16C-5+P was 2.2 ± 0.3, 5.7±0.3 and 5.1± 0.05 respectively. Therefore, it was unlikely that either the solubility or molecular interactions limited the release of Ptx from neat PU.

On the contrary, the hydrophobic nature of the drug could have an effect on limiting the release. An inversely proportional relationship between Ptx loading and percentage release from polymers was reported in several publications [289, 314]. The release of Ptx from PU film examined by Kang *et al*. [289] showed that Ptx at 5.4wt% loading released only 5%. A similar result was obtained by Shikanov *et al*. [314], where poly (sebacic acid-*co*-ricinoleic acid) paste containing 5wt% Ptx released 15% of the incorporated drug in 20 days, while the formulation that contained 10wt% only released 6% in 20 days [314]. The high affinity of Ptx for the hydrophobic matrix does not allow water to penetrate and dissolve the drug. Furthermore, the low solubility of the Ptx meant that even after water has penetrated the polymer matrix, Ptx may not be in a completely dissolved state [314, 315].

For drugs to diffuse out of the films, only those in the dissolved state can be pushed out through the narrow water channels. If both dissolved and undissolved states were present in the PU matrix, then the aggregated state of Ptx molecules cannot be released from the film [315]. Studies have shown that aggregates or crystals can be formed during the last stage of solvent evaporation when using highly hydrophobic drugs [316]. As the concentration of Ptx used in the coating process was at 10wt%, the formation of micro-aggregates within the matrix is very likely to occur.

Lastly is the possibility of Ptx being too large to be released. Similar to the trend presented in Figure 4.5 for heparin, the early plateau indicated that there was no further release of Ptx after the initial burst. The hypothesis proposed for Ptx was that the hydrophobicity could overcome the size restrictions seen in hydrophilic molecules due to lesser interactions with the host system. However, the limited release from Ptx suggested that drug size is still a dominating factor which limits the release from a PUNC system. That is, despite CB and Ptx having different charge, hydrophilicity and smaller in size than unfractionated heparin, they could still be too large for release, thereby leaving the majority trapped within the PU matrix.

Interestingly, after the addition of silicates, PUNCs loaded with Ptx showed a slow but continuous release after the initial burst. The reason for the release was thought to be caused by the disruptions to the PU matrix, thereby changing the hard-soft segment morphology as well as increasing the number of available water channels. It is possible that the addition of silicate particles increased the number of pores and free volume at the interface, allowing water to penetrate easier [166]. This suggested that the limited

release of Ptx from PU matrices can be promoted through the addition of silicates. The ability of silicate to modulate the release was also evidenced by the decrease in total Ptx released from increasing silicate loading. The rate of release for PUNCs loaded with 5wt% clay was also slower than those loaded with 1wt% clay, suggesting that the release was retarded accordingly to the tortuous pathway model. In addition, the van der Waals interactions occurring between surfaces of MMT and the NH or hydroxyl bonds (OH) of Ptx could decrease the release.

7.4.2 Biological response of PUNCs

The biological response between PUNCs and mammalian cell lines was investigated using a cell growth inhibition assay. An arbitrary value of 0.7 was used as an indicator in this assay for assessing the "acceptable level" of cell inhibition. PUNC films resulted in a slightly lower CGI ratio compared to that of pristine PU films, but were still above 0.7 and maintained a high viability of 94%. One of the reasons that could inhibit cell growth was due to the presence of OM in the material extracts. It has been reported in the literature that OM during PUNC fabrication could leach out from the material, thus disrupting the cell growth and membrane integrity [303]. Since OMs were not bound to silicate surfaces by covalent bonding but rather through electrostatic interactions, it is possible that these small molecular weight OM can still migrate out of the NC system and impact on the cell growth [303, 317].

A comparison between PUNCs fabricated either as films or coatings did not show any significant differences at the level of inhibition. This suggested that PUNCs can also be fabricated by an industrial coating system without causing adverse biological response.

The CGI ratios of P16 at 1wt% loading were slightly lower than the acceptable level of inhibition with ratios of 0.68 and 0.65 for the film and coating respectively.

The borderline CGI ratio of these samples however, does not necessarily rule out its use within a biological environment. A CGI ratio of 0.7 used in this assay was simply an indicator for assessing the cellular growth. Studies have shown that materials exhibiting adverse *in vitro* behaviour may still show appropriate results *in vivo* [318, 319]. Rosengren *et al*. [319] implanted PU disc mixed with the toxic substance Zincdiethyldithiocarbamate (ZDEC) into rat models for 6 weeks. The study showed that explanted materials remained highly toxic after 1 week implantation from *in vitro* assays, but showed no cytotoxicity *in vivo* during the 6 weeks of implantation [319]. The differences between *in vitro* and *in vivo* studies may be due to higher localised concentrations of cytotoxic or leachable products *in vitro* versus a more diluted case in an implant [318].

7.4.3 Drug activity

7.4.3.1 Dexamethasone

The activity of DexA after being released from the PUNC system was assessed by a cell growth assay. The number of cells in wells with DexA loaded samples did not increase over the 10 day period as compared to their relative controls, demonstrating that DexA was continuously released over the 10 day period and was still active after release. A similar result was shown by the decrease in CGI ratio of PU+1%DA and P16C-1+1%DA as compared to PU and P16C-1 from the CGI assay. The ability of DexA to

inhibit cell growth was in accordance with the literature where DexA can induce cell cycle arrest in the late G1 phase which prevents further growth of cells [293]. This inhibition was found to be related to the decrease in activity of a cell cycle-specific gene, thymidine kinase gene (*Tk-1)*, which is mainly expressed from cells moving from late G1 to S phase [294, 320].

Of interest were the benefits of using PUNCs in prolonged release. The cell growth assay however, could not assess the sustained activity of drugs from NCs. There was no significant difference in the number of viable cells at day 10 between neat PU and PUNCs. This was probably due to the small difference (~4%) in total drug release between PU+1% and P16C-1+1% after 10 days as shown in Chapter 6. However, it is expected that cells in contact with PU+1% will eventually resume growth, but over periods longer than 10 days. In addition, it may show a similar trend to cells exposed to DexA solution since only a continuous dosage of DexA can inhibit cell growth.

The anti-inflammatory activity of DexA from PUNCs was assessed by monitoring the secretion of a pro-inflammatory cytokine, TNF-α. The addition of DexA to U937 either in solution or being released from samples, have significantly decreased the amount of TNF-α produced ($p<0.05$). This was consistent with the effects of DexA in suppressing TNF-α secretion [292]. Interestingly, the sample PU+L appeared to produce a higher TNF-α response than P16C-5+L**.** This may be due to the surface chemistry of PUNCs which is more hydrophobic than pristine PU.

Adherent macrophages on biomaterials up-regulate cytokine secretion in an attempt to phagocytose the biomaterial [321]. The adherence of macrophages is dependent on the surface chemistry and surface topography of a material, where smooth and hydrophobic surfaces show far less cell adherence than rough and porous surfaces [322-324]. The high affinity of cells towards PU surface has been reported to be as a result of high surface energy arising from the polar groups on the surface and the hard-soft segment microstructure [325, 326]. However, when OMS were being incorporated into PU, the presence of hydrophobic alkyl tails on MMT surfaces and the lower surface energy of the resultant PUNC makes the surface unfavourable for cells to adhere [49, 85]. It is possible that the surface properties of PUNCs, which were more hydrophobic than PU prevented easy adhesion of U937*, thereby creating less chances for phagocytosis and an up-regulation of TNF-α.

7.4.3.2 Paclitaxel

The decrease in CGI ratio for samples incorporated with Ptx as compared to samples without Ptx, indicated that the activity of Ptx is still present after the fabrication process and can be released in sufficient amounts to inhibit cell growth. This is consistent with the effects of Ptx on preventing cell proliferation and migration through stabilising the microtubule assembly [327]. Noticeably, the viability of L929s in samples with added Ptx was maintained at above 80%. The concentration applied in the current experimental setup was thought to be cytotoxic since amounts as low as 2-10nM have been reported in literature to be cytotoxic against a wide range of tumour cell lines [302, 315, 328].

However, the fact that cells were still viable was reported by some studies to be caused by the low sensitivity of L929s to Ptx than other tumour cell lines [329, 330].

Kim *et al*. [329] compared the effects of Ptx on the viability and morphological changes in HeLa and L929s cells. It was found that upon treating L929s to low concentrations (1μM) and high concentrations (10uM) of Ptx, the cells exhibited a 10% and 17% decrease in viability on the first day respectively. Compared to HeLa cells that showed viability decrease up to 28% and 40% upon treating to low and high concentrations of Ptx respectively, the marginal decrease demonstrated by L929s and the more pronounced morphological changes, was related to the different origins and tumour type [329] The two cell lines were distinctive in their ability to adapt to changing environments [329], and the more apparent morphological changes in L929s indicated better survival mechanisms [331]. Another study by Akgun *et al* [330] also found similar results, where Ptx still showed 90% and 70% viability after treating with 1μM and 10μM of Ptx for 2 days.

The positive ethanol controls utilised in the CGI assay were 4% ethanol, 5% ethanol and 7.5% ethanol. These controls resulted in a cell viability of 91%, 89% and 27% respectively after 2 days. From the results, it is reasonable to suggest that L929s may still maintain good viability (~80%) after exposure to Ptx when the ethanol controls in this study only started to show cytotoxic effects at the highest concentration. The robust nature and low sensitivity of L929s towards Ptx suggested that these cells may not be the ideal cell line to test the cytotoxic effects of Ptx. Nevertheless, L929s still demonstrated

a strong dose-dependent relationship with Ptx concentration, where increasing Ptx concentration leads to increased cell growth inhibition.

7.5 Conclusion

The release of Ptx from coated coils in this study demonstrated the importance in considering the molecular size of the incorporated drug. The retarded release of Ptx from PU supported the hypothesis proposed for CB in chapter 5, where the size of the incorporated drug can impact on the release behaviour. If the molecular size is too large, the molecule cannot be released by diffusion through the bulk polymer. Interestingly, the release of Ptx was enhanced through the addition of silicate particles, possibly due to the disruption to the PU matrix and increases to the number of pores and free volume at the interface [166]. Ptx was also seen to be modulated by silicates, with slower release rates and lower total release observed from PU incorporated with higher clay loadings.

PUNCs fabricated (coils and films) in this research were not cytotoxic as examined by the CGI assay. However, the CGI ratio of PUNCs was slightly lower than the acceptable level of growth inhibition. This was possibly due to OMs migrating out from the NC system. The activity of DexA was demonstrated through the inhibition in cell growth and the decrease in TNF-α secretion.

The results from CGI assay of Ptx coated coils also indicated that the drug was active after release. The cytotoxic effect of the drug however, was not reflected by the CGI assay and a viability of above 80% was observed. Research into the literature found similar reports suggesting that L929s utilised in this study were less sensitive to Ptx and

have better survival mechanisms compared to other tumour cell lines. Further investigation using a different cell line should allow a better assessment of the effects of Ptx on cell viability and proliferation.

Although the drug activity assays suggested that DexA were active after release, the cell growth assay conducted could not show if the therapeutic activity of DexA can be prolonged by an NC system. However, given the lower drug release rates of DexA loaded PUNCs as compared to PU, it is expected that cells in contact with PUNCs will have a prolonged effect in inhibiting cell growth over longer periods. Future studies could focus into examining the period of efficacy of PUNCs versus PU. For DexA, extending the period of testing to more than 10 days or increasing the clay loading should allow a better evaluation of sustained drug activity.

In summary, PUNCs fabricated as films or as coatings demonstrated the capability to delivery active drugs within a biological environment without inducing cytotoxicity. It was also demonstrated that the molecular size and hydrophobicity of the drug were important factors that need to be considered in a controlled drug delivery system. The understanding of these factors is essential to accurately predict the release profile and to design a PUNC based drug delivery system.

Chapter 8: Conclusions and Recommendations for Future Work

8.1 Introduction

The improvement in mechanical and barrier performance of polymer NCs as a result of incorporation of nanoparticulates has attracted attention in the field of controlled drug delivery. One of the key factors contributing to accurate prediction of drug release behaviour in polymer NCs is by understanding the interactions that occur between the drug, polymer, nanofiller and modifier. In this thesis, a poly (ether) urethane based NC with silicate inclusions was investigated. Three main hypotheses of this thesis were examined. First, modification of silicates using longer chain length modifiers promotes dispersion and improves the barrier and mechanical performance of the resulting NC. These improvements can be achieved without significantly affecting the biological performance of PU. Second, addition of a drug into the PUNC system impacts on the structure and perturbs the release behaviour through competitive interactions with the NC constituents. Finally, PUNCs can release biologically active drugs regardless of being fabricated as films or coatings. The following sections are summaries for the three hypotheses in this research.

8.2 Overall conclusions

8.2.1 Silicate dispersion and biological interactions with PUNCs

A range of PUNC films with varying clay loading and modifier chain length were fabricated to study the effect of these parameters on the dispersion, morphology, and

mechanical properties. A summary of the results is shown in Table 8.1.

Table 8.1 Summary of silicate spacing, morphology and mechanical properties of PUNCs

	Structure		Mechanical properties (relative to PU control)		
	Silicate spacing (nm)	Morphology[a]	UTS	Strain	E (5%)
PU	-	-	-	-	-
P12C-1	-	PE	Decreased *	Increased *	Maintained
P12C-3	3.40	I	Decreased *	Maintained	Increased *
P12C-5	2.55	I	Decreased *	Decreased *	Increased *
P16C-1	-	PE	Maintained	Increased *	Maintained
P16C-3	4.78	PE	Decreased *	Increased *	Decreased
P16C-5	3.26	I	Decreased *	Increased *	Increased *

* Indicates significant difference compared to PU control ($p<0.05$)

[a] PE= partially exfoliated, I= intercalated

It was shown that silicate spacing and mechanical properties of PUNCs were both dependent on the type of modifier and the silicate loading. The most balanced enhancement in strain, UTS and modulus resulted from P16 at 1wt% clay loading. It was found that the optimal clay loading is at 1wt% for both lengths of modifiers due to the disappearance of peak and the presence of smaller aggregates as observed from XRD and TEM respectively. Dispersion of silicates within PUNCs was better among PUNCs modified with longer chain modifiers. Better dispersion also conferred better mechanical properties.

PUNCs based on longer chain modifiers were able to show significantly improved ultimate strain across all clay loadings ($p<0.05$), while shorter chain modifiers demonstrated a decreasing trend in strain with clay loading. Increasing the clay loading for both modifiers significantly increased Young's modulus ($p=0.009$), but had a detrimental effect on the UTS ($p<0.05$). This is with the exception of P16C-1 that was able to maintain the UTS of pristine PU. The decrease in UTS was mainly thought to be caused by agglomeration of clay particles, thereby creating a poor interface and decreases the number of available reinforcements [90].

To examine whether the addition of OMS would affect the biological performance, assessments using an *in vitro* cell growth inhibition (CGI) assay and a thrombin generation assay were conducted. Another variable that was also studied in the CGI assay was the fabrication method. The CGI assay showed that P16C-1 both fabricated as films or coatings resulted in slightly lower CGI ratio as compared to PU, but was within the acceptable level of inhibition and the cells maintained a high viability. The slightly lower CGI ratio to PU could be due to the migration of OM out of the NC system as these were not bound to silicate surfaces by covalent bonding, but rather through electrostatic interactions.

A comparison between PUNCs fabricated as films or coatings also showed no significant difference in the level of inhibition, suggesting that PUNCs can be fabricated consistently by both methods. The blood compatibility of PUNCs as assessed by thrombin generation assays showed that the addition of silicate particles did not significantly decrease the thrombin generation lag time ($p=0.659$) or the peak thrombin ($p=0.999$) of PU. Therefore, the addition of silicates does not increase the thrombogenicity of PU according to these two measures.

8.2.2 Impact of drug addition on the structure and drug release of PUNCs

Another hypothesis of this thesis was that the addition of drugs into PUNCs would impact on the structure and release behaviour due to interactions that can occur between each of the components. Much research was focused towards modulating drug release from NCs by adjusting filler content, filler type and dispersion. However, few have considered the effect of interactions between the drug and the constituents of NC and that they may have a more dominant role in affecting drug release.

An initial investigation to address the importance of drug properties and subsequent interactions that affect the release was by a proof-of-principle study focusing on blood related applications. The cumulative release profile of heparin indicated that heparin was too large to diffuse through the bulk polymer and therefore could not be modulated by varying the clay loading or OM chain length. The electrostatic interaction between heparin and clay also assisted in retaining most of the heparin within the bulk polymer. Based on the findings with heparin, further investigation on interactions was conducted using a range of therapeutic and model drugs with different charge, size and polarity as shown in Table 8.2. An overall guide for predicting drug release from PU and PUNCs based on the physiochemical properties of the added drug is shown in Figure 8.1.

It was necessary to consider the impact of drug addition to PU prior to the addition of silicates, since the majority of polymer NC is comprised of the host polymer. It was shown that the release of drugs from PU can be restricted by the size of the molecule.

Although molecules, such as CB and Ptx, were several magnitudes smaller in size than heparin, the trace amounts of release observed in both drugs suggested that the majority remaining were still trapped within PU. In addition, even though the total release of Ptx from neat PU over 3 weeks was around 16%, the effect was not thought to be from diffusion, but rather from the high initial drug loading (10wt%) causing a larger burst release. The hydrophilic or hydrophobic nature of the drug therefore has little effect in perturbing the release when they are above a critical size.

Table 8.2 Summary of drugs used in this study

Drugs	MW (g/mol)	Total Release (%)[c]	Type	Solubility (mg/ml)[d]	Charge
Model[a]					
CV	407.9	97.9	Hydrophilic	1	Positive
BB	669.9	87.9	Hydrophilic	4	Anionic
CB	825.9	0.9	Hydrophilic	1	Positive/ Negative
Therapeutic[b]					
DexA	434.5	65.0	Hydrophobic	0.1	Neutral
DexP	516.4	15.8	Hydrophilic	500	Negative
Ptx	853.9	16.4	Hydrophobic	0.001	Neutral

[a] Model drugs: CV= Crystal violet; BB= Bromophenol blue; CB= Coomassie Blue

[b] Therapeutic drugs: DexA= Dexamethasone acetate; DexP= Dexamethasone phosphate; Ptx= Paclitaxel

[c] Percentage loaded. Based on release from neat PU

[d] Aqueous solubility at 37°C

For drugs that are smaller than CB (825 g/mol) or Ptx (853 g/mol), the release of hydrophobic drugs was shown to be more sustained than drugs of hydrophilic nature. The release rates of hydrophilic CV and BB from PU were faster and higher than the hydrophobic DexA. The case where hydrophilic drugs do not release faster than hydrophobic drugs is when there are strong interactions with the host polymer. Using a drug that belonged to the same family of steroids as DexA but with different functional groups, DexP is a negatively charged hydrophilic drug. Results from ATR-FTIR and MD simulation suggested that DexP has strong attractive interactions with the soft segments of PU, which as a result largely limited the release from PU. On the contrary, the absence of obvious peak shifts with DexA, CV or BB suggested that the interactions between these drugs and PU were not very strong.

The attempt to modulate and sustain release from the subsequent introduction of silicates was found to be dependent on the net charge and polarity of the drug. Positively charged drugs have the potential to displace modifiers from the MMT surface through electrostatic interactions, while anionic and neutral drugs can only interact with clay through hydrogen bonding and dipole interactions. This was evidenced by larger changes to the silicate spacings and from the disappearance of characteristic peaks that belonged to the bending of OM head groups in PUNCs with added CV. On the other hand, PUNCs with added BB or DexA only showed slight shifts in characteristic peaks and minor changes in silicate spacings. Therefore, the release of positively charged drugs, such as CV, was significantly decreased by the introduction of clay, while the release of anionic (BB) and neutral (DexA and Ptx) drugs was modulated by a lesser extent. Interestingly, the introduction of clay to PU added with negatively charged drugs (DexP) promoted the release. The release of

DexP from PUNCs increased with increasing clay content due to the repulsive nature between the phosphate groups of DexP and the MMT surface.

In summary, the release behaviour from PUNCs was largely dependent on the interactions between the drug, polymer, clay and modifier. These interactions arise from the different physical and chemical properties of the added drug and can result in deviation from the predicted drug release based on the tortuous pathway model.

8.2.3 Drug activity

The final hypothesis of this thesis was that drugs released from PUNCs can remain biologically active and should not be affected by different fabrication methods. The drug activity of DexA was assessed using a cell growth assay and an inflammatory response assay, while a cell growth inhibition assay was used to assess the activity of Ptx. The cell growth assay demonstrated that samples with added DexA were able to inhibit cell growth over 10 days. There was no difference in cell inhibition between PU+1%DA and P16C-1+1%DA, showing that the concentrations released from both systems were therapeutically efficient over the period tested.

Further assessment of the activity of DexA by an inflammatory response assay showed that the release of DexA from PU+1% and P16C-5+1% significantly decreased the secretion of TNF-α as compared to their relative controls. Using cell growth inhibition assay, the activity of Ptx after release was also found to be active. Interestingly, the cytotoxic effect of the drug was not reflected in the assay and a viability of above 80% was observed. It was thought that L929s utilised in this study were less sensitive to Ptx and have better survival mechanisms compared to other tumour cell lines.

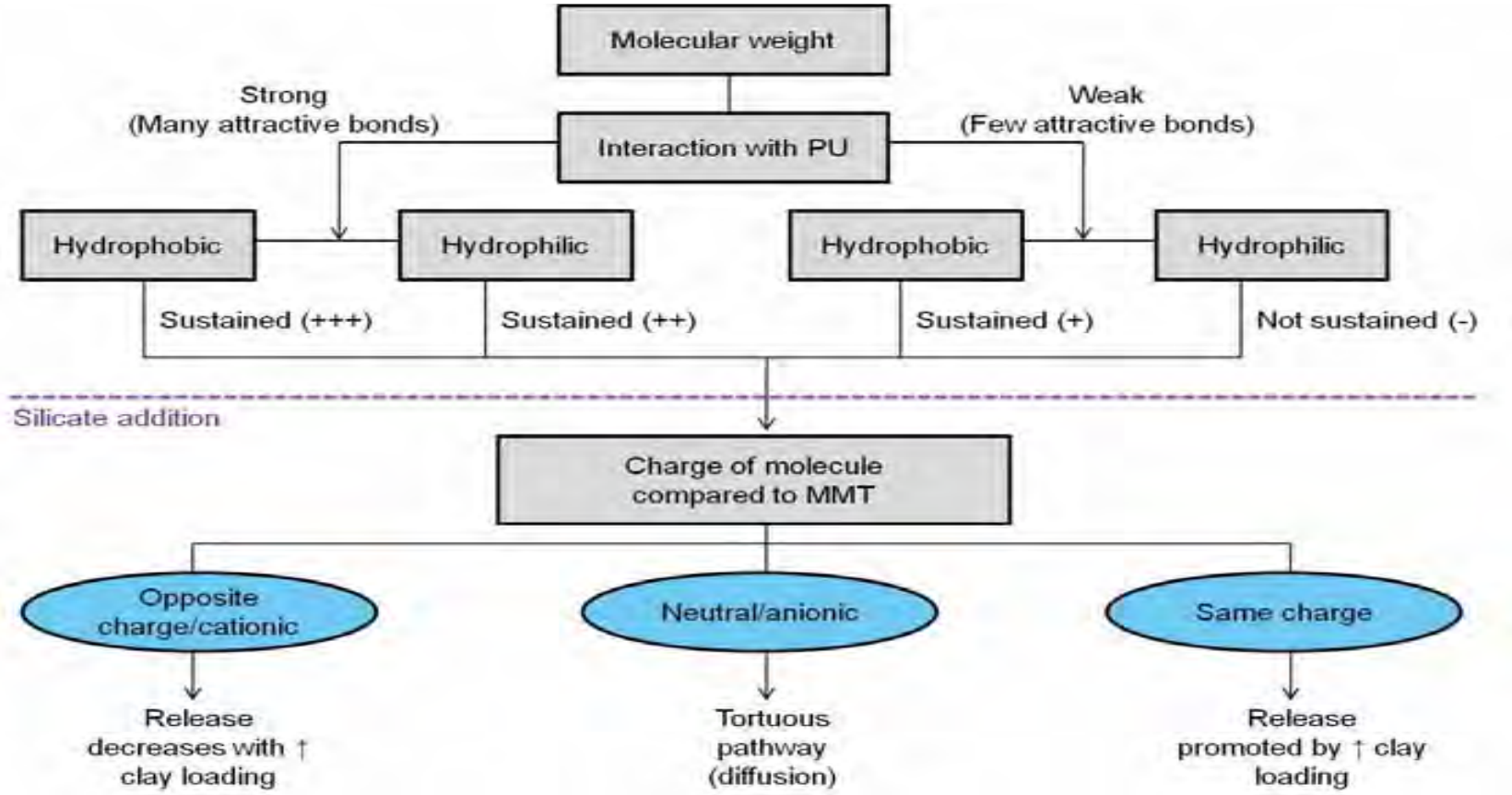

Figure 8.1 General guide for predicting the drug release profile from PUNCs based on tested model and therapeutic drugs. The magnitude of sustained release is represented by (+) and (-). '+++' indicates low total release and early plateau, '++' indicates low total release and no early plateau, '+' indicates high total release and no early plateau, '-' indicates high total release and early plateau.

In conclusion and summary, this thesis explores the potential of using polyurethane nanocomposites as drug delivery coatings on existing medical devices. The outcomes of this thesis are that:

1. Improvements in mechanical properties can be accomplished by using longer chain length modifiers, provided that optimal silicate dispersion is achieved throughout the polymer matrix.

2. Biological interactions with nanocomposites in terms of cell growth inhibition and blood compatibility were not detrimentally affected by the addition of OMS. A slightly higher level of cell inhibition from nanocomposites was observed and was due to the effects of the organic modifier.

3. Interactions that impact on the structure and drug release behaviour are largely dependent on the characteristics of the incorporated drug. A larger change in silicate spacing appeared in drugs that carried a net charge due to greater interactions with OMS from electrostatic interactions or hydrogen bonding. The release rate and level of retardation was governed largely by the size, polarity and hydrophilicity of the incorporated drug. In the absence of strong attractive interactions with the host polymer, the release of hydrophobic drugs from neat PU was more sustained than that for hydrophilic drugs. The subsequent introduction of silicates has an "additive" effect that perturbs the release profile based on the net charge of the drug. If the added drug is negatively charged, the release will be enhanced by the introduction of clay. On the contrary, if the drug

is neutral or positively charged, the addition of clay will retard the release to a greater extent.

4. PUNCs fabricated as films or as coatings did not induce cytotoxicity within a biological environment and can be used to deliver drugs that are active and therapeutically efficient.

8.3 Recommendations for Future Work

8.3.1 PUNC structure

By increasing the clay content, the permeability of NCs can be decreased based on the tortuous pathway model. However, the reduction in permeability is at the expense of mechanical performance as increasing the clay content inevitably decreases the quality of dispersion due to the hydrophilic nature of silicates. The effect of drug properties and interactions also affects the degree to which silicates can modulate or sustain the release. The selection of the most suitable combination of loadings and materials is therefore a challenging task that requires further refinement and investigation. In addition, there is a need for a single and more reliable technique to assess the overall dispersion of silicates within the bulk polymer.

The current gold standard for assessing NC dispersion and structure is from the combined use of XRD and TEM. An indirect measurement of dispersion can also be conducted through mechanical testing. In XRD, peak broadening and decreases in intensity can occur from silicates that do not inhibit a well defined basal reflection. This

decreases the accuracy in identifying the peak of the diffractograms which can result in a large difference in silicate spacing when converted by Bragg's law. TEM on the other hand can only examine a small region within the NC and cannot represent the overall dispersion of silicates without supplementing with XRD.

With the rapid development in analytical tools for characterising in nanoscale dimensions, assessment of dispersion in future studies could extend into using nuclear magnetic resonance (NMR) or nanoindentation. The former relies on the presence of Fe^{3+} within MMT that creates relaxation sinks at the clay surface. The better the dispersion, the more relaxation sinks and the shorter the proton longitudinal relaxation time (T_1^H). Using appropriate mathematical models, information regarding the degree of separation of the platelets and the homogeneity of the dispersion in the bulk can be obtained [332, 333]. The latter looks at the load-depth compliance curves, where the softer the material, the deeper the depth of loading. Information on dispersion can then be translated from modulus mapping [334, 335].

8.3.2 Drug-NC interaction

A major objective of this thesis was to understand the interactions between the drug and the constituents of the PUNC system. Through various characterisation techniques, it was found that the molecular size of the drug added could be the most dominating factor that will determine the release profile. Molecules such as heparin, Coomassie blue and paclitaxel, have all shown limited release from pristine PU due to the difficulty in diffusing out of the bulk polymer. On the contrary, the release of bromophenol blue with

molecular weight of 669 g/mol was rapid. Since the difference in size between bromophenol blue and Coomassie blue (825 g/mol) was not significant, there is a need to investigate further to determine the actual size above which molecules cannot be released. Molecules with sizes around 700-750 g/mol could be explored.

In an attempt to further understand drug properties and interactions, an approach that was not taken in this research due to the cost and quantity needed was to choose model dyes that belong to the same family. Apart from dexamethasone acetate (DexA) and phosphate (DexP) that belongs to the same family of drugs, all other model and active drugs selected in this thesis were not related. If the basic shape and structure of each dye or drug is the same, a more controlled and detailed understanding of drug interactions can be achieved. The family of dyes can include ATTO dyes [336], Alexa Fluor [337] and DyLight Fluor [338]. All of these dyes have several members that differ in molecular weight and net charge through the addition of different functional groups. Since all of these drugs are fluorescent dyes with emission/excitation spectra covered in the visible spectrum, it also allows faster analysis of samples through a plate reader rather than a UV-spectrophometer.

8.3.3 Drug release

In chapter 4, the cumulative release studies suggested that heparin was a drug more suitable to improve the blood compatibility of a material, rather than a drug for controlled release in NC. For a better assessment of PUNCs in blood related applications, the selection of lower molecular weight anti-thrombotic or anti-platelet drugs may be

better. Based on the results obtained with other model and active drugs, anti-platelet molecules such as aspirin [339], or genistein [340], can be used. The smaller molecular weight of these drugs with no charged functional groups should permit release and allow modulation by silicates.

Another area worth investigating is the use of PUNCs for dual drug release. Patients after coronary stenting are often immediately given anti-thrombotics to minimise the initial thrombus formation that could lead to restenosis or device failure at later stages. This meant that large quantities are administered initially and could lead to bleeding or surgical complications. Through appropriate selection of drugs, PUNCs could initially deliver anti-thrombotics followed by a sustained release of anti-inflammatory drugs over 3-4 weeks to prevent restenosis.

Drug properties suitable for the initial phase are hydrophilic molecules that are neutral or anionic in nature, so that they can only be modulated slightly by silicates. This is because a fast initial release is required. The use of larger molecular weight drugs such as heparin may also be feasible since the profiles desired are ones that have a significant burst release followed by an early plateau. As to the latter phase, drugs should have properties that are similar to DexA, where the hydrophobic and neutral properties allow a sustained release through modulation with silicates.

Cell studies conducted in Chapter 7 evaluated the impact of drug activity following release from PUNCs. One of the aspects these assays did not address is whether these NC materials prolong release while maintaining drug bioactivity. Therefore, it is

recommended that further studies should examine the drug activity over longer periods of time. Additionally, using flow cytometry to supplement the cell growth assays used in this thesis could provide information on the cell cycle, metabolism and cell surface receptor expression. These methods may offer a more sensitive and detailed approach to examining the cellular response to the released drug. Studies could also involve the use of higher clay loadings to further examine its impact on drug release. The limiting factor from using higher clay loadings would be the decrease in mechanical performance. However, this approach could still be undertaken if the aim was to prolong drug release and to assess drug activity.

An interesting finding between PU+L and P16C-5+L in the inflammatory response assay was that PU+L secreted higher amounts of TNF-α than P16C-5+L. The high affinity of cells for PU could increase the likelihood for PU to degrade from macrophage attack, thereby increasing TNF-α production [196]. The hypothesis that PU is more susceptible to oxidative attack than PUNCs could be examined by an enzymatic study measuring the cholesterol esterase (CE). Enzymes, such as CE, are thought to be potential degradative enzymes that cause hydrolytic degradation and are released upon contact with materials surfaces [341]. If PUNCs are more biostable and less susceptible to macrophage attack, then the production of CE should also be less. This could also be used to compare samples with added DexA. In addition, a measurement of the cell numbers on the sample surface and the presence of degradation products could also provide valuable information regarding the biostability of PU as compared to PUNCs. Progressing from this could involve *in vivo* animal tests. Drug concentrations that were effective *in vitro* does not necessarily have the same effect *in vivo* due to the different

physiological conditions. It is therefore necessary to determine the maximal drug concentration suitable for release from samples that are implanted.

In summary, PUNCs show much promise for use in drug delivery applications. Through understanding drug-NC interactions and from selecting appropriate silicate loadings and modifiers to achieve the best balance between mechanical and barrier performance, PUNCs can accommodate a wide variety of drugs for applications that require different release mechanisms.

Bibliography

1. The Freedonia group, 2009 *Medical plastics. US industry study with forecast for 2012 &2017*: Cleveland, OH. p. 1-338.
2. Sastri V. R., *Materials used in medical devices*. Plastics in medical devices: properties, requirements, and applications, 2010, Massachusetts, Elsevier Inc
3. Kohane D. S. ,Langer R. Polymeric biomaterials in tissue engineering. *Pediatric research* 2008; **63**: 487-491.
4. Modi C., 2010 *Medical plastics- engineered for precision*, Modern Plastics & Polymers.
5. *Biomaterials Science: A Multidisciplinary Endeavor*. 2nd ed. Biomaterials science an introduction to materials in medicine, ed. Ratner B.D., Hoffman, A.S, Schoen, F.J, Lemons, J.E, 2004, San Diego, Elsevier Academic Press
6. Bhat S. V., *Overview of biomaterials*. 2nd edition ed. Biomaterials, 2006, Harrow, Alpha Science International Ltd
7. Xu R. , Manias E. , Snyder A. J. ,Runt J. Low permeability biiomedical polyurethane nanocomposites. *Journal of biomaterial research* 2002; **64A**: 114-119.
8. Gunatillake P. A. , Martin D. J. , Meijs G. F. , McCarthy S. J. ,Adhikari R. Designing biostable polyurethane elastomers for biomedical implants. *Australia journal of chemistry* 2003; **56**: 545-557.
9. Iskakov R. , Batyrbekov E. , Zhubanov B. , Teleuova T. ,Volkova M. Polyurethanes as Carriers of Antitumorous Drugs. *Polymers for Advanced Technologies* 1998; **9**: 266-270.
10. Simmons A. , Padsalgikar A. D. , Ferris L. M. ,Poole-Warren L. A. Biostability and biological performance of a PDMS-based polyurethane for controlled drug release. *Biomaterials* 2008; **29**: 2987-2995.
11. Guo Q. , Knight P. T. ,Mather P. T. Tailored drug release from biodegradable stent coatings based on hybrid polyurethanes. *Journal of Controlled Release* 2009; **137**: 224-233.
12. Lee Y.K. , Jae H. P. , Hyun T. M. , Dong Y. L. , Jung H. Y. ,Byun Y. The short-term effects on restenosis and thrombosis of echinomycin-eluting stents topcoated with a hydrophobic heparin-containing polymer. *Biomaterials* 2007; **28**: 1523-1530.
13. Huang X. ,Brazel C. S. On the importance and mechanisms of burst release in matrix-controlled drug delivery systems. *Journal of Controlled Release* 2001; **73**: 121-136.
14. Goldberg M. , Langer R. ,Jai X. Nanostructured matrials for applications in drug delivery and tissue engineering. *Journal of Biomaterial science: Polymer edition* 2007; **18**: 241-268.
15. Deconinck E., Sohier, J, Scheerder, I.D, Van den Mooter, G. Pharmaceutical aspects of drug eluting stents. *Journal of Pharmaceutical Sciences* 2008; **97**: 5047-5060.

16. Chen C.-W. ,Lin C.-L. The Current Status of Coronary Drug-Eluting Stents. *Tzu Chi Medical Journal* 2009; **21**: 18-27.
17. Zilg C. , Mulhaupt R. ,Finter J. Morphology and toughness/stiffness balance of nanocomposites based upon anhydride-cured epoxy resins and layered silicates. *Macromolecular Chemistry and Physics* 1999; **200**: 661-670.
18. LeBaron P. C. , Wang Z. ,Pinnavaia T. J. Polymer-layered silicate nanocomposites: an overview. *Applied Clay Science* 1999; **15**: 11-29.
19. Utracki L. A., *Clay-containing polymeric nanocomposites*, 2004, Smithers Rapra Technology
20. Chen C. , Khobaib M. ,Curliss D. Epoxy layered-silicate nanocomposites. *Progress in Organic Coatings* 2003; **47**: 376-383.
21. Pavlidou S. ,Papaspyrides C. D. A review on polymer-layered silicate nanocomposites. *Progress in Polymer Science* 2008; **33**: 1119-1198.
22. Paul D. R. ,Robeson L. M. Polymer nanotechnology: Nanocomposites. *Polymer* 2008; **49**: 3187-3204.
23. Jones R. M., *Mechanics of composite materials*. 2nd ed, 1998, Taylor & Francis
24. Eckel D. F. , Balogh M. P. , Fasulo P. D. ,Rodgers W. R. Assessing organo-clay dispersion in polymer nanocomposites. *Journal of Applied Polymer Science* 2004; **93**: 1110-1117.
25. Hauser E. A., Modified gel-forming clay and process of producing same, in *United States Patent Office 2,531,427*. 1950: Cambridge, Mass.
26. Theng B. K. G. ,Walker G. F. Interactions of clay minerals with organic modifiers. *Israel journal of chemistry* 1970; **8**: 417-424.
27. Blumstein A. Polymerization of adsorbed monolayers. i. preparation of clay-polymer complex. *Journal of polymer science part A: general papers* 1965; **3**: 2653-2664.
28. Blumstein A. Polymerization of adsorbed monolayers. ii. thermal degradation of the inserted polymer. *Journal of polymer science part A: general papers* 1965; **3**: 2665-2672.
29. Usuki A. Swelling behaviour of montmorillonite cation exchanged for ω-amino acids by ε-caprolactam. *Journal of Materials Research* 1993; **8**: 1174-1178.
30. Usuki A. , Koiwai A. , Kojima Y. , Kawasumi M. , Okada A. , Kurauchi T. ,Kamigaito O. Interaction of nylon 6-clay surface and mechanical properties of nylon 6-clay hybrid. *Journal of Applied Polymer Science* 1995; **55**: 119-123.
31. Thostenson E. T. , Li C. ,Chou T. W. Nanocomposites in context. *Composites Science and Technology* 2005; **65**: 491-516.
32. Wu C. J. , Gaharwar A. K. , Schexnailder P. J. ,Schmidt G. Development of biomedical polymer-silicate nanocomposites: a materials science perspective. *Materials* 2010; **3**: 2896-3005.
33. Viseras C. , Aguzzi C. , Cerezo P. ,Bedmar M. C. Biopolymer-clay nanocomposites for controlled drug delivery. *Materials Science and Technology* 2008; **24**: 1020-1036.
34. Chung J. H. Y. , Simmons A. ,Poole-Warren L. A. Non-degradable polymer nanocomposites for drug delivery. *Expert opinion on drug delivery* 2011; **8**: 1-14.
35. Lan T. ,Pinnavaia T. J. Clay-reinforced epoxy nanocomposites. *Chemistry of Materials* 1994; **6**: 2216-2219.

36. Nah C. , Han S. H. , Lee J. H. , Lee M. H. ,Chung K. H. Preparation and properties of montmorillonite based polyimide nanocomposites. *Polymer International* 2004; **53**: 891-897.
37. Xie W. , Hwu J. M. , Jiang G. J. , Buthelezi T. M. ,Pan W. P. A study of the effect of surfactants on the properties of polystyrene-montmorillonite nanocomposites. *Polymer engineering and science* 2003; **43**: 214-222.
38. Pavlikova S. , Thomann R. , Reichert P. , Mulhaupt R. , Marcincin A. ,Borsig E. Fiber spinning from poly(propylene)-organoclay nanocomposites. *Journal of Applied Polymer Science* 2003; **89**: 604-611.
39. Hasegawa N. , Okamoto H. , Kawasumi M. , Kato M. , Tsukigase A. ,Usuki A. Polyolefin-clay hybrids based on modified polyolefins and organophilic clay. *Macromolecular Material Engineering* 2000; **280/281**: 76-79.
40. Dan C. H. , Lee M. H. , Kim Y. D. , Min B. H. ,Kim J. H. Effect of clay modifiers on the morphology and physical properties of thermoplastic polyurethane/clay nanocomposites. *Polymer* 2006; **47**: 6718-6730.
41. Bhat S. V., *Synthetic polymers*. 2nd edition ed. Biomaterials, 2006, Alpha Science International Ltd
42. Park J. ,Lakes R. S., *Polymeric implant materials*. 3rd edition ed. Biomaterials: An introduction, 2007, New York, Springer
43. Cypes S. H. , Saltzman W. M. ,Giannelis E. P. Organosilicate-polymer drug delivery systems: controlled release and enhanced mechanical properties. *Journal of Controlled Release* 2003; **90**: 163-169.
44. Wu S. , Cheng A. , Hua H. ,Shen J. A study on structure and mechanical properties of polyurethane/organic-montmorillonite nanocomposites. *Polymer-plastics technology and engineering* 2006; **45**: 685-689.
45. Hyvarinen J. Polyurethane biostability. *Chemistry in Australia* 2000; **67**: 42-46.
46. Szycher M., *Szycher's handbook of polyurethane*, 1999, New York, CRC Press
47. Estes G. M. , Seymour R. W. ,Cooper S. L. Infrared studies of segmented polyurethane elastomers II. Infrared dichroism. *Macromolecules* 1971; **4**: 452.
48. Tanaka T. , Yokoyama T. ,Yamaguchi Y. Quantitative study on hydrogen bonding between urethane compound and thers by infrared spectroscopy. *Journal of Polymer Science Part A* 1968; **6**: 2137.
49. Song M. , Xia H. S. , Yao K. J. ,Hourston D. J. A study on phase morphology and surface properties of polyurethane organoclay/nanocomposite. *European Polymer Journal* 2005; **41**: 259-266.
50. Blackwell J. ,Lee C. D. Hard segment domain sizes in MDI/diol polyurethane elastomers. *Journal of Polymer Science Polymer Physics Ed.* 1983; **21**: 2169.
51. Boretos J. H. ,Pierce W. S. Segmented polyurethane: a new elastomer for biomedical applications. *Science* 1967; **158**: 1481-1487.
52. Lamba N. M. K. , Woodhouse K. A. ,Cooper S. L., *Polyurethanes in biomedical applications*, ed. Schapiro F., 1997, CRC Press LLC
53. Kim J. H. , Jeong S. Y. , Jung M. H. ,Hwang J. M. Use of polyurethane with sustained release dexamethasone in delayed adjustable strabismus surgery. *British Journal of Ophthalmology* 2004; **88**: 1450-1454.

54. Hwang J. M. ,Chang B. L. Use of physical barriers for delayed adjustable strabismus surgery: the effect of Interceed and polyglactin 910 mesh. *British Journal of Ophthalmology* 1996; **80**: 759-762.
55. Chou C. W. , Hsu S. H. ,Wang P. H. Biostability and biocompatibilty of poly(ether)urethane containing gold or silver nanoparticles in porcine model. *Journal of Biomedical Materials Research* 2008; **84A**: 785-794.
56. Hsu S. , Chou C. ,Tseng S. Enhanced thermal and mechanical properties in polyurethane/Au nanocomposites. *Macromolecular Material Engineering* 2004; **289**: 1096-1101.
57. Lai L. C. , Tyson D. R. , Clayman R. V. ,Earthman J. C. Encrustation of nanostructured Ti in a simulated urinary tract environment. *Materials Science and Engineering: C* 2008; **28**: 460-464.
58. Maensiri S. , Laokul P. , Klinkaewnarong J. ,Amornkitbamrung V. Carbon nanofiber-reinforced alumina nanocomposites: fabrication and mechanical properties. *Materials science and Engineering: A* 2007; **447**: 44-50.
59. Chang T. E. , Jensen L. R. , Kisliuk A. , Pipes R. B. , Pyrz R. ,Sokolov A. P. Microscopic mechanism of reinforcement in single-wall carbon nanotube/polypropylene nanocomposite. *Polymer* 2005; **46**: 439-444.
60. Komareni S. Nanocomposites. *Journal of materials chemistry* 1992; **2**: 1219-1230.
61. Koyama S. , Haniu H. , Osaka K. , Koyama H. , Kuroiwa N. , Endo M. , Kim Y. A. ,Hayashi T. Medical Application of Carbon-Nanotube-Filled Nanocomposites: The Microcatheter. *Small* 2006; **2**: 1406-1411.
62. Zhang W. , Blackburn R. S. ,Dehghani-Sanij A. A. Carbon Black Reinforced Epoxy Resin Nanocomposites as Bending Sensors. *Journal of Composite Materials* 2009; **43**: 367-376.
63. Vaia R. A., *Structural characterization of polymer-layered silicate nanocomposites*. Polymer-clay nanocomposites, ed. Pinnavaia T.J., Beall, G.W, 2000, New York, John Wiley & Sons
64. Kormann X. , Lindberg H. ,Berglund L. A. Synthesis of epoxy-clay nanocomposites: influence of the nature of the clay on structure. *Polymer* 2001; **42**: 1303-1310.
65. Ng C. B. , Schadler L. S. ,Siegel R. W. Synthesis and mechanical properties of TiO_2-epoxy nanocomposites. *Nanostructured materials* 1999; **12**: 507-510.
66. Chen C. , Lv G. , Pan C. , Song M. , Wu C. , Guo D. , Wang X. , Chen B. ,Gu Z. Poly(lactic acid) (PLA) based nanocomposites;a novel way of drug-releasing. *Biomedical Materials* 2007; **2**: L1-L4.
67. Böswald M. , Girisch M. , Greil J. , Spies T. , Stehr K. , Krall T. ,Guggenbichler J. P. Antimicrobial activity and biocompatibility of polyurethane and silicone catheters containing low concentrations of silver: a new perspective in prevention of polymer-associated foreign-body-infections. *Zentralbl Bakteriol* 1995; **283**: 187-200.
68. Hung H. S. ,Hsu S. H. Biological performances of poly(ether) urethane-silver nanocomposites. *Nanotechnology* 2007; **18**: 1-9.

69. Hsu S. H. , Tang C. M. ,Tseng H. J. Gold nanoparticles induce surface morphological transformation in polyurethane and affect cellular response. *Biomacromolecules* 2008; **9**: 241-248.
70. Iijima S. Helical microtubules of graphitic carbon. *Nature* 1991; **354**: 56-58.
71. Endo M., Koyama, S, Matsuda, Y, Hayashi, T, Kim, Y.A. Thrombogenicity and blood coagulation of a microcatheter prepared from carbon nanotubes-nylon based composite. *Nano letters* 2004; **5**: 101-105.
72. Koh L. B. , Rodriguez I. ,Zhou J. Platelet adhesion studies on nanostructured poly(lactic-co-glycolic-acid)-carbon nanotube composite. *Journal of biomaterial research* 2008; **86A**: 394-401.
73. Costa F. , Saphiannikova M. , Wagenknecht U. ,Heinrich G., *Layered Double Hydroxide Based Polymer Nanocomposites*, in *Wax Crystal Control · Nanocomposites · Stimuli-Responsive Polymers*, Dusek K., Editor. 2008, Springer-Verlag: Berlin-Heidelberg. p. 101-168.
74. Li B. , He J. , Evans D. G. ,Duan X. Enteric-coated layered double hydroxides as a controlled release drug delivery system. *International Journal of Pharmaceutics* 2004; **287**: 89-95.
75. Costa F. R. , Leuteritz A. , Wagenknecht U. , Jehnichen D. , Häußler L. ,Heinrich G. Intercalation of Mg-Al layered double hydroxide by anionic surfactants: Preparation and characterization. *Applied Clay Science* 2008; **38**: 153-164.
76. Tammaro L. , Costantino U. , Bolognese A. , Sammartino G. , Marenzi G. , Calignano A. , Tete S. , Mastrangelo F. , Califano L. ,Vittoria V. Nanohybrids for controlled antibiotic release in topical applications. *International Journal of Antimicrobial Agents* 2007; **29**: 417-423.
77. Choi S. J. , Oh J. M. ,Choy J. H. Anticancer drug-layered hydroxide nanohybrids as potent cancer chemotherapy agents. *Journal of Physics and Chemistry of Solids* 2008; **69**: 1528-1532.
78. Ambrogi V. , Fardella G. , Grandolini G. ,Perioli L. Intercalation compounds of hydrotalcite-like anionic clays with antiinflammatory agents -- I. Intercalation and in vitro release of ibuprofen. *International Journal of Pharmaceutics* 2001; **220**: 23-32.
79. Wei M. , Shi S. , Wang J. , Li Y. ,Duan X. Studies on the intercalation of naproxen into layered double hydroxide and its thermal decomposition by in situ FT-IR and in situ HT-XRD. *Journal of Solid State Chemistry* 2004; **177**: 2534-2541.
80. Oh J.-M. , Kwak S.-Y. ,Choy J.-H. Intracrystalline structure of DNA molecules stabilized in the layered double hydroxide. *Journal of Physics and Chemistry of Solids* 2006; **67**: 1028-1031.
81. Berber M. R. , Hafez I. H. , Mingawa K. , Mori T. ,Tanaka M. Nanocomposite formulation system of lipid-regulating drugs based on layered double hydroxide: synthesis, characterization and drug release properties. *Pharmaceutical Research* 2010; **27**: 2394-2401.
82. Leroux F. ,Besse J. P. Polymer Interleaved Layered Double Hydroxide: A New Emerging Class of Nanocomposites. *Chemistry of Materials* 2001; **13**: 3507-3515.

83. Chavarria F. ,Paul D. R. Morphology and properties of thermoplastic polyurethane nanocomposites: Effect of organoclay structure. *Polymer* 2006; **47**: 7760-7773.
84. Kalendova A. , Posposil M. , Kovarova L. , Merinska D. , Valaskova M. , Vlkova H. , Simonik J. ,Capkova P. Influence of chain length on intercalation process of polyvinylchloride/clay nanocomposites based on alkyl-amine. *Plastics, Rubbers and Composites* 2004; **33**: 279-285.
85. Chen C., Curliss .D. Preparation, characterization, and nanostructural evolution of epoxy nanocomposites. *Journal of Applied Polymer Science* 2003; **90**: 2276-2287.
86. Soundararajah Q. Y. ,Karunaratne B. S. B. Mechanical Properties of Poly(vinyl alcohol) Montmorillonite Nanocomposites. *Journal of Composite Materials* 2010; **44**: 303-311.
87. Yasue K. , Katahira S. , Yoshikawa M. ,Fujimoto K., *In situ polymerization route to nylon 6-clay nanocomposites*. Polymer-clay nanocomposites, ed. Pinnavaia T.J.,Beall G.W., 2000, New York, John Wiley & Sons
88. Messersmith P. B. ,Giannelis E. P. Synthesis and characterization of layered silicate-epoxy nanocomposites. *Chemisty of Materials* 1994; **6**: 1719-1725.
89. Kato M., Usuki, A, *Polymer-clay nanocomposites*. Polymer-clay nanocomposites, ed. Pinnavaia T.J, Beall G.W., 2000, New York, John Wiley & Sons
90. Chang J. H. ,An Y. U. Nanocomposites of polyurethane with various organoclays: Thermomechanical properties, morphology, and gas permeability. *Journal of Polymer Science Part B: Polymer Physics* 2002; **40**: 670-677.
91. Favre H. ,Lagaly G. Organo-bentonites with quaternary alkylammonium ions. *Clay Minerals* 1991; **26**: 19-26.
92. Lagaly G. Interaction of alkylamines with different types of layered compounds. *Solid State Ionics* 1986; **22**: 43-51.
93. Goh P. S. , Ng B. C. , Ismail A. F. , Aziz M. ,Sanip S. M. Surfactant dispersed multi-walled carbon nanotube/polyetherimide nanocomposite membrane. *Solid State Sciences* 2010; **12**: 2155-2162.
94. Gong X., Liu, J, Baskaran, S, Voise, R.D, Young, J.S. Surfactant-assisted processing of carbon nanotube/polymer composite. *Chemistry of Materials* 2000; **12**: 1049-1052.
95. Zheng M. , Jagota A. , Semke E. D. , Diner B. A. , McLean R. S. , Lustig S. R. , Richardson R. E. ,Tassi N. G. DNA-assisted dispersion and separation of carbon nanotubes. *Nature Materials* 2003; **2**: 338-342.
96. Enyashin A. N. , Gemming S. ,Seifert G. DNA-wrapped carbon nanotubes. *Nanotechnology* 2007; **18**: 1-10.
97. Fong N. , Simmons A. ,Poole-Warren L. A. Antibacterial polyurethane nanocomposites using chlorhexidine diacetate as an organic modifier. *Acta Biomaterialia* 2010; **6**: 2554-2561.
98. Alexandre M. ,Dubois P. Polymer-layered silicate nanocomposites: preparation, properties and uses of a new class of materials. *Materials Science and Engineering* 2000; **28**: 1-63.

99. Vaia R. A. , Ishii H. ,Giannelis E. P. Synthesis and properties of two-dimensional nanostructures by direct intercalation of polymer melts in layered silicates. *Chemistry of Materials* 1993; **5**: 1694-1696.
100. Liu X. ,Wu Q. PP/clay nanocomposites prepared by grafting melt intercalation. *Polymer* 2001; **42**: 10013-10019.
101. Karapınar-Kazandağ M. , Bayrak Ö. F. , Yalvaç M. E. , Ersev H. , Tanalp J. , Şahin F. ,Bayırlı G. Cytotoxicity of 5 endodontic sealers on L929 cell line and human dental pulp cells. *International Endodontic Journal* 2011; **44**: 626-634.
102. Beriat N. C. , Ertan A. A. C., S , Gurpinar A. ,Onur M. A. Effect of different polymerization methods on the cytotoxicity of dental composites. *European Journal of Denstistry* 2010; **4**: 287-292.
103. Finnigan B. , Martin D. , Halley P. , Truss R. ,Campbell K. Morphology and properties of thermoplastic polyurethane nanocomposites incorporating hydrophilic layered silicates. *Polymer* 2004; **45**: 2249-2260.
104. Han B., Cheng, A, Ji, G, Wu, S, Shen, J. Effect of organophilic montmorillonite on polyurethane/montmorillonite nanocomposites. *Journal of Applied Polymer Science* 2004; **91**: 2536-2542.
105. Xu R. , Manias E. , Snyder A. J. ,Runt J. New biomedical poly(urethane urea)-layered silicate nanocomposites. *Macromolecules* 2001; **34**: 337-339.
106. Gilman J. W. Flammability and thermal stability studies of polymer layered-silicate (clay) nanocomposites. *Applied Clay Science* 1999; **15**: 31-49.
107. Camino G. , Tartaglione G. , Frache A. , Manferti C. ,Costa G. Thermal and combustion behaviour of layered silicate-epoxy nanocomposites. *Polymer Degradation and Stability* 2005; **90**: 354-362.
108. Matayabas J. C. ,Turner S. R., *Nanocomposite technology for enhancing the gas barrier of polyethylene terephthalate*. Polymer-clay nanocomposites, ed. Pinnavaia T.J, Beall G.W., 2000, New York, John Wiley & Sons
109. Zeng Q. H. , Yu A. B. , Lu M. ,Paul D. R. Clay-based polymer nanocomposites: research and commercial development. *Journal of nanoscience and nanotechnology* 2005; **5**: 1574-1592.
110. Alt V. , Bechert T. , Steinrücke P. , Wagener M. , Seidel P. , Dingeldein E. , Domann E. ,Schnettler R. An in vitro assessment of the antibacterial properties and cytotoxicity of nanoparticulate silver bone cement. *Biomaterials* 2004; **25**: 4383-4391.
111. Damm C. , Munstedt H. ,Rosch A. The antimicrobial efficacy of polyamide 6/silver-nano-and microcomposites. *Materials chemistry and physics* 2008; **108**: 61-66.
112. Li D. , He Q. ,Li J. Smart core/shell nanocomposites: Intelligent polymers modified gold nanoparticles. *Advances in Colloid and Interface Science* 2009; **149**: 28-38.
113. Corr S. A. , Rakovich Y. P. ,Gun'ko Y. K. Multifunctional magnetic-fluorescent nanocomposites for biomedical applications. *Nanoscale research letters* 2008; **3**: 87-104.
114. Alvarez-Lorenzo C. , Bromberg L. ,Concheiro A. Light-sensitive Intelligent Drug Delivery Systems. *Photochemistry and Photobiology* 2009; **85**: 848-860.

115. Wu C. , Chen C. , Lai J. , Chen J. , Mu X. , Zheng J. ,Zhao Y. Molecule-scale controlled-release system based on light-responsive silica nanoparticles. *Chemical Communications* 2008: 2662-2664.
116. Slowing I. I. , Trewyn B. G. , Giri S. ,Lin V. S. Y. Mesoporous Silica Nanoparticles for Drug Delivery and Biosensing Applications. *Advanced Functional Materials* 2007; **17**: 1225-1236.
117. Mal N. K. , Fujiwara M. ,Tanaka Y. Photocontrolled reversible release of guest molecules from coumarin-modified mesoporous silica. *Nature* 2003; **421**: 350-353.
118. Wei Q. , Ji J. ,Shen J. Synthesis of Near-Infrared Responsive Gold Nanorod/PNIPAAm Core/Shell Nanohybrids via Surface Initiated ATRP for Smart Drug Delivery. *Macromolecular Rapid Communications* 2008; **29**: 645-650.
119. Kost J. , Wolfrum J. ,Langer R. Magnetically enhanced insulin release in diabetic rats. *Journal of Biomedical Materials Research* 1987; **21**: 1367-1373.
120. Paoli V. M. D. , De paoli lacerda S. H. , Spinu L. , Ingber B. , Rosenzweig Z. ,Rosenzweig N. Effect of an oscillating magnetic field on the release properties of magnetic collagen gels. *Langmuir* 2006; **22**: 5894-5899.
121. Gupta R. K. ,Bajpai A. K. Magnetically Guided Release of Ciprofloxacin from Superparamagnetic Polymer Nanocomposites. *Journal of Biomaterials Science, Polymer Edition* 2011; **22**: 893-918.
122. Kaushik A. , Khan R. , Solanki P. R. , Randey P. , Alam J. , Ahmad S. ,Malhotra B. D. Iron oxide nanoparticles-chitosan composite based glucose biosensor. *Biosensors and Bioelectronics* 2008; **24**: 676-689.
123. Neuberger T. , Schopf B. , Hofmann H. , Hofmann M. ,von Rechenberg B. Superparamagnetic nanoparticles for biomedical applications: possibilities and limitations of a new drug delivery system. *Journal of magnetism and magnetic materials* 2005; **293**: 483-496.
124. Satarkar N. S. ,Hilt J. Z. Magnetic hydrogel nanocomposites for remote controlled pulsatile drug release. *Journal of Controlled Release* 2008; **130**: 246-251.
125. Banerjee S. S. , Roy M. ,Bose S. pH Tunable Fluorescent Calcium Phosphate Nanocomposite for Sensing and Controlled Drug Delivery. *Advanced Engineering Materials* 2011; **13**: B10-B17.
126. Brazel C. Magnetothermally-responsive Nanomaterials: Combining Magnetic Nanostructures and Thermally-Sensitive Polymers for Triggered Drug Release. *Pharmaceutical Research* 2009; **26**: 644-656.
127. Liu K. H. , Liu T. Y. , Chen S. Y. ,Liu D. M. Drug release behavior of chitosan-montmorillonite nanocomposite hydrogels following electrostimulation. *Acta Biomaterialia* 2008; **4**: 1038-1045.
128. Xu Z. , Li C. , Kang X. , Yang D. , Yang P. , Hou Z. ,Lin J. Synthesis of a multifunctional nanocomposite with magnetic, mesoporous, and near-IR absorption properties. *Journal of physical chemistry C* 2010; **114**: 16343-16350.
129. Weissleder R. ,Ntziachristos V. Shedding light onto live molecular targets. *Nature Medicine* 2003; **9**: 123-128.

130. Zhao L. , Xu X. , Wang X. , Zhang X. , Gao F. ,Tang J. Fabrication, characterization and in-vitro cytotoxicity of magnetic nanocomposite polymeric film for multi-functional medical application. *Proceedings of SPIE* 2009; **7493**: 749304.
131. Zhou N. L. , Liu Y. , Li L. , Meng N. , Huang Y. X. , Zhang J. , Wei S. H. ,Shen J. A new nanocomposite biomedical material of polymer/Clay-Cts-Ag nanocomposites. *Current Applied Physics* 2007; **7**: e58-e62.
132. Silva G. R. D. , Ayres E. , Orefice R. L. , Moura S. A. L. , Cara D. C. ,Cunha A. D. S. Controlled release of dexamethasone acetate from biodegradable and biocompatible polyurethane and polyurethane nanocomposite. *Journal of Drug Targeting* 2009; **17**: 374 - 383.
133. Salahuddin N. , El-Barbary A. ,Abdo N. Effect of polymethylmethacrylate–montmorillonite nanocomposite on the release of some biologically active 1,2,4-triazine derivatives. *Polymer Composites* 2009; **30**: 1190-1198.
134. Shaikh S. , Birdi A. , Qutubuddin S. , Lakatosh E. ,Baskaran H. Controlled Release in Transdermal Pressure Sensitive Adhesives using Organosilicate Nanocomposites. *Annals of Biomedical Engineering* 2007; **35**: 2130-2137.
135. Styan K. , Abrahamian M. , Hume E. ,Poole-Warren L. A. Antibacterial polyurethane organosilicate nanocomposites. *Key Enginnering Materials* 2007; **342-343**: 757-760.
136. Meng N. , Zhou N. L. , Zhang S. Q. ,Shen J. Synthesis and antimicrobial activities of polymer/montmorillonite-chlorhexidine acetate nanocomposite films. *Applied Clay Science* 2009; **42**: 667-670.
137. Choudalakis G. ,Gotsis A. D. Permeability of polymer/clay nanocomposites: A review. *European Polymer Journal* 2009; **45**: 967-984.
138. Nielson L. E. Models for the permeability of filled polymer systems. *Journal of macromolecular science A* 1967; **1**: 929-942.
139. Bharadwaj R. K. Modeling the Barrier Properties of Polymer-Layered Silicate Nanocomposites. *Macromolecules* 2001; **34**: 9189-9192.
140. Cussler E. L. , Hughes S. E. , Ward W. J. ,Aris R. Barrier membranes. *Journal of Membrane Science* 1988; **38**: 161-174.
141. Fredrickson G. H. ,Bicerano J. Barrier properties of oriented disk composites. *The Journal of Chemical Physics* 1999; **110**: 2181-2188.
142. Gusev A. A. ,Lusti H. R. Rational Design of Nanocomposites for Barrier Applications. *Advanced Materials* 2001; **13**: 1641-1643.
143. Aris R. On a problem in hindered diffusion. *Archive for Rational Mechanics and Analysis* 1986; **12**: 83-91.
144. Sorrentino A. , Tortora M. ,Vittoria V. Diffusion behavior in polymer-clay nanocomposites. *Journal of Polymer Science, Part B: Polymer Physics* 2006; **44**: 265-274.
145. Yano K. , Usuki A. ,Okada A. Synthesis and properties of polyimide-clay hybrid films. *Journal of Polymer Science Part A: Polymer Chemistry* 1997; **35**: 2289-2294.
146. Herrara-Alonso J. M. , Marand E. , Little J. C. ,Cox S. S. Transport properties in polyurethane/clay nanocomposites as barrier materials: Effect of processing conditions. *Journal of Membrane Science* 2009; **337**: 208-214.

147. Kim J. K. , Hu C. , Woo R. S. C. ,Sham M. L. Moisture barrier characteristics of organoclay-epoxy nanocomposites. *Composites Science and Technology* 2005; **65**: 805-813.
148. Wang Z. ,Pinnavaia T. J. Nanolayer reinforcement of elastomeric polyurethane. *Chemistry of Materials* 1998; **10**: 3769-3771.
149. Chen G. , Yao K. ,Zhao J. Montmorillonite clay/poly(methyl methacrylate) hydrbid resin and its barrier property to the plasticizer within poly(vinyl chloride) composite. *Journal of Applied Polymer Science* 1998; **73**: 425-430.
150. Tien Y. I., Wei, K.H. The effect of nano-sized silicate layers from montmorillonite on glass transition, dynamic mechanical, and thermal degradation properties of segmented polyurethane. *Journal of Applied Polymer Science* 2002; **86**: 1741-1748.
151. Wang S. J. , Liu L. M. , Fang P. F. , Chen Z. , Wang H. M. ,Zhang S. P. Microstructure of polymer-clay nanocomposites studied by positrons. *Radiation Physics and Chemistry* 2007; **76**: 106-111.
152. Xia H., Shaw S.J, Song,M. Relationship between mechanical properties and exfoliation degree of clay in polyurethane nanocomposites. *Polymer International* 2005; **54**: 1392-1400.
153. Xia H. , Song M. , Zhang Z. ,Richardson M. Microphase separation, stress relaxation, and creep behavior of polyurethane nanocomposites. *Journal of Applied Polymer Science* 2007; **103**: 2992-3002.
154. Tien Y. I., Wei, K.H. Hydrogen bonding and mechanical properties in segmented montmorillonite/polyurethane nanocomposites of different hard segment ratios. *Polymer* 2001; **42**: 3213-3221.
155. Finnigan B. , Martin D. , Halley P. , Truss R. ,Campbell K. Morphology and properties of thermoplastic polyurethane nanocomposites incorporating hydrophobic layered silicates. *Journal of Applied Polymer Science* 2005; **97**: 300-309.
156. Xia H., Song,M. Intercalation and exfoliation behaviour of clay layers in branched poyol and polyurethane/clay nanocomposites. *Polymer International* 2006; **55**: 229-235.
157. Jia Q. M. , Zheng M. S. , Chen H. X. ,Shen R. J. Morphologies and properties of polyurethane/epoxy resin interpenetrating network nanocomposites modified with organoclay. *Materials Letters* 2006; **60**: 1306-1309.
158. Wetzel B. , Haupert F. , Friedrich K. , Zhang M. Q. ,Rong M. Z. Impact and wear resistance of polymer nanocomposites at low filler content. *Polymer engineering and science* 2002; **42**: 1919-1927.
159. Zeng Q. , Yu A. ,Lu G. Interfacial interactions and structure of polyurethane intercalated nanocomposite. *Nanotechnology* 2005; **16**: 2757-2763.
160. Qi B., Zhang, Q.X, Bannister, M, Mai, Y.W. Investigation of the mechanical properties of DGEBA-based epoxy resin with nanoclay additives. *Composite Structures* 2006; **75**: 514-519.
161. Agag T., Koga, T, Takeichi, T. Studies on thermal and mechanical properties of polyimide-clay nanocomposites. *Polymer* 2001; **42**: 3399-3408.

162. Gurmendi U., Eguiazabal, J. I, Nazabal, J. Morphology and mechanical properties of polymer nanocomposites with a poly(hydroxy ether of bisphenol A) matrix. *Polymer International* 2006; **55**: 399-404.
163. Wang X. , Du V. ,Luo L. Biopolymer/montmorillonite nanocomposite: preparation, drug-controlled release property and cytotoxicity. *Nanotechnology* 2008; **19**: 065707-065714.
164. Strawhecker K. E. ,Manias E. Structure and Properties of Poly(vinyl alcohol)/Na+ Montmorillonite Nanocomposites. *Chemistry of Materials* 2000; **12**: 2943-2949.
165. Gorrasi G. , Tortora M. ,Vittoria V. Synthesis and physical properties of layered silicates/polyurethane nanocomposites. *Journal of Applied Polymer Science Part B: Polymer Physics* 2005; **43**: 2454-2467.
166. Osman M. A. , Mittal V. , Morbidelli M. ,Suter U. W. Polyurethane Adhesive Nanocomposites as Gas Permeation Barrier. *Macromolecules* 2003; **36**: 9851-9858.
167. Chen T. K., Tien, Y.I, Wei, K.H. Synthesis and characterization of novel segmented polyurethane/clay nanocomposites. *Polymer* 1999; **41**: 1345-1353.
168. Zilg C. , Thomann R. , Mülhaupt R. ,Finter J. Polyurethane Nanocomposites Containing Laminated Anisotropic Nanoparticles Derived from Organophilic Layered Silicates. *Advanced Materials* 1999; **11**: 49-52.
169. Chen-Yang Y. W., Lee, Y.K, Chen, Y.T, We, J.C. High improvement in the properties of exfoliated PU/clay nanocomposites by the alternative swelling process. *Polymer* 2007; **48**: 2969-2979.
170. Choi M. Y. , Anandhan S. , Youl J. H. , Baik D. H. , Seo S. W. ,Lee H. S. Synthesis and characterization of *in situ* polymerized segmented thermoplastic elastomeric polyurethane/layered silicate clay nanocomposites. *Journal of Applied Polymer Science* 2006; **102**: 3048-3055.
171. Choi W. J. , Kim H. J. , Young J. K. ,Kim S. C. Synthesis of chain-extended organifier and properties of polyurethane/clay nanocomposites. *Polymer* 2004; **45**: 6045-6067.
172. Lee W. F. ,Chen Y. C. Effect of bentonite on the physical properties and drug-release behavior of poly(AA-PEGMEA)/bentonite nanocomposite hydrogels for mucoadhesive. *Journal of Applied Polymer Science* 2004; **91**: 2934-2941.
173. Lee W. F. ,Fu Y. T. Effect of montmorillonite on the swelling behavior and drug-release behavior of nanocomposite hydrogels. *Journal of Applied Polymer Science* 2003; **89**: 3652-3660.
174. Zeng Q. , Yu A. B. , Lu G. Q. ,Standish R. K. Molecular Dynamics Simulation of Organic-Inorganic Nanocomposites: Layering Behavior and Interlayer Structure of Organoclays. *Chemistry of Materials* 2003; **15**: 4732-4738.
175. Jordan J. W., Modified clay complexes and methods of preparation, in *United States Patent Office*. 1960: New Jersey.
176. Norrish K., Quirk, J.P. Manner of swelling of montmorillonite. *Nature* 1954; **173**: 255-256.
177. Mizutani T., Takano, T, Ogoshi, H. Selectivity of adsorption of organic ammonium ions onto smetite clays. *Langmuir* 1995; **11**: 880-884.

178. Bellucci R. , Terenzi A. , Leuteritz A. , Pospiech D. , Frache A. , Traverso G. ,Camino G. Intercalation degree in PP/organoclay nanocomposites: role of surfactant structure. *Polymers for Advanced Technologies* 2008; **19**: 547-555.
179. Weiss A. Organic derivatives of mica-type layer-silicate. *Angewandte Chemie (International ed. in English)* 1963; **2**: 134-144.
180. Lan T. , Kaviratna P. D. ,Pinnavaia T. J. Mechanism of clay tactoid exfoliation in epoxy-clay nanocomposite. *Chemistry of Materials* 1995; **7**: 2144-2150.
181. Pluart L. L. , Duchet J. , Sautereau H. ,Gerard J. F. Tailored Interfaces in Nanocomposites. *Macromolecular symposia* 2003; **194**: 155-160.
182. Kim J. T. , Oh T. S. ,Lee D. H. Morphology and rheological properties of nanocomposites based on nitrile rubber and organophilic layered silicates. *Polymer International* 2003; **52**: 1203-1208.
183. Reichert P. , Nitz H. , Kinke S. , Bramndsch R. , Thomann R. ,Mulhaupt R. Poly(propylene)/organoclay nanocomposite formation: Influence of compatibilizer functionality and organoclay modification. *Macromolecular Materials and Engineering* 2000; **275**: 8-17.
184. Kormann X. , Rees M. , Thomann Y. , Necola A. , Barbezat M. ,Thomann R. Epoxy-layered silicate nanocomposites as matrix in glass fibre-reinforced composites. *Composites Science and Technology* 2005; **65**: 2259-2268.
185. Osman M. A. , Rupp J. E. P. ,Suter U. W. Gas permeation properties of polyethylene-layered silicate nanocomposites. *Journal of materials chemistry* 2005; **15**: 1298-1304.
186. Tien Y. I. ,Wei K. H. High-Tensile-Property Layered Silicates/Polyurethane Nanocomposites by Using Reactive Silicates as Pseudo Chain Extenders. *Macromolecules* 2001; **34**: 9045-9052.
187. Song L. , Hu Y. , Tang Y. , Zhang R. , Chen Z. ,Fan W. Study on the properties of flame retardant polyurethane/organoclay nanocomposite. *Polymer Degradation and Stability* 2005; **87**: 111-116.
188. Pattanayak A. ,Jana S. C. Properties of bulk-polymerized thermoplastic polyurethane nanocomposites. *Polymer* 2005; **46**: 3394-3406.
189. Xu Z. , Tang X. , Gu A. , Fang Z. ,Tong L. Surface-modifiers of clay on mechanical properties of rigid polyurethane foams/organoclay nanocomposites. *Journal of Applied Polymer Science* 2007; **105**: 2988-2995.
190. Deng , Ran Q. , Wu S. ,She J. Study on polyurethane/MDI-modified-organic montmorillonite nanocomposites. *polymer-plastics technology and engineering* 2008; **47**: 1200-1204.
191. Zou H. , Ran Q. , Wu S. ,Shen J. Study of nanocomposites prepared by melt blending TPU and montmorillonite. *Polymer Composites* 2008; **29**: 385-389.
192. Causin V., Marega, C, Marigo, A, Ferrara, G. Assessing organo-clay dispersion in polymer layered silicate nanocomposites: A SAXS approach. *Polymer* 2005; **46**: 9533-9537.
193. Samakande A. , Hartmann P. C. , Cloete V. ,Sanderson R. D. Use of acrylic based surfmers for the preparation of exfoliated polystyrene-clay nanocomposites. *Polymer* 2007; **48**: 1490-1499.

194. Xie W. , Gao Z. , Pan W.-P. , Hunter D. , Singh A. ,Vaia R. Thermal Degradation Chemistry of Alkyl Quaternary Ammonium Montmorillonite. *Chemistry of Materials* 2001; **13**: 2979-2990.
195. *Southern clay products, Inc*. [cited 2009 October 8th]; Available from: http://www.nanoclay.com/testdata.asp#.
196. Poole-Warren L. A. , Farrugia B. , Fong N. , Hume E. ,Simmons A. Controlling cell-material interactions with polymer nanocomposites by use of surface modifying additives. *Applied Surface Science* 2008; **255**: 519-522.
197. Okada A., Usuki, A. Twenty years of polymer-clay nanocomposites. *Macromolecular Materials and Engineering* 2006; **291**: 1449-1476.
198. Yasmin A. , Luo J. J. , Abot J. L. ,Daniel I. M. Mechanical and thermal behavior of clay/epoxy nanocomposties. *Composite science and technology* 2006; **66**: 2415-2422.
199. Finnigan B. , Jack K. , Campbell K. , Halley P. , Truss R. , Casey P. , Cookson D. , King S. ,Martin D. Segmented Polyurethane Nanocomposites: Impact of Controlled Particle Size Nanofillers on the Morphological Response to Uniaxial Deformation. *Macromolecules* 2005; **38**: 7386-7396.
200. Hehrlein C. , Arab A. ,Bode C. Drug-eluting stent: the "magic bullet" for prevention of restenosis? *Basic Research in Cardiology* 2002; **97**: 417-423.
201. 1997 *Coronary stenting; a literature review*. Australian health technology advisory committee: Australia.
202. Knetsch M. L. W., *Blood-contacting surfaces*. Biomaterials fabrication and processing, ed. Chu P.K.,Liu X., 2008, United States of America, CRC Press
203. Ikada Y. Surface modification of polymers for medical applications. *Biomaterials* 1994; **15**: 725-736.
204. McNeely T. B. ,Griffith M. J. The anticoagulant mechanism of action of heparin in contact-activated plasma: inhibition of factor X activation. *Blood* 1985; **65**: 1226-1231.
205. Byun Y. , Jacobs H. A. ,Kim S. W. Mechanism of thrombin inactivation by immobilized heparin. *Journal of Biomedical Materials Research* 1996; **30**: 423-427.
206. Han D. K. , Park K. D. , Ahn K. D. , Jeong S. Y. ,Kim Y. H. preparation and surface characterization of PEO-grafted and heparin immobilized polyurethanes. *Journal of biomaterial research* 1989; **23**: 87-104.
207. Du Y. J. , Klement P. , Berry L. R. , Tressel P. ,Chan A. K. C. In vivo rabbit acute model tests of polyurethane catheters coated with a novel antithrombin-heparin covalent complex. *Thrombosis and Haemostasis* 2005; **94**: 366-372.
208. Zhou Z. ,Meyerhoff M. E. Preparation and characterization of polymeric coatings with combined nitric oxide release and immobilized active heparin. *Biomaterials* 2005; **26**: 6506-6517.
209. Riedl C. R. , Witkowski M. , Plas E. ,Pflueger H. Heparin coating reduces encrustation of ureteral stents: a preliminary report. *International Journal of Antimicrobial Agents* 2002; **19**: 507-510.
210. Fu J. , Ji J. , Fan D. ,Shen J. Construction of antibacterial multilayer films containing nanosilver via layer-by-layer assembly of heparin and chitosan-silver ions complex. *Journal of biomaterial research* 200; **79A**: 665-674.

211. Tan Q. , Ji J. , Barbosa M. A. , Fonseca C. ,Shen J. Constructing thromboresistant surface on biomedical stainless steel via layer-by-layer deposition anticoagulant. *Biomaterials* 2003; **24**: 4699-4705.
212. Tan Q. , Ji J. , Zhao F. , Fan D. Z. , Sun F. Y. ,Shen J. C. Fabrication of thromboresistant multilayer thin film on plasma treated poly(vinyl chloride) surface. *Journal of Materials Science: Materials in Medicine* 2005; **16**: 687-692.
213. van der Heiden A. P. , Goebbels D. , Pijpers A. P. ,Koole L. H. A photochemical method for the surface modification of poly(etherurethanes) with phosphorylcholine-containing compounds to improve hemocompatibility. *Journal of biomaterial research* 1997; **37**: 282-290.
214. Desai N. P. ,Hubbell J. A. Solution technique to incorporate polyethylene oxide and other water-soluble polymers into surfaces of polymeric biomaterials. *Biomaterials* 1991; **12**: 144-153.
215. Mazid M. A. , Scott E. ,Nai-Hong L. New biocompatible polyurethane-type copolymer with low molecular weight heparin. *Clinical Materials* 1991; **8**: 71-80.
216. Labarre D. , Jozefowicz M. ,Boffa M. C. Properties of heparin-poly (methyl methacrylate) copolymers. II. *Journal of Biomedical Materials Research* 1977; **11**: 283-295.
217. Moon H. T. , Lee L. K. , Han J. K. ,Byun Y. A novel formulation for controlled release of heparin-DOCA conjugate dispersed as nanoparticles in polyurethane film. *Biomaterials* 2001; **22**: 281-289.
218. Park K. D. , Okano T. , Nojiri C. ,Kim S. W. Heparin immobilization onto segmented polyurethaneurea surfaces-effect of hydrophili spacers. *Journal of biomaterial research* 1988; **22**: 977-992.
219. Chen M. C. , Chang Y. , Liu C. T. , Lai W. Y. , Peng S. F. , Hung Y. W. , Tsai H. W. ,Sung H. W. The characteristics and in vivo suppression of neointimal formation with sirolimus-eluting polymeric stents. *Biomaterials* 2009; **30**: 79-88.
220. Lee P. I. Effect of non-uniform initial drug concentration distribution on the kinetics of drug release from glassy hydrogel matrices. *Polymer* 1984; **25**: 973-978.
221. Kannan R. Y., Salacinski, H.J, Groot, J.D, Clatworthy, I, Bozec, L, Horton, M, Butler, P.E, Seifalian, A.M. The antithrombogenic potential of a polyhedral oligomeric silsesquioxane (POSS) nanocomposite. *Biomacromolecules* 2006; **7**: 215-223.
222. Zhou N., Fang, S, Xu, D, Zhang, J, Mo, H, Shen, J. Montmorillonite-phosphatidyl choline/PDMS films: A novel antithrombogenic material. *Applied Clay Science* 2009; **46**: 401-403.
223. Asmatulu R. , Claus R. O. , Mecham J. B. , Corcoran S. G. ,Wang Y. X. Nanocomposite thin film coatings for protection of materials surfaces. *Materials research society symposia proceedings* 2005; **872**: J13.14.1-J13.14.6.
224. Zaporojtchenko V. ,et al. Physico-chemical and antimicrobial properties of co-sputtered Ag–Au/PTFE nanocomposite coatings. *Nanotechnology* 2006; **17**: 4904.
225. Courtney J. M. , Lamba N. M. K. , Sundaram S. ,Forbes C. D. Biomaterials for blood-contacting applications. *Biomaterials* 1994; **15**: 737-744.

226. Meng J. , Kong H. , Xu H. Y. , Song L. , Wang C. Y. ,Xie S. S. Improving the blood compatibility of polyurethane using carbon nanotubes as fillers and its implications to cardiovascular surgery. *Journal of Biomedical Materials Research Part A* 2005; **74A**: 208-214.
227. Hong J. , Larsson A. , Ekdahl K. N. , Elgue G. , Larrsson R. ,Nilsson B. Contact between a polymer and whole blood: Sequence of events leading to thrombin generation. *Journal of laboratory clinical medicine* 2001; **138**: 139-145.
228. Mackman N. , Tilley R. E. ,Key N. S. Role of the extrinsic pathway of blood coagulation in hemostasis and thrombosis. *Arteriosclerosis, Thrombosis, and Vascular Biology* 2007; **27**: 1687-1693.
229. Davie E. W. A Brief Historical Review of the Waterfall/Cascade of Blood Coagulation. *Journal of Biological Chemistry* 2003; **278**: 50819-50832.
230. Dellinger R. P. Inflammation and Coagulation: Implications for the Septic Patient. *Clinical Infectious Diseases* 2003; **36**: 1259-1265.
231. Jaques L. B. , Monkhouse F. C. ,Stewart M. A method for the determination of heparin in blood. *The Journal of Physiology* 1949; **109**: 41-48.
232. Smith P. K. , Mallia A. K. ,Hermanson G. T. Colorimetric method for the assay of heparin content in immobilized heparin preparations. *Analytical Biochemistry* 1980; **109**: 466-473.
233. Hemker H. C. , Giesen P. , AlDieri R. , Regnault T. , de Smed E. ,Wagenvoord R. The calibrated automated thrombogram (CAT): a universal routine test for hyper- and hypocoagulability *Pathophysiology of haemostasis and thrombosis* 2002; **32**: 249-253.
234. Aldenhoff Y. B. J. , Hanssen J. H. L. , Knetsch M. L. W. ,Koole L. H. Thrombus formation at the surface of guide-wire models: effetcs of heparin-releasing or heparin-exposing surface coatings. *Journal of Vascular and interventional radiology* 2007; **18**: 419-425.
235. Aldenhoff Y. B. J. , Knetsch M. L. W. , Hanssen J. H. L. , Lindhout T. , Wielders S. J. H. ,Koole L. H. Coils and tubes releasing heparin. Studies on a new vascular graft prototype. *Biomaterials* 2004; **25**: 3125-3133.
236. Al Dieri R. , Alban S. , Beguin S. ,Hemker H. C. Thrombin generation for the control of heparin treatment comparison with the activated partial thrombo-plastin time. *Journal of Thrombosis and Haemostasis* 2004; **24**: 1395-1401.
237. Hemker H. C. , Al Dieri R. ,Beguin S. Thrombin generation assays: accruing clinical relevance. *Current Opinion in Hematology* 2004; **11**: 170-175.
238. Munro M. S. , Eberhart R. C. , Maki N. J. , Brink B. E. ,Fry W. J. Thromboresistant alkyl derivatized polyurethanes. *American Society in Artificial Internal Organs* 1983; **6**: 65-75.
239. Duncan A. C. , Sefton M. V. ,Brash J. L. Effect of C4-, C8- and C18- alkylation of poly(vinyl alcohol) hydrogels on the adsorption of albumin and fibrinogen from buffer and plasma: limited correlation with platelet interactions. *Biomaterials* 1997; **18**: 1585-1592.
240. Pitt W. G. ,Cooper S. L. Albumin adsorption on alkyl chain derivatized polyurethanes: I. The effect of C-18 alkylation. *Journal of Biomedical Materials Research* 1988; **22**: 359-382.

241. Day J. R. S. , Landis R. C. ,Taylor K. M. Heparin is much more than just an anticoagulant. *Journal of Cardiothoracic and Vascular Anesthesia* 2004; **18**: 93-100.
242. Lv Q. , Cao C. ,Zhu H. A novel solvent system for blending of polyurethane and heparin. *Biomaterials* 2003; **24**: 3915-3919.
243. Bounameaux H. Unfractionated versus low-molecular-weight heparin in the treatment of benous thromboembolism. *Vascular Medicine* 1998; **3**: 41.
244. Heuck C. C. , Schiele U. , Horn D. , Fronda D. ,Ritz E. The role of surface charge on the accelerating action of heparin on the antithrombin III-inhibited activity of α-Thrombin. *The journal of biological chemistry* 1985; **260**: 4598-4603.
245. Porubcan L. S. , Serna S. J. , White J. L. ,Hem S. L. Mechanism of adsorption of clindamycin and tetracycline by montmorillonite. *Journal of Pharmaceutical Sciences* 1978; **67**: 1081-1087.
246. Aguzzi C. , Cerezo P. , Viseras C. ,Caramella C. Use of clays as drug delivery systems: Possibilities and limitations. *Applied Clay Science* 2007; **36**: 22-36.
247. Patel H. , Somani R. , Bajaj H. ,Jasra R. Nanoclays for polymer nanocomposites, paints, inks, greases and cosmetics formulations, drug delivery vehicle and waste water treatment. *Bulletin of Materials Science* 2006; **29**: 133-145.
248. Piozzi A. Polyurethanes loaded with antibiotics: Influence of polymer-antibiotic interactions on In Vitro activity against staphylococcus epidermidis. *Journal of Chemotherapy* 2004; **16**: 446-452.
249. Shi H. , Lan T. ,Pinnavaia T. J. Interfacial Effects on the Reinforcement Properties of Polymer-Organoclay Nanocomposites. *Chemistry of Materials* 1996; **8**: 1584-1587.
250. Serizawa T. , Matsukuma D. ,Akashi M. Loading and Release of Charged Dyes Using Ultrathin Hydrogels. *Langmuir* 2005; **21**: 7739-7742.
251. Lee W.-F. ,Chen Y.-C. Effects of intercalated hydrotalcite on drug release behavior for poly(acrylic acid-co-N-isopropyl acrylamide)/intercalated hydrotalcite hydrogels. *European Polymer Journal* 2006; **42**: 1634-1642.
252. Lee W. F. ,Chen Y. C. Effect of hydrotalcite on the physical properties and drug-release behavior of nanocomposite hydrogels based on poly[acrylic acid-poly(ethylene glycol) methyl ether acrylate] gels. *Journal of Applied Polymer Science* 2004; **94**: 692-699.
253. Lee W. F. ,Jou L. L. Effect of the intercalation agent content of montmorillonite on the swelling behavior and drug release behavior of nanocomposite hydrogels. *Journal of Applied Polymer Science* 2004; **94**: 74-82.
254. Hanley H. J. M. , Muzny C. D. , Ho D. L. ,Glinka C. J. A Small-Angle Neutron Scattering Study of a Commercial Organoclay Dispersion. *Langmuir* 2003; **19**: 5575-5580.
255. Sigma-Aldrich, *Brilliant blue R product information*. 2003.
256. Sigma-Aldrich, *Crystal violet product specification*. 2010.
257. Chemicalland21, *Bromophenol Blue product description*. 2010.
258. Graham N. B. , Zulfiqar M. , MacDonald B. B. ,McNeill M. E. Caffeine release from fully swollen poly(ethylene oxide) hydrogels. *Journal of Controlled Release* 1988; **5**: 243-252.

259. Ritger P. L. ,Peppas N. A. A simple equation for description of solute release I. Fickian and non-fickian release from non-swellable devices in the form of slabs, spheres, cylinders or discs. *Journal of Controlled Release* 1987; **5**: 23-36.
260. Crank J., *The mathematics of diffusion*. 2nd edition ed, 1975, New York, Oxford University Press Inc
261. Chen G. , Liu S. , Chen S. ,Qi Z. FTIR spectra, thermal properties, and dispersibility of a polystyrene/montmorillonite nanocomposite. *Macromolecular Chemistry and Physics* 2001; **202**: 1189-1193.
262. Madejová J. FTIR techniques in clay mineral studies. *Vibrational Spectroscopy* 2003; **31**: 1-10.
263. Dillon J., *Infrared Spectroscopic Atlas of Polyurethanes*, 1989, Pennsylvannia, Tachnomic Publishing Company, Inc
264. Simmons A. , Hyvarinen J. , Odell R. A. , Martin D. J. , Gunatillake P. A. , Noble K. R. ,Poole-Warren L. A. L. A. Long-term in vivo biostability of poly(dimethylsiloxane)/poly(hexamethylene oxide) mixed macrodiol-based polyurethane elastomers. *Biomaterials* 2004; **25**: 4887-4900.
265. Kozak M. ,Domka L. Adsorption of the quaternary ammonium salts on montmorillonite. *Journal of Physics and Chemistry of Solids* 2004; **65**: 441-445.
266. Hongping H. , Ray F. L. ,Jianxi Z. Infrared study of $HDTMA^+$ intercalated montmorillonite. *Spectrochimica Acta Part A* 2004; **60**: 2853-2859.
267. van der Marel H. W. ,Beutelspacher H., *Atlas of Infrared spectroscopy of clay minerals and their admixtures*, 1976, Elsevier Scientific Publishing Company
268. Silverstein R. M. ,Webster F. X., *Spectrometric identification of organic compounds*. 6th edition ed, 1998, John Wiley & Sons Inc
269. Huang T. H. ,Wu T. M. Spectral analysis of ball pen script by FTIR microscopy with ATR objective. *Spectroscopy and spectral analysis* 2007; **27**: 2200-2202.
270. Dillon J. G., *Infrared spectroscopic atlas of polyurethanes*, 1989, Technomic Publishing Company Inc
271. Silberberg M., *Chemistry: The Molecular Nature of Matter and Change*, 2004, McGraw-Hill
272. Kohjiya S. , Ikeda Y. , Takesako S. ,Yamashita S. Drug release behavior from polyurethane gel. *Reactive Polymers* 1991; **15**: 165-175.
273. Piozzi A. , Francolini I. , Occhiaperti L. , Venditti M. ,Marconi W. Antimicrobial activity of polyurethanes coated with antibiotics: a new approach to the realization of medical devices exempt from microbial colonization. *International Journal of Pharmaceutics* 2004; **280**: 173-183.
274. Chan C.-K. ,Chu I. M. In vitro release of incorporated model compounds in poly(sebacic anhydride-co-ethylene glycol). *European Polymer Journal* 2005; **41**: 1403-1409.
275. Lao L. L. , Venkatraman S. S. ,Peppas N. A. A novel model and experimental analysis of hydrophilic and hydrophobic agent release from biodegradable polymers. *Journal of Biomedical Materials Research Part A* 2009; **90A**: 1054-1065.
276. Huang Y. Y. , Chung T. W. ,Tzeng T. W. Drug release from PLA/PEG microparticulates. *International Journal of Pharmaceutics* 1997; **156**: 9-15.

277. Einmahl S. , Zignani M. , Varesio E. , Heller J. , Veuthey J. L. , Tabatabay C. ,Gurny R. Concomitant and controlled release of dexamethasone and 5-fluorouracil from poly(ortho ester). *International Journal of Pharmaceutics* 1999; **185**: 189-198.
278. Kim D. H. , Kang S. G. , Park S. S. , Lee D. H. , Lee G. H. , Lee C. G. ,Song H. Y. Evaluation of the release behavior of the dexamethasone embedded in polycarbonate polyurethane membrances: an invitro study. *Journal of the Korean Radiological Society* 2003; **48**: 7-11.
279. Thote A. J. ,Gupta R. B. Formation of nanoparticles of a hydrophilic drug using supercritical carbon dioxide and microencapsulation for sustained release. *Nanomedicine: Nanotechnology, Biology and Medicine* 2005; **1**: 85-90.
280. Guy R. K., Bioactive Database, St. Jude Childrens Research Hospital.
281. Heinz H. , Koerner H. , Anderson K. L. , Vaia R. A. ,Farmer B. L. Force Field for Mica-Type Silicates and Dynamics of Octadecylammonium Chains Grafted to Montmorillonite. *Chemistry of Materials* 2005; **17**: 5658-5669.
282. Amarasinghe P. M. , Katti K. S. ,Katti D. R. Nature of organic fluid-montmorillonite interactions: An FTIR spectroscopic study. *Journal of Colloid and Interface Science* 2009; **337**: 97-105.
283. Rodrigues L. B. , Leite H. F. , Yoshida M. I. , Saliba J. B. , Junior A. S. C. ,Faraco A. A. G. In vitro release and characterization of chitosan films as dexamethasone carrier. *International Journal of Pharmaceutics* 2009; **368**: 1-6.
284. Zignani M. , Einmahl S. , Baeyens V. , Varesio E. , Veuthey J. L. , Anderson J. , Heller J. , Tabatabay C. ,Gurny R. A poly(ortho ester) designed for combined ocular delivery of dexamethasone sodium phosphate and 5-fluorouracil: subconjunctival tolerance and in vitro release. *European Journal of Pharmaceutics and Biopharmaceutics* 2000; **50**: 251-255.
285. Daemen J. ,Serruys P. W. Drug-Eluting Stent Update 2007: Part I: A Survey of Current and Future Generation Drug-Eluting Stents: Meaningful Advances or More of the Same? *Circulation* 2007; **116**: 316-328.
286. Suk K. T. , Kim J. W. , Kim H. S. , Baik S. K. , Oh S. J. , Lee S. J. , Kim H. G. , Lee D. H. , Won Y. H. ,Lee D. K. Human application of a metallic stent covered with a paclitaxel-incorporated membrane for malignant biliary obstruction: multicenter pilot study. *Gastrointestinal Endoscopy* 2007; **66**: 798-803.
287. Shin J. H. , Song H.-Y. , Seo T.-S. , Yuk S. H. , Kim Y.-H. , Cho Y.-M. , Choi G. B. , Kim T.-H. ,Suh J.-Y. Influence of a dexamethasone-eluting covered stent on tissue reaction: an experimental study in a canine bronchial model. *European Radiology* 2005; **15**: 1241-1249.
288. Shin J. H. , Kim J. S. , Kim T. H. , Kim E. Y. , Choi W. C. , Woo C. W. , Yuk S. H. , Lee Y. S. , Di Z. ,Song H. Y. Influence of a Paclitaxel-eluting Expandable Metallic Stent on Tissue Hyperplasia: An Experimental Study in a Canine Tracheal Model. . *Journal of Korean Radiology Society* 2005; **52**: 233-240.
289. Kang S.-G. , Lee S. , Choi S. , Park S. , Jeong S. , Lee D. ,Kim M. Paclitaxel-polyurethane film for anti-cancer drug delivery: Film characterization and preliminary in vivo study. *Macromolecular Research* 2010; **18**: 680-685.

290. Guo Q. , Knight P. T. , Wu J. ,Mather P. T. Blends of Paclitaxel with POSS-Based Biodegradable Polyurethanes: Morphology, Miscibility, and Specific Interactions. *Macromolecules* 2010; **43**: 4991-4999.
291. Newton R. Molecular mechanisms of glucocorticoid action: what is important? *Thorax* 2000; **55**: 603-613.
292. Barnes P. J. Anti-inflammatory actions of glucocorticoids: molecular mechanisms. *Clinical Science* 1998; **94**: 557-572.
293. Adcock I. M. Molecular Mechanisms of Glucocorticosteroid Actions. *Pulmonary Pharmacology & Therapeutics* 2000; **13**: 115-126.
294. Reil T. D. , Sarkar R. , Kashyap V. S. , Sarkar M. ,Gelabert H. A. Dexamethasone Suppresses Vascular Smooth Muscle Cell Proliferation. *Journal of Surgical Research* 1999; **85**: 109-114.
295. Ramalingam A. , Hirai A. ,Thompson E. A. Glucocorticoid Inhibition of Fibroblast Proliferation and Regulation of the Cyclin Kinase Inhibitor p21Cip1. *Molecular Endocrinology* 1997; **11**: 577-586.
296. da Silva G. , da Silva Cunha A. , Ayres E. ,Oréfice R. Effect of the macromolecular architecture of biodegradable polyurethanes on the controlled delivery of ocular drugs. *Journal of Materials Science: Materials in Medicine* 2009; **20**: 481-487.
297. Singarayar S. , Kistler P. M. , De Winter C. ,Mond H. A Comparative Study of the Action of Dexamethasone Sodium Phosphate and Dexamethasone Acetate in Steroid-Eluting Pacemaker Leads. *Pacing and Clinical Electrophysiology* 2005; **28**: 311-315.
298. Shin J. H. , Song H. Y. , Chol C. G. , Yuk S. H. , Kim J. S. , Kim Y. M. , Yoong C. J. , Kim T. H. , Suh J. Y. ,He X. Tissue hyperplasia: influence of a paclitaxel-eluting covered stent-preliminary study in a canine urethral model. *Radiology* 2005; **234**.
299. Moura S. A. L. , Lima L. D. C. , Andrade S. P. , Silva-Cunha Junior A. D. , Órefice R. L. , Ayres E. ,Da Silva G. R. Local drug delivery system: Inhibition of inflammatory angiogenesis in a murine sponge model by dexamethasone-loaded polyurethane implants. *Journal of Pharmaceutical Sciences* 2011: 2886-2895.
300. da Silva G. R. , da Silva-Cunha Jr A. , Behar-Cohen F. , Ayres E. ,Oréfice R. L. Biodegradable polyurethane nanocomposites containing dexamethasone for ocular route. *Materials Science and Engineering: C* 2011; **31**: 414-422.
301. Lao L. L. ,Venkatraman S. S. Adjustable paclitaxel release kinetics and its efficacy to inhibit smooth muscle cells proliferation. *Journal of Controlled Release* 2008; **130**: 9-14.
302. Liebmann J. E. , Cook J. A. , Lipschultz C. , Teague D. , Fisher J. ,Mitchell J. B. Cytotoxic studies of paclitaxel (Taxol) in human tumour cell lines. *British Journal of Cancer* 1993; **68**: 1104-1109.
303. Styan K. E. , Martin D. J. ,Poole-Warren L. A. In vitro fibroblast response to polyurethane organosilicate nanocomposites. *Journal of Biomedical Materials Research Part A* 2008; **86A**: 571-582.
304. Mirabedini S. M. , Sabzi M. , Zohuriaan-Mehr J. , Atai M. ,Behzadnasab M. Weathering performance of the polyurethane nanocomposite coatings containing silane treated TiO2 nanoparticles. *Applied Surface Science* 2011; **257**: 4196-4203.

305. Solarski S. , Benali S. , Rochery M. , Devaux E. , Alexandre M. , Monteverde F. ,Dubois P. Synthesis of a polyurethane/clay nanocomposite used as coating: Interactions between the counterions of clay and the isocyanate and incidence on the nanocomposite structure. *Journal of Applied Polymer Science* 2005; **95**: 238-244.
306. Devaux E. , Rochery M. ,Bourbigot S. Polyurethane/clay and polyurethane/POSS nanocomposites as flame retarded coating for polyester adn cotton fabrics. *Fire and materials* 2002; **26**: 149-154.
307. Bakhshi R. , Darbyshire A. , Evans J. E. , You Z. , Lu J. ,Seifalian A. M. Polymeric coating of surface modified nitinol stent with POSS-nanocomposite polymer. *Colloids and Surfaces B: Biointerfaces* 2011; **86**: 93-105.
308. Kannan R. Y. , Salacinski H. J. , Edirisinghe M. J. , Hamilton G. ,Seifalian A. M. Polyhedral oligomeric silsequioxane-polyurethane nanocomposite microvessels for an artificial capillary bed. *Biomaterials* 2006; **27**: 4618-4626.
309. Grabow N. , Martin D. P. , Schmitz K.-P. ,Sternberg K. Absorbable polymer stent technologies for vascular regeneration. *Journal of Chemical Technology & Biotechnology* 2010; **85**: 744-751.
310. Alexis F. , Venkatraman S. S. , Rath S. K. ,Boey F. In vitro study of release mechanisms of paclitaxel and rapamycin from drug-incorporated biodegradable stent matrices. *Journal of Controlled Release* 2004; **98**: 67-74.
311. AS-ISO-10993, Biological evaluation of medical devices. 2004. p. AS ISO-10993
312. Burt H. M. , Zhang X. , Toleikis P. , Embree L. ,Hunter W. L. Development of copolymers of poly(,-lactide) and methoxypolyethylene glycol as micellar carriers of paclitaxel. *Colloids and Surfaces B: Biointerfaces* 1999; **16**: 161-171.
313. Bouquet W. , Ceelen W. , Fritzinger B. , Pattyn P. , Peeters M. , Remon J. P. ,Vervaet C. Paclitaxel/[beta]-cyclodextrin complexes for hyperthermic peritoneal perfusion - Formulation and stability. *European Journal of Pharmaceutics and Biopharmaceutics* 2007; **66**: 391-397.
314. Shikanov A. , Ezra A. ,Domb A. J. Poly(sebacic acid-co-ricinoleic acid) biodegradable carrier for paclitaxel--effect of additives. *Journal of Controlled Release* 2005; **105**: 52-67.
315. Elkharraz K. , Faisant N. , Guse C. , Siepmann F. , Arica-Yegin B. , Oger J. M. , Gust R. , Goepferich A. , Benoit J. P. ,Siepmann J. Paclitaxel-loaded microparticles and implants for the treatment of brain cancer: Preparation and physicochemical characterization. *International Journal of Pharmaceutics* 2006; **314**: 127-136.
316. Zilberman M. , Schwade N. D. , Meidell R. S. ,Eberhart R. C. Structured drug-loaded bioresorbable films for support structures. *Journal of Biomaterials Science, Polymer Edition* 2001; **12**: 875-892.
317. Joshi G. V. , Patel H. , Bajaj H. ,Jasra R. Intercalation and controlled release of vitamin B_6 from montmorillonite-vitamin B_6 hybrid. *Colloid & Polymer Science* 2009; **287**: 1071-1076.
318. Suggs L. J. , Shive M. S. , Garcia C. A. , Anderson J. M. ,Mikos A. G. In vitro cytotoxicity and in vivo biocompatibility of poly(propylene fumarate-co-ethylene glycol) hydrogels. *Journal of Biomedical Materials Research* 1999; **46**: 22-32.

319. Rosengren A. , Faxius L. , Tanaka N. , Watanabe M. ,Bjursten L. M. Comparison of implantation and cytotoxicity testing for initially toxic biomaterials. *Journal of Biomedical Materials Research Part A* 2005; **75A**: 115-122.
320. Frost G. H. , Rhee K. ,Thompson E. A. Glucocorticoid regulation of thymidine kinase (Tk-1) expression in L929 cells. *Journal of Biological Chemistry* 1993; **268**: 6748-6754.
321. Thomsen P. ,Gretzer C. Macrophage interactions with modified material surfaces. *Current Opinion in Solid State and Materials Science* 2001; **5**: 163-176.
322. Lee J. H. , Jung H. W. , Kang I. K. ,Lee H. B. Cell behaviour on polymer surfaces with different functional groups. *Biomaterials* 1994; **15**: 705-711.
323. Lin D. T. , Young T. H. ,Fang Y. Studies on the effect of surface properties on the biocompatibility of polyurethane membranes. *Biomaterials* 2001; **22**: 1521-1529.
324. Anderson J. M. , Rodriguez A. ,Chang D. T. Foreign body reaction to biomaterials. *Seminars in Immunology* 2008; **20**: 86-100.
325. Lee P. C. , Chen L. W. , Lin J. R. , Hsieh K. H. ,Huang L. L. Influence of hard segments of polyurethane on cell growth. *Polymer International* 1996; **41**: 419-425.
326. Khorasani M. T. , MoemenBellah S. , Mirzadeh H. ,Sadatnia B. Effect of surface charge and hydrophobicity of polyurethanes and silicone rubbers on L929 cells response. *Colloids and Surfaces B: Biointerfaces* 2006; **51**: 112-119.
327. Schiff P. B. ,Susan Band H. Taxol Stabilizes Microtubules in Mouse Fibroblast Cells. *Proceedings of the National Academy of Sciences of the United States of America* 1980; **77**: 1561-1565.
328. Chang Y. F. , Li L. L. , Wu C. W. , Liu T. Y. , Lui W. Y. , P'eng F. K. ,Chi C. W. Paclitaxel-induced apoptosis in human gastric carcinoma cell lines. *Cancer* 1996; **77**: 14-18.
329. Kim J. Y. , Liu Y. , Sung H. K. , Park J. H. , Song I. H. , Sung E. G. ,Lee Y. H. Effect of paclitaxel on the β-actin, fibronectin, laminin and fine structure in HeLa and L929 cells. *The Korean Journal of Anatomy* 2001; **34**: 1-11.
330. Akgun H. , Berk B. , Erol D. D. , Mercanoglu G. , Bayrak O. F. , Caglayan B. , Dedeagac A. ,Kurnaz I. A. Nitric oxide releasing derivatives of [(2-Chloroethyl) ureido] benzoic acid esters as potential antineoplastic agents. *Turkish Journal of Chemistry* 2009; **33**: 107-121.
331. Danesi R. , Figg W. D. , Reed E. ,Myers C. E. Paclitaxel (Taxol) inhibits isoprenylation and induces apoptosis in PC-3 human prostate cancer cells. *Molecular Pharmacology* 1995; **47**: 1106-1111.
332. Samyn F. , Bourbigot S. , Jama C. , Bellayer S. , Nazare S. , Hull R. , Castrovinci A. , Fina A. ,Camino G. Crossed characterisation of polymer-layered silicate (PLS) nanocomposite morphology: TEM, X-ray diffraction, rheology and solid-state nuclear magnetic resonance measurements. *European Polymer Journal* 2008; **44**: 1642-1653.
333. Grandjean J. Solid-state NMR study of modified clays and polymer/clay nanocomposites. *Clay Minerals* 2006; **41**: 567-586.
334. Sikdar D. , Pradhan S. M. , Katti D. R. , Katti K. S. ,Mohanty B. Altered Phase Model for Polymer Clay Nanocomposites. *Langmuir* 2008; **24**: 5599-5607.

335. Dhakal H. N. , Zhang Z. Y. ,Richardson M. O. W. Nanoindentation behaviour of layered silicate reinforced unsaturated polyester nanocomposites. *Polymer Testing* 2006; **25**: 846-852.
336. ATTO-TEC, *fluorescent labels and dyes catalogue*. 2011/2013.
337. Panchuk-Voloshina N. , Hauglang R. P. , Bishop-Steward J. , Bhalgat M. K. , Millard P. J. , Mao F. , Leung W. Y. ,Haugland R. P. Alexa Dyes, a series of new fluorescent dyes that yield exceptionally bright, photostable conjugates. *The Journal of histochemistry & cytochemistry* 1999; **47**: 1179-1188.
338. Thermoscientific, *Thermo Scientific Pierce Fluorescent Products Guide*. 2008.
339. Ajun W. , Yan S. , Li G. ,Huili L. Preparation of aspirin and probucol in combination loaded chitosan nanoparticles and in vitro release study. *Carbohydrate Polymers* 2009; **75**: 566-574.
340. Kukreja N. ,Onuma Y. The future of drug-eluting stents. *Pharmacological Research* 2008; **57**: C.
341. Matheson L. A. , Labow R. S. ,Santerre J. P. Biodegradation of polycarbonate-based polyurethanes by the human monocyte-derived macrophage and U937 cell systems. *Journal of Biomedical Materials Research* 2002; **61**: 505-513.

Appendix A- Statistical analysis

A.1 Mechanical testing data

A1.1 Chapter 3-Table 3.3

Polyurethane was added with MMT at loadings of 1%, 3% or 5% in combination with OM using either P12 or P16. Each material (formulation, F) was prepared (batch, B) and subdivided into specimens that were tested to determine the mechanical properties. The data are measurements of ultimate tensile strength (UTS), ultimate strain (ε) and Young's modulus (E). Each material tested contained 16-28 specimens in total from 3-7 different batches. The experiment design was a mixed design with the formulation being the fixed factor and the batch number being a random factor nested within the formulation. A two-way analysis of variance (ANOVA) was performed to assess whether there was a significant difference between batches.

UTS

```
Analysis of Variance for UTS, using Adjusted SS for Tests

Source   DF    Seq SS    Adj SS   Adj MS      F      P
F         6  25563.98  21007.07  3501.18  13.40  0.000 x
B(F)     27   7059.74   7059.74   261.47   6.90  0.000
Error   117   4435.29   4435.29    37.91
Total   150  37059.01

x Not an exact F-test.


S = 6.15699   R-Sq = 88.03%   R-Sq(adj) = 84.66%
```

Strain

```
Analysis of Variance for strain, using Adjusted SS for Tests

Source   DF    Seq SS    Adj SS   Adj MS      F      P
F         6  202.1790  195.9675  32.6613  14.03  0.000 x
B(F)     27   62.9001   62.9001   2.3296   9.85  0.000
Error   117   27.6765   27.6765   0.2366
Total   150  292.7555

x Not an exact F-test.


S = 0.486365   R-Sq = 90.55%   R-Sq(adj) = 87.88%
```

Young's modulus

```
Analysis of Variance for E, using Adjusted SS for Tests

Source   DF    Seq SS   Adj SS  Adj MS     F      P
F         6   462.149  410.188  68.365  4.01  0.005 x
B(F)     27   461.109  461.109  17.078  6.89  0.000
Error   117   290.200  290.200   2.480
Total   150  1213.457

x Not an exact F-test.


S = 1.57491   R-Sq = 76.08%   R-Sq(adj) = 69.34%
```

The analysis of UTS, strain and modulus data indicated that there was a significant different between formulations and between each batch. The batch mean square must then be used as the error term in testing for difference between formulations.

Comparison of strain, UTS and modulus of samples against PU control using Dunnett's test

In order to determine whether the strain, UTS and modulus of the samples were significantly different to the PU control, the batch and error were pooled and Dunnett's test was used. The output for UTS is shown.

UTS

```
Analysis of Variance for UTS, using Adjusted SS for Tests

Source   DF   Seq SS   Adj SS  Adj MS      F      P
F         6  25564.0  25564.0  4260.7  53.37  0.000
Error   144  11495.0  11495.0    79.8
Total   150  37059.0

S = 8.93457   R-Sq = 68.98%   R-Sq(adj) = 67.69%

Dunnett Simultaneous Tests
Response Variable UTS
Comparisons with Control Level
F  = 1  subtracted from:

      Difference       SE of           Adjusted
F       of Means  Difference  T-Value   P-Value
2         -15.26       2.680    -5.69    0.0000
3         -20.31       2.997    -6.78    0.0000
4         -41.29       2.760   -14.96    0.0000
5          -0.11       2.825    -0.04    1.0000
6         -11.52       2.825    -4.08    0.0004
7         -20.69       2.616    -7.91    0.0000
```

The analysis showed that only formulation 5 was not significantly different from the control. Using similar methods of analysis, the analysis of variance for strain indicated that only formulation 3 was not significantly different (p=1.0000) to the PU control (formulation 1). For Young's modulus, analysis indicated that formulations 3, 4 and 7 were significantly different to that of control.

A two-way analysis of variance (ANOVA) without PU control

The effect of clay loading (L), modifier type (M) and their interaction were assessed using a two-way ANOVA. The analysis was performed without PU control for easier assessment of the factors (loading and modifier).

UTS

```
Analysis of Variance for UTS, using Adjusted SS for Tests

Source   DF    Seq SS    Adj SS   Adj MS      F      P
L         2  11146.68  11100.12  5550.06  18.75  0.000 x
M         1   7742.76   5668.89  5668.89  19.38  0.000 x
L*M       2    721.23    721.23   360.62   1.22  0.315 x
B(L M)   22   6838.21   6838.21   310.83  13.34  0.000
Error   103   2400.10   2400.10    23.30
Total   130  28848.98

x Not an exact F-test.

S = 4.82721   R-Sq = 91.68%   R-Sq(adj) = 89.50%
```

Strain

```
Analysis of Variance for Strain, using Adjusted SS for Tests

Source   DF    Seq SS    Adj SS    Adj MS      F      P
L         2    7.1852   18.6244    9.3122   4.96  0.017 x
M         1  152.6271  137.2780  137.2780  73.92  0.000 x
L*M       2   16.8068   17.5150    8.7575   4.66  0.020 x
B(L M)   22   43.2582   43.2582    1.9663   7.87  0.000
Error   103   25.7325   25.7325    0.2498
Total   130  245.6098

x Not an exact F-test.


S = 0.499830   R-Sq = 89.52%   R-Sq(adj) = 86.78%
```

Young's modulus

```
Analysis of Variance for E, using Adjusted SS for Tests

Source   DF    Seq SS   Adj SS   Adj MS     F      P
L         2   252.325  222.702  111.351  5.92  0.009 x
M         1   153.945  134.926  134.926  7.25  0.013 x
L*M       2    26.176   31.241   15.620  0.83  0.449 x
B(L M)   22   433.409  433.409   19.700  7.71  0.000
Error   103   263.027  263.027    2.554
Total   130  1128.882

x Not an exact F-test.


S = 1.59802   R-Sq = 76.70%   R-Sq(adj) = 70.59%
```

The large F-ratio for both the clay loading (L) ($p<0.05$) and modifier ($p<0.05$) indicated that there was a significant effect in these 2 factors on the UTS of samples. The L*M

interaction was not significantly different (p=0.315). The clay loading and modifier had a significant effect on the strain. Although the L*M was found to be significantly different (p=0.02), the main effect for the fixed factor L and M over the interaction mean square was tested and found to be not significantly different. The analysis for modulus also indicated that clay loading and modifier type had a significant effect on the modulus of the material. The L*M interaction had no significant effect (p=0.449) implying that the significant effect of modifier type across all clay loadings were consistent.

A.2 Blood compatibility assays

A2.1 Chapter 4-Table 4.2

Release 24 hours versus 48 hours

A two-way analysis of variance (ANOVA) was used to determine significant differences between different release times (time). Five materials (F) were compared; PU+H, P12C-1+H, P12C-5+H, P16C-1+H, P16C-5+H. The design has a fixed factor (F) and the response being heparin released. The analysis indicated that there was no significant difference in heparin released between 24 hours and 48 hours.

Comparison of heparin release (24 hour) between PUNCs and PU using Dunnett's test

In order to determine whether the heparin released in 24 hours from PUNCs was significantly different to PU control, Dunnett's test was used. The design has a fixed factor (F) and response being release (24 hr). Results showed that there were no

significant differences across all samples when compared to PU+H control, except for P16C-1+H (p=0.0586) that was considered to be significantly different as the p-value was close to the value assigned in this test to indicate significant difference (p<0.05).

Comparison of heparin release (48 hour) between PUNCs and PU using Dunnett's test

The same analysis was conducted to determine significant differences in the release after 48 hours. Results showed that there were no significant differences across all samples when compared to PU+H control.

A2.2 Chapter 4-Figure 4.6

The data are measurements of amounts of surface heparin (H) after different washing time (time) comparing five materials (F), PU+H, P12C-1+H, P12C-5+H, P16C-1+H, P16C-5+H. The experiment was conducted in triplicates. The design has fixed factor (F) and a two-way analysis of variance (ANOVA) was used.

Washing time

```
Analysis of Variance for TGT, using Adjusted SS for Tests

Source  DF  Seq SS  Adj SS  Adj MS      F      P
F        4  301132  301132   75283  47.57  0.001
time     1    2564    2564    2564   1.62  0.272
Error    4    6331    6331    1583
Total    9  310027

S = 39.7834   R-Sq = 97.96%   R-Sq(adj) = 95.41%
```

The analysis indicated that there was no significant difference in the extent of washing (p=0.272)

Pairwise comparison of the amount of surface heparin across samples using Tukey's method

The analysis between the amounts of surface heparin (H) among samples (F) was conducted using Tukey's method.

Surface heparin (H)

```
Tukey Simultaneous Tests
Response Variable H
All Pairwise Comparisons among Levels of F
F = P12C-1+H  subtracted from:

Difference       SE of           Adjusted
F           of Means  Difference  T-Value   P-Value
P12C-5+H      -347.1       39.78    -8.73    0.0045
P16C-1+H      -118.9       39.78    -2.99    0.1633
P16C-5+H      -414.0       39.78   -10.41    0.0023
PU+H            -1.7       39.78    -0.04    1.0000


F = P12C-5+H  subtracted from:

Difference       SE of           Adjusted
F           of Means  Difference  T-Value   P-Value
P16C-1+H      228.21       39.78    5.736    0.0210
P16C-5+H      -66.89       39.78   -1.681    0.5276
PU+H          345.46       39.78    8.684    0.0046


F = P16C-1+H  subtracted from:

Difference       SE of           Adjusted
F           of Means  Difference  T-Value   P-Value
P16C-5+H      -295.1       39.78   -7.418    0.0083
PU+H           117.2       39.78    2.947    0.1695


F = P16C-5+H  subtracted from:

Difference       SE of           Adjusted
F       of Means  Difference  T-Value   P-Value
PU+H       412.3       39.78    10.36    0.0023
```

There was no significant difference between PU+H, P12C-1+H and P16C-1+H. There was also no difference between P12C-5 and P16C-5. Significant differences were observed when 5wt% loaded NCs were compared to PU. In addition, a significant difference was found when clay loading increases from 1 to 5wt% ($p=0.0045$ for P12s and 0.0083 for P16s)

A2.3 Chapter 4-Figure 4.8

Statistical analysis was performed using a two-way analysis of variance (ANOVA) to assess the effects of washing time (time) on TGT. The materials tested (F) were PU+H and P16C-5+H. The analysis indicated that there was no difference between washing time ($p=0.131$).

A2.4 Chapter 4-Figure 4.9 & Figure 4.10

The data are measurements of TGT of static thrombin generation assay. Ten materials (PU, P12C-1, P12C-5, P16C-1, P16C-5, PU+H, P12C-1+H, P12C-5+H, P16C-1+H, P16C-5+H) were conducted in 3 replicates. In order to determine whether TGT and peak thrombin of samples without heparin (5 types) were significantly different to the PU control, the Dunnett's test was used.

TGT

```
Analysis of Variance for TGT, using Adjusted SS for Tests

Source  DF  Seq SS  Adj SS  Adj MS     F      P
Type     4   61.14   61.14   15.28  0.61  0.659
Error   15  372.84  372.84   24.86
Total   19  433.98


S = 4.98561   R-Sq = 14.09%   R-Sq(adj) = 0.00%


Dunnett Simultaneous Tests
Response Variable TGT
Comparisons with Control Level
Type = 1  subtracted from:

      Difference       SE of           Adjusted
Type    of Means  Difference  T-Value   P-Value
2          5.346       3.525   1.5164    0.3915
3          2.618       3.525   0.7427    0.8689
4          3.436       3.525   0.9746    0.7327
5          3.669       3.525   1.0406    0.6896
```

Peak thrombin

```
Analysis of Variance for Peak, using Adjusted SS for Tests

Source  DF  Seq SS  Adj SS  Adj MS     F      P
Type     4    46.4    46.4    11.6  0.03  0.999
Error   15  6677.8  6677.8   445.2
Total   19  6724.2


S = 21.0995   R-Sq = 0.69%   R-Sq(adj) = 0.00%


Dunnett Simultaneous Tests
Response Variable Peak
Comparisons with Control Level
Type = 1  subtracted from:

      Difference       SE of            Adjusted
Type    of Means  Difference   T-Value   P-Value
2        -0.0878       14.92  -0.00588    1.0000
3        -0.1724       14.92  -0.01156    1.0000
4         2.3453       14.92   0.15720    0.9995
5         3.5083       14.92   0.23515    0.9977
```

Results showed that there was no significant difference between the TGT and peak thrombin of PUNC coils compared to PU.

Comparison of TGT of heparin loaded NC coils against PU using Dunnett's test

The same analysis was conducted to determine significant differences in the TGT of heparin loaded samples. Results showed that there were significant differences across all samples when compared to PU+H control.

A two-way analysis of variance (ANOVA) comparing heparin loaded coils to non-heparin loaded coils

The effects of TGT and peak thrombin between heparin (H) loaded coils and non heparin loaded was assessed. The output for analysis of variance for TGT is given.

TGT

```
Analysis of Variance for TGT, using Adjusted SS for Tests

Source  DF   Seq SS   Adj SS  Adj MS      F      P
F        4   511.11   511.11  127.78   2.86  0.038
H        1   679.31   679.31  679.31  15.19  0.000
Error   34  1521.00  1521.00   44.74
Total   39  2711.41
S = 6.68844   R-Sq = 43.90%   R-Sq(adj) = 35.65%
```

The analysis of this data indicated that there was a significant difference ($p<0.05$) between heparin and non-heparin coils. A similar effect was observed for peak thrombin ($p=0.008$).

A2.5 Chapter 4-Table 4.3

The data are measurements of TGT from dynamic thrombin generation assay. Ten materials (PU, P12C-1, P12C-5, P16C-1, P16C-5, PU+H, P12C-1+H, P12C-5+H, P16C-

1+H, P16C-5+H) from 2 donors (Donor) were analysed. The effects of donor on the TGT of samples were assessed using a two-way analysis of variance (ANOVA) with donor and formulation as fixed factors.

Donor

```
Analysis of Variance for TGT, using Adjusted SS for Tests

Source  DF   Seq SS   Adj SS  Adj MS      F      P
Donor    1    30.28    30.28   30.28   3.31  0.102
F        9  3092.36  3092.36  343.60  37.60  0.000
Error    9    82.25    82.25    9.14
Total   19  3204.90

S = 3.02308   R-Sq = 97.43%   R-Sq(adj) = 94.58%
```

The results indicated that there were no differences to the TGT of samples among donors (p=0.102).

Comparison of TGT of heparin loaded NC coils against PU using Dunnett's test

The analysis was conducted by the same method as described in the static thrombin generation assay. The TGT of NC coils without heparin (5 types) were compared to the PU control using Dunnett's test. Results did not show significant differences between PUNC and PU coils without heparin

A two-way analysis of variance (ANOVA) comparing heparin loaded coils to non-heparin loaded coils.

The analysis was conducted by the same method as described in the static thrombin generation assay. The differences in TGT between heparin (H) loaded coils and non-

heparin loaded coils were assessed. Results indicated a significant difference between heparin and non-heparin samples ($p<0.05$).

A Pairwise comparison of the TGT across coils with added heparin using Tukey's method

The analysis between the TGT of heparin loaded coils were compared using Tukey's method. The results indicated that there were no significant differences between the samples except between P16C-1 and PU ($p=0.0161$).

A.3 Cell studies

A3.1 Chapter 7-Figure 7.9

The analysis was performed on cell numbers (C) at day 10 of the cell proliferation assay, comparing six materials (F), PU, PU+1%DA, P16C-1, P16C-1+1% DA, Null, and Dex solution. The experiment was conducted in 3 replicates with 3 samples for each material in each replicate. The design has fixed factor (F) and a two-way analysis of variance (ANOVA) was used followed by a pairwise comparison between the samples using Tukey's method. The analysis indicated that there was no difference between PU and P16C-1 ($p=0.2478$), suggesting that the addition of NC did not significantly affect the growth of cells. The addition of DexA resulted in significant differences when compared to their relative controls. PU ($p=0.0001$) was different to PU+1% and P16C-1 ($p=0.004$) was different to P16C-1+1% DA.

A3.2 Chapter 7-Figure 7.10

Eight materials (+ve, blank, Dex, Dex+L, P16C-5+1%+L, P16C-5+L, PU+1%, PU+1%+L) were assessed in triplicates with 3 samples for each material in each replicate. The formulation (F) was a fixed factor and a two-way analysis of variance (ANOVA) was used to assess the variations amongst the materials. Subsequently, Tukey's method was used to determine whether drug loaded samples were different to their relative controls. The analysis indicated a significant difference between PU+L and PU+1%+L ($p=0.0011$). Similarly, a significant difference was observed between P16C-5+L and P16C-5+1%+L ($p=0.0162$) owing to the same reason.

Appendix B

B.1 Static thrombin generation assay

A typical thrombin generation curve is shown in Figure B.1. From the curve, the thrombin generation lag time (TGT) can be determined by marking the time where thrombin rises above 2nM, while the peak thrombin is the thrombin generated at the highest point of the curve. Both PU+H and P16C-1+H in Figure A1 showed improved lag time compared to their respective controls as well as a lower peak thrombin due to the lesser formation of thrombus. These results suggested that the heparin is still active after the coating process.

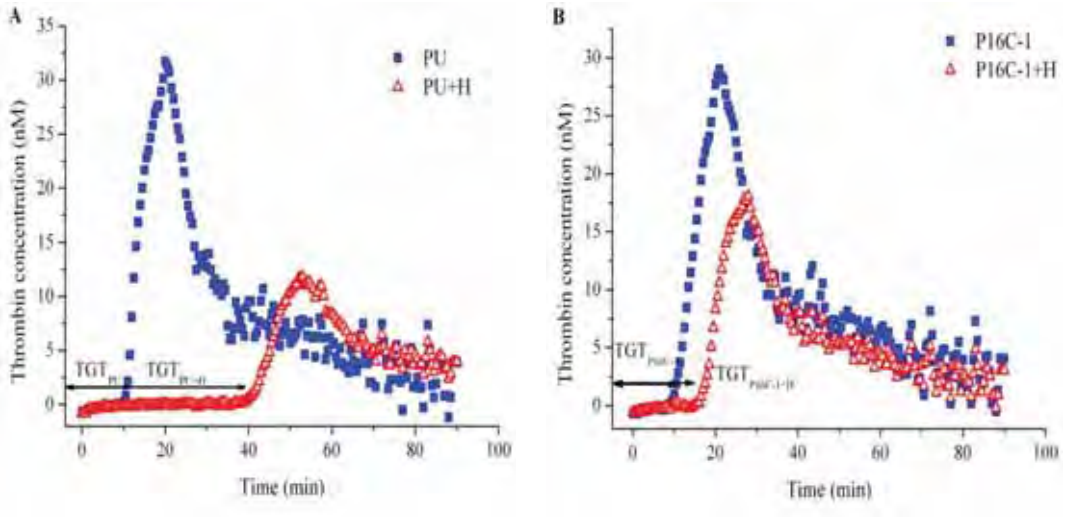

Figure B.1 Representative thrombin generation curves for: A) PU and B) P16C-1. The time between the start of the experiment and the sudden rise in thrombin levels represents the thrombin generation lag time (TGT). Notice how the onset of thrombin between the controls and samples with heparin differs.

B.2 Dynamic thrombin generation assay

The thrombin generation plots for PUNC coils with and without heparin were shown in Figure B.2. The threshold value marking the onset of clotting was consistently taken at

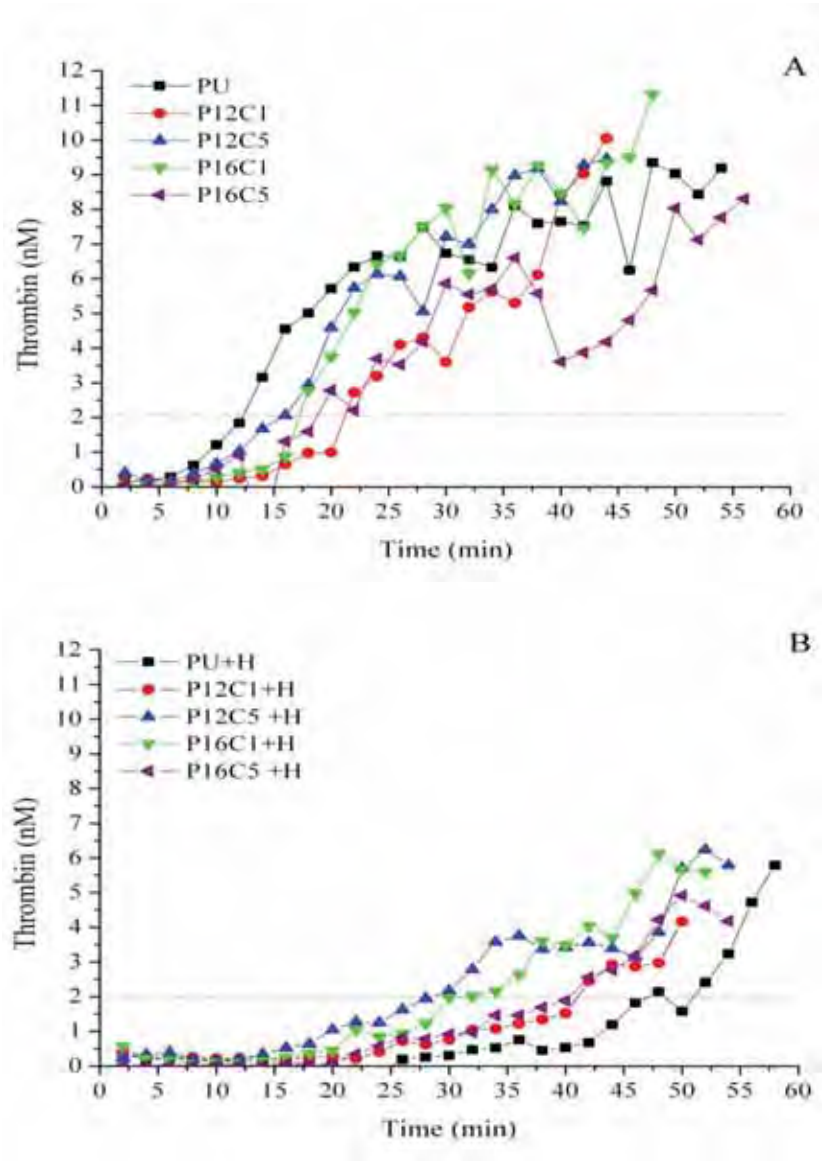

Figure B.2 Dynamic thrombin generation curve of A) PUNC controls and B) incorporated with heparin. The error bars in this figure was neglected for ease of interpretation. Dotted lines represent the threshold (2nM) taken for this assay (n=2).

2nM for all thrombin generation assays and is illustrated in Figure B.2 by the dotted line. The time taken for samples to produce 2nM is the thrombin generation lag time (TGT).

The errors bars in Figure B.2 were neglected for ease of interpretation but were included in Table 4.3 (TGT only). A sudden decrease in thrombin concentration was observed in some samples during the duration of the experiment. These are caused by the loss and removal of thrombus during sample collection into the vials. The concentration of thrombus will eventually build up again until the flow of blood is completely occluded marking the end point of the experiment. PUNC coated coils without heparin showed a slightly longer TGT as compared to PU control. Noticeably, coils with added heparin as shown in Figure B.2 displayed much longer TGT than ones without due to the anti-thrombotic effects of heparin.

Appendix C

C.1 ATR-FTIR spectra of $16CH_3MMT$ and $12CH_3MMT$

The ATR-FTIR spectra for MMT and OMS are shown in Figure C.1. Distinct peaks for MMT were in agreement with those reported in literature [261, 262] occurring at 3626 cm^{-1} (stretching of structural OH), 3425cm^{-1} (stretching of H-O-H water) and 986cm^{-1} (Si-O-Si stretch). Both $12CH_3MMT$ and $16CH_3MMT$ displayed peaks corresponding to the asymmetric and symmetric stretching of CH_2 at 2926cm^{-1} and 2854cm^{-1} respectively. The intensities at those peaks were larger for $16CH_3MMT$ since the carbon chain length was longer.

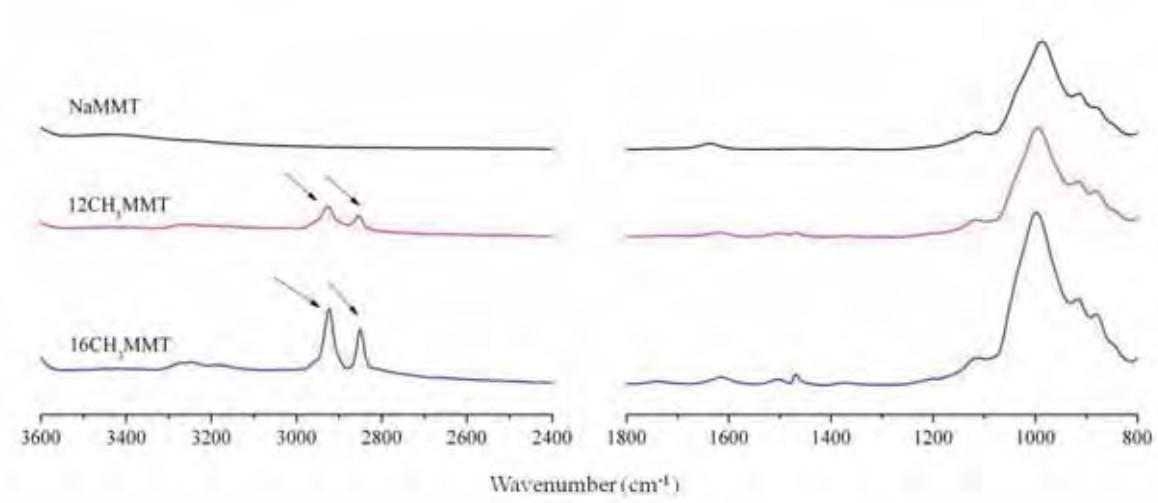

Figure C.1 ATR FTIR spectra for NaMMT, $12CH_3MMT$ and $16CH_3MMT$ showing successful modification. Peaks labelled with arrows indicate the presence of alkylamine modifiers.

C.2 Release kinetics of crystal violet and bromophenol blue

The release data was analysed to assess the drug release kinetics by using equation presented in Chapter 5 for: zero order, first order and Higuchi's model. Release kinetics from crystal violet and bromophenol blue were shown in graphs in Figure C.2-C.4 and Figure C.5-C.7 respectively. The coefficient of determination (r^2) and release constant (*k*), shown in Table 5.10 were determined from the R^2 and slope of the linear regression equation. The data analysed are only limited to the initial section of the in vitro drug release curve (Figure 5.14 and Figure 5.15) before the release profile plateaus. This is because as the curve plateaus, it indicates that the model drugs from the samples reached maximum release and there will be no further drug, hence no mechanism of release. Therefore, the data after the initial increase were omitted. Kinetic analysis was not performed on samples incorporated with Coomassie blue.

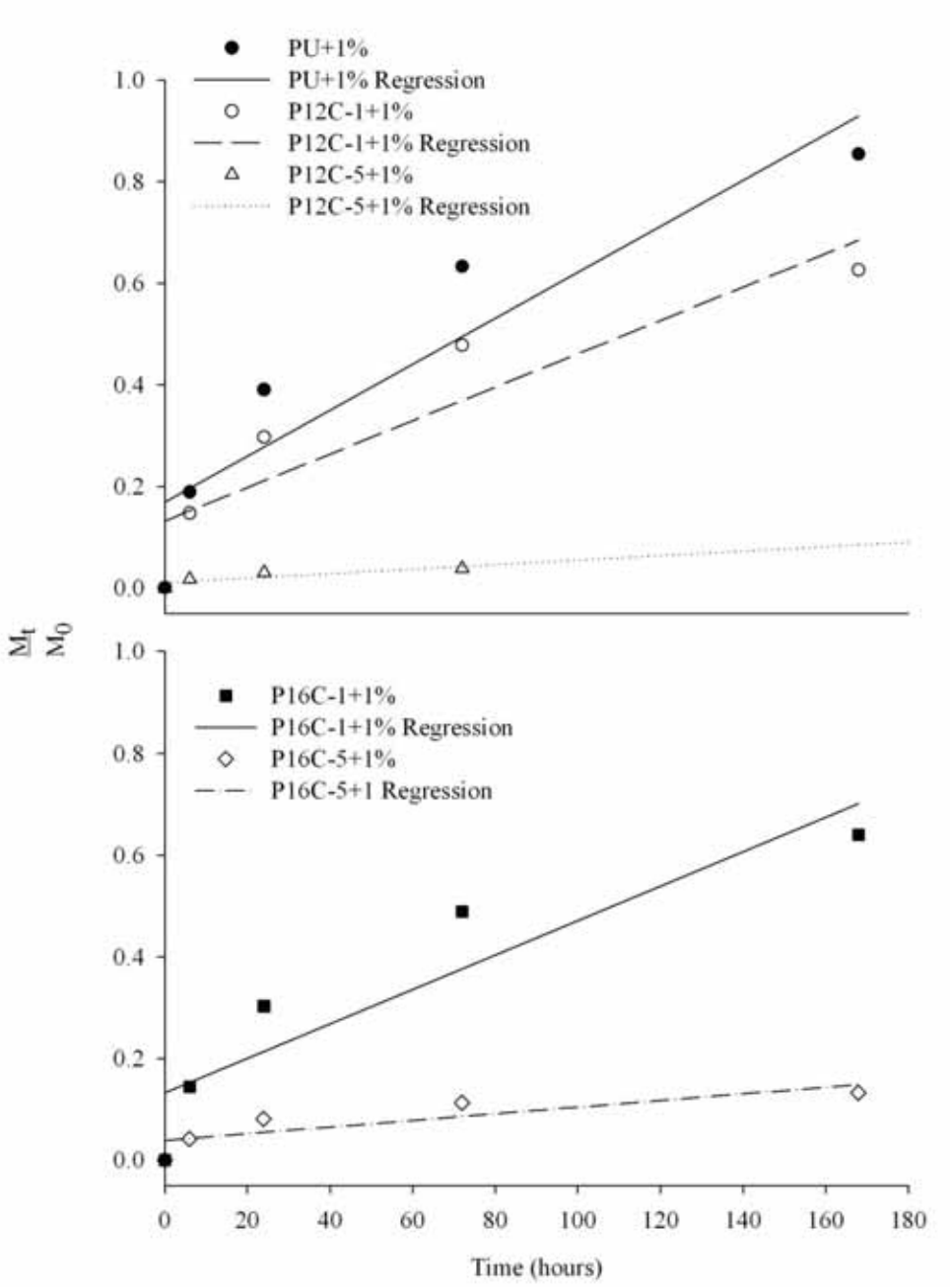

Figure C.2 Zero order release kinetics. The ratio of cumulative release of CV from PU and PUNCs as a function of time.

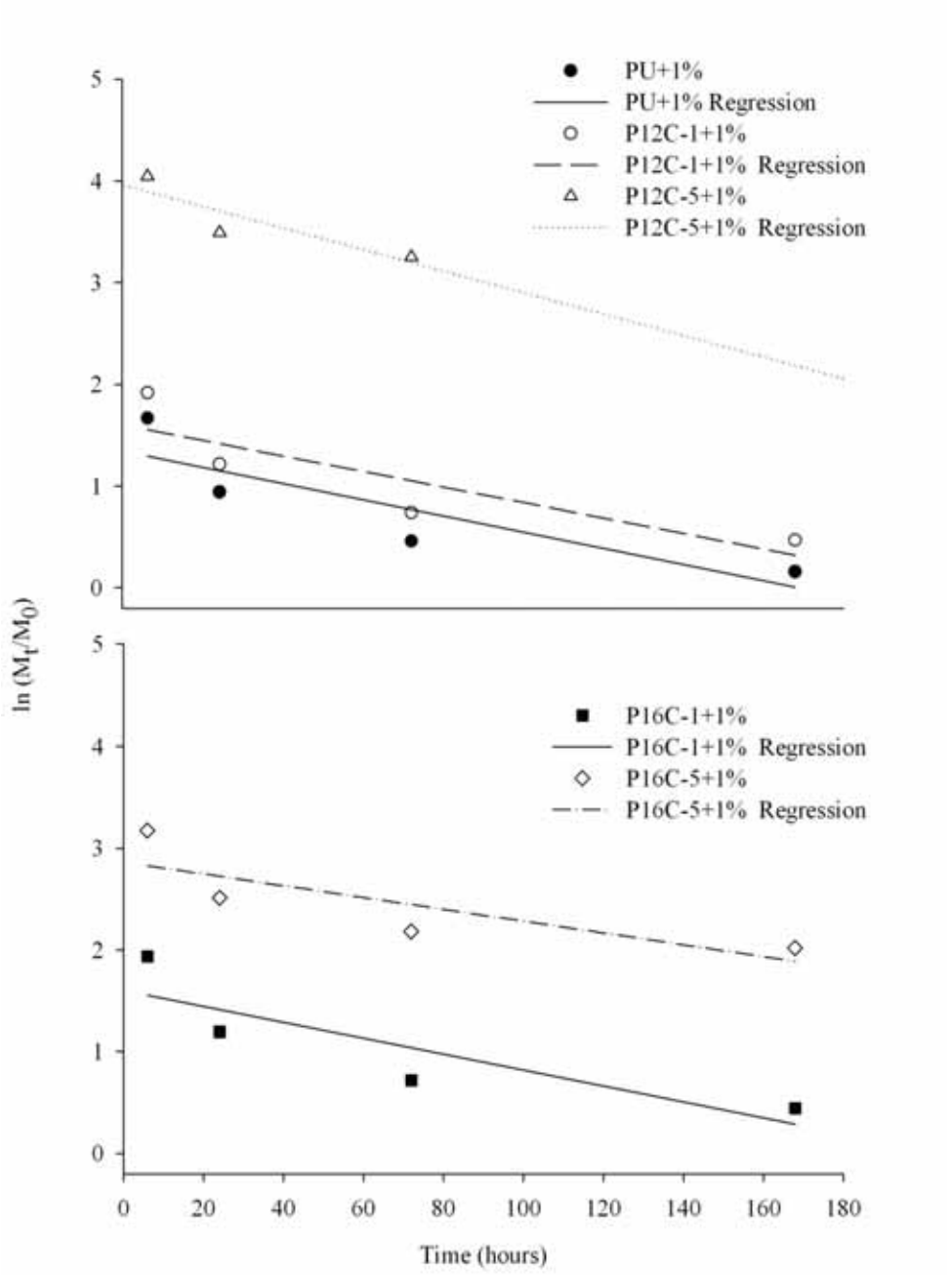

Figure C.3 First order release kinetics. The logarithm of cumulative release of CV over initial concentration as a function of time.

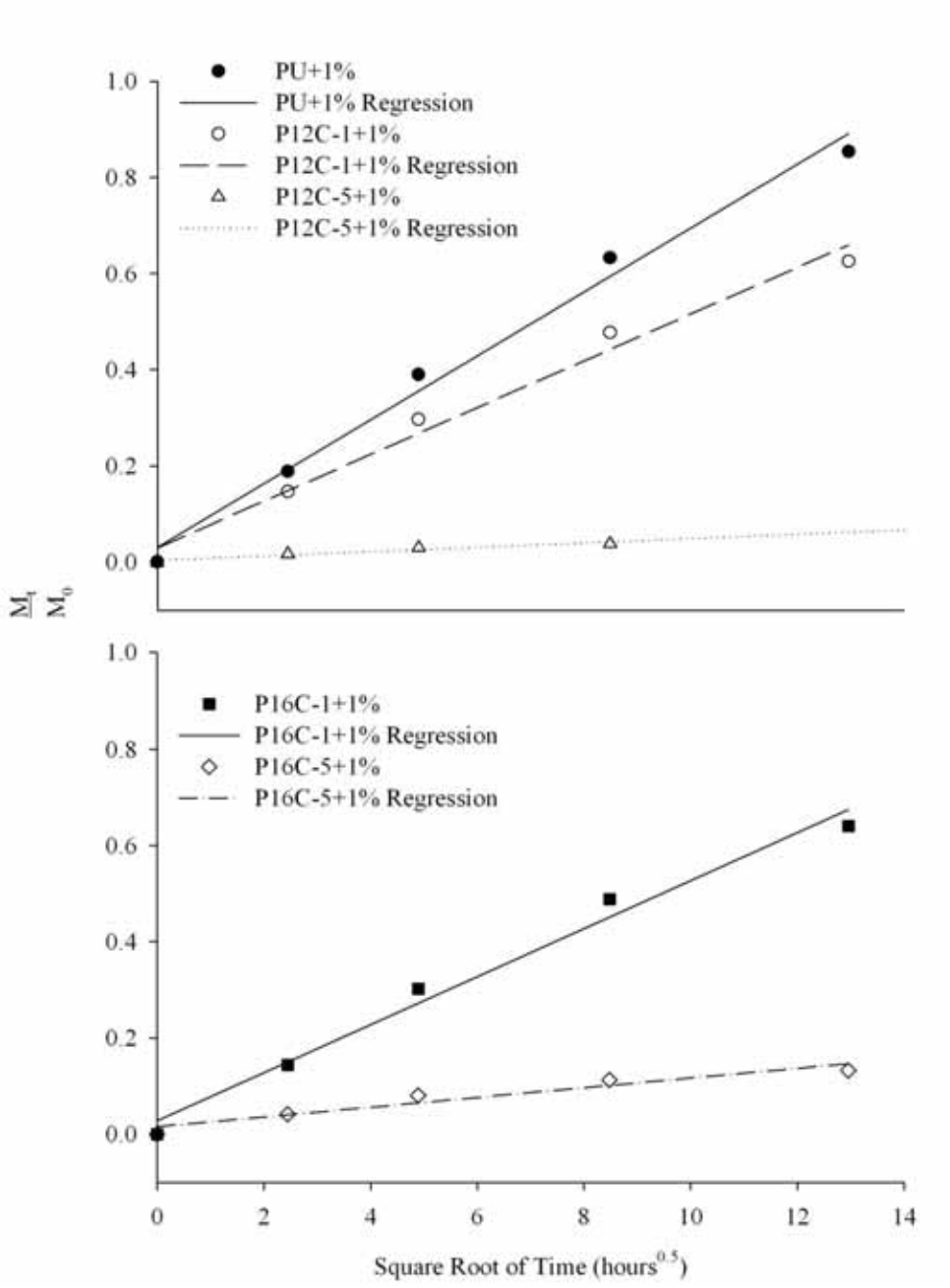

Figure C.4 Higuchi's square root model. The ratio of cumulative release of CV from PU and PUNCs as a function of the square root of time.

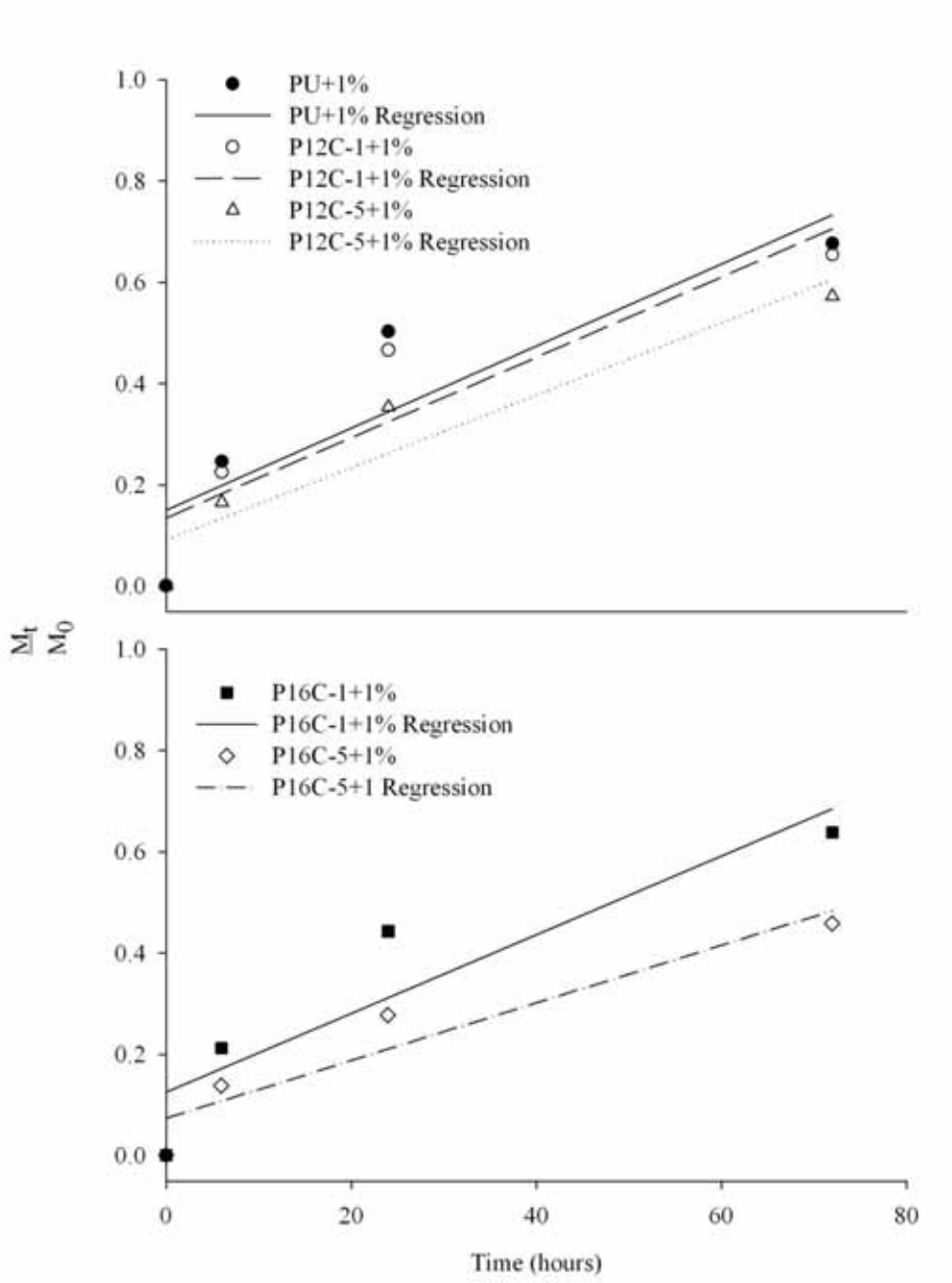

Figure C.5 Zero order release kinetics. The ratio of cumulative release of BB from PU and PUNCs as a function of time.

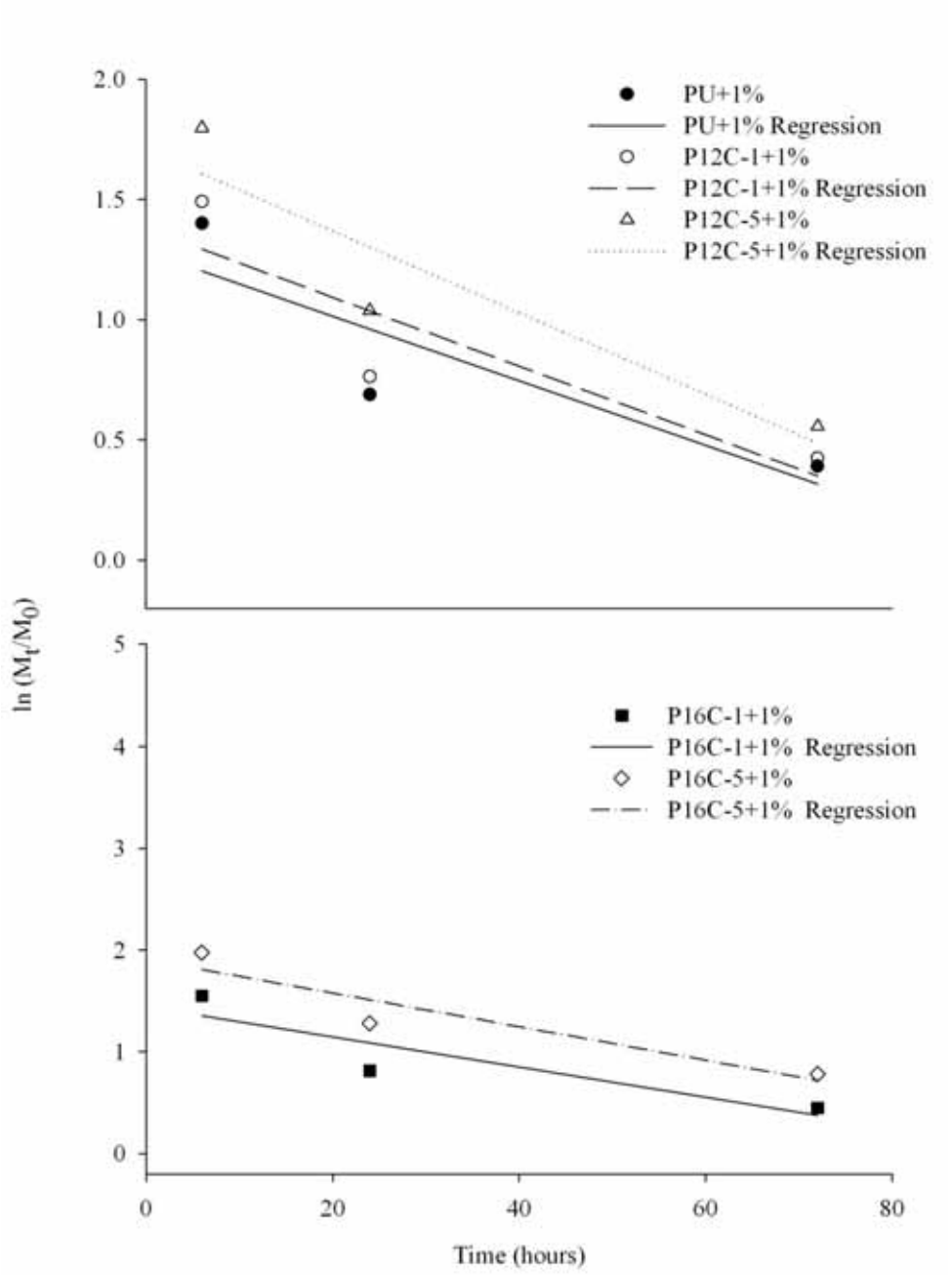

Figure C.6 First order release kinetics. The logarithm of cumulative release of BB over initial concentration as a function of time.

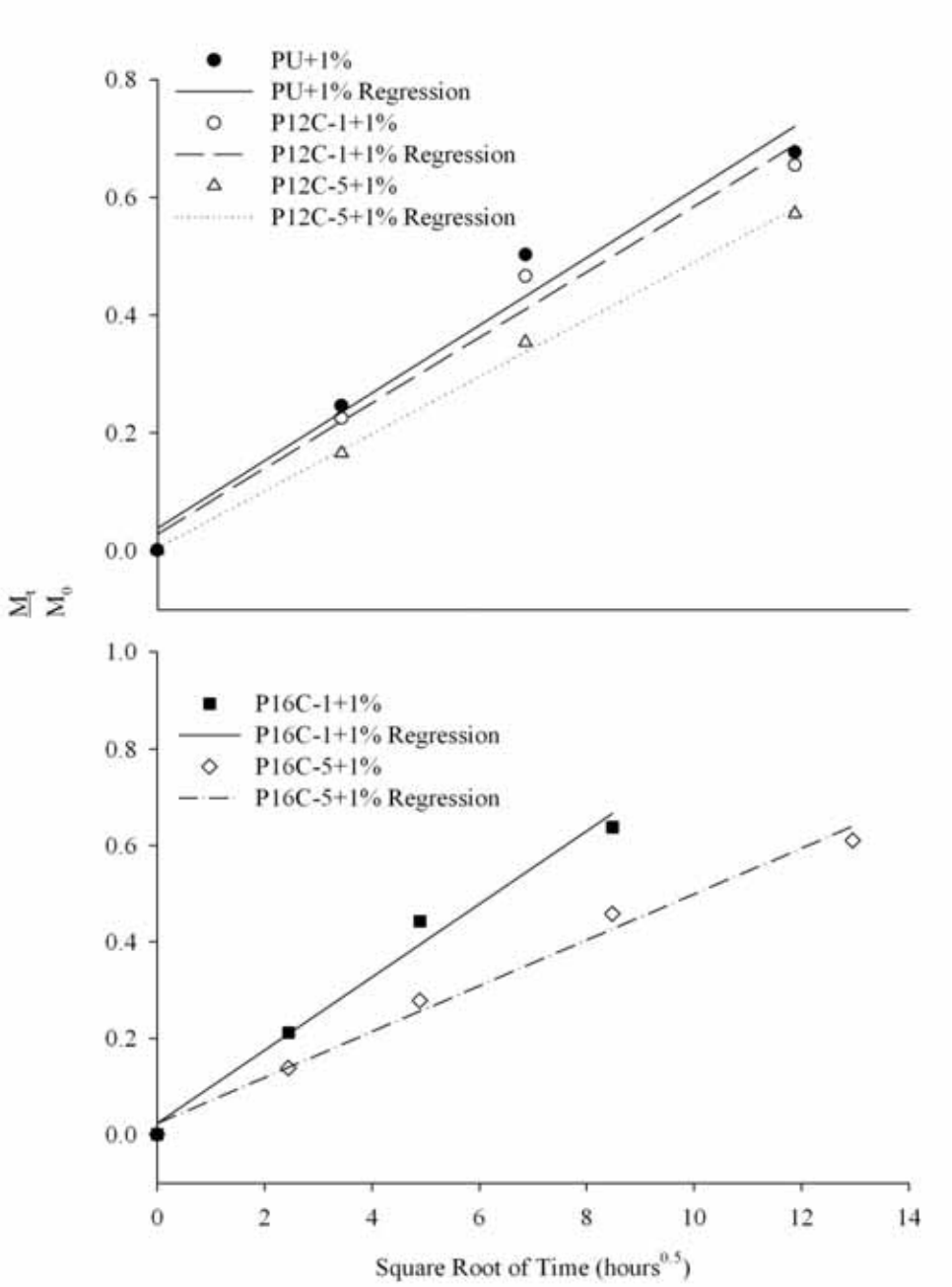

Figure C.7 Higuchi's square root model. The ratio of cumulative release of BB from PU and PUNCs as a function of the square root of time.

Appendix D

D.1 Cell growth inhibition assay of DexA and DexP

The cell growth inhibition results with DexP and DexA in solution is shown in Figure D.1 a) and b) respectively. The CGI ratio across all concentrations tested was similar for both drugs since both drugs belong to the same family of glucocorticoid steroids [297].

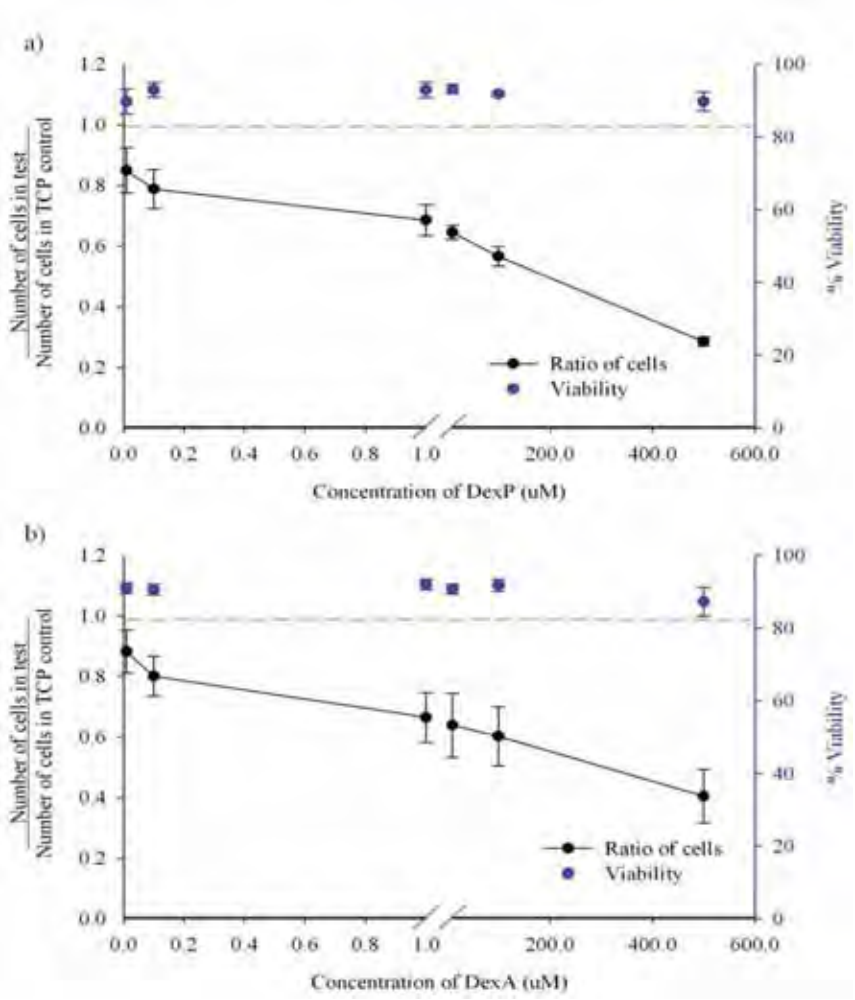

Figure D.1 CGI standard curve for: a) DexP (n=2) and b) DexA (n=3). Data represents a ratio of cells in test against cells in positive control. Dotted line represents the positive tissue culture plate.